Targeted degradation of Myc-interacting oncoproteins

Gezielte Degradation von mit Myc interagierenden Onkoproteinen

Doctoral thesis for a doctoral degree
at the Graduate School of Life Sciences,
Julius-Maximilians-Universität Würzburg

Section: Biomedicine

submitted by

Bikash Adhikari

from

Chitwan, Nepal

Würzburg 2022

Submitted on: .....

Members of the Thesis Committee

Chairperson: **Prof. Dr. Manfred Gessler**

Primary Supervisor: **Prof. Dr. Elmar Wolf**

Supervisor (Second): **Dr. Sonja Lorenz**

Supervisor (Third): **Prof. Dr. Claudia Höbartner**

Supervisor (Fourth): **Prof. Dr. Martin Sos**

TABLE OF CONTENTS

Table of Contents

Summary

The hallmark oncoprotein Myc is a major driver of tumorigenesis in various human cancer entities. However, Myc's structural features make it challenging to develop small molecules against it. A promising strategy to indirectly inhibit the function of Myc is by targeting its interactors. Many Myc-interacting proteins have reported scaffolding functions which are difficult to target using conventional occupancy-driven inhibitors. Thus, in this thesis, the proteolysis targeting chimera (PROTAC) approach was used to target two oncoproteins interacting with Myc which promote the oncogenicity of Myc, Aurora-A and WDR5. PROTACs are bifunctional small molecules that bind to the target protein with one ligand and recruit a cellular E3-ligase with the other ligand to induce target degradation via the ubiquitin-proteasome system. So far, the most widely used E3-ligases for PROTAC development are Cereblon (CRBN) and von Hippel–Lindau tumor suppressor (VHL). Furthermore, there are cases of incompatibility between some E3-ligases and proteins to bring about degradation. Hence there is a need to explore new E3-ligases and a demand for a tool to predict degradative E3-ligases for the target protein in the PROTAC field.

In the first part, a highly specific mitotic kinase Aurora-A degrader, JB170, was developed. This compound utilized Aurora-A inhibitor alisertib as the target ligand and thalidomide as the E3-ligase CRBN harness. The specificity of JB170 and the ternary complex formation was supported by the interactions between Aurora-A and CRBN. The PROTAC-mediated degradation of Aurora-A induced a distinct S-phase defect rather than mitotic arrest, shown by its catalytic inhibition. The finding demonstrates that Aurora-A has a non-catalytic role in the S-phase. Furthermore, the degradation of Aurora-A led to apoptosis in various cancer cell lines.

In the second part, two different series of WDR5 PROTACs based on two protein-protein inhibitors of WDR5 were evaluated. The most efficient degraders from both series recruited VHL as a E3-ligase and showed partial degradation of WDR5. In addition, the degradation efficiency of the PROTACs was significantly affected by the linker nature and length, highlighting the importance of linker length and composition in PROTAC design. The degraders showed modest proliferation

defects at best in cancer cell lines. However, overexpression of VHL increased the degradation efficiency and the antiproliferative effect of the PROTACs.

In the last part, a rapamycin-based assay was developed to predict the degradative E3-ligase for a target. The assay was validated using the WDR5/VHL and Aurora-A/CRBN pairs. The result that WDR5 is degraded by VHL but not CRBN and Aurora-A is degraded by CRBN, matches observations made with PROTACs. This technique will be used in the future to find effective tissue-specific and essential E3-ligases for targeted degradation of oncoproteins using PROTACs.

Collectively, the work presented here provides a strategy to improve PROTAC development and a starting point for developing Aurora-A and WDR5 PROTACs for cancer therapy.

Zusammenfassung

Das Onkoprotein Myc ist ein wichtiger Faktor bei der Tumorentstehung in verschiedenen menschlichen Krebsarten. Die strukturellen Merkmale von Myc machen es jedoch schwierig, kleine Moleküle gegen dieses Protein zu entwickeln. Eine vielversprechende Strategie zur indirekten Hemmung der Funktion von Myc besteht darin, auf seine Interaktoren abzuzielen. Viele Proteine, die mit Myc interagieren, haben Gerüstfunktionen, die mit herkömmlichen Inhibitoren nur schwer zu hemmen sind. Daher wurde in dieser Arbeit der PROTAC-Ansatz (Proteolysis Targeting Chimera) verwendet, um zwei Onkoproteine, die mit Myc interagieren und die Onkogenität von Myc fördern, ins Visier zu nehmen: Aurora-A und WDR5. PROTACs sind bifunktionale kleine Moleküle, die mit einem Liganden an das Zielprotein binden und mit dem anderen Liganden eine zelluläre E3-Ligase rekrutieren, um den Abbau des Zielproteins über das Ubiquitin-Proteasom-System einzuleiten. Die bisher am häufigsten verwendeten E3-Ligasen für die Entwicklung von PROTACs sind Cereblon (CRBN) und der von Hippel-Lindau-Tumorsuppressor (VHL). Außerdem gibt es Fälle von Inkompatibilität zwischen einigen E3-Ligasen und Proteinen, die abgebaut werden sollen. Daher besteht die Notwendigkeit, neue E3-Ligasen zu erforschen und Werkzeuge zur Vorhersage abbauender E3-Ligasen für das Zielprotein zu entwickeln.

Im ersten Teil wurde ein hochspezifischer Degrader der mitotischen Kinase Aurora-A, JB170, entwickelt. Bei dieser Verbindung wurde der Aurora-A-Inhibitor Alisertib als Zielligand und Thalidomid als Binder für die E3-Ligase CRBN verwendet. Die Spezifität von JB170 und die ternäre Komplexbildung wurden durch die Wechselwirkungen zwischen Aurora-A und CRBN unterstützt. Der durch PROTAC vermittelte Abbau von Aurora-A führte zu einem deutlichen Defekt in der S-Phase und nicht zu einem mitotischen Stillstand, wie es für dessen katalytische Hemmung beobachtet wurde. Dies zeigt, dass Aurora-A eine nicht-katalytische Funktion in der S-Phase hat. Außerdem führte der Abbau von Aurora-A in verschiedenen Krebszelllinien zur Apoptose.

Im zweiten Teil wurden zwei verschiedene Serien von WDR5 PROTACs auf der Grundlage von zwei Protein-Protein-Inhibitoren von WDR5 untersucht. Die effizientesten Degrader aus beiden Serien rekrutierten VHL als E3-Ligase und

zeigten einen teilweisen Abbau von WDR5. Darüber hinaus wurde die Abbaueffizienz der PROTACs erheblich von der Art und Länge des Linkers beeinflusst, was die Bedeutung der Linkerlänge und -zusammensetzung bei der Entwicklung von PROTACs unterstreicht. Die Abbauprodukte zeigten bestenfalls bescheidene Proliferationsdefekte in Krebszelllinien. Eine Überexpression von VHL erhöhte jedoch die Abbaueffizienz und den antiproliferativen Effekt der PROTACs.

Im letzten Teil wurde ein auf Rapamycin basierender Assay entwickelt, um die abbauende E3-Ligase für ein Target vorherzusagen. Der Assay wurde anhand der Paare WDR5/VHL und Aurora-A/CRBN validiert. Das Ergebnis, dass WDR5 von VHL, aber nicht von CRBN abgebaut wird und Aurora-A von CRBN abgebaut wird, stimmt mit den Beobachtungen überein, die mit PROTACs gemacht wurden. Diese Technik wird in Zukunft eingesetzt werden, um wirksame gewebespezifische und essentielle E3-Ligasen für den gezielten Abbau von Onkoproteinen mit Hilfe von PROTACs zu finden.

Insgesamt bieten die hier vorgestellten Arbeiten eine Strategie zur Verbesserung der PROTAC-Entwicklung und einen Ausgangspunkt für die Entwicklung von Aurora-A- und WDR5-PROTACs für die Krebstherapie.

1 Introduction

1.1 Myc protein family

The Myc protein family consists of three members, c-Myc (hereafter written as Myc), N-Myc, and L-Myc, which are required for the development and maintenance of proliferative tissues. Myc, N-Myc, and L-Myc are encoded by *MYC*, *MYCN,* and *MYCL* genes. Initially, *MYC* was discovered as avian tumor viral transforming gene v-Myc (Duesberg et al., 1977; Sheiness et al., 1978). Later, in humans, Myc was found to be translocated in Burkitt's Lymphoma, where it was fused to IgG enhancer leading to its overexpression (Dalla-Favera et al., 1982; Taub et al., 1982). Soon *MYCN* and *MYCL* were also identified in human neuroblastoma (Kohl et al., 1983; Schwab et al., 1983) and small cell lung carcinoma (SCLC) cell lines (Nau et al., 1985), respectively. All three homologs of Myc share conserved regions known as Myc homology boxes.

Myc is a transcription factor and is essential for the functioning of normal cells by regulating cellular processes like proliferation, differentiation, and apoptosis (Eilers & Eisenman, 2008; Facchini & Penn, 1998). Many studies have shown Myc's essentiality for growth and development. For example, the complete deletion of *MYC* alleles in mice embryos resulted in a severe decrease in embryo size and eventual embryonic lethality before 10.5 days of gestation (Davis et al., 1993; Dubois et al., 2008; Trumpp et al., 2001). Moreover, conditional deletion of *MYC* in mice during adult hematopoiesis resulted in severe cytopenia and accumulation of hematopoietic stem cells due to their inability to start differentiation (Wilson et al., 2004). In addition, mice with epidermal *MYC* knockdown showed severe skin defects like impaired wound healing and fragile skin (Zanet et al., 2005). In another study, conditional depletion of *MYC* in mice resulted in rapid loss of intestinal crypts (Muncan et al., 2006).

Besides being an essential protein, Myc is dysregulated in most cancers. A large body of evidence has shown the role of Myc in both tumor initiation and maintenance.

1.2 Hallmark oncogene: Myc

Over the years, it has become increasingly apparent that Myc is overexpressed in many different human cancer entities (Dang, 2012). In normal, untransformed cells Myc is a short-lived protein with an mRNA half-life of ~30 minutes (Dani et al., 1984) and a protein half-life of ~20 minutes (Hann & Eisenman, 1984). The expression of Myc is stringently regulated at different cellular levels of transcription and translation (Farrell & Sears, 2014; Lemm & Ross, 2002; Yeilding et al., 1996). In cancer cells, up to date, Myc is found to be overexpressed due to chromosomal translocation, gene amplification, point mutations, enhanced translation, deregulation or mutation in upstream pathways, and increased protein stability via mutation in E3 ligases (Choi et al., 2010; Hemann et al., 2005; Kalkat et al., 2017; Meyer & Penn, 2008; Welcker et al., 2004). Myc can enable all the processes, annotated under the umbrella term “cancer hallmarks” (Fig. 1.1), which provides an explanation of why Myc is so frequently deregulated in tumors (Gabay et al., 2014; Hanahan, 2022; Hanahan & Weinberg, 2011; Llombart & Mansour, 2022).

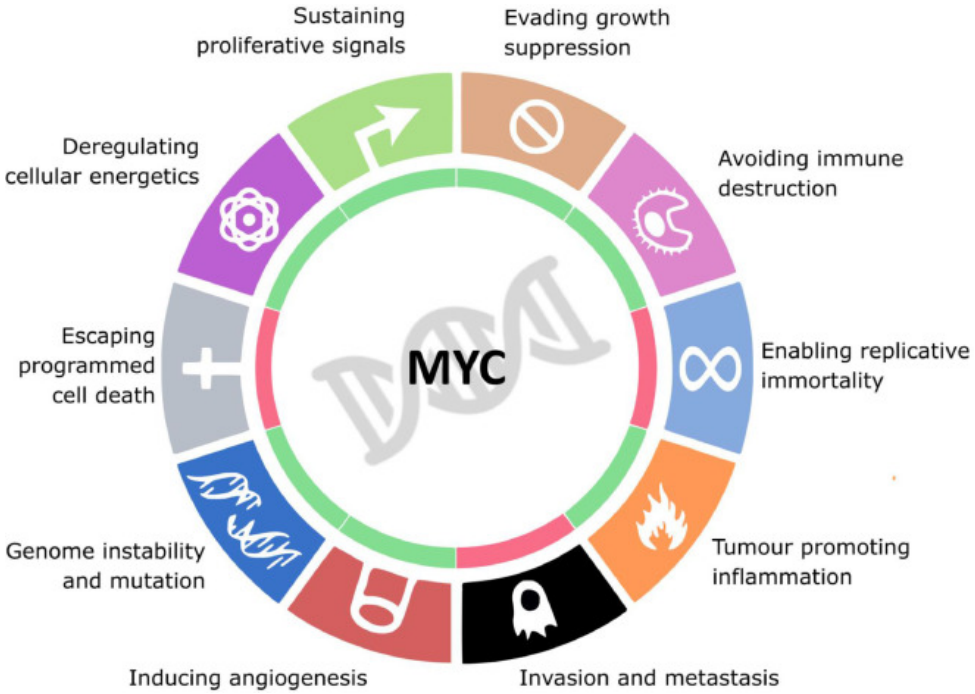

Figure 1.1: Hallmarks of cancer regulated by MYC.
adapted from Llombart & Mansour, 2022.

The following sub-chapters highlight why Myc is a critical oncogene and potential target for cancer therapy.

1.2.1 Upregulation of Myc in human patients and human samples

Pan-cancer analysis showed that one of the Myc paralogs is amplified in more than 28% across 33 cancers of The Cancer Genome Atlas (TCGA) (Schaub et al., 2018). Myc is frequently amplified in tumors where the tumor cells contain many copies of the *MYC* gene. However, there are many other ways by which Myc can be overexpressed and that differs from tumor-to-tumor entities. Some relevant examples are discussed below.

The third most frequent cancer type, colorectal cancer (CRC), is characterized by activation of the WNT/ β-catenin signaling pathway, which induces increased expression of the target genes like Myc (Cancer Genome Atlas, 2012; Guinney et al., 2015; van de Wetering et al., 2002). Human primary colorectal carcinomas show Myc overexpression and amplification in almost 70% and 10% cases, respectively (Erisman et al., 1985; Rochlitz et al., 1996; Sikora et al., 1987; Smith et al., 1993). Myc overexpression in CRC can also result from an inactivating missense mutation in FBXW7 (F-box/WD repeat-containing 7), an E3-ubiquitin ligase for Myc, which results in increased Myc protein stability (Kogita et al., 2015; Korphaisarn et al., 2017).

Neuroblastoma, a malignant tumor of the peripheral nervous system, accounts for ~10% of all tumors in children and ~15% of cancer-related deaths in children (Otte et al., 2020). *MYC* paralog, *MYCN* is amplified in 20-30% of all neuroblastoma patients and accounts for more than 50% of high-risk neuroblastoma patients (Huang & Weiss, 2013; Otte et al., 2020), who have a five-year survival of less than 50% (Rickman et al., 2018). Similarly, in the most malignant brain tumor in children, medulloblastoma, two subgroups illustrate high overexpression of one or two Myc isoforms. The overexpression is linked to poor prognosis and eventually lead to shorter survival (Kawauchi et al., 2012; Northcott et al., 2011; Roussel & Robinson, 2013).

All three *MYC* family genes are amplified in ~ 20% of small cell lung cancer (SCLC) in a mutually exclusive manner (Gugger et al., 2002; Mollaoglu et al., 2017; Sos et al., 2012). SCLC tumors harboring MYC amplification exhibited poor survival compared to tumors without MYC amplification (Johnson et al., 1987). It has also been shown that Myc can promote the evolution of different molecular subtypes of SCLC (Bragelmann et al., 2017; Ireland et al., 2020). Furthermore, a whole-genome sequencing-based study performed on 183 non-small-cell lung cancer

(NSCLC) tumors spotted MYC amplification in 31% of cases (Imielinski et al., 2012).

Similarly, in hepatocellular carcinoma (HCC), *MYC* is amplified in more than 30% of the tumors and is recurrent in larger tumors (Kaposi-Novak et al., 2009; Kawate et al., 1999). In alcohol-related HCC, a gain of ~77 % of the region harboring *MYC* is observed (Schlaeger et al., 2008). In this cancer entity, *MYC* amplification is found to correlate with poorer survival. (Kawate et al., 1999). A meta-analysis performed on publications from 1999-2016, which included 981 patients with HCC, revealed that high Myc expression levels signified poor overall and disease-free survival (Min et al., 2021).

Amplification and overexpression of Myc are also found in hematopoietic malignancies like lymphomas and leukemias (Ahmadi et al., 2021; Ohanian et al., 2019). Overexpression of Myc in these cancers is aided by mutation of *MYC* at T58 (threonine 58) (Brown et al., 2012; Chang et al., 2000; Malempati et al., 2006). Myc phosphorylation at T58 residue is essential for recognition by E3-ubiquitin ligase FBXW7, leading to ubiquitylation and eventual degradation of Myc via the proteasome (Welcker et al., 2004; Yada et al., 2004). Moreover, the mutation in *FBXW7* is also seen in these malignancies (Brown et al., 2012; O'Neil et al., 2007; Thompson et al., 2007). These mutations in *MYC* and *FBXW7* collectively impair FBXW7-mediated degradation of Myc. Similarly, chromosomal translocation in the proximity of gene encoding immunoglobulin heavy (*IGH)* and light chain (*IGL)* is another critical cause of the Myc upregulation in leukemia and lymphoma (Avet-Loiseau et al., 2001; Chiecchio et al., 2009; Dalla-Favera et al., 1982; Taub et al., 1982).

Myc overexpression and amplification in various cancer entities indicate that tumor cells benefit from increased Myc levels. This leads to the question of whether the upregulation of Myc leads to cancer.

1.2.2 Overexpression of Myc induces tumor in mice

The causal relationship between Myc overexpression and tumorigenesis has been demonstrated in various tumor xenografts and transgenic mouse models. Adams et al. described one of the first mouse models for Myc-activated tumorigenesis (Adams et al., 1985). In this transgenic mouse model, *MYC* was coupled to the immunoglobulin μ enhancer. These E_{μ}-*MYC* mice showed aggressive lymphoma, where 94% of mice died within four months after birth. The onset of lymphoma was

observed in pups as early as three weeks of age. All the tumors were of B-lymphoid lineage with both pre-B and mature B-cell lymphoma. In a further study, Park and colleagues inserted 6x His-tagged *MYC* into the mouse's *IGH* locus (Park et al., 2005). This resulted in the development of B-cell and plasma-cell neoplasms within the age of six months. Similarly, another research approach used a construct with the control promoter region of human *CD2* fused to *MYC* to create a transgenic mouse. Almost one-quarter of the *CD2-MYC* transgenic mice developed thymic lymphoma (Stewart et al., 1993). These mouse models thus demonstrated that high Myc is sufficient for the tumor formation.

Mouse models were also employed to test the ability of Myc and N-Myc overexpression to initiate various tumors of the nervous system, such as neuroblastoma, medulloblastoma, and retinoblastoma. A pTH-*MYCN* mouse model was designed to overexpress human N-Myc in neural crest cells (Weiss et al., 1997). The promotor tyrosine hydroxylase (pTH) was used, which is active in the neural crest, sympathetic ganglia, and adrenal (Banerjee et al., 1992). These mice developed neuroblastoma showing characteristics of human disease. Wu and colleagues generated a retinoblastoma mouse model using the Tet-On system driven by retina-specific *PAX6* α-enhancer to overexpress N-Myc in mice where tumor suppressor gene retinoblastoma (*RB*) was deleted. N-Myc over-expression led to retinoblastoma even without the inactivation of other tumor suppressors like 107 kDa retinoblastoma-associated protein (p107) and 130 kDa retinoblastoma-associated protein (p130). Retinoblastoma formation was rapid, with an average time of 54 days from the onset of N-Myc overexpression to tumor development (Wu et al., 2017).

Various studies have also been performed to investigate the carcinogenic nature of Myc in breast cancers. In one model, the *MYC* gene was attached to the mouse mammary tumor virus's (*MMTV*) long terminal repeats (*LTR*). The overexpression of Myc in mammary tissue led to the development of mammary adenocarcinomas during early to second pregnancies (Stewart et al., 1984). Similar observations of mammary tumor formation upon expression of *MYC* were seen in other independent studies (D'Cruz et al., 2001; Liao et al., 2000; Schoenenberger et al., 1988).

In a study by Shroff et al., Myc overexpression in kidneys using the g-glutamyl transferase gene promoter (*GGT*) led to the formation of renal cell carcinoma (RCC). Myc-induced RCC in this mouse model was shown to occur via glutamine

metabolism (Shroff et al., 2015). In a lung tumor mouse model developed by Ehrhardt and colleagues, a lung-specific surfactant protein C (SP-C) promoter was used to control the expression of murine Myc. These mice developed multifocal bronchiolo-alveolar adenomas and bronchiolo-alveolar carcinomas (Ehrhardt et al., 2001). Activation of Myc in β cells of the pancreas using the *MYC-ER* mouse model showed rapid islet tumor development (Lawlor et al., 2006). Using a different mouse model for pancreatic cancer, where *MYC* was delivered to mice using avian retroviruses, Myc exclusively induced endocrine tumors (Lewis et al., 2003). Similarly, in a skin mouse model, expression of human *MYC* under the keratin 14 (K14) promoter in transgenic mice induced differentiation of the basal layer of the mouse epidermis (Arnold & Watt, 2001).

1.2.3 Addiction of tumors on Myc

From the studies mentioned, it remained unclear if Myc overexpression is necessary for established tumors or just for their initiation. Several conditional mouse models were exploited to investigate this. These mouse models often utilize different systems to manipulate Myc levels. On the one hand, in Myc-coupled Tet-O promoter-based systems, the expression of Myc depends on the activity of a second transgene, which is usually tissue-specific. The second transgene is combined with either a tetracycline-controlled transactivator protein (tTA, Tet-Off system) or reverse tetracycline-controlled transactivator (rtTA, Tet-On system) (Kistner et al., 1996; Schonig & Bujard, 2003). In the presence of doxycycline (Dox), the expression of Myc is turned off in the Tet-Off system, whereas the expression of Myc is activated in the Tet-On system. The presence of a tissue-specific transgene helps to activate Myc only in the specific tissue. On the other hand, in the estrogen receptor (ER)-based model, the Myc-ER fusion protein is only activated in the presence of 4-Hydroxytamoxifen (OHT), which translocates the protein from the cytoplasm to the nucleus (Blyth et al., 2000; Eilers et al., 1989; Pelengaris et al., 1999). Tissue specificity is rendered in the *MYC-ER* model by adding a tissue-specific promoter, which drives the expression of the fusion protein. The reversal of tumorigenesis after Myc removal was shown by many groups using such conditional transgenic mouse models. In such models, Myc expression was deactivated after tumor formation (D'Cruz et al., 2001; Felsher & Bishop, 1999; Kistner et al., 1996; Marinkovic et al., 2004; Pelengaris et al., 2002; Shachaf et al., 2004). This dependency of tumors on high Myc levels is known as oncogene

addiction (here, Myc addiction). It implies that Myc is essential not only for tumor development but also for tumor maintenance.

The first mouse model to show Myc addiction used a Tet-Off system to manipulate Myc expression in hematopoietic cells. After the development of hematopoietic malignancies, namely, T-cell lymphomas and acute myeloid leukemia, when Myc was inactivated by Dox addition, all the established tumors regressed. Proliferation arrest and apoptosis of the malignant cells were the leading cause of tumor collapse (Felsher & Bishop, 1999). When the Felsher group used the same model for osteogenic sarcoma, they observed tumor regression upon brief Myc inactivation. Moreover, the malignancy did not recur even after Myc was reactivated, as apoptosis was induced in those cells (Jain et al., 2002). Tumor regression upon removal of Myc was also observed in other cancer entities, like T- and B-cell lymphomas (Marinkovic et al., 2004), HCC (Shachaf et al., 2004), and RCC (Shroff et al., 2015). However, this was not exclusive to the Tet-Off system, since similar observations were made using the *MYC-ER* system in skin cancer models (Flores et al., 2004; Pelengaris et al., 1999) and pancreatic tumor model (Pelengaris et al., 2002).

So far, studies have shown that tumors depend on elevated Myc expression, but it remains elusive if systemic depletion or inhibition of Myc is tolerated by healthy tissue. Systemic inhibition of Myc by expressing a dominant negative allele called OmoMyc was used to study this. OmoMyc comprises the leucine-zipper (LZ) region of Myc with four mutations. This Myc mutant, OmoMyc, can homodimerize and heterodimerize with Myc and MYC-associated factor X (Max) (Soucek et al., 1998; Soucek et al., 2008). OmoMyc inhibits Myc-dependent transcriptional activation as OmoMyc-Max dimerization opposes the availability of Max to Myc, and OmoMyc-Myc heterodimer cannot bind the E-boxes (Jung et al., 2017; Soucek et al., 1998; Soucek et al., 2002). In lung adenocarcinomas, inhibition of Myc by OmoMyc led to tumor regression and extension of overall survival, even in the presence of oncogenic Kras with G12D mutation and deficiency of tumor suppressor, p53 (Beaulieu et al., 2019; Soucek et al., 2008; Soucek et al., 2013). The therapeutic potential of OmoMyc was further demonstrated in the NSCLC mouse model, where the purified OmoMyc protein was administered intravenously and intranasally (Beaulieu et al., 2019). Tumor growth arrest by OmoMyc was reported in pancreatic ductal adenocarcinoma (PDAC) and pancreatic β-cell tumors (Sodir et al., 2020; Sodir et al., 2011). OmoMyc also resulted in complete or partial reduction

of tumor volume in skin cancer (Soucek et al., 2004), mammary tumor (von Eyss et al., 2015), and glioblastoma (Galardi et al., 2016). Furthermore, the mice can tolerate the damage in the normal tissue, which shows the therapeutic window in cancer therapy to target Myc (Soucek et al., 2008).

Established tumors depend on elevated Myc expression and genetic inhibition of Myc eradicates tumors in mice and is tolerated by healthy tissue. But what molecular function of Myc is responsible for this?

1.3 Transcription factor: Myc

Like all transcription factors, Myc proteins are modular and are composed of a DNA-binding- and a trans-regulatory domain. The N-terminal transactivation domain (TAD) and Myc homology boxes (MBs) interact with the myriads of coactivators (Fig.1.2). Heterodimerization of the C-terminal basic helix-loop-helix leucine zipper (bHLH-LZ) region of Myc with Max facilitates binding to DNA. This interaction is key to the general functions of Myc. *In vitro* Myc-Max binds to a specific sequence CACGTG of DNA called enhancer box or E-box (Blackwell et al., 1990; Blackwood & Eisenman, 1991). However, *in vivo* basically all promotors of active genes are bound by Myc (Lin et al., 2012; Nie et al., 2012; Walz et al., 2014), independent of if these promoters are transcribed by RNA polymerase I, II, or III (Gomez-Roman et al., 2006; Gomez-Roman et al., 2003; Grandori et al., 2005). However, how Myc functions as an oncogene and transforms cells is still an open question. Several models have been postulated to explain the function of Myc (Baluapuri et al., 2020).

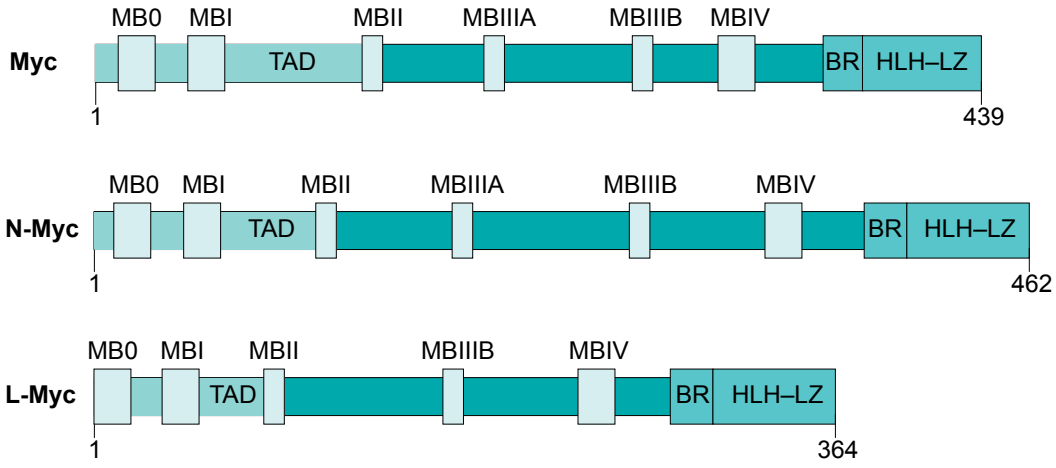

Figure 1.2: Domain structure of Myc protein family.
MYC homology box (MB), transactivation domain (TAD), basic region (BR), and helix-

loop-helix leucine zipper (HLH-LZ). adapted from Lourenco et al., 2021.

1.3.1 Amplifier model

The amplifier model is based on the findings displaying that Myc binds to all active promoters and enhances their transcription and, in this way, “amplifies” already existing gene expression patterns (Lin et al., 2012; Nie et al., 2020; Nie et al., 2012). For example, in the study from Richard Young’s lab, when Myc was overexpressed in Burkitt’s Lymphoma cells by the Tet-Off system, it led to increased binding of Myc to open promoters and enhancer regions and triggered an increase in overall mRNA transcription and levels (Lin et al., 2012). Hence, the model proposes that this increased transcription overrides the barrier to the growth and proliferation of tumor cells in high (oncogenic) levels of Myc.

1.3.2 Specifier model

The specifier model suggests that even though Myc binds to thousands of promoters, it represses and activates only a set of specific genes. Various works performed using genome-wide chromatin immunoprecipitation (ChIP) and RNA sequencing techniques illustrated that only a small subset of Myc-bound genes was regulated upon alteration of Myc level (Sabo et al., 2014; Tesi et al., 2019; Walz et al., 2014). This model assumes that a fraction of promoters are bound by Myc in an unproductive way and thus their transcription output is not altered upon induction of MYC. Thus, the physiological changes due to the oncogenic level of Myc are bestowed by these specific genes.

1.3.3 Affinity model

In the affinity model, Myc target genes are classified into high-affinity and low-affinity target genes. At physiological levels, Myc preferentially binds to and regulates the high-affinity genes, so these genes are regulated when Myc expression is activated when entering the cell cycle. These promoters are not further bound and regulated when Myc levels reach oncogenic concentrations since they are already saturated, whereas it is recruited to the low-affinity genes resulting in oncogenic gene expression patterns (Lorenzin et al., 2016; Zeid et al., 2018). The low-affinity target genes contained a relatively low abundance of E-boxes and were often repressed by Myc (Allevato et al., 2017; Lorenzin et al.,

2016). According to this model, the low-affinity target genes contribute to Myc-driven tumorigenesis.

1.3.4 Target gene-independent model

Inspired by the observation that Myc binds to various promoters without influencing their transcription output, it has been suggested that Myc might also regulate nuclear processes, independent of the direct regulation of transcription activity. In this model, Myc interacts with various proteins and affects the function of many processes like transcription and coordination of transcription-replication conflicts (Baluapuri et al., 2019; Buchel et al., 2017; Cossa et al., 2021; Endres et al., 2021; Herold et al., 2019; Papadopoulos et al., 2022). In rapidly proliferating tumor cells, transcriptional stress and the transcription-replication conflict are incredibly high. Myc, in such circumstances, helps the tumor cells to handle transcription stress, prevents transcription-replication conflict, and maintains genome stability.

All the models mentioned above agree that Myc protein-protein interactions (PPIs) are vital for the function of Myc. The concept of Myc PPIs driving Myc functionality is a consensus in the Myc biology (Lourenco et al., 2021; Wolf & Eilers, 2020). Along similar lines, in a study by Kalkat and colleagues, when Myc mutants consisting of either deletion of MB0 or MBII were expressed in a mouse model, they did not show any transforming characteristics. The Myc oncogenic activity was only restored when both mutants were co-expressed, showing the importance of Myc PPIs for tumorigenesis (Kalkat et al., 2018). Many other studies have reported this essentiality of the interaction of Myc with partner proteins for tumor development and maintenance (Guarnaccia & Tansey, 2018; Nikiforov et al., 2002; Thomas et al., 2019).

Thus, the large protein-protein interface and protein-protein interaction of Myc with its interacting partners are essential for Myc-mediated transformation.

1.4 Targeting Myc via interactors

It is well established that Myc is a potential target for cancer therapeutics (see chapter 1.2). However, inhibiting Myc is challenging as it is not an enzyme, and it does not have an active site or well-defined pockets for compound binding. So, various alternative approach has been implemented to target Myc (Wolf & Eilers,

2020). There are three main approaches: targeting Myc directly, targeting Myc expression, and targeting Myc stability (Wolf & Eilers, 2020). However, none of these strategies have shown breakthroughs therapeutically.

Two strategies have been implemented to target Myc directly, one inhibiting Myc-Max interaction and the other via OmoMyc. Many small molecules have been synthesized to disrupt the Myc-Max interaction, of which 10058-F4 is the best characterized one. In cell culture, 10058-F4 inhibited Myc-Max dimerization and prevented the growth of various cancer cells expressing Myc (Huang et al., 2006; Nie et al., 2012; Wang et al., 2007; Yin et al., 2003). However, some xenograft mouse models were unable to recapitulate the *in cellulo* efficacy due to low stability and rapid clearance (Guo et al., 2009). The other method where OmoMyc is directly administered as therapy is discussed in section 1.2.3.

Next, to target Myc expression, stabilizers of a secondary structure, G-quadruplex, the negative regulatory element in Myc promoter, have been reported (Local et al., 2018; W. Wang et al., 2020). But the G4-stabilizers that reached clinical trials are shown to partially act in a Myc-independent manner (Drygin et al., 2009; Wang et al., 2017; Xu et al., 2017). Similarly, several inhibitors of BET proteins have demonstrated to downregulate Myc transcription (Duffy et al., 2021). Of them, the BRD4 inhibitor, JQ-1 suppressed tumor growth in various mouse models with Myc activation (Delmore et al., 2011; Shao et al., 2014). Nonetheless, some clinical trials based on JQ-1 were discontinued due to toxicity (Postel-Vinay et al., 2019). In the same line, clinical trials with antisense oligonucleotides against *MYC* mRNA were also discontinued (Devi et al., 2005; Kipshidze et al., 2007; Whitfield & Soucek, 2021).

To target the stability of Myc, compounds promoting recognition of Myc by E3-ligases and facilitating binding of Myc by E3-ligases have been developed. The recognition of Myc by E3-ligase FBXW7 requires dephosphorylation of the S62 residue of Myc. This dephosphorylation is carried by PP2A (protein phosphatase 2A. Small molecules increasing the activity of PP2A have been reported to reduce Myc activity (Janghorban et al., 2014). Nonetheless, further studies to investigate the direct role of Myc turnover with such strategies need to be studied.

These results suggest that indirectly targeting Myc expression and interaction with Max might not be viable, and newer approaches are necessary. Since Myc PPIs are essential for Myc's oncogenic function, another way to target Myc is via the

disruption of the large protein-protein interfaces required for these interactions. Nevertheless, this is challenging from a pharmacological point of view. Therefore, the easier alternative approach is to target those Myc-interacting partners directly. Recently, several large-scale proteomic analyses have been performed, revealing many functionally distinct interactors of the Myc proteins.

1.4.1 Myc-interacting proteins

The first extensive study to identify Myc-associated proteins was performed by Koch et al. They fused the open reading frame of *MYC* C-terminally to a tandem affinity purification (TAP) tag. The fusion protein was either transiently expressed in human embryonic kidney cells (HEK293T) or conditionally expressed in a colorectal cancer cell line, DLD1, via the Tet-Off system. After the expression of Myc-TAP, Myc and its complexes were separated from the cell lysate using the TAP tag. Using multidimensional protein identification technology (MudPIT), they could identify 221 proteins associated with Myc compared to the TAP-only control. Surprisingly, these 221 Myc-associated proteins had diverse functions like transcription, RNA processing, DNA repair, protein synthesis, degradation, and metabolism. They also used deletion mutants to show that proteins like SV40 Large T Antigen, MCM7, and DBC-1 interacted with Myc via MBII, whereas FBX29 and Mi22-β required bHLH-LZ region along with MBII for their interaction with Myc. Finally, they reported that Myc was present in various complexes with different molecular weights and compositions (Koch et al., 2007).

Agrawal and colleagues also applied the TAP-MudPIT method with additional approaches to identify Myc interactors. This study used human lung fibroblast cells and predominantly N-terminally TAP-tagged Myc (Agrawal et al., 2010). Notably, three different experimental procedures were used. In the first approach, purification was performed in two steps using the domains of TAP-tag. The second approach was called the label-free approach, where TAP-Myc was directly eluted from IgG beads by low pH. Furthermore, in the final approach, they used SILAC (stable isotope labeling with amino acids in cell culture) labeled cells, and complexes were purified as in the label-free approach. These approaches could identify 418 high-confidence Myc-interacting proteins, 389 of which were apparent novel interactors like Erbin (*ERBB2IP*) and RUNX1.

A thorough study of N-Myc interactome was shown by the study of Büchel et al. using a neuroblastoma cell line, SH-EP. Stable cells expressing hemagglutinin

(HA)-tagged wild-type N-Myc or mutant N-Myc (N-Myc T58A, S63A) were generated. This N-Myc mutant is more stable as it is not recognized by FBXW7 (Otto et al., 2009). The N-Myc complexes were isolated via HA-tag pull-down. They could pull down known interactors of Myc like Max, TRRAP, p400, and Aurora-A, along with subunits of TFIIIC complex, TOP2A, and TOP2B. However, the mutant N-Myc had less affinity towards Aurora-A and some subunits of TFIIIC. This suggested that the phosphorylation of these residues (T58, S62) in N-Myc is vital for interacting with Aurora-A and TFIIIC. Further studies could show that these interactions are vital during the cell cycle, especially in S-phase, and coordinate to prevent transcription-replication conflicts (Buchel et al., 2017).

Heidelberger and colleagues expressed GFP-tagged Myc in human U2OS cells and used GFP trap agarose to purify the Myc complexes from the cellular extracts. They identified 1413 proteins enriched in Myc immunoprecipitates using SILAC-based quantitative mass spectrometry. They found many proteins that were not described to interact with Myc. Among them was Valosin-containing protein (VCP, also known as p97) which was highly enriched. They also showed that the HUWE1-mediated ubiquitylation of Myc was crucial for the interaction. They suggested that VCP helps in the HUWE1-dependent degradation of Myc by dissociating it from the Myc-Max dimer (Heidelberger et al., 2018).

A comprehensive study to analyze the Myc interactome and characterize it according to interaction with the Myc boxes was done by Kalkat et al. This study applied a proximity-dependent labeling method called BioID. This method uses a mutant biotin ligase (BirA*), which labels proteins with biotin when they are in proximity. For this, the wild-type Myc and all six MB deletion mutants (Δ0, ΔI, ΔII, ΔIIIa, ΔIIIb, and ΔIV) were N-terminally tagged with FLAG-BirA* and expressed in engineered HEK293 cells using Dox-inducible system. Upon expression of the Myc constructs and addition of biotin, the proteins in the vicinity of the Myc are labeled by biotin. Finally, mass spectrometry analyzed the cell extract for the biotinylated protein. The study was able to identify 336 interactors for full-length Myc. The MB deletion resulted in a loss of proximal partners from 11% for MBI to 31% for MBIV. For MB0, II, IIIa, and IIIb, the reduction was 28, 13, 13, and 26%, respectively. However, the interactions were not mutually exclusive, as only 54% of the interactors were shown to be dependent on one or more MBs. The notable interactions of Myc were with RNA polymerase-associated proteins by MB0, components of the STAGA complex via MBI and MBIIIa, TRRAP and components

of TIP60 complexes via MBII, transcriptional regulators and spliceosome components via MBIIIb, and components of BRAF-HDAC complex and nucleosome remodelers through MBIV. They also showed that MB0 and MBII are crucial for Myc-mediated transformation (Kalkat et al., 2018).

Finally, a recent study was performed with the expression of HA-tagged Myc in U2OS and T-lymphoma cells. HA-immunoprecipitation followed by label-free quantitative mass spectrometry analysis showed 88 significant Myc interactors. Among them, two uncharacterized Myc-interactors, SPT5 and SPT6, were transcription factors. The group further studied RNA Polymerase II (RNAPII) interactome in the presence and absence of Myc. The binding of SPT5 to RNAPII was significantly attenuated in the absence of Myc. Additional studies showed that Myc transfers SPT5 to RNAPII for productive transcription (Baluapuri et al., 2019). The Myc interactors from all the recent publications are shown in Fig 1.3.

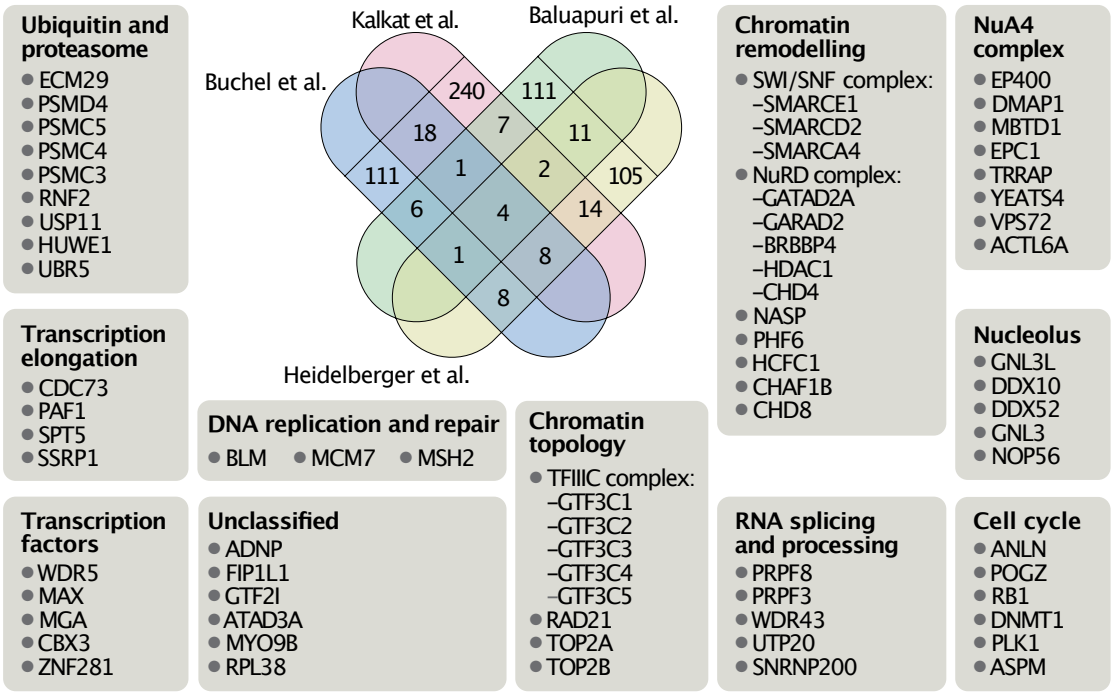

Figure 1.3: Myc-interactors.

Schematic overlap of recently published Myc and N-Myc associated proteins (Baluapuri et al., 2019; Buchel et al., 2017; Heidelberger et al., 2018; Kalkat et al., 2018). Proteins appearing in at least two datasets are functionally categorized and listed. adapted from Baluapuri et al., 2020.

Only few interactions of Myc and N-Myc with their interactors are characterized by crystal structures (Nair & Burley, 2003; Pineda-Lucena et al., 2005; Richards et al., 2016; Thomas et al., 2015; Wei et al., 2019; Welcker et al., 2022). For example, crystal structures have shown that N-Myc binds Aurora-A by its N-terminal region,

flanking MB0 to MBI (Richards et al., 2016) and WDR5 binds MBIIIb (Thomas et al., 2015). Due to the presence of crystal structures, not only their binding location but also their interacting protein-protein interface is known.

The presence of crystal structure with Myc and the link to the oncogenic function of Myc makes both Aurora-A and WDR5 potential candidates for cancer treatment. WDR5 is an adaptor protein and functions non-catalytically, whereas Aurora-A has reported non-catalytic functions (see section1.4.2 and 1.4.3). Even though ligands and inhibitors are available for both, targeting them using the conventional occupancy-driven method might not be optimal. The classical inhibitors do not inhibit all the functions of such multifunctional proteins. Instead, degradation-based approaches like proteolytic targeting chimeras (PROTACs) are ideal, eliminating all the protein functions.

1.4.2 Aurora-A

The aurora kinases are mitotic serine/threonine kinases homologous to the yeast kinase increased-in-ploidy 1 (Inp1). They are evolutionally conserved within eukaryotes (Brown et al., 2004). The human Aurora family consists of three members, namely Aurora-A (*AURKA*), Aurora-B (*AURK*B), and Aurora-C (*AURKC*). They share high amino acid sequence similarities (Fig. 1.4). Structurally, Aurora kinases consist of the N-terminal, kinase, and C-terminal domains. The kinase domain is the catalytic domain of the protein. They also contain degron motifs that are required for the degradation of aurora kinases through the anaphase-promoting complex/cyclosome (APC/C) complex (Castro et al., 2002; Lindon et al., 2015; Min et al., 2013; Stewart & Fang, 2005; Taguchi et al., 2002). Those motifs are KEN motif, destruction box (D-Box, sequence: RxxL), and D-box activating domain/ activation box (DAD/ A-Box, sequence: QRxLxPS) (Bischoff & Plowman, 1999; Castro et al., 2002; Littlepage & Ruderman, 2002).

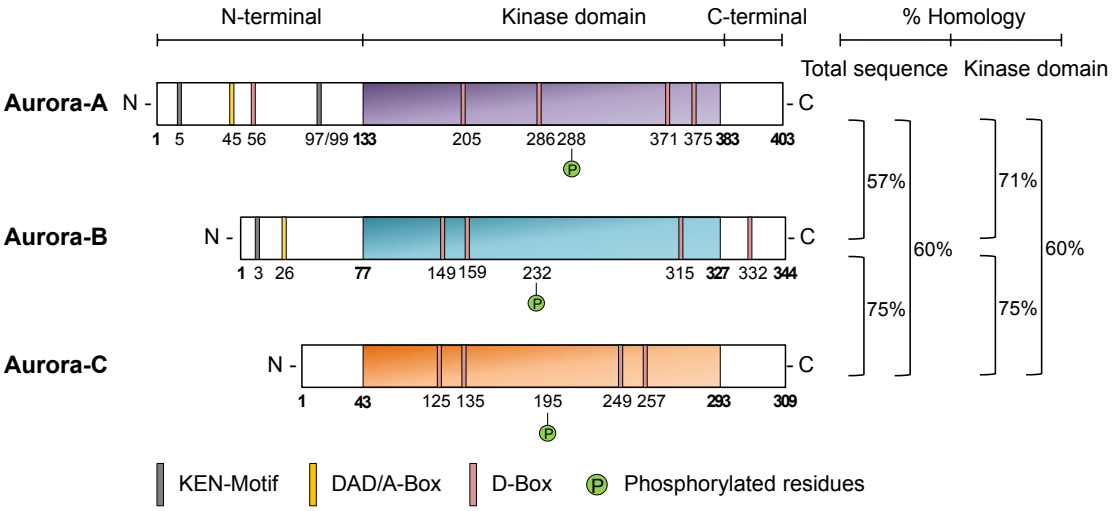

Figure 1.4: Structure of Aurora kinases: Aurora-A, Aurora-B, and Aurora-C.
The N-terminal domain, kinase domain, and C-terminal domain. The Destruction box (D-Box), KEN motif, Activation box (DAD/A-Box,) and the phosphorylated residues are highlighted. Percentage of amino acid sequence homology of the complete sequence and the kinase domain between the three proteins are also shown. adapted from Willems et al., 2018.

Aurora-A and -B are ubiquitously expressed in all human tissues, whereas Aurora-C is confined to germ cells (Carmena et al., 2009; Lin et al., 2006; Tseng et al., 1998). The expression and localization of Aurora kinases change throughout the cell cycle (Kimura et al., 1997; Rannou et al., 2008; Willems et al., 2018). For instance, Aurora-A level remains low during the G1 and early S-phase, increases during S-phase and G2-phase, and peaks in M-phase (Goldenson & Crispino, 2015; Willems et al., 2018). The degradation of Aurora-A starts upon mitotic exit (Barr & Gergely, 2007; Littlepage & Ruderman, 2002). Furthermore, Aurora-A is localized in the spindle throughout mitosis and in the centrosome from late S- and G2-phase (Barr & Gergely, 2007). The Aurora kinases regulate the progression of mitosis from onset to cytokinesis by phosphorylating their numerous substrates (Fu et al., 2007; Hochegger et al., 2013; Tang et al., 2017). The phosphorylation of the specific threonine residues of the kinase domain (T288, Aurora-A; T232, Aurora-B; T195, Aurora-C) via autophosphorylation or binding of co-factors like TPX2 is required for the activity of these kinases (Bayliss et al., 2017; Dodson & Bayliss, 2012; Dodson et al., 2010; Zorba et al., 2014).

1.4.2.1 Aurora-A in cancer

Several studies have demonstrated the upregulation of Aurora-A in various tumors. The chromosomal location of *AURKA*, 20q13.2 is mapped with frequent mutations

and amplifications (Bischoff et al., 1998; Staff et al., 2009; Tanner et al., 2000). The overexpression and mutation of Aurora-A are reported in both hematological and solid tumors, comprising breast cancer (Ali et al., 2012; Treekitkarnmongkol et al., 2016; Yamamoto et al., 2013), colorectal cancer (Bischoff et al., 1998; Casorzo et al., 2015), pancreatic cancer (Li et al., 2003), lung cancer (Chiu et al., 2019; Lo Iacono et al., 2011), leukemia (Ochi et al., 2009), and melanoma (Puig-Butille et al., 2017). Moreover, Aurora-A high expression level is linked to poor prognosis and survival (Guo et al., 2018; Landen et al., 2007; Xu et al., 2013). Aurora-A has been shown to promote tumorigenesis by inhibiting function of tumor suppressors like p53 (Katayama et al., 2004; Liu et al., 2004) and BRCA (Wang et al., 2014; Yang et al., 2010), increasing the stability of other oncogenes like Myc (Brockmann et al., 2013; Dauch et al., 2016; Otto et al., 2009) and FOXM1 (Yang et al., 2019), preventing apoptosis via activation of NF-κB signaling (Briassouli et al., 2007; Chefetz et al., 2011; Yao et al., 2009), and inducing epithelial-mesenchymal transition (EMT) (D'Assoro et al., 2014). Therefore, Aurora-A a is a bona fide oncoprotein and target for cancer therapy.

Various small molecule inhibitors have been produced over the years to inhibit the activity and expression of Aurora-A in tumors (Borisa & Bhatt, 2017; Falchook et al., 2015). Many of them are at various stages of clinical evaluations. However, none has been approved yet. Among them, alisertib (MLN8237) is the most extensively studied inhibitor, which has advanced to phase III of clinical trials (O'Connor et al., 2019; O'Shaughnessy et al., 2021). However, some of the studies in phase II showed low response rates (Beltran et al., 2019; Mosse et al., 2019). These inhibitors' failure to make a significant impact might be because Aurora-A also has several non-catalytic functions, which are challenging to address with the conventional inhibitors, and the potential off-targeting at effective concentrations.

1.4.2.2 Non-catalytic functions of Aurora-A

Over the years, various scaffolding or kinase-independent functions of Aurora-A have been proposed. Aurora-A prevents the FBXW7-mediated degradation of both N-Myc and Myc (Brockmann et al., 2013; Dauch et al., 2016; Otto et al., 2009). Aurora-A binds to Myc and blocks its attachment to and ubiquitylation by the E3-ligase FBXW7. Similarly, Aurora-A stabilizes another oncogene, FOXM1, independently of its kinase activity (Yang et al., 2019). The overexpression of the catalytically-inactive form of Aurora-A induced amplification of centrosome in HeLa

and CHO cells, highlighting the role of non-catalytic activity of Aurora-A (Meraldi et al., 2002). Toya et al. reported the kinase-independent role of Aurora-A in *Caenorhabditis elegans* in the assembly of mitotic spindle microtubules (Toya et al., 2011). They assumed that catalytically inactive Aurora-A was essential for stabilizing both γ-tubulin-dependent and -independent microtubules. Aurora-A is also described to enhance stemness of breast cancer in a kinase-independent manner (Zheng et al., 2016). It does so by transactivation of *MYC* transcription via interaction with heterogeneous nuclear ribonucleoprotein K (hnRNP K). They suggest that cytoplasmic Aurora-A has predominant kinase role, whereas nuclear Aurora-A has kinase-independent role. In a separate study, Almeida and colleagues showed that Aurora-A has non-catalytic functions in interphase, G1/S phase transition, and DNA replication firing (Guarino Almeida et al., 2020). It is also assumed that Aurora-A has distinct sets of interacting partners in kinase-active and -inactive forms, which aid in its diverse role.

Since kinase inhibitors cannot inhibit non-catalytic functions, some allosteric inhibitors like alisertib and CD352, which change the confirmation of the catalytic domain of Aurora-A upon binding, can target some non-kinase activity but to which extent still needs to be studied (Gustafson et al., 2014; Richards et al., 2016). To successfully target Aurora-A in cancer, both the catalytic and non-catalytic functions of Aurora-A need to be disabled. An attractive alternative is the complete degradation of this oncoprotein using targeted protein degradation methods like PROTACs.

1.4.3 WDR5

WD repeat-containing protein 5 (WDR5) is a remarkably well-conserved ubiquitous scaffolding protein. Human WDR5 shares more than 90% sequence similarities across all vertebrates and is identical to that of mice (Schuetz et al., 2006). WDR5 consists of seven WD domain repeats forming a seven-bladed propeller fold, which resembles a donut in structure (Fig. 1.5). It interacts with many different proteins and long non-coding RNAs (lncRNAs) to carry out various chromatin-associated processes. The interaction occurs via its two distinct binding sites: the WDR5 Binding Motif (WBM) site and the WDR5 interacting (Win) site (Fig. 1.5).

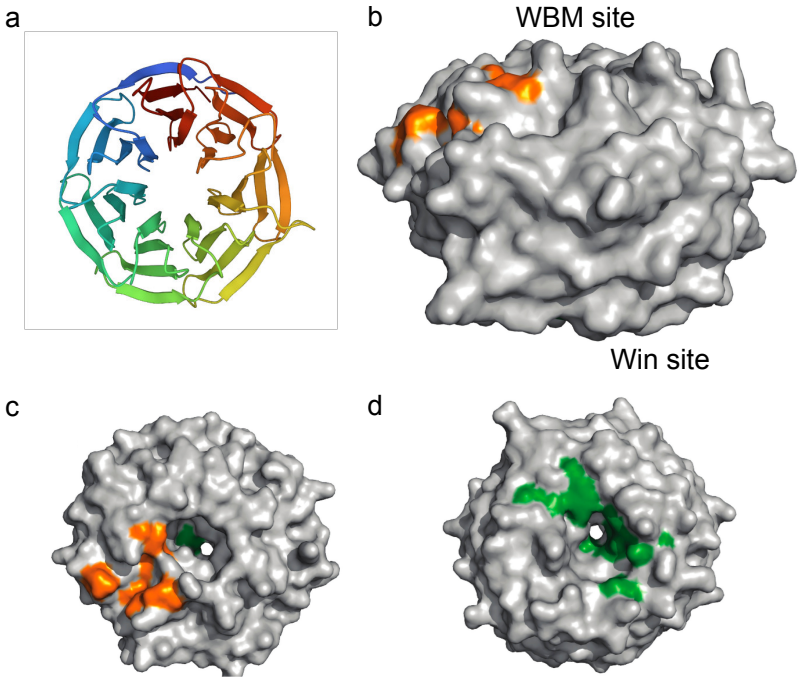

Figure 1.5: Structures of WDR5.
(a) *Cartoon structure of WDR5 showing seven β-propeller blades.* ***(b)*** *Surface structure of WDR5 with WDR5-binding motif (WBM) site and WDR5-interacting (Win) site.* ***(c, d)*** *Top view of (c) WBM site and (d) Win site of WDR5. The regions involved in interaction for each site are highlighted. adapted from Guarnaccia & Tansey, 2018.*

1.4.3.1 WDR5 and its interactors

One of the well-studied interactions of WDR5 is with the SET/MLL family of histone methyltransferases (HMTs). HMT proteins consist of a SET domain that catalytically transfers mono-, di-, and tri-methyl groups to the lysine residues of histones. There are six homologous proteins of HMT found in the humans: MLL1 (*KMT2A*), MLL2 (*KMT2B*), MLL3 (*KMT2C*), MLL4 (*KMT2D*), SETD1A (*KMT2F*) and SETD1B (*KMT2G*). The methyltransferase activity of SET/MLL is facilitated by a multi-protein complex whose core proteins are called the WRAD complex, which comprises WDR5, Retinoblastoma Binding Protein 5 (RBBP5), Absent-Small-Homeotic-2-Like protein (ASH2L), and Dumpy-30 protein (DPY30). WDR5 is the most critical adapter protein in this complex as it binds to SET/MLL via its Win-site and to RBBP5 via its WBM-site (Odho et al., 2010; Patel et al., 2008; Song & Kingston, 2008). Moreover, the binding of WDR5 to the SET/MLL proteins is crucial for methyltransferase activity (Alicea-Velazquez et al., 2016; Dou et al., 2006). The deposition of mono-, di-, and tri-methyl groups on the histone 3 Lysine 4 residue (H3K4) collectively regulates the transcription by acting as gene repression and

activation markers (Cheng et al., 2014; Pekowska et al., 2011; Pinskaya & Morillon, 2009; Soares et al., 2017).

Apart from HMT, WDR5 is found in the histone acetyltransferase (HAT) complex, non-specific lethal (NSL) (Cai et al., 2010; Dias et al., 2014). In the NSL complex, WDR5 binds the two core components: KAT8 regulatory NSL complex subunit-1 (*KANSL1*) and -2 (*KANSL2*) via its Win- and WBM-sites, respectively (Dias et al., 2014). In addition, studies have shown that the NSL complex promotes the activity of the SET/MLL complex (Zhao et al., 2013). As WDR5 is present in both complexes, it can be assumed that WDR5 might coordinate the histone acetylation and methylation by these two complexes. Furthermore, WDR5 is present in another HAT complex, the Ada2-containing (ATAC) complex (Guelman et al., 2009; Wang et al., 2008).

Moreover, WDR5 is associated with nucleosome remodeling and deacetylase (NuRD) complex. One subunit of NuRD, methyl-CpG binding domain protein 3 isoform C (MBD3C), which is expressed in embryonic stem cells (ESCs), interacts with WDR5 via the Win-site (Bode et al., 2016; Ee et al., 2017). WDR5 is vital for the function of this ESC-specific NuRD complex (Ee et al., 2017). Likewise, WDR5 directly interacts with histone deacetylase 3 (HDAC3) and regulates EMT during hypoxia (Wu et al., 2011).

Notably, WDR5 binds to all Myc family proteins via its WBM-site (Sun et al., 2015; Thomas et al., 2015). WDR5 is crucial for Myc binding to its target genes (Thomas et al., 2015). Mutations in Myc that disrupts the interaction with WDR5, but not the Myc-Max interaction, decreased binding of Myc to most target sites on chromatin (Thomas et al., 2015). A similar observation was made in neuroblastoma cells, where N-Myc binding to WDR5 was essential (Sun et al., 2015).

Besides these interactors, a SILAC-based mass spectrometry approach in the presence of the Win-site inhibitor, C6 has revealed many new Win-site interaction partners. The WDR5 Win-site-associated proteins ranged from proteins with tRNA ligase activity to proteins functioning in phosphatidyl inositol pathways. One of the interacting proteins was phosphoinositide-dependent protein kinase 1 (PDPK1), and the interaction of WDR5-PDPK1 was shown to regulate the expression of genes in the cell cycle phase G2 (Guarnaccia et al., 2021).

Moreover, WDR5 binds to lncRNAs HOTTIP (Liu et al., 2020; Wang et al., 2011), ANRIL (Zhang et al., 2020), NeST (Gomez et al., 2013) and GCAWKR (Ma et al., 2018). A study using chromatin RNA immunoprecipitation (ChRIP) in a breast

cancer cell line showed that more than 800 lncRNAs bind to WDR5, which are required to maintain transcriptionally efficient chromatin (Subhash et al., 2018). Similarly, another study illustrated that WDR5 binds over 1000 RNAs (~ 200 lncRNAs) in mouse ESCs and activates genes required for the maintenance of stem cell state (Yang et al., 2014). The binding to RNA increased the WDR5 protein stability.

1.4.3.2 WDR5 in cancer

WDR5 is over-expressed in various cancers, like leukemia (Ge et al., 2016), bladder cancer (Chen et al., 2015), prostate cancer (Zhou et al., 2021), breast cancer (Dai et al., 2015), lung cancer (Ji et al., 2021), gastric cancer (W. Sun et al., 2018), liver (Cui et al., 2018), colon cancer (Neilsen et al., 2018), and head and neck cancer (Wu et al., 2018). WDR5 overexpression correlates with poor prognosis and survival (Chen et al., 2015; Cui et al., 2018; Dai et al., 2015; Huang et al., 2020). WDR5 plays a critical role in the tumorigenesis of MLL-rearranged cancers, characterized by the translocation of the *MLL* gene to the chromosomal location of many partner genes resulting in the expression of MLL-fusion oncoproteins (Gole & Wiesmuller, 2015; Harper & Aplan, 2008). Indeed, inhibitors that target the interaction of MLL-WDR5 have been effective in preventing the proliferation of MLL-rearranged human cell lines and primary cells (Aho et al., 2019; Cao et al., 2014). The inhibition decreased the expression of genes required for leukemogenesis like, Hoxa9 and Myc, and increased p53-mediated dell death. Similarly, the WDR5 Win-site antagonist OICR-9429 has been reported to be successful in targeting CEBPA-mutant human cell lines (Grebien et al., 2015). Punzi et al. demonstrated that WDR5 induces metastasis in breast cancer by induction of EMT genes. OICR-9429 addition significantly reduced cell viability and migration of breast cancer cell lines. The inhibition even successfully sensitized the cells to chemotherapy (Punzi et al., 2019).

Moreover, Myc-WDR5 interaction is necessary for Myc-driven tumorigenesis and tumor maintenance (Thomas et al., 2019; Thomas et al., 2015). In a separate study, a small molecule that inhibits the binding of WDR5 to chromatin or depletion of WDR5 inhibited the proliferation of various N-Myc amplified cancer cell lines (Bryan et al., 2020). Furthermore, the WDR5-Myc interaction shields PDAC cells from DNA damage and replicative stress and supports their proliferation (Carugo et al., 2016). Recently, WDR5-Myc interaction inhibitors have also been discovered

using a fragment-based approach. However, their therapeutic efficacy still needs to be tested (Chacon Simon et al., 2020; Macdonald et al., 2019).

These observations suggest that WDR5 is a promising drug target in cancer therapy. The Win-site inhibitors have shown a promising result, however, it might not be optimal to target WDR5 with PPI inhibitors as it will not be sufficient to block all the oncogenic functions of WDR5. In a study by Siladi et al. in Burkitt's lymphoma cell line, when WDR5 degradation by auxin-inducible degron (AID) system was compared to WDR5 Win-site inhibition by inhibitor C6, inhibition caused only a small portion of WDR5-mediated transcriptome changes than that caused by degradation (Siladi et al., 2022). A similar observation was made in another study where WDR5 inhibition by C6 and depletion by degradation tag (dTAG, $FKBP12^{F36V}$) were carried out in the N-Myc amplified neuroblastoma cell line CHP134 (Bryan et al., 2020). Hence, the ideal way to target the multifunctional adapter protein WDR5 is via a targeted protein degradation approach.

1.5 Targeted protein degradation as a new therapeutic modality

Over the last decades, we understood many processes on oncogenesis, but significant oncogenic drivers are still difficult to target. Most pharmaceutical drugs are directed against enzymes that are easy to inhibit and receptors that are easily accessible (Fig 1.6a) (Ursu et al., 2017). This leaves many proteins currently undruggable or difficult to drug, like proteins functioning by protein-protein interaction, such as transcription factors and adaptor proteins, which comprise the majority of all cellular proteins (Ni et al., 2019). On the other hand, more than three-fourths of multifunctional proteins found in humans are associated with human diseases, and half of these proteins are the target of current drugs (Fig 1.6b) (Franco-Serrano et al., 2018). Remarkably, both the moonlighting and canonical functions of 50% of these proteins are associated with the disease (Franco-Serrano et al., 2018), implying that conventional inhibitors cannot inhibit their complete disease-related function. The solution is the targeted protein degradation (TPD) approach which eliminates the target, thereby abolishing all of its potential functions. TPD hijacks the pathways of protein homeostasis to target the protein of interest (POI).

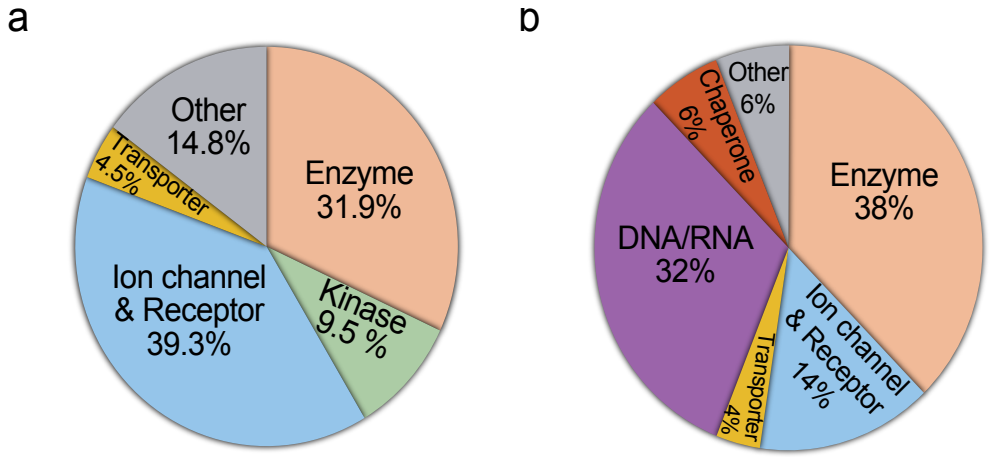

Figure 1.6: Distribution of drugs and targets.
(a) *Distribution of FDA-approved drugs by their targets. Data from DrugCentral 2021 (Ursu et al., 2017).* ***(b)*** *Distribution of the moonlighting proteins that are classified as drug-targets. adapted from Franco-Serrano et al., 2018.*

1.5.1 Targeted protein degradation strategies

Protein homeostasis is maintained by a delicate balance between protein synthesis, folding, transport, assembly, and clearance (Sala et al., 2017). Ubiquitin proteasome system (UPS) and autophagy-lysosome pathway (ALP) are the two notable pathways of protein clearance or degradation in eukaryotes (Dikic, 2017; Ursu et al., 2017). Various TPD approaches exploit these two protein degradation pathways.

1.5.1.1 TPD via the ubiquitin-proteasome system

The ubiquitin-proteasome machinery degrades normal short-lived, soluble misfolded, and damaged proteins (Hershko & Ciechanover, 1998; Hochstrasser, 1995). The UPS comprises a cascade for the ubiquitination of the proteins and the proteasome, which eventually degrades the ubiquitinated proteins (see section 1.5.2). The widely used targeted protein degradation approach by PROTACs and molecular glues depend on this system. Both PROTACs and molecular glues utilize molecules that bring the ubiquitinating apparatus into the vicinity of the protein of interest, thereby tagging the protein of interest with ubiquitin. The ubiquitin-tagged protein is later shuttled to the proteasome and degraded. PROTACs are described in detail in section 1.5.3.

Stuart Schreiber coined the term molecular glue for natural compounds like FK506, cyclosporin-a, and rapamycin (Liu et al., 1991; Michnick et al., 1991; Schreiber,

1992). These compounds bind one protein and stick it to another, forming a ternary complex. Decades after the application of the immunomodulatory drugs (IMiDs), thalidomide and its analogs, their mechanism of action was unearthed. It was found that they bind the E3-ligase, Cereblon (CRBN) and recruit neosubstrates like transcription factors, Ikaros (IKZF1) and Aiolos (IKZF3), thereby acting as a molecular glue (Ito et al., 2010). Since then, various labs have invested their efforts in using the property of molecular glue to guide and degrade protein of interest by inducing interaction with the E3-ubiquitin ligase complex. So far, Cyclin K (Mayor-Ruiz et al., 2020; Slabicki, Kozicka, et al., 2020), RBM39 (Han et al., 2017; Ting et al., 2019), RBM23 (Ting et al., 2019), β-catenin (Simonetta et al., 2019), and BCL6 (Kerres et al., 2017; Slabicki, Yoon, et al., 2020), have been successfully degraded using molecular glue. Molecular glues being monovalent are smaller than bivalent compounds like PROTACs, which can increase their oral bioavailability. However, their design is challenging, with only slight progress made in rational design.

Hydrophobic tagging (HyT) is another strategy that exploits the UPS/chaperone-mediated proteasomal degradation of POI. In this approach, hydrophobic tags, like the adamantyl group, are attached to the ligand of the POI. Upon binding to a protein, it mimics a partially unfolded protein, thus activating the UPS- or chaperone-mediated degradation (Choi et al., 2021; Gao et al., 2017; Gustafson et al., 2015; Ma et al., 2020; Xie et al., 2014). However, the exact mechanism of the HyT-mediated degradation, the bioavailability, and the efficacy of this approach still needs to be investigated.

1.5.1.2 TPD via the autophagy-lysosome pathway

The autophagy-lysosome pathway degrades organelles, unfolded proteins, insoluble aggregated proteins, long-lived proteins, bacteria, and viruses to retain cellular homeostasis (De Duve & Wattiaux, 1966; Kocaturk & Gozuacik, 2018). There are three autophagy pathways: micro-autophagy, macro-autophagy, and chaperone-mediated autophagy (CMA). Macro-autophagy involves merging of the autophagosome containing materials to be degraded and the lysosome. In micro-autophagy and CMA, the materials are directly taken up by the lysosome (Yim & Mizushima, 2020). The ALP-based degradation utilizes the proteins of the macro-autophagy and CMA pathway as harness in a targeted approach (Zhao et al., 2022).

Autophagosome-tethering compounds (ATTECs) bind the POI to autophagosome via Microtubule-associated *protein light chain 3 (*LC3), and by this designate POI for the degradation by lysosome. This approach was used to degrade mutant huntingtin protein in primary cells from Huntington's disease patients (Li et al., 2019) and lipid droplets in hepatic lipidosis mouse model (Fu et al., 2021). Autophagy targeting chimera (AUTAC) uses a cGMP-based degradation tag linked to a ligand for POI via a linker. The AUTAC upon binding induces ubiquitination of the target protein and eventually degradation via the lysosome (Takahashi et al., 2019). Takashaki et al. used this methodology to degrade methionine aminopeptidase 2 (MetAP2), 12-kDa FK506-binding protein (FKBP12), and dysfunctional mitochondria. Like ATTEC, AUTOphagy-TArgeting Chimera (AUTOTAC) brings the POI to the autophagosome by facilitating its binding to p62, a receptor of autophagy (Ji et al., 2022). Ji and colleagues demonstrated AUTOTAC-mediated degradation of METAP2 in glioblastoma, estrogen receptor β (ERβ) in breast carcinoma, androgen receptor (AR) in prostate carcinoma, and aggregation-prone tau in neuroblastoma cell lines. Moreover, Lysosomal-Targeting Chimeras (LYTACs) were utilized to degrade membrane-associated and extracellular proteins, which are not accessible by UPS (Ahn et al., 2021; Banik et al., 2020). New emerging technologies, namely, CMA-based degrader (Fan et al., 2014), bispecific-aptamer chimera (Miao et al., 2021), antibody-based PROTACs (AbTAC) (Cotton et al., 2021), and GlueTAC (Zhang et al., 2021) also employ ALP-based targeted degradation.

The autophagy-lysosome-mediated degradation of proteins is a promising strategy to degrade insoluble aggregated protein and extracellular proteins, which can overcome the limitations of UPS-based degradation. However, these are only proof-of-principle studies. Comprehensive applications and thorough understanding of these strategies need to be further explored

1.5.2 Ubiquitin-proteasome system

The UPS is the major pathway to govern protein quality in cells which is crucial for cell survival **(**Hershko & Ciechanover**,** 1998**)**. Ubiquitin mediated proteolysis pathway was discovered by Aaron Ciechanover, Avram Hershko, and Irwin Rose. In 2004 they were awarded Nobel Prize in Chemistry for their discovery. The UPS pathway consists of two distinct parts. First, linking of 76 amino acids containing

peptide, ubiquitin (Ub) to the protein, and second, the degradation of the Ub-tagged protein (Fig. 1.7).

The addition of Ub to a target protein is a well-regulated cascade executed by three sets of enzymes: the ubiquitin-activating enzyme (E1), the ubiquitin-conjugating enzyme (E2), and ubiquitin-protein ligase (E3). The carboxy-terminal of Ub is firstly activated in an ATP-dependent manner and covalently attached to the cysteine residue of the E1 by a thioester bond. Second, the Ub is transferred from E1 to E2 through a *trans*-thiolation reaction. Third, the Ub is linked by an amide bond to the lysine residue of the target protein, which is facilitated by E3 (Glickman & Ciechanover, 2002; Hershko & Ciechanover, 1998). The cycle is repeated several times to form a polyubiquitination chain, where the previously attached Ub acts as the receptor for the next Ub. Polyubiquitin chains can be linked through seven different lysine residues in Ub (K6, K11, K27, K29, K33, K48, and K63) (Tracz & Bialek, 2021). On the one hand, the E2 plays a major role in regulating the type of ubiquitin chain made (Stewart et al., 2016; Ye & Rape, 2009). The type of linkage of the ubiquitin chain determines the fate of the protein. Only distinct polyubiquitin chains, like K48, lead to proteasomal degradation, whereas the ubiquitination involved in subcellular localization is known to have a non-proteolytic function (Chen & Sun, 2009). On the other hand, E3 provides specificity toward the substrate proteins (Zheng & Shabek, 2017). Fourth, the Ub-tagged protein is degraded by 26S proteasome in an ATP-dependent manner. The substrate is degraded into small peptides, whereas ubiquitin is recycled (Fig. 1.7) (Hershko & Ciechanover, 1998).

For this complex process of protein degradation, the human genome encodes two E1s, 30-50 E2s, and more than 600 E3s (George et al., 2018). TPD approach particularly hijacks the E3 ligases to recruit UPS for degradation of the POI.

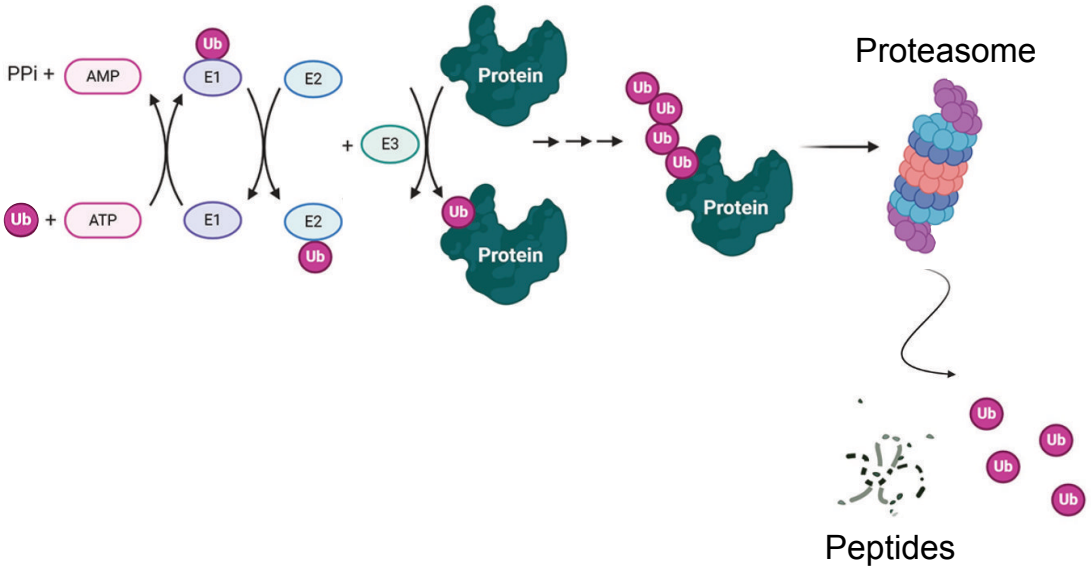

Figure 1.7: Schematic representation of Ubiquitin Proteasome System (UPS). *adapted from Scholz et al., 2020.*

1.5.3 PROTACs

1.5.3.1 Principle of PROTACs

PROTACs are small bifunctional molecules with two ligands bound together by a linker. One ligand binds to the target protein and the other binds to the E3-ubiquitin ligase, thereby bringing the target protein into vicinity of the E3-ligase to form a ternary complex. This induced proximity results in the ubiquitination of the POI by the E3-ligase followed by proteasomal degradation of the POI (Fig. 1.8) (Sakamoto et al., 2001; Schneekloth et al., 2008).

The first proof-of-concept PROTAC was peptidic and developed by the groups of Crews and Deshaies in the early 2000s (Sakamoto et al., 2001). In the study, they harnessed the Ub-ligase complex, Skp1-Cullin-F box (SCF), to degrade MetAP2 using a bivalent molecule consisting of the IκBα peptide (recognized by F-box protein) linked to ovalicin (binds MetAP2). A similar approach with IκBα peptide was used to show the degradation of estrogen and androgen receptors (Sakamoto et al., 2003). However, the first small-molecule PROTAC was developed in 2008 (Schneekloth et al., 2008). Nutlin, a ligand for the E3-ligase, MDM2, was connected to an androgen receptor ligand with a polyethylene glycol (PEG)- based linker to create the first PROTAC. Since then, many PROTACs have been developed for various targets.

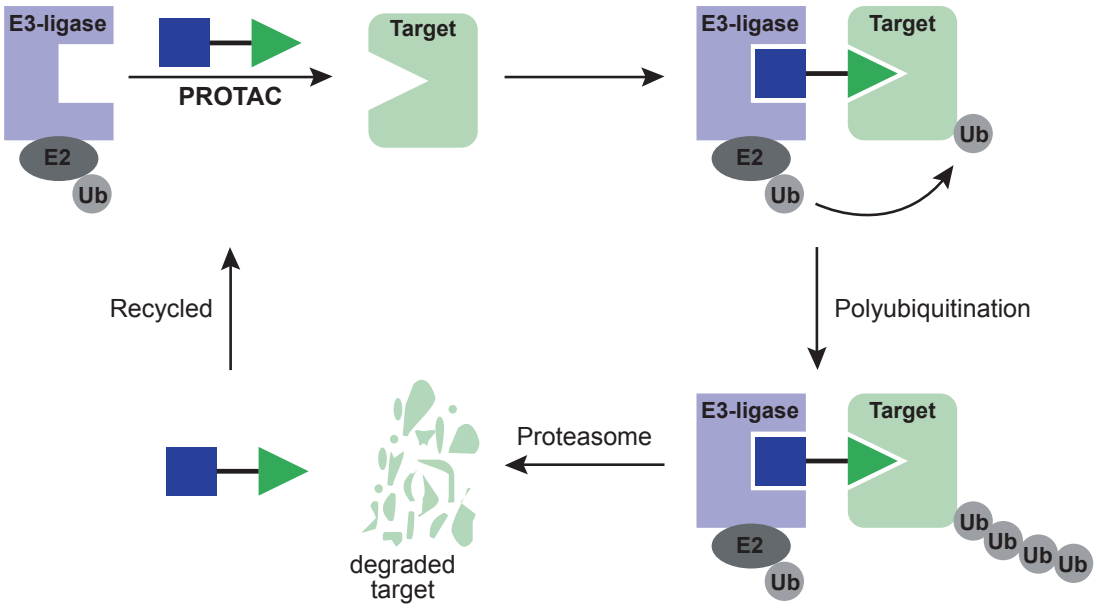

Figure 1.8: The mechanism of action of PROTACs.
adapted from Adhikari et al., 2020.

1.5.3.2 Advantages and disadvantages of PROTACs

This new modality offers a wide range of advantages over classical small molecule inhibitors. First, the conventional inhibitors are pharmacokinetically occupancy-driven, whereas PROTACs are event-driven. Conventional inhibitors require high-affinity binding to the active or allosteric site of the proteins to inhibit their function. On the contrary, PROTACs mediate transient ternary complex formation to induce ubiquitination and, thereby, degradation of the target. Therefore, this approach is viable to target the so far undruggable or difficult-to-target proteins, as a low-affinity ligand or a binder is sufficient to develop a degrader (Bond & Crews, 2021). Using this approach, the previously considered undruggable protein signal transducer and activator of transcription 3 (STAT3) has been targeted (Bai et al., 2019). Second, considering PROTACs degrade the whole protein, it overcomes the limit of traditional inhibitors in targeting proteins with multiple (moonlighting or scaffolding) functions. While inhibitors can only prevent one part of the function, PROTACs get rid of all the functions at once. PROTAC-induced degradation of kinases with scaffolding functions like BCR-ABL1 (Burslem et al., 2019), Fak (Cromm et al., 2018), FLT3 (Burslem, Song, et al., 2018), PARP1 (Wang et al., 2019), and RTK (Burslem, Smith, et al., 2018), have verified this benefit. Third, the catalytic mode of action of PROTACs (Fig. 1.8) enables low doses to achieve therapeutic efficacy, which reduces possible toxicity (Bondeson et al., 2015; Toure

& Crews, 2016). Fourth, inhibition of proteins is often associated with drug resistance, whereas PROTACs can eliminate resistance caused by target overexpression or target mutation (Burke et al., 2022; He et al., 2021). Resistance against inhibitors arises due to mutation in the target that hinders the effective binding of the small molecule. However, as PROTACs are effective with transient and low-affinity binding to the target, such mutation does not render resistance. For example, the ibrutinib-resistant BTK mutant was degraded by ibrutinib-based PROTACs (Buhimschi et al., 2018; B. Sun et al., 2018). Fifth, PROTACs offer high target selectivity to promiscuous inhibitors. PROTACs synthesized from a pan-inhibitor that binds many targets have shown selective degradation of targets (Bondeson et al., 2018). All these arguments highlight the superiority of this rising therapeutic modality.

However, PROTAC technology also has some limitations and challenges. PROTACs have a larger molecular size than inhibitors and thus sub-optimal pharmacological properties, resulting in limited oral bioavailability. Even though PROTACs can overcome the resistance in the target protein, there are additional resistance mechanisms compared to inhibitors. The UPS machinery consists of many non-essential proteins, which can be targeted by tumor cells to develop resistance against PROTACs (Hughes et al., 2021). A recent study by Ruiz et al. identified that changes in cullin-RING ligases (CRLs) components could drive resistance against PROTACs (Mayor-Ruiz et al., 2019). Moreover, although more than 600 E3-ligases are expressed in humans, only a handful of them, like CRBN, VHL, and MDM2 has been overly utilized for PROTAC development so far. Those E3-ligases are commonly expressed in all tissue types or are non-essential for the tumor tissue or both. In the first scenario, the PROTAC can also degrade the target in the healthy tissue causing unwanted side effects. In the second scenario, the tumor tissue can quickly develop resistance against the PROTAC by altering the E3-machinery, causing the failure of the degrader molecules (Scholes et al., 2021; Shirasaki et al., 2021; L. Zhang et al., 2019). Thus, there is a need to identify tissue-specific E3-ligases and to develop ligands for additional E3-ligases to expand the repertoire of this technology.

Also, most of the current degrader synthesis approach is hit and trial based. Generally, a series of degraders are synthesized using a combination of warheads for different E3-ligases, various linkers, and a few target ligands. However, even

synthesizing numerous degraders with this approach does not guarantee that the PROTAC will successfully degrade the target. The reasons for the high failure rate of such approach are due to the expression of E3-ligase and target in the different cellular compartments, incompatibility of the target/ E3-ligase, absence of Lysine residue on the target surface in the vicinity of the E3-ligase, and simply no K48 activity of the E3-ligase (Chen & Sun, 2009). In addition, the type of ubiquitin chains added by many E3-ligases is still unknown. Moreover, studies have shown that only certain E3-ligases are more suitable than others to degrade specific target proteins. It is also validated by the fact that protein-protein interactions (PPI) between the E3-ligase and the target critically support the PROTAC-induced ternary complex formation (Maniaci & Ciulli, 2019). So, the presence of an assay to predict the degradability of the target by the E3-ligase before starting the laborious and expensive process of PROTAC synthesis would be advantageous.

1.5.3.3 Recent developments in PROTACs

Since the development of the first small-molecule PROTAC in 2008, the PROTAC technology has made major advances. Fig. 1.9 shows the timeline highlighting the important events within this technology. Crews and Ciulli groups designed the first small molecule inhibitors of the E3-ligase, VHL (Buckley, Gustafson, et al., 2012; Buckley, Van Molle, et al., 2012). This led to the development of VHL-based PROTACs against BRD4, RIPK2, and ERRα (Bondeson et al., 2015; Zengerle et al., 2015). After identifying CRBN as a target for thalidomide and its derivative (Ito et al., 2010), efforts were made to develop PROTACs recruiting CRBN. In 2015, Bradner and Crews lab separately reported the CRBN-based PROTACs degrading BRD2/3/4 and FKBP12 (Winter et al., 2015), and BRD4 (Lu et al., 2015), respectively. Henceforth, various derivatives of ligands for CRBN and VHL have been developed and used to target numerous proteins. Besides CRBN and VHL, PROTACs harnessing E3-ligases MDM2, IAP, DCAF15, DCAF16, RNF4, RNF114, and KEAP1 have also been published (Ishida & Ciulli, 2021).

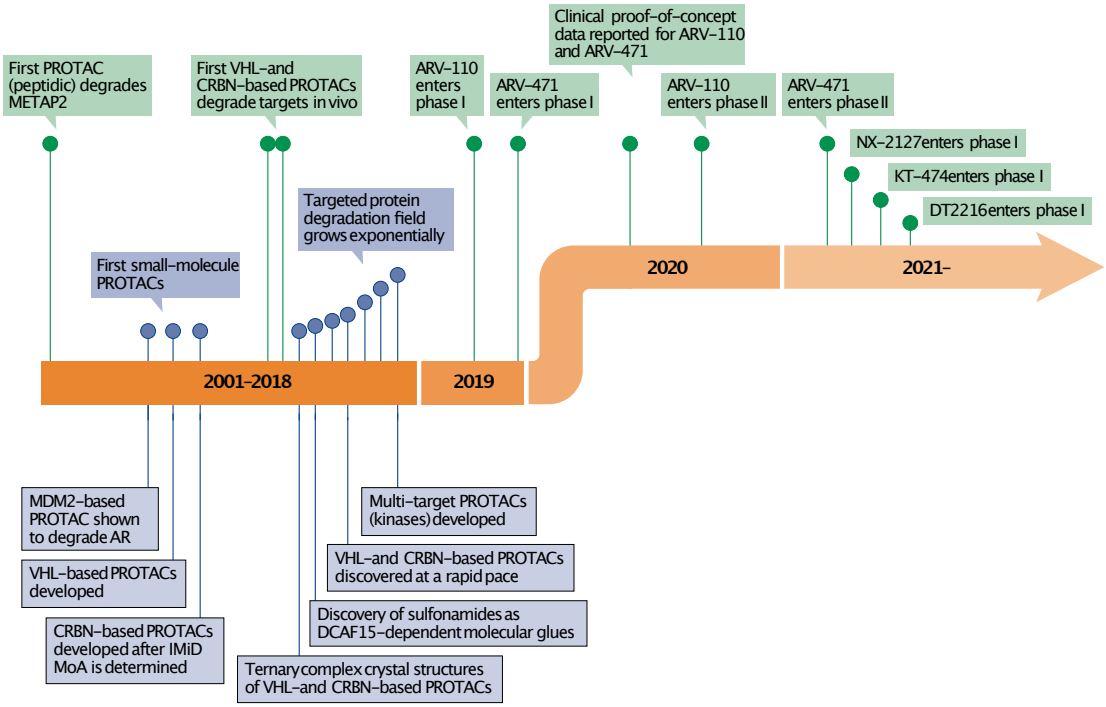

Figure 1.9: The timeline of PROTAC development.
adapted from Bekes et al., 2022.

The first crystal structure of a ternary complex consisting of VHL: MZ1: $BRD4^{BD2}$ was solved by the Ciulli group (Gadd et al., 2017). The structure has highlighted the importance of cooperativity in ternary complex formation and the need for structure-based PROTAC design to selectively degrade the target (Ahn et al., 2021; Farnaby et al., 2019). The breakthrough in the PROTAC field came in 2019 when two degraders from Arvinas, ARV-110, and ARV-471, targeting AR and ER, respectively entered phase I clinical trials. Both PROTACs are now in phase II trials and showing promising results (Gao et al., 2022; E. Hamilton et al., 2022; E. P. Hamilton et al., 2022). Currently, there are ten more PROTACs in phase I clinical trials targeting ER, AR, BCL-XL, BRD9, IRAK4, STAT3, and BTK (Bekes et al., 2022).

1.6 Aim of the thesis

Despite being deregulated in most human cancers, targeting oncoprotein Myc has been challenging due to its structure. So, various alternative approaches have been suggested to target Myc indirectly. One of them is targeting Myc via its interactors. Many Myc binding partners have reported scaffolding functions, indicating that degradation approach would be effective in targeting such proteins.

PROTAC-mediated targeted protein degradation has emerged as a new therapeutic modality in recent years. PROTACs utilize the UPS machinery and destroy the target protein, thereby eliminating all its functions, which were not achievable by conventional occupancy-driven inhibitors. Even though PROTACs are fascinating tools, the lack of a method to analyze the compatibility of E3-ligase and the target protein has impacted their design and synthesis processes.

One of the aims of this thesis was to explore the PROTAC approach to target two Myc-interacting oncogenic partners, Aurora-A and WDR5, and investigate the cellular consequences of their degradation. Another aim was to establish a system to predict the E3-ligases that can successfully induce target degradation.

2 Materials

2.1 Cell lines and bacteria strains

2.1.1 Cell lines

Cell line	Specification	Source
HEK293	Human embryonic kidney cell line, adherent, female	ATCC
HeLa	Human cervical carcinoma cell line, adherent, female	ATCC
HL-60	Human acute promyelocytic leukemia cell line, suspension, female	Schick Lab
HLE	Human hepatocellular carcinoma cell line, adherent, male	Eilers Lab
IMR5	Human neuroblastoma cell line, adherent, male	Eilers Lab
LS174T	Human colorectal carcinoma cell line, adherent, female	Eilers Lab
MCF7	Human breast carcinoma cell line, adherent, female	Eilers Lab
MV4-11	Human acute myeloid leukemia cell line, suspension, male	Eilers Lab
NCI-H1299	Human non-small cell lung cancer cell line, adherent, male	Diefenbacher Lab
NCI-H23	Human non-small cell lung cancer cell line, adherent, male	Diefenbacher Lab
NGP	Human neuroblastoma cell line, adherent, male	Eilers Lab
Sk-Mes-1	Human non-small cell lung cancer cell line, adherent, male	Diefenbacher Lab

SW620	Human colorectal carcinoma cell line, adherent, male	ATCC
U2OS	Human osteosarcoma cell line, adherent, female	ATCC

2.1.2 Bacterial strains

XL1 blue	*Escherichia coli*, genotype recA1 endA1 gyrA96 thi- 1hsdR17 supE44 relA1 lac [F´ proAB laclqZΔM15 Tn10 (Tetr)]

2.2 Cultivation media and supplements

2.2.1 Mammalian cell culture media

Name	Purpose	Composition
Culture media	Cell line propagation	DMEM or RPMI 1640 (Thermo Fisher Scientific) 10% (v/v) Fetal bovine serum (FBS; Capricorn Scientific GmbH) 1% (v/v) penicillin/streptomycin (Sigma)
SILAC media	SILAC mass spectrometry	RPMI-1640 Medium for SILAC (Thermo Fisher Scientific) 50 mg labeled or unlabeled Lysine 50 mg labeled or unlabeled Arginine 100 mg unlabeled Proline 10% (v/v) dialyzed FBS 1% (v/v) penicillin/streptomycin (Sigma)
Transfection media	Cell transfection	DMEM or RPMI-1640 2% (v/v) FBS
Freezing medium	Cell storage	50% (v/v) FBS 40% (v/v) Culture medium 10% (v/v) DMSO

2.2.2 Supplements for mammalian cell culture

Compound	Final concentration	Source
Alisertib (MLN8237)	0.1 – 1 µM	Absource Diagnostics / Selleckchem
Bromodeoxyuridine (BrdU)	10 µM	Sigma
Cycloheximide	10 – 50 µg/ml	Sigma
Doxycycline	1 µg/ml	Sigma
Hygromycin	100 – 200 µg/ml	InvivoGen
L-Arginine monohydrochloride	100 mg/l	Sigma
L-ARGININE:HCL (13C6, 15N4)	100 mg/l	Cambridge Isotope
L-ARGININE:HCL (13C6)	100 mg/l	Cambridge Isotope
L-Lysine monohydrochloride	100 mg/l	Sigma
L-Lysine-2HCl, 4,4,5,5-D4 for SILAC	100 mg/l	Thermo Fischer Scientific
L-LYSINE:2HCL (13C6; 15N2)	100 mg/l	Cambridge Isotope
L-Proline	200 mg/l	Sigma
MG132	10 µM	Calbiochem / Merck
Pevonedistat (MLN4924)	3 – 5 µM	Selleckchem / Biozol
Pomalidomide	1 – 10 µM	Selleckchem / Biozol
Puromycin	1 – 10 µg/ml	InvivoGen
Rapamycin	10 – 500 nM	Biozol
Thalidomide	1 – 20 µM	Cayman / Biomol
VHL-ligand	10 µM	Cayman / Biomol

2.2.3 Bacterial culture media

Name	Composition
LB Medium	10% (w/v) Bacto tryptone (Roth) 0.5% (w/v) yeast extract (Roth) 1% (w/v) NaCl (Roth)
LB agar	LB-medium with 1.2% (w/v) agar-agar (Roth);

	Autoclaved and cooled before addition of antibiotics

2.2.4 Supplements for bacterial culture media

Compound	Final concentration	Source
Ampicillin	100 µg/ml	Roth
Carbenicillin	100 µg/ml	Roth
Kanamycin	30 µg/ml	Roth

2.3 Buffers and solutions

If not stated otherwise all the buffers and solutions were prepared in ddH_2O.

Name	Composition	Storage
Ammonium persulfate (APS, 10 %)	5 g APS dissolved in 50 ml ddH_2O aliquoted	-20 °C
Annexin V binding buffer	10 mM HEPES, pH 7.4 140 mM NaCl 2.5 mM $CaCl_2$	4 °C
BCA solution A	1 % (w/v) BCA-Na_2 2 % (w/v) Na_2CO_3	4 °C / RT
BCA solution B	4% (w/v) $CuSO_4$	RT
Bis-Tris (3.5 x)	1.25 M Bis-Tris	4 °C
Bis-Tris stacking gel	1 x Bis-Tris 0.03 % (v/v) APS 0.05 % (v/v) TEMED	4 °C
Bis-Tris separation gel	8-12 % (v/v) acrylamide / bisacrylamide 1 x Bis-Tris 0.03 % (v/v) APS 0.05 % (v/v) TEMED	4 °C
Blocking solution for PVDF membranes (Fuji)	5 % (w/v) non-fat dry milk in TBS-T; sterile filtered	-20 °C
BSA/ PBS	0.5 % (w/v) BSA in PBS; sterile filtered	4 °C
Crystal violet solution	0.5 % (w/v) crystal violet 20 % (v/v) ethanol	RT

dNTPs mix stock (10 mM)	20 µl each dNTP (100 mM) mixed with 120 ddH_2O	-20 °C
DNA loading buffer (6 x)	10 mM EDTA, pH 8.0 0.2 % (w/v) Orange G 40 % (w/v) sucrose	-20 °C
Doxycycline stock (1 mg/ml)	50 mg doxycycline in 50 ml ethanol; aliquoted	-20 °C
EDTA stock (0.5 M)	93.05 gm EDTA in 400 ml ddH_20 adjusted to pH 8.0 using 10 M NaOH final volume 500 ml autoclaved and aliquoted	RT
IP buffer	20 mM HEPES, pH 7.9 200 mM NaCl 0.2 % (v/v) NP-40 0.5 mM EDTA 10 % (v/v) Glycerol	4 °C
Kinobead buffer	50 mM Tris-HCl, pH 7.5 0.8 % (v/v) NP-40 150 mM NaCl 1 mM Na_3VO_4 1.5 mM $MgCl_2$ 5.5 % (v/v) Glycerol 25 mM NaF 1 mM DTT	4 °C
Laemmli sample buffer (6 x)	12 % (w/v) SDS 0.06 % (w/v) bromophenol blue 40% (v/v) glycerol 60 mM Tris/HCl, pH 6.8 9.3% (w/v) DTT aliquoted	-20 °C
Miniprep lysis buffer (Solution 1)	1 % (w/v) SDS 200 mM NaOH	RT
Miniprep neutralization buffer (Solution 2)	11.5 % (v/v) acetic acid 3 M KOAc	4 °C

Miniprep resuspension buffer	TE buffer with freshly added 1:1000 RNase A (10 mg/ml)	RT
MOPS running buffer (20 x)	1 M MOPS 1 M Tris base 20 mM EDTA 2 % (w/v) SDS	4 °C
MOPS running buffer (ready-to-use)	1 x MOPS running buffer 5 mM sodium bisulfite	RT
MS IP buffer	20 mM HEPES, pH 7.9 180 mM NaCl 0.2 % (v/v) NP-40 1.5 mM $MgCl_2$ 10 % (v/v) Glycerol	4 °C
PBS	137 mM NaCl 2.7 mM KCl 10.1 mM Na_2HPO_4 1.76 mM KH_2PO_4 autoclaved	RT
Phosphatase inhibitor cocktail	Ser/Thr phosphatase inhibitor (Sigma) Tyr phosphatase inhibitor (Sigma) used 1:1000	-20 °C
Polybrene stock solution (4mg/ml)	200 mg dissolved in 50 ml ddH_2O sterile filtered and aliquoted	-20 °C
Polyethyleneimine (PEI)	0.09 % PEI 6 mM HCl sterile filtered and aliquoted	-20 °C
Primary antibody dilution buffer (Fuji)	5% BSA 0.02% NaN3 in TBS-T sterile filtered	4 °C
Propidium Iodide (PI)	1 mg/ml in PBS	4 °C
Protease inhibitor	Protease inhibitor cocktail (Sigma) used 1:1000	-20 °C

Proteinase K	10 mg/ml (Roth) aliquoted	-20 °C
RIPA lysis buffer	50 mM HEPES, pH 7.9 140 mM NaCl 1 mM EDTA 1 % (v/v) Triton X-100 0.1 % Na-deoxycholate 0.1 % (w/v) SDS sterile filtered 1:1000 protease and phosphatase inhibitors added fresh before use	4 °C
RNase A (10 mg/ml)	100 mg RNase A (Roth) in 27 µl 3 M sodium acetate, pH 5.2 9 ml ddH_2O 450 µl aliquots prepared and boiled for 30 min at 100°C to inactivate DNases 50 µl 1 M Tris, pH 7.4 added per aliquot	-20 °C
SDS lysis buffer	2 % (w/v) SDS 40 mM Tris-HCl, pH 7.6	RT
TAE (50 x)	2 M Tris, pH 8.0 5.71 % (v/v) acetic acid 50 mM EDTA, pH 8.0	RT
TBS (20 x)	500 mM Tris, pH 7.4 2.8 M NaCl	RT
TBS-T	1 x TBS 0.2 % (v/v) Tween-20	RT
TE	10 mM Tris pH 7.4 1 mM EDTA pH 8.0	RT
Transfer buffer (20 x)	500 mM Bicine 500 mM Bis-Tris 20.5 mM EDTA 0.1 mM chlorobutanol	4 °C
Transfer buffer (ready-to-use)	1x transfer buffer 40 % (v/v) methanol	4 °C

Trypsin solution	0.25 % trypsin 5 mM EDTA 22.3 mM Tris, pH 7.4 125 mM NaCl	-20 / 4 °C

2.4 Commercial reagents

Name	Source
Standards	
Gene Ruler™ 1 kb Plus DNA Ladder	Thermo Fisher Scientific
PageRule™ Prestained Protein Ladder	Thermo Fisher Scientific
Colour Prestained Protein Standard, Broad Range	New England Biolabs
Enzymes	
AgeI-HF	New England Biolabs
Benzonase nuclease purity >99%, 25 U/µl	Merk Millipore
EcoRI-HF	New England Biolabs
M-MLV reverse transcriptase	Promega
MluI-HF	New England Biolabs
Phusion	Thermo Fisher Scientific
Proteinase K	Roth
RNase A	Roth
SpeI-HF	New England Biolabs
T4 DNA ligase	Thermo Fisher Scientific
XhoI	New England Biolabs
Kits	
CloneJET PCR Cloning Kit	Thermo Fisher Scientific
GeneJET Gel Extraction Kit	Thermo Fisher Scientific
Nano-Glo® HiBiT Lytic Detection System	Promega
Nano-Glo® Luciferase Assay System	Promega
NEBNext® Poly(A) mRNA Magnetic Isolation Module	New England Biolabs
NEBNext® Ultra™ II Directional RNA Library Prep Kit for Illumina	New England Biolabs

NextSeq® 500/550 High Output Kit v2 (75 cycles)	Illumina
PowerUP™ SYBR® Green Master Mix	Thermo Fisher Scientific
PureLink HiPure Plasmid Maxiprep Kit	Invitrogen
RNeasy Mini Kit	Qiagen
Beads	
Dynabead Protein A for Immunoprecipitation	Thermo Fisher Scientific
Dynabead Protein G for Immunoprecipitation	Thermo Fisher Scientific
Pierc Anti-HA Magnetic Beads	Thermo Fisher Scientific
Chemicals and Reagents	
alamarBlue™ HS Cell Viability Reagent	Thermo Fischer Scientific
Ehidium bromide	Carl Roth
Lipofectamine 2000 Transfection Reagent	Thermo Fischer Scientific
Lipofectamine RNAiMAX Transfection Reagent	Thermo Fisher Scientific
peqGOLD TriFast reagent	Peqlab/ VWR international
Propidium iodide	Sigma

2.5 Nucleic acids

2.5.1 Oligonucleotides

Name	**Sequence (5' – 3')**
Primers for cloning	
EW_1551_AURKA_ AgeI_f	CGCACCGGTATGGACCGATCTAAAGAAAACTGC
EW_1552_cAURKA_HiBiT_MluI_r	CGCGACGCGTCTAGCTAATCTTCTTGAACAGCC GCCAGCCGCTCACACCGGAGCTCCCAGACTGTT TGCTAGCTGATTC
EW_1638_HA_AURKA _AgeI_f	CGCACCGGTATGTACCCTTACGACGTGCCCGAC TACGCCGGGATGGACCGATCTAAAGAAAACTGC
EW_1639_ AURKA_SpeI_r	GGACTAGTCTAAGACTGTTTGCTAGCTGATTC

EW_1763_SpeI_AURKA_HA_Cterm_r	GGACTAGTCTAGGCGTAGTCGGGCACGTCGTAAGGGTAACCGGAGCTCCCAGACTGTTTGCTAGCTGATTC
EW_1778_WDR5_AgeI_f	CGCACCGGTATGGCGACGGAGGAGAAGAAGC
EW_1779_WDR5_cHiBiT_MluI_r	CGCGACGCGTTTAGCTAATCTTCTTGAACAGCCGCCAGCCGCTCACACCGGAGCTCCCGCAGTCACTCTTCCACAGT
EW_1855_AURKA_Age_f	GTACCGGTATGTACCCTTACGAC
EW_1856_AURKA_Spe_r	CCACTAGTCTAAGACTGTTTGCT
EW_1985_AgeI_AURKB_nHA_f	CGCACCGGTATGTACCCTTACGACGTGCCCGACTACGCCGGGATGGCCCAGAAGGAGAACTC
EW_1988_SpeI_AURKB_r	CCACTAGTTCAGGCGACAGATTGAAG
EW_1989_AURKB_E161T_1_r	AGCTCCTTGTAGAGAGTCCCGCG
EW_1990_AURKB_E161T_2_f	CGCGGGACTCTCTACAAGGAGCT
EW_1991_AURKBx3_1_r	CTTCTGCAGCTCTCTGTAGAGAGTCCCTAAGGGGGCATAC
EW_1992_AURKBx3_2_f	GTATGCCCCCTTAGGGACTCTCTACAGAGAGCTGCAGAAG
EW_1941_AURKA_P191W_1_r	CTAAGAATATTCCAATGCCGAAGG
EW_1942_AURKA_P191W_2_f	CCTTCGGCATTGGAATATTCTTAG
EW2341_VHL_SpeI_r	GGACTAGTTCAATCTCCCATCCGTTGATGTG
EW2344_AgeI_nHA_VHL_f	CGCACCGGTATGTACCCTTACGACGTGCCCGACTACGCCGGGAGCTCCGGTCCCCGGAGGGCGGAGAAC
EW_2580_AgeI_FRB_f	CGCACCGGTATGATCCTCTGGCATGAGATGT
EW_2585_FRB_SpeI_r	GGACTAGTTCACTTTGAGATTCGTCGGAAC

EW2604_MluI_linker_nLuc_r	CGACGCGTACCGGAGCTCCCACCGGAGCTCCCCGCCAGAATGCGTTCGCACAGCC
EW2703_link_MluI_r	CGCGACGCGTACCGGAGCTCCCACCGGAGC
EW2704_CRBN_MluI_f	CGCGACGCGTGCCGGCGAAGGAGATCAGCAG
EW2705_CRBN_SpeI_r	GGACTAGTTTACAAGCAAAGTATTACTTTG
EW2706_CRBN_AgeI_f	CGCACCGGTATGGCCGGCGAAGGAGATCAGCAG
EW2707_CRBN_MluI_r	CGCGACGCGTCAAGCAAAGTATTACTTTGTC
EW2708_link_MluI_f	CGCGACGCGTGGGAGCTCCGGTGGGAGCTCCGGGTATC
EW2709_AURKA_XhoI_r	CCGCTCGAGAGACTGTTTGCTAGCTGATTC
EW2710_link_Nluc_XhoI_f	CCGCTCGAGGGGAGCTCCGGTGGGAGCTCCGGTGTCTTCACACTCGAAGATTTC
gBlocks	
EW_1861_HA_AURKA_Imut	ACCGGTATGTACCCTTACGACGTGCCCGACTACGCCGGGATGGACCGATCTAAAGAAAACTGCATTTCAGGACCTGTTAAGGCTACAGCTCCAGTTGGAGGTCCAAAACGTGTTCTCGTGACTCAGCAATTTCCTTGTCAGAATCCATTACCTGTAAATAGTGGCCAGGCTCAGCGGGTCTTGTGTCCTTCAAATTCTTCCCAGCGCGTTCCTTTGCAAGCACAAAAGCTTGTCTCCAGTCACAAGCCGGTTCAGAATCAGAAGCAGAAGCAATTGCAGGCAACCAGTGTACCTCATCCTGTCTCCAGGCCACTGAATAACACCCAAAAGAGCAAGCAGCCCCTGCCATCGGCACCTGAAAATAATCCTGAGGAGGAACTGGCATCAAAACAGAAAAATGAAGAATCAAAAAAGAGGCAGTGGGCTTTGGAAGACTTTGAAATTGGTGAACCTCTGGGTAAAGGAAAGTTTGGTAATGTTTATTTGGCAAGAGAAGAACAAAGCGAAGAAGAACTGGCTCTTAAAGTGTTATTTAAAGCTCAGCTGGAGAAAGCCGGAGTGGAGCATCAGCTCAGAAGAGAAGTAGAAATACAGTCCCACCTTGAACATTGGAATATTCTTAGACTGTATGGTTATTTCCATGATGCTACCAGAGTCTACCTAATTCTGGAATATGCACCACTTGGAACAGTTTATAGAGAACTTCAGGAACTTTCAAAGTTTGATGAGCAGAGAACTGCTACTTATATAACAAGATTGGCAAATGCCCTGTCTTACTGTCATTCGAAGAGAGTTATTCATAGAGACATTAAGCCAGAGAACTTACTTCTTGGATGGTGGGGAGAGCTT

	AAAATTGCAGATTTTGGGTGGTCAGTACATGCTCCATCT TCCAGGAGGACCACTCTCTGTGGCACCCTGGACTACCT GCCCCCTGAAATGATTGAAGGTCGGATGCATGATGAGA AGGTGGATCTCTGGAGCCTTGGAGTTCTTTGCTATGAAT TTTTAGTTGGGAAGCCTCCTTTTGAGGCAAACACATACC AAGAGACCTACAAAAGAATATCACGGGTTGAATTCACAT TCCCTGACTTTGTAACAGAGGGAGCCAGGGACCTCATT TCAAGACTGTTGAAGCATAATCCCAGCCAGAGGCCAAT GCTCGAAGAAGTACTTGAACACCCCTGGATCACAGCAA ATTCATCAAAACCATCAAATTGCCAAAACAAAGAATCAG CTAGCAAACAGTCTTAGACTAGT
EW_1862_HA_K162R_b	TGGGCTTTGGAAGACTTTGAAATTGGTCGCCCTCTGGG TAAAGGAAAGTTTGGTAATGTTTATTTGGCAAGAGAAAA GCAAAGCAAGTTTATTCTGGCTCTTAGAGTGTTATTTAA AGCTCAGCTGGAGAAAGCCGGAGTGGAGCATCAGCTC AGAAGAGAAGTAGAAATACAGTCCCACCTTCGGCATCC TAATATTCTTAGACTGTATGGTTATTTCCATGATGCTACC AGAGTCTACCTAATTCTGGAATATGCACCACTTGGAACA GTTTATAGAGAACTTCAGAAACTTTCAAAGTTTGATGAG CAGAGAACTGCTACTTATATAACAGAATTGGCAAATGCC CTGTCTTACTGTCATTCGAAGAGAGTTATTCATAGAGAC ATTAAGCCAGAGAACTTACTTCTTGGATCAGCTGGAGAG CTTAAAATTGCAGATTTTGGGTGGTCAGTACATGCTCCA TCTTCCAGGAGGACCACTCTCTGTGGCACCCTGGACTA CCTGCCCCCTGAAATGATTGAAGGTCGGATGCATGATG AGAAGGTGGATCTCTGGAGCCTTGGAGTTCTTTGCTAT GAATTTTTAGTTGGGAAGCCTCCTTTTGAGGCAAACACA TACCAAGAGACCTACAAAAGAATATCACGGGTTGAATTC ACATTCCCTGACTTTGTAACAGAGGGAGCCAGGGACCT CATTTCAAGACTGTTGAAGCATAATCCCAGCCAGAGGC CAATGCTCAGAGAAGTACTTGAACACCCCTGGATCACA GCAAATTCATCAAAACCATCAAATTGCCAAAACAAAGAA TCAGCTAGCAAACAGTCTTAGACTAGT
EW_1863_HA_K162R_a	ACCGGTATGTACCCTTACGACGTGCCCGACTACGCCGG GATGGACCGATCTAAAGAAAACTGCATTTCAGGACCTGT TAAGGCTACAGCTCCAGTTGGAGGTCCAAAACGTGTTC TCGTGACTCAGCAATTTCCTTGTCAGAATCCATTACCTG TAAATAGTGGCCAGGCTCAGCGGGTCTTGTGTCCTTCA AATTCTTCCCAGCGCGTTCCTTTGCAAGCACAAAAGCTT GTCTCCAGTCACAAGCCGGTTCAGAATCAGAAGCAGAA

	GCAATTGCAGGCAACCAGTGTACCTCATCCTGTCTCCA GGCCACTGAATAACACCCAAAAGAGCAAGCAGCCCCTG CCATCGGCACCTGAAAATAATCCTGAGGAGGAACTGGC ATCAAAACAGAAAAATGAAGAATCAAAAAAGAGGCAGTG GGCTTTGGAAGACTTTGAAATTGGTCGC
Primers for sequencing	
EW_859_SFFV_seq	CTTCTGCTTCCCGAGCTCTA
IREShygRn	CAGACCTTGCATTCCTTTGG
pJET1.2-F	CGACTCACTATAGGGAGAGCGGC
pJET1.2-R	AAGAACATCGATTTTCCATGGCAG
Primers for RT-qPCR	
EW316_B2MG_F	GTGCTCGCGCTACTCTCTC
EW317_B2MG_R	GTCAACTTCAATGTCGGAT
EW_1312_AURKA_ f	TTCAGGACCTGTTAAGGCTACA
EW_1313_AURKA_r	ATTTGAAGGACACAAGACCCG
EW2306_WDR5_f	CCAGTCTCGGCCGTTCATTT
EW2307_WDR5_r	CGTTCGGGGAGAACTTCACA

2.5.2 Plasmids

Name	Description	Source
psPAX2	Lentiviral packing plasmid	Addgene #12260
pMD2.G	VSV-G envelope expressing plasmid	Addgene #12259
pRRL-SFFV-IRES-puro	Lentiviral expression vector; SFFV promoter; puromycin resistance	AG Eilers
pRRL-SFFV-IRES-hygro	Lentiviral expression vector; SFFV promoter; hygromycin resistance	AG Eilers
pRRL-PGK-IRES-hygro	Lentiviral expression vector; PGK promoter; hygromycin resistance	AG Wolf

pcDNA3 HA-AURKA wt	Eukaryotic expression vector; expresses Aurora A with N-terminal HA-tag; CMV promoter	AG Eilers
pTREpur HA-AURKA-A wt	Eukaryotic inducible expression vector; expresses Aurora A with N-terminal HA-tag	AG Eilers
pcDNA3 HA-AURKA T217D	Eukaryotic expression vector; expresses Aurora A harboring T217D mutation with N-terminal HA-tag; CMV promoter	AG Eilers
pTREpur HA-AURKA T217D	Eukaryotic inducible expression vector; expresses Aurora A harboring T217D mutation with N-terminal HA-tag	AG Eilers
pcDNA3 HA-AURKB	Eukaryotic expression vector; expresses Aurora B isoform 5 (69-69: T → TR) with N-terminal HA-tag; CMV promoter	AG Eilers
pRRL-PGK -AURKA-HiBiT	Lentiviral expression vector; expresses Aurora A with C-terminal HiBiT-tag; SFFV promoter; hygromycin resistance	This study
pRRL_puro_HA-AURKA	Lentiviral expression vector; expresses Aurora A with N-terminal HA-tag; SFFV promoter; puromycin resistance	This study
pRRL_puro_AURKA-HA	Lentiviral expression vector; expresses Aurora A with C-terminal HA-tag; SFFV promoter; puromycin resistance	This study
pRRL_puro_HA-AURKA_Imut	Lentiviral expression vector; expresses Aurora A mutant Imut with N-terminal HA-tag; SFFV promoter; puromycin resistance	This study

pRRL_puro_HA-AURKA_D274N	Lentiviral expression vector; expresses Aurora A containing mutation D274N with N-terminal HA-tag; SFFV promoter; puromycin resistance	This study
pRRL_puro_HA-AURKA_K162R	Lentiviral expression vector; expresses Aurora A containing mutation K162R with N-terminal HA-tag; SFFV promoter; puromycin resistance	This study
pRRL_PGK_HA-AURKA-HiBIT	Lentiviral expression vector; expresses Aurora A with N-terminal HA-tag and C-terminal HiBiT-tag; PGK promoter; hygromycin resistance	This study
pRRL_PGK_HA-Imut-HiBIT	Lentiviral expression vector; expresses Aurora A mutant Imut with N-terminal HA-tag and C-terminal HiBiT-tag; PGK promoter; hygromycin resistance	This study
pRRL_PGK_HA-AURKA_P191W-HiBIT	Lentiviral expression vector; expresses Aurora A containing mutation P191W with N-terminal HA-tag and C-terminal HiBiT-tag; PGK promoter; hygromycin resistance	This study
pRRL-Puro_HA-AURKB-wt	Lentiviral expression vector; expresses Aurora B isoform 5 with N-terminal HA-tag; SFFV promoter; puromycin resistance	This study
pRRL-Puro_HA-AURKB-E162T	Lentiviral expression vector; expresses Aurora B isoform 5 harboring E162T mutation with N-terminal HA-tag; SFFV promoter; puromycin resistance	This study

pRRL-Puro_HA-AURKB-x3	Lentiviral expression vector; expresses Aurora B isoform 5 harboring triple mutations (R160L,E162T,K165R) with N-terminal HA-tag; SFFV promoter; puromycin resistance	This study
pRRL_PGK_WDR5_HiBiT	Lentiviral expression vector; expresses WDR5 with C-terminal HiBiT-tag; SFFV promoter; hygromycin resistance	This study
pRRL_Puro_HA_VHL	Lentiviral expression vector; expresses VHL isoform 1 with N-terminal HA-tag; SFFV promoter; puromycin resistance	This study
pRRL_Hygro_VHL-FRB	Lentiviral expression vector; expresses VHL tagged with FRB in C-terminal; SFFV promoter; hygromycin resistance	Bachelor thesis (Isabella Kurrer)
pRRL_Hygro_FRB-VHL	Lentiviral expression vector; expresses VHL tagged with FRB in N-terminal; SFFV promoter; hygromycin resistance	Bachelor thesis (Isabella Kurrer)
pRRL_Hygro_FRB	Lentiviral expression vector; expresses FRB; SFFV promoter; hygromycin resistance	Bachelor thesis (Isabella Kurrer)
pRRL_puro_WDR5-NLuc-FKBP12	Lentiviral expression vector; expresses WDR5 tagged with NLuc-FKBP12 fusion protein in C-terminal; SFFV promoter; puromycin resistance	Bachelor thesis (Isabella Kurrer)

pRRL_puro_NLuc-WDR5-FKBP12	Lentiviral expression vector; expresses WDR5 tagged with NLuc in N-terminal and FKBP12 in C-terminal; SFFV promoter; puromycin resistance	Bachelor thesis (Isabella Kurrer)
pRRL_puro_NLuc-FKBP12	Lentiviral expression vector; expresses NLuc tagged with FKBP12 in C-terminal; SFFV promoter; puromycin resistance	Bachelor thesis (Isabella Kurrer)
pRRL _Hygro_CRBN-FRB	Lentiviral expression vector; expresses CRBN tagged with FRB in C-terminal; SFFV promoter; hygromycin resistance	This study
pRRL _Hygro_FRB-CRBN	Lentiviral expression vector; expresses CRBN tagged with FRB in N-terminal; SFFV promoter; hygromycin resistance	This study
pRRL _Puro_AURKA-NLuc-FKBP12	Lentiviral expression vector; expresses Aurora A tagged with NLuc-FKBP12 fusion protein in C-terminal; SFFV promoter; puromycin resistance	This study

2.6 Antibodies

Name	**Source**	**Identifier**
Primary antibodies		
Anti-Dicer antibody [13D6]	Abcam	Cat# ab14601
Aurora A/AIK Antibody	Cell Signaling Technology	Cat# 3092S
Aurora B Antibody	Bethyl Laboratories	Cat# A300-431A
Endophilin II Antibody (A-11)	Santa Cruz Biotechnology	Cat# sc-365704
HA-probe Antibody (Y-11)	Santa Cruz Biotechnology	Cat#sc-805X
Ikaros Antibody (E-2)	Santa Cruz Biotechnology	Cat# sc-398265

Mouse monoclonal anti-CRBN (D8H3S)	Cell Signaling Technology	Cat# 71810S
Mouse monoclonal anti-vinculin, clone*hv	Sigma	Cat#V9131
VHL Antibody (VHL40)	Santa Cruz Biotechnology	Cat#sc-135657
WDR5 Antibody (G-9)	Santa Cruz Biotechnology	Cat#sc-393080
FITC anti-BrdU, Mouse IgG1, kappa, Clone: 3D4	BioLegend	Cat#364104
Secondary antibodies		
ECL-anti-mouse IgG Horseradish Peroxidase	GE Healthcare / FisherScientific GmbH	Cat#1079-4347
ECL-anti-rabbit IgG Horseradish Peroxidase	GE Healthcare / FisherScientific GmbH	Cat#1079-4347

2.7 Consumables

Name	**Source**
Cell culture plates and reaction tubes	
Cell culture plates (10 cm, 15 cm)	Greiner Nunc Sarstedt
Cell culture well plates (6 well, 12 well, 24 well, 96 well)	Greiner Nunc Thermo Fisher Scientific
CellCarrier 96 ultra, black	Perkin Elmer
Glass pipettes (5 ml, 10 ml, 25 ml)	Roth
Glass Pasteur pipettes	Roth
PCR tubes	Sarstedt Starlab
Pipette Tips	Sarstedt Greiner
Eppendorf tubes (1.5 ml, 2 ml)	Sarstedt
Falcon tubes (15 ml, 50 ml)	Sarstedt

Immunoblots

Whatman filter paper	Sigma
Immobilon-P Membrane, PVDF	Merck
Immobilon-FL Membrane, PVDF	Merck

2.8 Equipments

Utility	**Type**	**Source**
Analytical balance	PCB 2500-2 PT 600	KERN Satorius GmbH
Cell counter	Casy cell counter	Innovatis
Cell culture incubator	BBD 6220	Heraeus
Centrifuges	5417R / 5424 Avanti J-26 XP Multifuge plus Sorvall Legend Micro 17R	Eppendorf Beckman Coulter Starlab Thermo Fisher
Chemiluminescence imager	LAS-4000 mini	Fujifilm
Flow cytometer	BD FACS Canto II	BD Biosciences
Fluorescence image reader	Odyssey CLx Infrared Imaging System	LI-COR
Freezing container	Mr. Frosty	Thermo Fisher
Microliter syringes	20 µl and 50 µl	Hamilton
Heating block	Thermomixer Comfort	Eppendorf
Immunoblot transfer chamber	PerfectBlue Tank Electro Blotter Web S	Peqlab
Incubator shaker	Multitron Standard	INFORS HT
Luminescence reader	GloMax 96 Microplate Luminometer	Promega
Microscope	Axiovert 40CFL	Zeiss
PCR thermal cycler	C1000 Thermal cycler Mastercycler proS ProFlex PCR System	Bio-Rad Eppendorf Thermo Fisher

Multipurpose plate reader	Tecan Spark Multiplate reader	Tecan
Photometers	Multiscan Ascent Spectrofluorometer NanoDrop 1000	Thermo Labsystems Thermo Fisher
Power supply	PowerPac HC Consort EV 243	Bio-Rad Sigma
Quantitative RT-PCR machine	StepOne plus	Applied Biosystem
Roller mixer	SRT9	Stuart
Rotator mixer	SB2	Stuart
SDS-PAGE system	Mini-PROTEAN Tetra Cell	Bio-Rad
Sequencer	NextSeq500	Illumina
Ultrasonifier	Digital Sonifier W-250 D	Branson
UV table	ECX-F26MX	Vilber
Vortex	Vortex-Genie 2	Scientific Industries
Water bath	Water bath WB14	Memmert
Water purification system	Milli-Q Integral 5	Millipore

2.9 Software and programs

Software	**Source**
Affinity Designer v1.10.5	Pantone LLC
ApE- A plasmid Editor v2.0	M. Wayne Davis
BD FACSDIVA Software v6.1.2	BD Biosciences
Bowtie2 (v2.3.4.1)	(Langmead et al., 2009)
EdgeR	(Robinson et al., 2010)
EndNote 20.4	Clarivate Analytics
FlowJo (version 8.8.6)	https://www.flowjo.com/
GraphPad Prism v5/6.0 for Mac	Graph Pad Software Inc.
Image Studio Lite (Version 5.2.5)	LI-COR
ImageJ (version 1.52q)	Wayne Rasband

LAS-4000 mini-2.1	Fujifilm
Max Quant (version 1.6.2.10)	(Cox & Mann, 2008)
Microsoft Excel (v16.16.24)	Microsoft
Multiscan Ascent	Thermo Fisher Scientific
Perseus (version 1.5.8.5)	(Tyanova et al., 2016)
R v3.5.2	https://www.r-project.org/
Samtools (v1.3)	http://samtools.sourceforge.net
SnapGene Viewer v6.1.2	GSL Biotech LLC
SparkControl	Tecan
Spotfire	TIBCO Software
StepOne software v2.3	Applied Biosystems
Tm Calculator	Thermo Fisher Scientific (online page)

3 Methods

3.1 Cell biology methods

3.1.1 Cell culture

MV4-11, IMR5, Sk-Mes-1, HL-60, HLE, NCI-H1299, NCI-H23, and NGP cells were cultured in RPMI 1640 medium supplemented with 10% FBS and 1% penicillin/ streptomycin. HEK293, U2OS, Hela, SW620, LS174T, and MCF7 cells were grown in DMEM medium supplemented with 10% FBS and 1% penicillin/ streptomycin. For stable isotope labeling of MV4-11 cells, cells were cultured in RPMI 1640 medium for SILAC containing 10% dialyzed FBS, 200 mg/l L-proline, and supplemented with either 100 mg/l L-arginine and 100 mg/l L-lysine (light) or [$^{13}C_6$]-L-arginine and [$^{2}H_4$]-L-lysine (medium) or [$^{13}C_6$,$^{15}N_4$]-L-arginine and [$^{13}C_6$,$^{15}N_2$]-L-lysine (heavy). Cells were cultured at 37 °C in the presence of 5 % CO_2. All cells were routinely examined and found negative for mycoplasma contamination by PCR-based assay.

For splitting the suspension cells (MV4-11, HL-60), the cells were homogenously distributed by pipetting up and down gently, and a portion of the cells was transferred to a new dish with fresh media. For passaging the adherent cells, the cells were detached using trypsin/EDTA after a PBS wash, resuspended in culture media, centrifuged, and the required amount was seeded into a new dish with fresh media. For seeding the specific cell numbers for experiments, cells were counted using the Casy cell counter or Neubauer chamber using the manufacturer's instructions.

To freeze the cells, both suspension and adherent cells (after trypsinization) were pelleted, resuspended in the freezing medium, and transferred to cryo-vials. The vials were frozen slowly at -80 °C using Mr. Frosty overnight. For thawing the cells, the cells were quickly thawed in a water bath, and resuspended in culture media. The cell suspension was centrifuged and cell pellet was transferred to a cell culture dish with media.

3.1.2 Transfection of plasmid

For the Rapamycin induced proximity (RIP) assay, 5 million HEK293 cells were seeded in 10 ml media per 10 cm dish or 800,000 cells in 2ml per well of a 6-well plate. The cells were allowed to attach and recover for at least 6 hours before transfection. For transfection, two Eppendorf tubes were prepared containing 700 µl Opti-MEM each (140 µl of 6-well plate). 30 µl PEI or lipofectamine 2000 (6 µl for 6-well plate) was added to one tube while an appropriate amount of FRB and FKBP12 plasmids were added to another (0.8 – 12 µg for 10 cm dish; 0.2 – 2 µg for 6-well plate). The mixtures were vortexed and incubated for 5 minutes at RT. Then the DNA mixture was added to the PEI mixture dropwise, incubated for 20 minutes at RT, and added to the dish with cells. The cells were left in the cell culture incubator for at least 20 hours for protein expression. Next, the cells were reseeded, left overnight to recover, and finally treated with rapamycin or vehicle.

3.1.3 Lentivirus production

Five million HEK293 cells were seeded per 10 cm dish 24 hours before transfection. For transfection, a DNA-mixture consisting of 10 µg PAX2, 2.5 µg pMD2G, and 10 µg of the plasmid of interest in 500 µl Opti-MEM and PEI mixture containing 30 µl PEI in 500 µl Opti-MEM were prepared. The mixtures were incubated for 5 minutes, combined (DNA mixture added to PEI mixture), and further incubated for 20 minutes. During incubation, cells were washed with PBS, and 5 ml transfection media was added per dish. The transfection mixture was added to the cells and the cells were taken to the S2 cell incubator. 6-8 hours post-transfection, the media was removed, and 6 ml fresh media was added. After 24 hours of transfection, the supernatant containing the virus was collected and stored at 4 °C. The viral supernatant was collected every 12 hours for a total of four times, replenishing with 6 ml fresh media after each harvest. The pooled supernatant was filtered with a 0.45 µm filter and either stored at 4 °C for immediate use or flash frozen and stored at -80 °C for long-term use.

3.1.4 Lentiviral infection

For lentiviral infection of MV4-11 and HL-60 cells, 3ml of viral supernatant was added to 3 ml cell suspension (200,000 cells/ml) along with 6 µl of polybrene stock

solution. The day after the first infection, a second round of infection was carried out by adding 6 ml viral supernatant and 6 µl polybrene. 24 hours after the second infection, selection with antibiotics was started (depending upon the resistance marker present in the plasmid) and continued until the uninfected control cells were completely dead.

3.1.5 Flow cytometry

For BrdU/PI flow cytometry, the cells were labeled with 10 µM BrdU for 1-hour prior to harvest. The suspension cells were directly collected in 15 ml low binding affinity falcon, whereas adherent cells were collected after trypsinization followed by resuspension in the media the cells were cultured in. The cells were centrifuged for 5 minutes at 400x g at 4 °C, washed with 5 ml cold PBS, fixed in 80 % ice-cold ethanol, and stored at -20 °C overnight. The next day, the cells were pelleted, washed with 5 ml cold PBS, and incubated at RT for 30 minutes after resuspending in 1 ml 2 M HCl containing 0.5 % TritonX-100. The cells were neutralized with 0.1 M $Na_2B_4O_7$ (pH 8.5). The cells were then centrifuged, resuspended in 100 µl 1 % BSA in PBS-T containing 5 µl anti-BrdU-FITC antibody, and incubated in the dark for 30 minutes at RT. Further, the cells were washed once with 1 % BSA in PBS-T, resuspended in 400 µl PBS with PI (54 µM) and RNase (24 µg/ml), and incubated for 30 minutes at 37 °C in the dark. Finally, the cells were transferred to ice and kept in the dark until analysis.

The cells were collected for annexin/PI flow cytometry as for BrdU/PI flow cytometry. The cells were washed with 10 ml cold PBS and pelleted at 400x g for 5 minutes at 4 °C. The cells were resuspended in 100 µl annexin V binding buffer with 2 µl annexin V conjugated with Pacific Blue dye. Then, the cells were incubated for 15 minutes at RT, followed by the addition of 400 µl PBS with PI (18.5 µM). Finally, the cells were stored on ice and kept in the dark until analysis.

3.1.6 Cell growth assays

For crystal violet staining, at the endpoint of treatment, the cells were washed with PBS once and incubated with crystal violet solution (0.7 ml per well of 6-well plate) for 30 minutes at RT. The cells were carefully washed with desalted water to remove the excess dye. The plates were turned upside down and air-dried at RT before imaging.

For the alamarBlue assay, a few hours before the experimental endpoint, cells were incubated with alamarBlue. 10x alamarBlue was added to the media containing cells to reach a final concentration of 1x. Next, the cells were incubated until the color of the media for untreated cells was changed from blue to purple due to the reduction of resazurin in alamarBlue to resorufin. Finally, the fluorescence was measured on the Tecan Spark Multiplate reader using excitation and emission wavelength of 550 nm and 600 nm, respectively.

For the cumulative growth curve, the cells were seeded at the density of 100,000 cells/ml and treated with various compounds. Every third day the cells were counted and reseeded to the initial cell density (100,000 cells/ml) in fresh media with compounds. The cumulative cell number for a particular time point was calculated using the final cell density and seeding density of that particular time point and the previous time point.

3.2 Molecular biology methods

3.2.1 Primer design and polymerase chain reaction (PCR)

To clone a new expression vector, the required DNA fragment was amplified from existing vectors, gBlocks or complementary DNA (cDNA) using forward and reverse primers. The primers were designed using the coding sequence (CDS) of the protein of interest and sequence for appropriate restriction sites. The primers were ordered from Sigma.

For the amplification of the DNA fragments, a Phusion polymerase was used. The following reagents were pipetted into a reaction tube:

Components	**Final amount**
Template DNA	100 ng
5x buffer	10 µl
dNTPs	200 µM
Forward primer	0.4 µM
Reverse primer	0.4 µM
Phusion polymerase	1 U
DMSO	0 – 10 %
ddH_2O	Fill up to 50 µl

The annealing temperature for the primers was calculated using T_m calculator. The reaction tube was placed in a thermocycler and PCR was carried out using the following program:

Step	Temperature	Time	Cycles
Initial Denaturation	98 °C	30 sec	1x
Denaturation	98 °C	10 sec	
Annealing	55 – 71 °C	10 sec	4x
Extension	72 °C	30 sec per kb	
Denaturation	98 °C	10 sec	
Annealing	55 – 71 °C	10 sec	28x
Extension	72 °C	30 sec per kb	
Final extension	72 °C	5 min	1x
Hold	4 °C	∞	1x

3.2.2 Restriction digest

The restriction enzymes were bought from NEB. At least two enzymes simultaneously digested the vector backbone or the PCR fragments in the cut smart buffer. For preparative digestion, 1.5 µl of each restriction enzyme and 5 µl of 10x cut smart buffer were used in a final reaction volume of 50 µl. The reaction mixture was incubated for at least 3 hours at 37 °C and the enzymes were heat inactivated whenever required. The amount of DNA, enzymes, reaction volume, and digestion time were adjusted for analytical digestion.

3.2.3 Agarose gel electrophoresis

Agarose gel electrophoresis was carried out to visualize and extract the undigested and digested vector backbone or PCR fragments. Based on the DNA fragment size, 0.8 – 3 % agarose gel was prepared in TAE buffer. Ethidium bromide was added to the melted agarose gel before solidification, and the gel was cast using a gel chamber with combs. The DNA fragments were mixed with DNA loading buffer, loaded into the wells, and separated for 1 hour at 150 V. The DNA fragments were visualized using a UV table, imaged, and the expected DNA fragment was cut-out for further use, when required.

3.2.4 Extraction and purification of DNA fragments

For the purification of the vector backbone or PCR fragments, digested or extracted DNA fragments from agarose gel, the GeneJET Gel Extraction Kit was utilized according to the manufacturer's instructions. The DNA fragments were eluted in 30 – 50 µl ddH_2O.

3.2.5 Ligation

The digested PCR fragments (inserts) and vector backbone were ligated using 2 µl T4 DNA ligase in a total reaction volume of 20 µl. The insert and plasmid were used in molar ratio of 3:1 with a 100g vector backbone. A mixture without inserts was used as religation control. The reaction mixtures were incubated at 16 °C overnight or 22 °C for 1 hour.

3.2.6 Transformation of competent bacterial cells

Chemically competent *E. coli* XL1 blue was thawed on ice and 50 µl of the cell suspension was mixed with 50 ng plasmid or 10 µl of ligation mixture (see section 3.2.5). The bacteria were incubated on ice for 10- 30 minutes followed by heat shock at 42 °C for 45 seconds. After heat shock, the bacteria were transferred to the ice for 3 minutes, 0.5 ml LB medium was added and allowed to regenerate for up to one hour at 37 °C with shaking. The bacteria were pelleted at 900x g for 2 minutes, resuspended in 100 µl LB medium, and streaked onto LB-agar plates with appropriate antibiotics (depending on the antibiotic resistance present in the transformed plasmid backbone). The plate was incubated upside down at 37 °C overnight.

3.2.7 Plasmid isolation from bacteria

For analytical preparation of plasmid (miniprep), a single colony of transformed bacteria was propagated overnight at 30 °C with shaking (200 rpm) in 3 ml LB medium with appropriate antibiotics. 1 ml of overnight culture was pelleted at 900x g for 5 minutes at RT, resuspended in 300 µl LB medium and mixed with 300 µl miniprep solution 1. The solution was mixed by inverting the tube and incubated for 5 minutes at RT to lyse the cell. The lysis was stopped by the addition of 300 µl miniprep solution 2 and the mixture was further incubated for 5 minutes at RT. The

sample was centrifuged at 14000x g for 5 minutes at RT to remove the bacterial debris. 800 µl of the supernatant was transferred to a new tube and the plasmid was precipitated by intense vortexing after adding 600 µl isopropanol. The plasmid was pelleted by centrifugation at 14000x g for 10 minutes at 4 °C and washed twice with 1ml ice-cold 70 % ethanol. The plasmid was air-dried and resuspended in 50 µl of miniprep resuspension buffer.

For preparative plasmid isolation (maxiprep), 1 ml of the overnight bacterial culture used for miniprep was further cultured overnight in 200 ml LB medium with antibiotics. The bacterial pellet was harvested by centrifugation at 9000x g for 25 minutes at 4 °C and the plasmid was isolated using PureLink HiPure Plasmid Maxiprep Kit according to the manufacturer's protocol. The extracted plasmid was solubilized in ddH_2O, and the concentration was adjusted at 1 mg/ml using NanoDrop 1000. The sequence of the plasmid was confirmed by Sanger sequencing.

3.2.8 RNA isolation

Total RNA was extracted using pegGOLD TriFast reagent. Media was removed from the adherent cells, whereas suspension cells were pelleted before lysis with 1 ml TriFast. The lysed cells were transferred to Eppendorf tubes, triturated 6x with a 0.6 mm syringe and incubated at RT for 5 minutes. To the lysate, 200 µl chloroform was added, vortexed intensely for 30 seconds, and centrifuged at 16,000x g for 10 minutes at 4 °C. The upper aqueous phase was transferred into another tube with 1 µl glycoblue and an equal volume of isopropanol was added. The resultant mixture was vortexed, incubated at -20 °C for at least 5 minutes, and centrifuged at 16,000x g for 10 minutes at 4 °C. The RNA pellet was washed twice with 75 % 1 ml ethanol, air-dried, and dissolved in 30 µl RNase-free ddH_2O. The concentration of the RNA was measured using NanoDrop and the RNA was either directly utilized for cDNA synthesis or flash frozen and stored at -80 °C.

For the RNA sequencing experiment, RNA was isolated using the miRNeasy Mini kit according to the manufacturer's protocol.

3.2.9 cDNA synthesis

For cDNA synthesis, 1 µl of the isolated RNA was mixed with 4 µl random primers to a final volume of 20 µl using ddH_2O. The solution was incubated at 65 °C for 1 minute and transferred to the ice for 2 minutes. To the mixture, 20 µl MLV buffer (5x), 0.4 µl Ribolock RNase inhibitor, 2.5 µl dNTPs (10 mM), and 2 µl MLV reverse transcriptase were added, and a final volume of 100 µl was maintained using ddH_2O. The resultant mixture was incubated at 23 °C for 10 minutes, followed by incubation at 37 °C for 50 minutes, and at 70 °C for 15 minutes. Finally, 400 µl of ddH_2O was added to the cDNA solution and stored at -20 °C until used for qPCR analysis.

3.2.10 Quantitative PCR (qPCR)

The SYBR Green Master mix was combined with 10 µM primer pairs in a ratio of 9:1. 10 µl of the resulting mixture was added to 10 µl of cDNA. The qPCR was performed in Real-Time PCR System using the following program:

Step	Temperature	Time	Cycles
Initial Denaturation	50 °C	2 min	1x
	95 °C	2 min	
Denaturation	95 °C	3 sec	40x
Annealing and extension	60 °C	30 sec	
Melt curve	95 °C	15 sec	1x
	60 °C	1 min	
	0.3 °C increment to 95 °C		
	95 °C	15 sec	

The relative mRNA expression of a protein of interest was normalized to housekeeping gene (B2-microglobulin) expression and calculated using C_T (cycle threshold) values.

3.3 Biochemical methods

3.3.1 Whole cell protein extracts

Depending on the experiment, the cells were lysed using 1 – 1.5x laemmli sample buffer, RIPA buffer, or IP buffer. The adherent cells were directly lysed in the cell culture plates and transferred to an Eppendorf tube, whereas suspension cells

were lysed after pelleting them via centrifugation. For laemmli whole cell extract, the cells were washed once with cold PBS and lysed using laemmli buffer. The lysates were incubated with 1 µl benzonase for at least 30 minutes at RT with constant shaking to reduce the viscosity. The samples were eventually denatured by heating at 95 °C for 5 min and stored at -20 °C.

For RIPA and IP lysate, the cells were washed twice with cold PBS and lysed with the corresponding lysis buffer in the presence of protease and phosphatase inhibitors. The cell lysates were incubated on a rotating wheel for 30 minutes at 4 °C and then centrifuged at 14,000 for 10 minutes at 4 °C to remove the cell debris. The supernatant was transferred to a new tube and stored at -20 °C (RIPA lysate) or flash-frozen and stored at -80 °C (IP lysate).

3.3.2 Protein concentration determination

RIPA lysates were pipetted in triplicates (1.5 µl each) in 96 well plate. As standards, BSA solutions with concentrations of 0, 0.5, 1, 2, 4, 8, and 16 mg/ml were used. To the lysate and standards, 150 µl of a mixture of BCA solutions A and B in a ratio of 50:1 was added. The plate was incubated for 15 minutes at 37 °C and the absorbance was measured at 550 nm using the Multiskan Ascent plate reader or Tecan Spark Multiplate reader. The protein concentration of the samples was calculated by comparing the standard curve generated from BSA dilutions.

3.3.3 Polyacrylamide Gel Electrophoresis (PAGE)

Based on the protein concentration of RIPA lysate, 6x laemmli and ddH_2O were added to the lysates to load an equal amount of protein (in the same volume). The samples were heated at 95 °C for 5 min. The samples were loaded on Bis-Tris polyacrylamide gel consisting of a 4 % stacking gel and an 8 – 12 % resolving gel. The electrophoresis was performed in ready-to-use MOPS running buffer at 80 – 100 V. Protein ladder was also loaded in the gel to determine the size and running behavior of the protein of interest.

3.3.4 Immunoblot

After separating the proteins according to their molecular weight by PAGE, the Whatman filter paper, methanol-activated PVDF membranes, sponges, and gel

were briefly incubated in the transfer buffer. Then a sandwich with the order: sponge, Whatman filter paper, gel, membrane, Whatman filter paper, and sponge was prepared. The transfer was carried out in a transfer chamber filled with running buffer at 300 mA for 3.5 hours at 4 °C. After transfer, the membranes were blocked with blocking solution for 1 hour at RT. Next, the membranes were briefly washed with TBS-T, cut into pieces for different proteins using the ladder as guide, and incubated with corresponding primary antibodies overnight at 4 °C. Next day, the membranes were washed with TBS-T and incubated with HRP-labelled secondary antibodies for 1 hour at RT. Finally, the membranes were washed with TBS-T and visualized using chemiluminescent HRP substrate in LAS4000 Mini.

3.3.5 HiBiT assay

The cells stably expressing HiBiT-tagged protein were seeded and treated with various compounds for desired time points. At the endpoint, the assay was performed using the HiBiT lytic detection system according to the manufacturer's instructions. Luminescence was measured on a GloMax 96 Microplate Luminometer or Tecan Spark Multiplate reader. DC_{50} was calculated using lower concentrations showing sigmoidal behavior with the dose−response (four parameters) equation in GraphPad Prism.

3.3.6 Luciferase assay

The cells stably or transiently expressing Nanoluciferase fusion proteins were seeded and treated with rapamycin or vehicle (DMSO) for desired time points. Afterward, the cells were lysed with Nano-Glo Luciferase Assay Reagent according to the manufacturer's protocol, and luminescence was measured on the Tecan Spark Multiplate reader with an integration time of 1 second.

3.3.7 HA immunoprecipitation

Cells stably expressing HA-tagged protein were washed with cold PBS and lysed in IP buffer (see section 3.3.1). For immunoprecipitation (IP), the lysate was used directly after lysis or thawed quickly by placing the frozen vial with lysate in a metal block if stored at -80 °C. The HA-coupled magnetic beads (20 µl per sample) were washed with IP buffer and incubated with lysate for 3 hours at 4 °C. Beads were then washed at least 4 times with IP buffer and eluted in 1x LDS buffer by

incubating for 30 min at 37 °C with 450 rpm shaking. Finally, the eluate was transferred to a new tube, DTT was added to the final concentration of 50 mM, heated at 95 °C for 5 min, and stored at -20 °C.

3.3.8 Cycloheximide assay

Cells were seeded one day before the cycloheximide (CHX) treatment. Then, the cells were treated with 10 – 50 µg/ml CHX with or without degrader for various time points. The cells were harvested in RIPA buffer (see section 3.3.1) and used for immunoblotting (see section 3.3.4). The intensity of the protein of interest band at timepoint zero was set as 1. The mean intensity for different timepoints were plotted as log_{10} values and half-life ($t_{1/2}$) was calculated in GraphPad Prism using nonlinear regression (curve fit) with a semilog line (x is linear and y is log).

3.3.9 Quantitative SILAC mass spectrometry

MV4-11 cells were grown in light, medium, and heavy labeled media for at least five doubling or until their labeling efficiency was more than 95 %. The cells were seeded at a density of 300,000 cells/ml (total 10 ml) in triplicates the day before treatment. The cells were treated with DMSO (light), JB170 (medium), and alisertib (heavy) for 6 hours. A total of 3.5 million cells per treatment (per replicate) were combined in a tube, washed twice with cold PBS supplemented with protease and phosphatase inhibitors, and lysed with 500 µl 1.5x laemmli sample buffer. To reduce the viscosity, the lysate was incubated with 25 U benzonase for 20 minutes at RT, followed by heating samples for 5 minutes at 95 °C.

Sample preparation after lysis and further analysis were performed by the research group of Andreas Schlosser (Rudolf Virchow Center, Wuerzburg). Briefly, the protein was precipitated using acetone at -20 °C overnight and washed three times with acetone. The protein pellet was dissolved in LDS sample buffer, reduced with 50 mM DTT, and alkylated with 120 mM iodoacetamide. The proteins were separated in NuPAGE Novex 4 – 12% Bis-Tris gels using MOPS buffer and stained with Simply Blue Safe Stain. Then the gels were washed with ddH_2O for 2 hours. Each gel lane was cut into 15 pieces and destained with 30 % acetonitrile in a 0.1 M ammonium bicarbonate of pH 8. Afterward, the bands were shrunk with 100 % acetonitrile, dried under vacuum, and digested with 0.1 µg trypsin (per gel band) in 0.1 M ammonium bicarbonate of pH 8 overnight at 37 °C. Peptides were extracted

from gel slices using 5 % formic acid and pooled together. The peptides were measured using nanoLC-MS/MS on the Orbitrap Fusion system. The raw MS files were analyzed with MaxQuant software (Cox & Mann, 2008) and UniProt human database search was done with Andromeda within MaxQuant. Protein identification was controlled with a false discovery rate (FDR) of <1 % on both protein and peptide levels. For SILAC-labeled protein quantification, means were calculated for log_2-transformed medium-to-light (M/L) and heavy-to-medium (H/L) peptide ratios for each protein. For each experiment, protein ratios were normalized in intensity bins.

3.3.10 Quantitative tandem mass tag (TMT) mass spectrometry

Four million IMR5 cells were seeded 24 hours before treatment with JB170, JB211, and alisertib for 6 hours. Four replicates were used for each treatment. Cells were washed twice with cold PBS and lysed with SDS buffer. The viscosity of the samples was reduced by sonication (15 cycles, 30 seconds sonication, 30 seconds pause, 4 °C) followed by heating for 10 minutes at 95 °C and the addition of trifluoroacetic acid to a final concentration of 1 %. The pH of the samples was neutralized with 300 mM *N*-methylmorpholine, and the protein amount was quantified using the BCA assay.

The proteins were cleaned up to remove the contaminants using the SP3 workflow. Briefly, per sample, 10 µl each of SeraMag-A and SeraMag-B magnetic beads were mixed, washed with ddH_2O, and added to 50 µg of the sample. The samples were incubated with 70 % acetonitrile and washed twice with 80 % ethanol. The beads with samples were reduced and alkylated with 10 mM DTT and 55 mM chloroacetamide, respectively, in a solution of 8 M urea in 40 mM Tris pH 7.6. The beads were incubated with 70 % acetonitrile, washed with 80 % ethanol, air-dried, and kept in 25 mM HEPES pH 8.5. The protein was digested with trypsin overnight at 37 °C, centrifuged, sonicated, and the supernatant was collected. The peptides were further released from pelleted beads by the addition of ddH_2O and sonication. The supernatant was collected and combined to the previous supernatant. The peptide concentration was determined using NanoDrop and 20 µg peptides per condition were labeled with tandem mass tags 11 (TMT11)-plex (Thermo Fisher Scientific). Three samples were from the JB211 treatment, and four samples each from JB170 and alisertib treatments. TMT labeled samples were measured by LC-

MS/MS using Dionex UltiMate 3000 RSLCnano System coupled to an Orbitrap Fusion Lumos mass spectrometer (Thermo Fisher Scientific). The MS3 files were analyzed with MaxQuant software (Cox & Mann, 2008) to quantify and identify proteins and peptides. Andromeda was used to search all canonical protein sequences in the UniProt reference database. The protein and peptide identification were regulated by keeping the minimum peptide length to seven and protein FDR to 1 %. The resultant data were analyzed using the Perseus software suite (Tyanova et al., 2016) and Microsoft Excel to calculate the p-values and log_2FC between different treatments. Replicate 4 of the JB170 treatment was detected as a technical outlier and excluded from the analysis. The sample preparation after lysis and further analysis was performed by Stephanie Heinzlmeir from the group of Prof. Dr. Bernhard Kuster (Technical University of Munich).

3.3.11 Quantitative unlabeled mass spectrometry

Four million MV4-11 cells in 10 ml were seeded the evening before and treated with AD100, AD122, JW48, JW39, and DMSO for 9 hours. Four replicates were used per treatment. The cells were lysed, and protein concentration was quantified as in TMT mass spectrometry (MS) (see section 3.3.10)

The samples were continued with SP3 workflow followed by trypsinization and release of peptides from beads as in TMT-MS (see section 3.3.10). However, a total of 200 µg sample was used for unlabeled MS, while 50 µg was used in TMT-MS. Further, the peptide supernatants were acidified with formic acid (final concentration 1 %), desalted with solid-phase extraction cartridges, and dried in a SpeedVac. The sample was reconstituted in 0.1 % formic acid and peptide concentration was determined using NanoDrop. 50 µg of peptides per sample was analyzed by LC-MS/MS setup with a Q Exactive HF-X mass spectrometer (Thermo Fisher Scientific). The protein and peptide identification and quantification were performed with MaxQuant with minimum peptide length set to seven and protein FDR to 1 %. Perseus software suite and Microsoft Excel were used for data analysis and calculating p-values and log_2FC between various treatments. Replicate 1 of the JW39 treatment showed significant differences with other samples and was not used for the analysis. The sample preparation after lysis and further analysis was performed by Nicola Berner from the group of Prof. Dr. Bernhard Kuster (Technical University of Munich).

3.3.12 Immunoprecipitation mass spectrometry

MV4-11 cells stably expressing HA-tagged Aurora-A and control cells were washed twice with cold PBS and lysed in MS IP buffer containing protease and phosphatase inhibitor by homogenization and sonication. The chromatin-bound proteins were solubilized by incubation with 100 U/ml benzonase at 4 °C for 40 minutes. Next, the soluble protein fraction was immunoprecipitated with 80 µl HA-coupled magnetic beads at 4 °C for 3 hours with constant mixing. Beads were washed three times with MS IP buffer supplemented with 0.1 % TritonX-100 and two times with MS IP buffer. The elution was performed with 100 µl 1x LDS buffer by incubation at 37 °C for 30 minutes, and the eluted proteins were reduced with 50 mM DTT, followed by heating for 5 minutes at 95 °C.

The eluted proteins were alkylated with 120 mM iodoacetamide, precipitated with acetone at -20 °C overnight, and washed thrice with acetone. The digestion was carried out with LysC protease in 0.5 % sodium deoxycholate and trypsin. The digested peptides were extracted in sodium deoxycholate using 0.5 % trifluoroacetate and ethyl acetate. The peptides were dried under vacuum and desalted using three C18 Empore SPE disks (3 M). The peptides were eluted with 0.1% formic acid and 60% acetonitrile, dried under vacuum, and dissolved in 0.1% formic acid and 2 % acetonitrile. NanoLC-MS/MS on the Orbitrap Fusion system was used for the measurement of samples. The raw MS files were analyzed with MaxQuant software and the search for protein sequence was performed against the UniProt human database with Andromeda. FDR of <1 % was used on protein and peptide levels to control protein identification. Label-free quantitation (LFQ) intensities were used for protein quantitation and the p-values were calculated in the limma package in R using the linear method. The immunoprecipitation was performed by Julia Hoffstetter from the group of Prof. Dr. Elmar Wolf (University of Wuerzburg) and further sample preparation of eluted HA-immunoprecipitated material along with analysis was performed by the research group of Andreas Schlosser (Rudolf Virchow Center, Wuerzburg).

3.3.13 Kinobead selectivity profiling

The kinobead selectivity profiling experiments were performed by Stephanie Heinzlmeir from the group of Prof. Dr. Bernhard Kuster (Technical University of

Munich). MV4-11 cells were lysed with kinobead buffer supplemented with protease and phosphatase inhibitors, and the lysate was ultracentrifuged. The supernatant was diluted with kinobead buffer without NP-40 to a concentration of 5 mg/ml. For selectivity profiling, 2.5 mg protein per pulldown was pre-incubated with DMSO and an increasing concentration of JB170 and alisertib before incubating with kinobeads epsilon. The proteins bound to beads were eluted by 2x LDS sample buffer, reduced by 50 mM DTT, and alkylated by 55 mM chloroacetamide. The protein was concentrated and desalted by short PAGE followed by tryptic in-gel digestion.

The digested peptides were measured using a nano HPLC system coupled with Orbitrap Fusion Lumos mass spectrometer. The peptides and proteins were identified by searching against the UniProt reference database and quantified using MaxQuant and Andromeda. To make the identification stringent, protein FDR of 1 % and the minimum amino acid length of seven were set. For the binding assay, relative binding was calculated based on the LFQ intensity ratio of every concentration of JB170 or alisertib to that of DMSO. The binding constant (K_d^{app}) was calculated from EC_{50} derived from a four-parameter log-logistic regression using the 'drc' package in R and correction factor.

3.3.14 RNA-sequencing (RNA-seq)

RNA was isolated from MV4-11 cells after DMSO, JB170, and alisertib treatment using miRNeasy Mini kit (see section 3.2.8). The RNA quality was analyzed using a Fragment analyzer and 1 µg of total RNA was used to isolate mRNA using NEBNext Poly(A) mRNA magnetic isolation module following the manufacturer's instructions. Library preparation was performed using the NEBNext Ultra II Directional RNA Library Prep Kit for Illumina using the manufacturer's protocol. The libraries were amplified with 8 PCR cycles, and library size and concentration were determined with the Fragment Analyzer High Sense DNA kit. The sequencing was performed on a NextSeq500 Illumina platform for 75 cycles. The data was analyzed by Apoorva Baluapuri from the group of Prof. Dr. Elmar Wolf (University of Wuerzburg).

3.4 Computational methods

The computational experiments were performed by Mathias Diebold from the group of Prof. Dr. Christoph Sotriffer (University of Wuerzburg). Briefly, the complex of Aurora-A with alisertib was prepared using the crystal structure of Aurora-A with MLN8054 (PDB 2X81) (Sloane et al., 2010) and Aurora-A PDB structure 6R4A (R. Zhang et al., 2019). The CRBN/lenalidomide complex was obtained from the crystal structure of CRBN and DDB1 in complex with lenalidomide (Chamberlain et al., 2014). The Aurora-A/alisertib complex and the CRBN/lenalidomide complex were used for protein/protein docking within the molecular operating environment (MOE) ("Molecular Operating Environment (MOE)," 2019). The Aurora-A/alisertib was used as a ligand, whereas the CRBN/lenalidomide complex was used as a receptor, with lenalidomide atoms as a binding site. The 100 solutions generated were checked for the compatibility with the linker used in JB170. Rank 1 and rank 15 were the best two solutions compatible for modification and joining the alisertib and lenalidomide with the JB170 linker. Finally, the contribution of Aurora-A side chains for the formation of the ternary complex was determined using molecular dynamics simulations where Aurora-A and JB170 served as receptor and CRBN as ligand.

4 Results

The result chapter is subdivided into three sub-chapters. The first two sub-chapters detail the targeted protein degradation approach for two Myc-interacting oncogenes, Aurora-A and WDR5. The third sub-chapter describes an assay to predict the E3-ligase that can successfully degrade the target protein.

4.1 Aurora-A degradation

A substantial part of the results shown in this section was published in Adhikari, Bozilovic et al. (Adhikari et al., 2020). Additional data, which was performed by others but is required to convey the message, are acknowledged and cited accordingly. Most of the figures presented in this section are modified or taken from Adhikari et al., 2020.

4.1.1 Design of Aurora-A PROTACs

For the synthesis of Aurora-A PROTACs, the Aurora-A inhibitor alisertib (MLN8237) was used as Aurora-A warhead. Alisertib was previously characterized as a selective and effective Aurora-A inhibitor (Manfredi et al., 2011; Sells et al., 2015). Since the crystal structure of Aurora-A with structurally similar compound MLN8054 was reported (Sloane et al., 2010), the design of PROTACs was straightforward. While bound with Aurora-A, the carboxyl group of MLN8054 was exposed to solvent, which was an ideal attachment point for the linker (Fig. 4.1a). Then, the alisertib-coupled linker was either connected to thalidomide to recruit Cereblon (CRBN) or to VHL-ligand to harness von Hippel-Lindau Tumor Suppressor (VHL). Altogether, five PROTACs with thalidomide (JB158, JB159, JB169, JB170, and JB171) and two PROTACs with VHL-ligand (JB160 and JB161) were synthesized (Fig. 4.1b). For the synthesis of thalidomide-based PROTACs, polyethylene glycol (PEG) and aliphatic linkers were used, whereas for VHL-based degraders only PEG linkers were used. All the PROTACs were synthesized by Jelena Bozilovic, from the group of Prof. Dr. Stefan Knapp, Goethe-Universität Frankfurt.

Target engagement assay and thermal shift assay were performed to validate the binding of the degraders to Aurora-A. Both assays showed that all the degraders bind to Aurora-A but with different affinities (Adhikari et al., 2020).

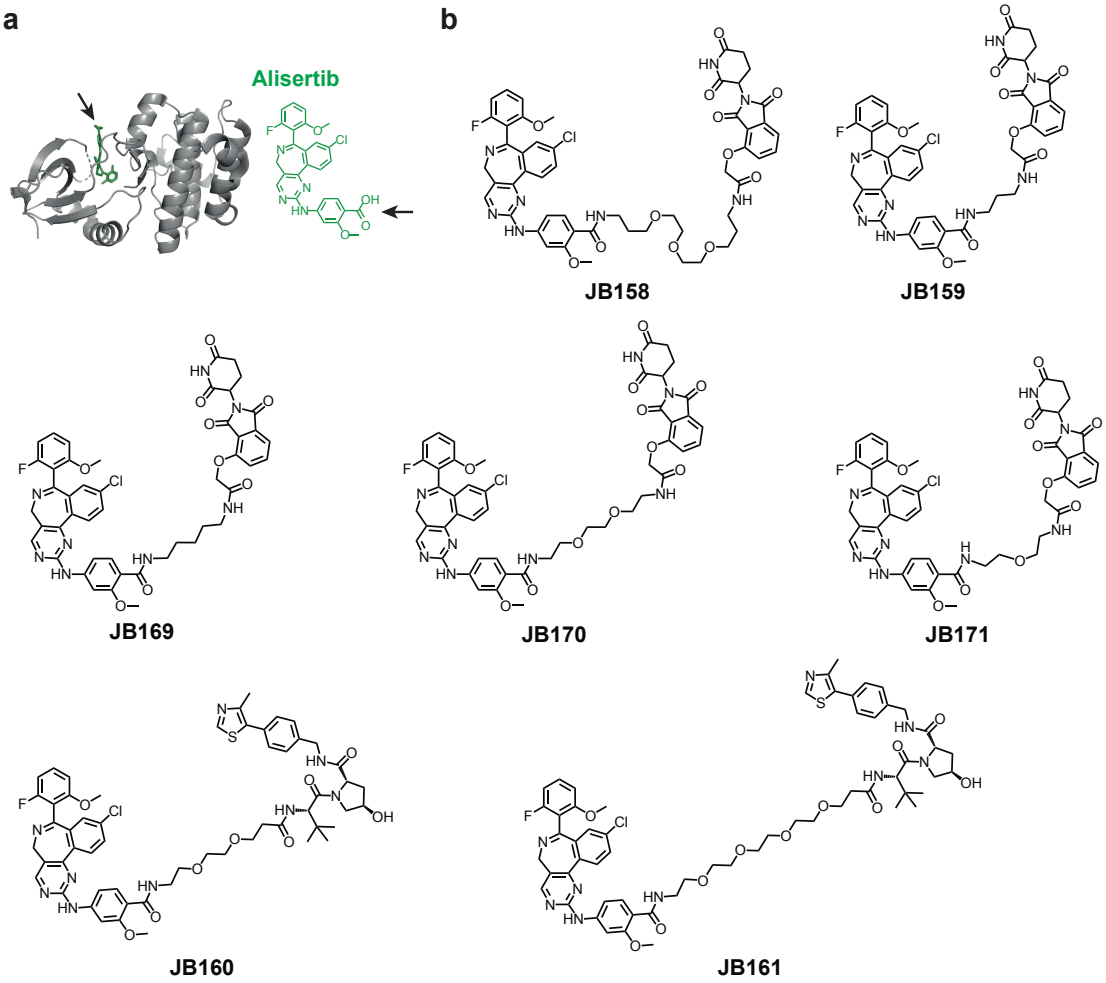

Figure 4.1: Design and structure of Aurora-A PROTACs.

(a) *Crystal structure of Aurora-A and structure of alisertib. The structure of Aurora-A with MLN8054 (PDB: 2X81) showing its free carboxyl group exposed to the solvent (highlighted by an arrow). This carboxyl group of alisertib (highlighted by an arrow) was used to attach the linkers.* ***(b)*** *Structure of Aurora-A PROTACs. Five degraders (JB158, JB159, JB169, JB170, and JB171) were cereblon-recruiting and two degraders (JB160 and JB161) were VHL-recruiting. The compounds were synthesized by Jelena Bozilovic.*

The figures were taken and modified from Adhikari et al., 2020.

4.1.2 Evaluation of Aurora-A PROTACs

4.1.2.1 CRBN-based PROTACs, JB158 and JB170 induced Aurora-A degradation

4.1.2.1.1 Cereblon-based JB170 and JB158 robustly reduce Aurora-A levels

All synthesized PROTACs were investigated for their ability to degrade Aurora-A in cellular systems. For this, the acute myeloid leukemia (AML) cell line, MV4-11 was used. The cells were treated with a single dose of the degraders. After 6 hours, proteins were harvested from the treated cells and immunoblotting was performed with antibodies against Aurora-A and Vinculin as a loading control. The upper band recognized by the Vinculin antibody is a Vinculin splice variant called Meta-vinculin (Fig. 4.2a). The upper band were detected in some cell lines used in this study like MV4-11 and HLE. The comparison of the Aurora-A levels to their corresponding vehicle (dimethyl sulfoxide, DMSO) treated control showed that VHL-based PROTACs (in orange) could not reduce the protein level of Aurora-A (Fig. 4.2a, b). However, all five CRBN-based degraders (in blue) were able to decrease the steady state levels of Aurora-A. JB158 and JB170 were the most potent PROTACs and degraded 62% and 69% of Aurora-A, respectively (Fig. 4.2b) as quantified from four independent experiments. Due to their better degradation efficiency, these two compounds were further characterized.

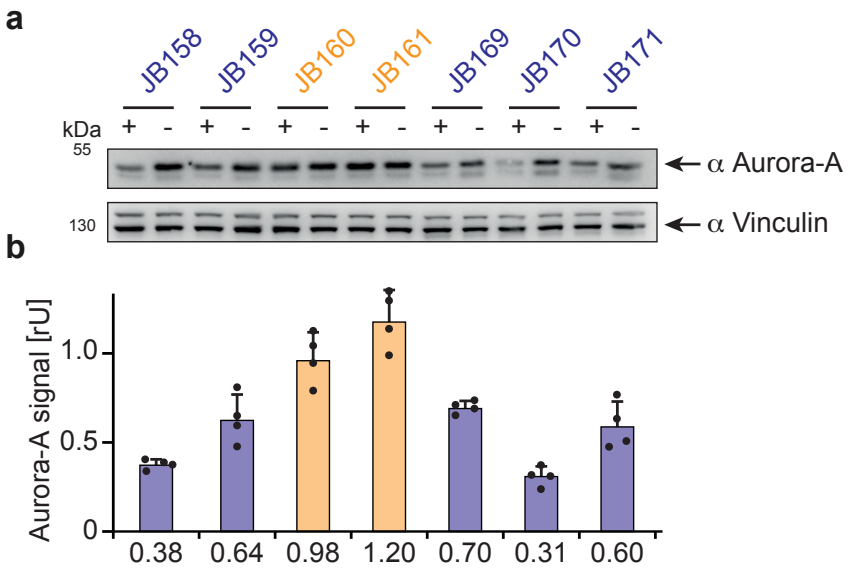

Figure 4.2: Assessment of Aurora-A PROTACs.

(a) *Immunoblot of Aurora-A. MV4-11 cells were treated with CRBN-recruiting (blue) and VHL-recruiting (orange) PROTACs for 6 hours, and the Aurora-A levels were*

quantified against the vehicle-treated controls. JB159 and JB171 were used at 1 μM, whereas the rest were 0.1μM. Vinculin was used as a loading control (as in all other immunoblotting experiments in this thesis). ***(b)*** *The quantification of Aurora-A degradation by different PROTACs. The bars represent mean ± SD from four biological replicates. One of the replicate is shown in (a).*
The figures were taken and modified from Adhikari et al., 2020.

4.1.2.1.2 Both JB170 and JB158 degrade Aurora-A rapidly

Time-course experiments were performed to check the swiftness of the degradation. For this, the MV4-11 cells were treated with 100 nM JB158 or JB170, or DMSO, and harvested after various time points. Indeed, immunoblotting revealed that both PROTACs degraded Aurora-A rapidly. Both degraders reduced ~25% of Aurora-A within 1 hour of treatment and ~65% after 3 hours (Fig. 4.3a, b). The degradation was persistent for 24 hours with 50% Aurora-A degradation by both degraders.

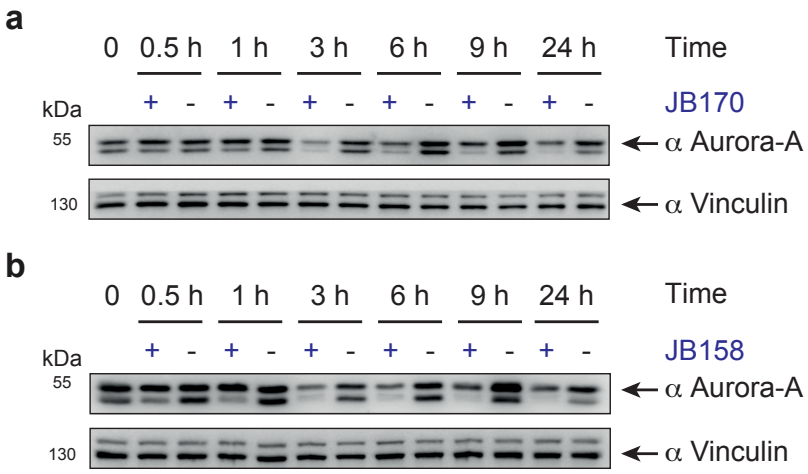

Figure 4.3: Time-course of JB170 and JB158.
(a, b) *Immunoblots of Aurora-A. MV4-11 cells were treated with 0.1 μM (a) JB170 or (b) JB158 for designated time points, and Aurora-A levels were compared to vehicle-treated cells by immunoblotting.*
The figures were taken and modified from Adhikari et al., 2020.

4.1.2.1.3 Optimal concentration of degradation is between 0.1 to 1 μM

Next, concentration course experiments were performed to determine the concentration of PROTAC for optimal Aurora-A degradation. MV4-11 cells were treated with 10 nM, 0.1 μM, 1 μM, and 10 μM concentrations of JB158 or JB170 for 6 hours. Furthermore, as a control, the Aurora-A warhead alisertib was added at 1 μM. Around 40% degradation of Aurora-A was observed at 10 nM, whereas degradation of 89% and 75% was observed at 0.1 μM and 1 μM of JB170,

respectively (Fig. 4.4a). However, the highest concentration of JB170, 10 µM, did not induce any degradation. This effect is described as “Hook effect”, where at high PROTAC concentrations binary complexes (JB170: Aurora-A and JB170: CRBN) are predominant and prevent ternary complex (Aurora-A: JB170: CRBN) formation (Douglass et al., 2013; Pettersson & Crews, 2019). Moreover, as expected, alisertib did not induce protein degradation but even increased Aurora-A levels (Fig. 4.4a). It can be speculated that alisertib addition might increase Aurora-A protein stability and this effect has been previously reported (Buchel et al., 2017; Gustafson et al., 2014). Similar observations were made for JB158 (Fig. 4.4b). Thus, for all the subsequent cellular experiments, PROTAC concentrations between 0.1 µM and 1 µM was used.

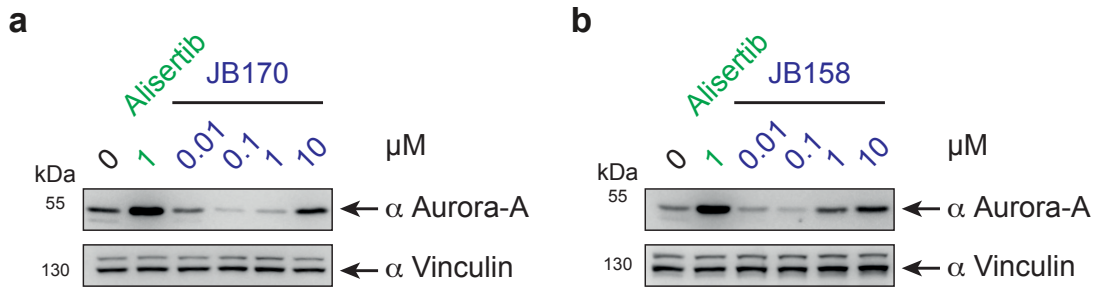

Figure 4.4: Concentration-course of JB170 and JB158.
(a, b) *Immunoblots of Aurora-A. MV4-11 cells were treated with 1 µM alisertib and indicated concentrations of (a) JB170 or (b) JB158 for 6 hours, and Aurora-A levels were compared to vehicle-treated cells by immunoblotting.*
The figures were taken and modified from Adhikari et al., 2020.

4.1.2.1.4 HiBiT assay for optimal concentration of JB170

Along with immunoblots, a HiBiT assay was performed to confirm the degradation efficiency of JB170. HiBiT assay is a split luciferase assay, in which the 1.3 kDa HiBiT peptide makes a functional nanoluciferase (NLuc) when complemented with the 18kDa subunit of NLuc, LgBiT (Schwinn et al., 2018). So, the C-terminus of Aurora-A was tagged with HiBiT, and MV4-11 cells were generated stably expressing this Aurora-A-HiBiT construct. The cells were then treated for 6 hours with 3-fold serially diluted JB170 with starting concentration of 25 µM. After the treatment, cells were lysed, complemented with LgBiT, and luminescence was measured to quantify the Aurora-A levels. Similar to the immunoblot result, the three highest concentrations of JB170 induced less or no degradation due to the Hook-effect (Fig. 4.5). The maximum degradation of 63.4% was achieved at 300 nM (DC_{max}) and the half-maximal degradation was observed at 28 nM (DC_{50}) (Fig.

4.5). The HiBiT assay, thus, reconfirmed an optimal degradation concentration of JB170 was between 0.1 to 1 µM.

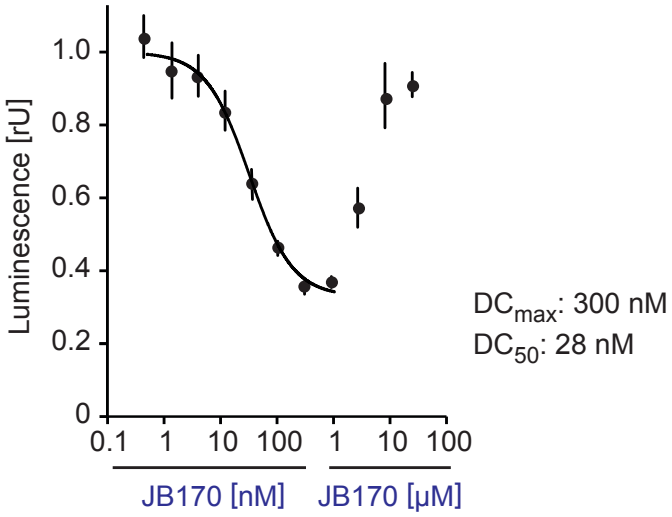

Figure 4.5: HiBiT assay with JB170.
Aurora-A levels based on luciferase measurements. MV4-11 cells stably expressing Aurora-A-HiBiT were treated with various concentrations of JB170 for 6 hours, lysed, and complemented with LgBiT, and luminescence was measured to quantify Aurora-A levels. DC_{max}, concentration for maximal degradation; DC_{50}, concentration for half of the maximal degradation. DC_{50} was calculated with the sigmoidal dose-response (four parameters) equation using only the lower eight concentrations. The data represent mean ± SD from three replicates.
The figure was taken and modified from Adhikari et al., 2020.

Hence, out of initially tested seven PROTACs, only the CRBN-recruiting degraders were successful in Aurora-A degradation. Among those five CRBN-based degraders, JB170 and JB158 showed strong and fast depletion of Aurora-A at concentrations between 0.1 and 1 µM.

4.1.2.2 Aurora-A degradation is via ubiquitin-proteasome system

Further experiments were performed to prove that the observed reduction in Aurora-A levels was via PROTAC-induced ubiquitination and proteasomal degradation and not by any other mechanisms.

4.1.2.2.1 JB170 and JB158 do not decrease Aurora-A mRNA levels

The first experiment was to inspect the changes in Aurora-A transcripts after PROTAC treatment. MV4-11 cells were treated with 100 nM JB170, alisertib, or vehicle for 6 hours and 24 hours. The same cell suspension was used to check Aurora-A protein level by immunoblot and mRNA level by quantitative PCR

(qPCR). Even though JB170 decreased the Aurora-A protein level at both time points (Fig. 4.6a), mRNA levels were not diminished, but rather increased by 25% and 38% after 6 and 24 hours of JB170 treatment (Fig. 4.6b). On the one hand, due to this increase in mRNA level, the actual decrease of Aurora-A protein level after JB170 treatment might have been underestimated when comparing to vehicle treatment. On the other hand, alisertib increased both the protein and mRNA levels after 6- and 24-hours treatment (Fig. 4.6b). The increase in Aurora-A mRNA might be due to the feedback loop on loss of Aurora-A function. Likewise, JB158-treated MV4-11 cells showed a similar decrease in Aurora-A protein but not mRNA levels after 6 hours (Fig. 4.6c, d). Thus, the observed decrease in Aurora-A protein level by both degraders was not due to changes in Aurora-A transcription.

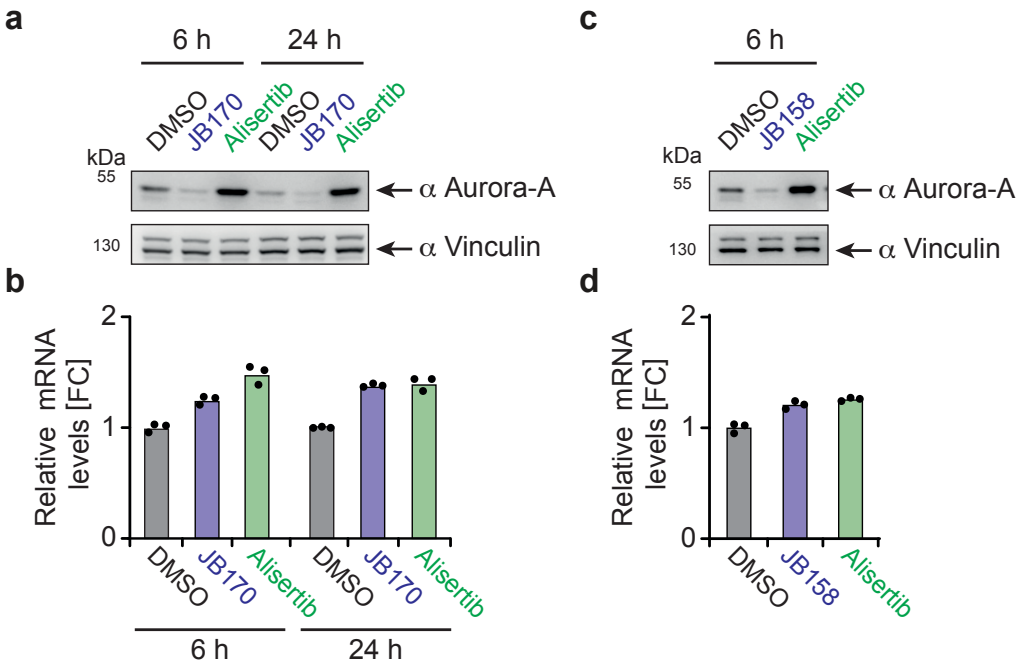

Figure 4.6: Aurora-A transcript levels after JB170 and JB158 treatment.
(a) *Aurora-A protein levels in response to JB170. MV4-11 cells were treated with 0.1 µM JB170 or alisertib for 6 and 24 hours. Proteins were isolated and Aurora-A levels were analyzed by immunoblot.* ***(b)*** *Aurora-A mRNA levels in response to JB170. RNA was isolated from MV4-11 after treatment with 0.1 µM JB170 or alisertib. Aurora-A mRNA levels were analyzed by quantitative rtPCR. Aurora-A expression levels were normalized to vehicle-treated cells (DMSO). Bars represent the mean of technical replicates.* ***(c)*** *Aurora-A protein levels in response to JB158. MV4 -11 cells were treated for 6 hours with 0.1 µM JB158 or alisertib and Aurora-A levels were analyzed by immunoblot.* ***(d)*** *Aurora-A mRNA levels in response to JB158. Aurora-A mRNA levels were analyzed by quantitative rtPCR after 6 hours treatment with 0.1 µM JB158 or alisertib. Bars represent the mean of technical replicates.*
The figures were taken and modified from Adhikari et al., 2020.

4.1.2.2.2 JB170 diminishes Aurora-A protein stability

Since both PROTACs behaved similar so far, further characterization was done for JB170 only. To measure the steady-state protein stability, cycloheximide (CHX) chase assay was performed in the presence and absence of JB170. CHX prevents protein synthesis by inhibiting the translocation step during protein translation (Schneider-Poetsch et al., 2010). Thus, this assay helps to determine the degradation kinetics and half-life of the target protein. MV4-11 cells were treated with 10 µg/ml CHX in the presence of either vehicle or 1 µM JB170 for different time points. Then Aurora-A abundance was quantified based on immunoblots. JB170 treatment reduced the Aurora-A half-life from 3.8 to 1.3 hours (Fig. 4.7a, b), confirming Aurora-A protein degradation by JB170.

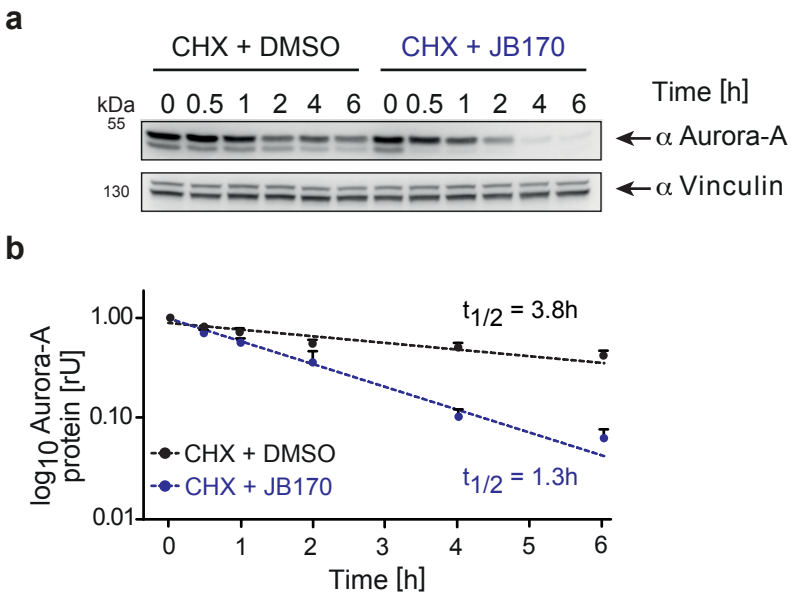

Figure 4.7: Aurora-A protein stability after JB170 treatment.
(a) *Cycloheximide (CHX) chase assay with JB170. MV4-11 cells were incubated with 10 µg/ml CHX for indicated time points in the presence or absence of 1 µM JB170. Aurora-A protein level was evaluated by immunoblotting.* ***(b)*** *The quantification of Aurora-A half-life. MV4-11 cells were treated with JB170 for various time-points, Aurora-A levels were quantified, and half-life ($t_{1/2}$) was calculated by linear regression. The data represent mean ± SEM from three biological replicates. One of the replicate is shown in (a).*
The figures were taken and modified from Adhikari et al., 2020.

4.1.2.2.3 JB170-mediated degradation requires Cereblon and Aurora-A binding

The binding of the PROTAC to the POI and the E3-ligase is essential for the functionality of the PROTAC. Blocking this binding should abrogate PROTAC-

mediated degradation. To test this, MV4-11 cells were treated with 0.1 µM JB170 in the presence of increasing concentrations of POI and E3-ligase warheads, alisertib and thalidomide, respectively. Co-incubation of the warheads completely abrogated the JB170-induced Aurora-A degradation (Fig. 4.8a, b). However, the concentration of the ligands required for complete rescue were different. For complete abrogation of degradation, 100 nM alisertib was sufficient (Fig. 4.8a), whereas 20 µM thalidomide was required (Fig. 4.8b). This discrepancy in concentration was possibly due to the diverse cellular levels of Aurora-A and CRBN and the different cell permeability of the ligands.

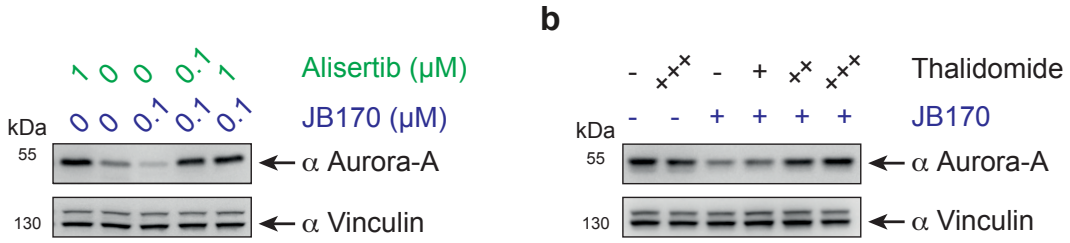

Figure 4.8: Competition assay of JB170 with Aurora-A and CRBN ligands.
(a, b) *Immunoblots of Aurora-A. MV4-11 cells were treated with 0. 1 µM JB170 and various concentrations of (a) alisertib or (b) thalidomide for 6 hours and compared to single compound or vehicle-treated cells. +: 1 µM, ++: 10 µM and +++: 20 µM.*
The figures were taken and modified from Adhikari et al., 2020.

4.1.2.2.4 Proteasomal and neddylation inhibition blocks JB170-mediated degradation

To further demonstrate UPS-mediated Aurora-A degradation by JB170, the inhibitors MG132 and MLN4924 were used. MG132 is a 26S proteasomal inhibitor (Lee & Goldberg, 1998), and MLN4924 is an inhibitor of the NEDD8-activating enzyme (NAE) (Soucy, Smith, Milhollen, et al., 2009). The Cullin-RING ubiquitin E3-ligases (CRLs) like $CRL4^{CRBN}$ are activated only after conjugation of NEDD8, which is mediated by NAE (Soucy, Smith, & Rolfe, 2009). The co-treatment of MV4-11 cells with JB170 and 10 µM MG132 or 3 µM MLN4924 suppressed the degradation of Aurora-A (Fig. 4.9a, b), displaying the dependence on $CRL4^{CRBN}$ and the proteasome.

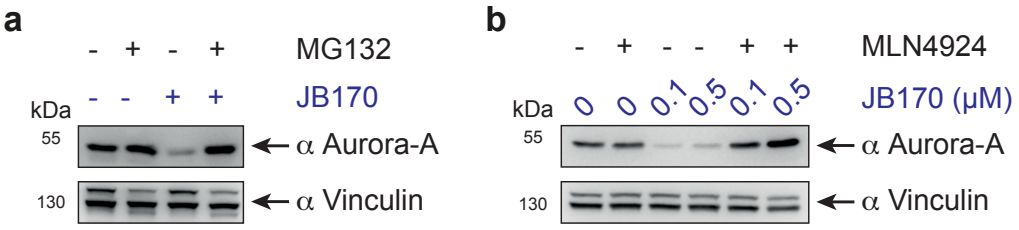

Figure 4.9: Effect of proteasomal and neddylation inhibition on JB170-mediated Aurora-A degradation.

(a) *Immunoblots of Aurora-A. MV4-11 cells were treated for 6 hours with 0.1 μM JB170 and 10 μM MG132 as indicated.* ***(b)*** *Immunoblots of Aurora-A. MV4-11 cells were incubated with specified concertation of JB170 and 3 μM MLN4924 for 6 hours.*
The figures were taken and modified from Adhikari et al., 2020.

4.1.2.2.5 N-methylated JB170 analog does not degrade Aurora-A

The NH group in the glutarimide ring of thalidomide is vital for its binding to CRBN and methylation of this residue causes a substantial loss of CRBN binding (Lu et al., 2015). So, the N-methylated JB170 analog, named JB211, was synthesized and its efficiency in degrading Aurora-A was assessed (Fig. 4.10a). As expected, JB211 did not induce Aurora-A degradation in MV4-11 cells after 6 hours of treatment, while JB170 caused substantial degradation using similar concentrations (Fig. 4.10b). JB211 was synthesized by Jelena Bozilovic.

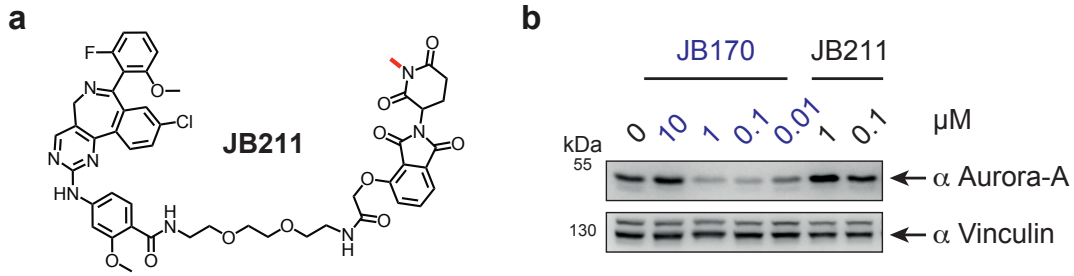

Figure 4.10: N-methylated JB170 analog does not degrade Aurora-A.

(a) *Structure of N-methylated JB170 analog, JB211. The methyl group in the glutarimide ring of thalidomide is highlighted by a red line.* ***(b)*** *Immunoblot of Aurora-A. MV4-11 cells were treated with indicated concentrations of JB170 or JB211 for 6 hours and compared to vehicle-treated cells.*
The figures were taken and modified from Adhikari et al., 2020.

These experiments proved the functionality of the PROTAC JB170 in the leukemia cell line MV4-11. To validate its effectiveness in other cell lines as well, JB170 was used in neuroblastoma (IMR5 and NGP), osteosarcoma (U2OS), hepatocellular carcinoma (HLE), breast cancer (MCF7), colorectal carcinoma (LS174T), lung carcinoma (NCI-H1299), and cervical cancer (HeLa) cell lines. Like in MV4-11 cells, JB170 rapidly reduced Aurora-A levels in all these cancer cell lines (Fig.

4.11a-h). This revealed that JB170 is potent across various cancer entities, and JB170-mediated Aurora-A degradation was not cell-line dependent.

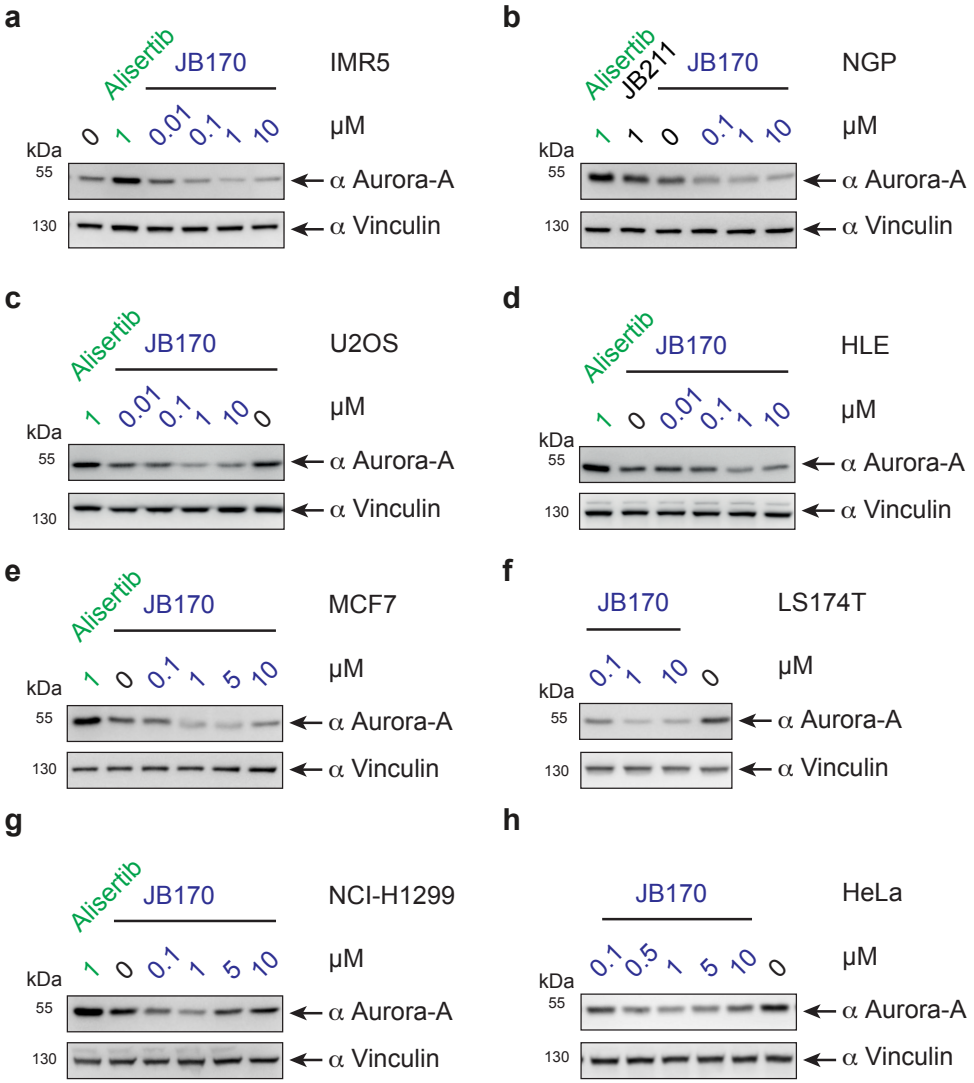

Figure 4.11: JB170-mediated Aurora-A degradation in various cancer cell lines. ***(a-h)*** *Immunoblots of Aurora-A. (a) IMR5, (b) NGP, (c) U2OS, (d) HLE, (e) MCF7, (f) LS174T, (g) NCI-H1299, and (h) HeLa cells were incubated with the specified concentration of JB170 for 6 hours and compared to control cells (0 μM).*
The figure panels (c) and (d) were taken and modified from Adhikari et al., 2020.

In summary, all the experiments undoubtedly demonstrated that upon JB170 treatment the Aurora-A protein level decreases via the PROTAC mode of action.

4.1.3 Aurora-A PROTAC JB170 is highly specific

Immunoblots showed JB170 degraded Aurora-A in various cell lines. However, the ability of JB170 to bind and degrade Aurora-A from a plethora of cellular proteins was not possible to assess using immunoblots. So, the binding and degradation

potential of JB170 were characterized on a large-scale using Kinobead selectivity profiling and quantitative proteomics.

4.1.3.1 Kinobead assay shows JB170 is more specific than its warhead

In order to study the binding characteristics of the Aurora-A warhead, alisertib and the PROTAC JB170 towards various proteins in the cells, kinobead selectivity profiling was performed in MV4-11 cells. The profiling was done by Stephanie Heinzlmeir from the group of Prof. Dr. Bernhard Kuster, Technical University of Munich. A kinobead assay utilizes beads containing immobilized ATP-competitive broad-spectrum kinase inhibitors (Klaeger et al., 2017). The cell lysate was incubated with increasing concentration of compounds and subsequently incubated with kinobeads. Depending on the binding affinity of the compound to the proteins, the proteins were enriched in the kinobeads. The higher the compound's affinity, the less protein binds to kinobeads. Finally, the proteins were pulled-down and analyzed via mass spectrometry and compared to the DMSO control.

As expected, alisertib bound to Aurora-A with the maximal affinity, K_d^{app}, of 7 nM (Fig. 4.12a, b). However, it was also bound by various other ATP-binding proteins like ACAD10, Aurora-B, ABL2, and AK2 with the affinity (K_d^{app}) of 19 nM, 92 nM, 214 nM, and 215 nM, respectively. Similarly, JB170 bound Aurora-A strongest with 99 nM K_d^{app}, but also to ACAD10 (K_d^{app}:253 nM) and Aurora-B (K_d^{app}:5102 nM) (Fig. 4.12a, b). The affinity differed between Aurora-A and Aurora-B and was more pronounced for JB170 than for alisertib. Aurora-A to Aurora-B binding affinity for JB170 was 52-fold higher, whereas for alisertib was 13-fold. Moreover, JB170 lost binding to several targets compared to alisertib, possibly due to steric hindrances. The kinobead selectivity profiling showed that JB170 was more selective and specific for Aurora-A than alisertib.

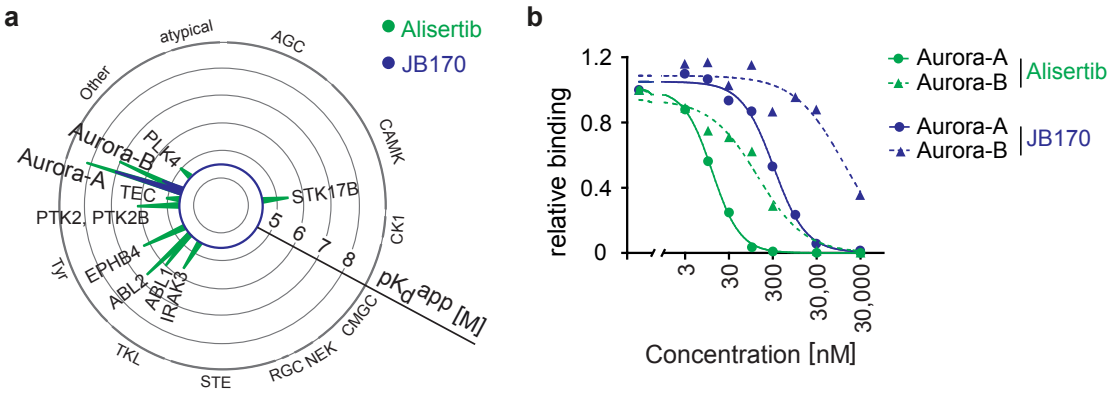

Figure 4.12: Kinobead selectivity profiling with JB170 and alisertib.
(a) *Radar plot for JB170 and alisertib. Shown are the kinobead selectivity profiles of JB170 (blue) and alisertib (green) in MV4-11 cell lysate. Each spike depicts a protein, and the spike's length indicates binding affinity, pK_d^{app} ($-log_{10}K_d^{app}$).* ***(b)*** *Full dose-response curves of Aurora-A and -B for JB170 and alisertib. The curve shows the relative binding of Aurora-A and -B to kinobeads at various concentrations of alisertib and JB170. K_d^{app} was calculated using four-parameter non-linear regression. These experiments were performed by Stephanie Heinzlmeir.*
The figures were taken and modified from Adhikari et al., 2020.

4.1.3.2 SILAC mass spectrometry in MV4-11 cells shows JB170 is specific

Proteomics analysis was conducted with MV4-11 cells in a quantitative and unbiased manner to investigate the selectivity of JB170 towards Aurora-A. Stable isotope labeling by amino acids in cell culture (SILAC) mass spectrometry approach was used, which has the advantage of quantitative accuracy and reproducibility. MV4-11 cells were cultured in light, medium, and heavy medium until more than 95% of proteins were labeled with the respective amino acid isotope. Then, the cells were treated for 6 hours with vehicle (light), 0.1 µM JB170 (medium), and 0.1 µM alisertib (heavy) in triplicate experiments. An equal number of cells from each condition was combined, lysed, digested with trypsin, and subsequently analyzed by mass spectrometry. The analysis was performed by Andreas Schlosser from Rudolf Virchow Center, University of Wuerzburg.

In the analysis more than 4200 proteins were identified in all conditions. In both comparisons, JB170- vs vehicle-treated and JB170- vs alisertib-treated, only Aurora-A was downregulated fulfilling the criteria of p-value < 0.001 and log_2FC of < -1 (Fig. 4.13a). JB170 degraded 73% Aurora-A with a p-value of $1.68x\ 10^{-5}$ when compared to alisertib treatment (Fig. 4.13a) and 57% with a p-value of $4.2x\ 10^{-5}$ in comparison to vehicle treatment (Adhikari et al., 2020). The changes in abundance of Aurora-B, another mitotic kinase and member of the Aurora kinase family with

high structural similarity with Aurora-A, were not statistically significant (Adhikari et al., 2020). Most importantly, the abundance of none of the alisertib-binding proteins (in orange) was significantly altered upon JB170 treatment. Unfortunately, ACAD10, which has a serine/ threonine kinase domain and was bound by JB170 in the kinobead assay, was not detected in the proteomic analysis. To confirm the observation, the Aurora-B levels were analyzed by immunoblotting after incubating MV4-11 cells with JB170. As expected, Aurora-B did not decrease after the treatment (Fig. 4.13b).

The CRBN-warhead thalidomide is an immunomodulatory imide drug (IMiD), which binds CRBN and alters the substrate specificity of CRBN to degrade neosubstrates (Ito & Handa, 2016). Therefore, proteomics data were investigated for JB170-induced changes in CRBN neosubstrates, but no depletion of the identified neosubstrates could be observed (Fig. 4.13a, in red). For confirmation, MV4-11 cells were treated with different concentrations of JB170, thalidomide, and pomalidomide (thalidomide analog) and immunoblotted for one of the neosubstrate, Ikaros (IKZF1) (Kronke et al., 2014; Lu et al., 2014). As anticipated, thalidomide and its analog degraded IKZF1, whereas JB170 did not affect the IKZF1 levels (Fig. 4.13c).

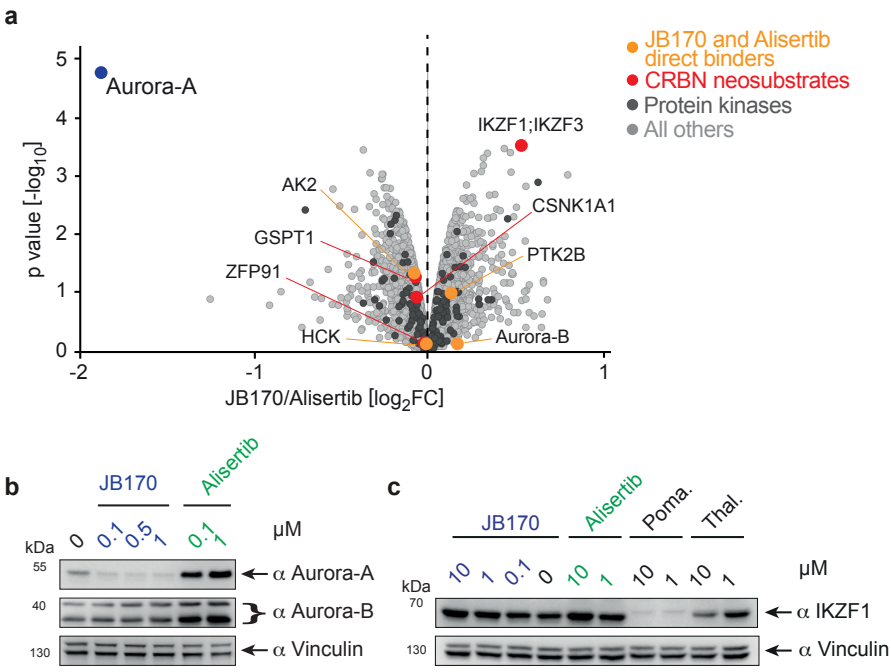

Figure 4.13: JB170 is highly specific for Aurora-A.

(a) *Volcano plot displaying alteration in cellular proteome. SILAC-labeled MV4-11 cells were treated with 0.1 μM JB170 or 0.1 μM alisertib for 6 hours and proteins were analyzed by mass spectrometry. The x-axis shows the log_2 fold change of protein*

abundance by JB170 treatment compared to alisertib. Y-axis shows a negative log_{10} of the p-value from triplicate experiments. JB170 and alisertib binding proteins are labeled in orange, and the neosubstrates of CRBN in red. ***(b)*** *Immunoblots of Aurora-A and -B. MV4-11 cells were treated with various concentrations of JB170 and alisertib for 24 hours.* ***(c)*** *Immunoblot of Ikaros. MV4-11 cells were treated with specified concentrations of JB170, alisertib, pomalidomide (Poma.), and thalidomide (Thal.) for 18 hours, and the protein levels were compared to the vehicle-treated cells.*
The figures were taken and modified from Adhikari et al., 2020.

4.1.3.3 TMT mass spectrometry in IMR5 cells confirms JB170 specificity

The selectivity of JB170 was analyzed in yet another cell line, IMR5, using a different quantitative proteomics approach, tandem mass tag (TMT) mass spectrometry. In TMT proteomics, the samples are labeled separately with isobaric tags after harvest and all samples are combined before mass spectrometry analysis. IMR5 cells were treated with 1 µM JB170, JB211, and alisertib for 6 hours in quadruplicate experiments. Then, 11plex-TMT was carried out with four samples of JB170 and alisertib while three samples of JB211. The TMT labeling and analysis were performed by Stephanie Heinzlmeir from the group of Prof. Dr. Bernhard Kuster, Technical University of Munich.
Similar to the SILAC mass spectrometry, of 6485 identified proteins, JB170 only decreased Aurora-A significantly with $log_2FC < -1$ and p-value < 0.001, compared to both alisertib- and JB211-treated conditions (Fig. 4.14a). JB170 degraded 66.3% (p-value: $3.7x\ 10^{-6}$) and 54.5% (p-value: $8.9x\ 10^{-5}$) of Aurora-A in comparison to alisertib and JB211, respectively (Adhikari et al., 2020). Immunoblot of Aurora-B from IMR5 cells reinforced that its protein levels were not reduced upon 1 µM JB170 treatment for 6 hours (Fig. 4.14b).

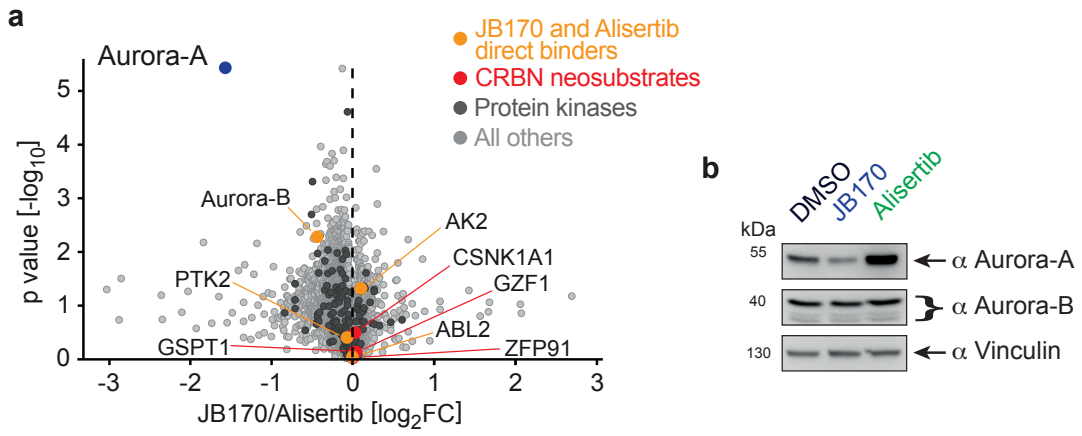

Figure 4.14: TMT proteomics of IMR5 cells after JB170 treatment.
(a) *Volcano plot displaying alteration in cellular proteome. IMR5 cells were treated with*

1 µM JB170 or alisertib for 6 hours, labeled with tandem mass tags 11 (TMT11)-plex, and analyzed by mass spectrometry. The x-axis shows the log_2 fold change of protein abundance by JB170 treatment compared to alisertib. Y-axis shows a negative log_{10} of the p-value from triplicate experiments. JB170 and alisertib binding proteins are labeled in orange, and the neosubstrates of CRBN are in red. ***(b)*** *Immunoblots of Aurora-A and -B. IMR5 cells were treated with vehicle (DMSO), 1 µM JB170, and alisertib for 6 hours.*
The figures were taken and modified from Adhikari et al., 2020.

In summary, the kinobead selectivity profiling and both quantitative proteomics approach collectively demonstrated that JB170 is highly specific to Aurora-A.

4.1.4 Ternary complex formation is supported by cooperativity

Data so far illustrated the potency and selectivity of JB170 towards Aurora-A, even greater than alisertib, but further experiments were required to elucidate the reason behind it. What does JB170 make more effective when compared to the other PROTACs examined in the beginning? We hypothesized that the interaction between Aurora-A and CRBN is responsible for this selectivity, which was strengthened by the fact that none of the tested VHL-recruiting PROTACs were functional. Previous studies have demonstrated that ternary complex formation (E3-ligase:PROTAC:POI) stabilized by protein-protein interactions (PPI) shows positive cooperativity and leads to selective degradation (Brand et al., 2019; Gadd et al., 2017). To test this hypothesis, modeling studies were performed, and these observations were subsequently inspected in cellular models.

4.1.4.1 Modeling studies identify amino acids in Aurora-A critical for ternary complex formation

The modeling studies were executed by Mathias Diebold from the group of Prof. Dr. Christoph Sotriffer, Institute for Pharmacy and Food Chemistry, University of Wuerzburg. First, protein-protein docking was performed between Aurora-A/alisertib and CRBN/lenalidomide complexes. The complexes were prepared based on crystal structure of Aurora-A in complex with MLN8054 (PDB: *2X81*) (Sloane et al., 2010) and a crystal structure of CRBN in complex with lenalidomide (PDB: *4TZ4*) (Chamberlain et al., 2014). The best-scored complex, Aurora-A-CRBN complex 1 (ACc1), displayed a considerable interface between Aurora-A and CRBN (Fig. 4.15a). Moreover, the corresponding linker of JB170 could be

joined to the alisertib and lenalidomide without significant distortion in ACc1 (Fig. 4.15b). Apart from JB170, only JB158 would fit in ACc1, while other thalidomide-derived degraders could not fit without major displacement (Adhikari et al., 2020). This is in line with the finding that these very two PROTACs, JB170 and JB158, showed strongest degradation of Aurora-A.

To further identify the amino acids crucial for ternary complex formation, molecular dynamics (MD) simulations were carried out using ACc1 and the second-best model, in which JB170 could be fitted without major rearrangements. Twelve amino acids in Aurora-A were determined to contribute to the formation of the ternary complex using the energy decomposition function (R137, K153, K156, F157, I158, R189, P191, K224, E239, S266, A267, and R375).

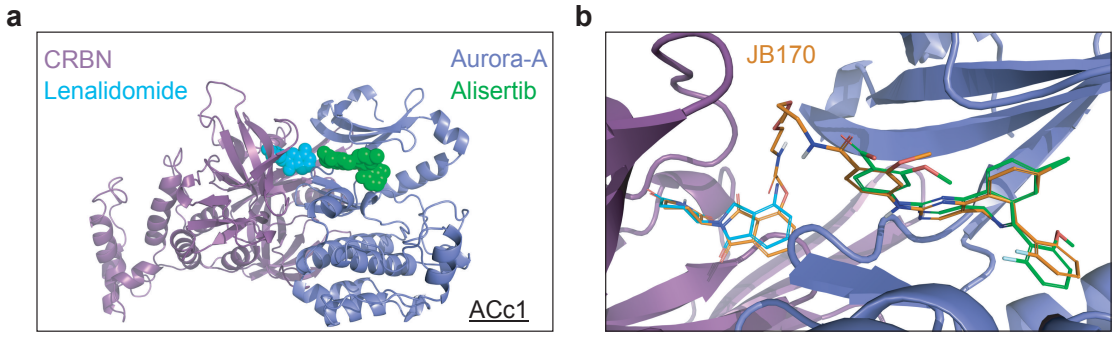

Figure 4.15: Modeling JB170 into Aurora-A and CRBN complex.
(a) *Model of Aurora-A-CRBN complex with JB170. The top-scoring complex, Aurora-A-CRBN complex 1 (ACc1), from protein-protein docking using Aurora-A/alisertib and CRBN/lenalidomide.* ***(b)*** *Modeled ACc1 with JB170. Alisertib and lenalidomide were modified, connected, and minimized to give JB170. Aurora-A, alisertib, CRBN, lenalidomide, and JB170 are shown in blue, green, purple, aqua, and orange, respectively. These analyses were performed by Mathias Diebold.*
The figures were taken and modified from Adhikari et al., 2020.

4.1.4.2 PPI supports the ternary complex formation

4.1.4.2.1 Aurora-A interface mutants are not degraded by JB170

To confirm the observations made from MD simulation, Aurora-A wild-type (WT) and a mutant were generated fused to HA-tag and HiBiT-tag. In the mutant Aurora-A (Imut), all the 12 amino acids of Aurora-A identified to be critical for interacting with CRBN were mutated. The HA- and HiBiT-tagged Aurora-A WT and Imut were cloned by Ashwin Narain from the group of Prof. Dr. Elmar Wolf, University of Wuerzburg. The mutations in Imut were: R137E, K153E, K156E, F157E, I158E, R189E, P191W, K224E, E239R, S266W, A267W, and R375E. MV4-11 cell lines

were generated stably expressing the HA- or HiBiT-tagged versions of WT and Imut Aurora-A. These MV4-11 cells were treated with 1 µM JB170 and alisertib for 6 hours. Immunoblotting proved our hypothesis since no degradation of Imut was observed upon JB170 treatment (Fig. 4.16a). The HiBiT assay also confirmed this result. When cells expressing HiBiT-tagged Aurora-A versions were treated with various concentrations of JB170, no significant degradation of Imut-HiBiT was detected (Fig. 4.16b).

Finally, pulldown experiments were performed with HA-tagged versions of Aurora-A in the presence and absence of JB170. The cells were treated with JB170 for 6 hours, and Aurora-A was immunoprecipitated using an HA-tag specific antibody to investigate co-immunoprecipitation (co-IP) of CRBN. As expected, WT Aurora-A heavily co-precipitated CRBN in the presence of JB170 (even though the amount of immunoprecipitated Aurora-A was less), while Imut did not (Fig. 4.16c).

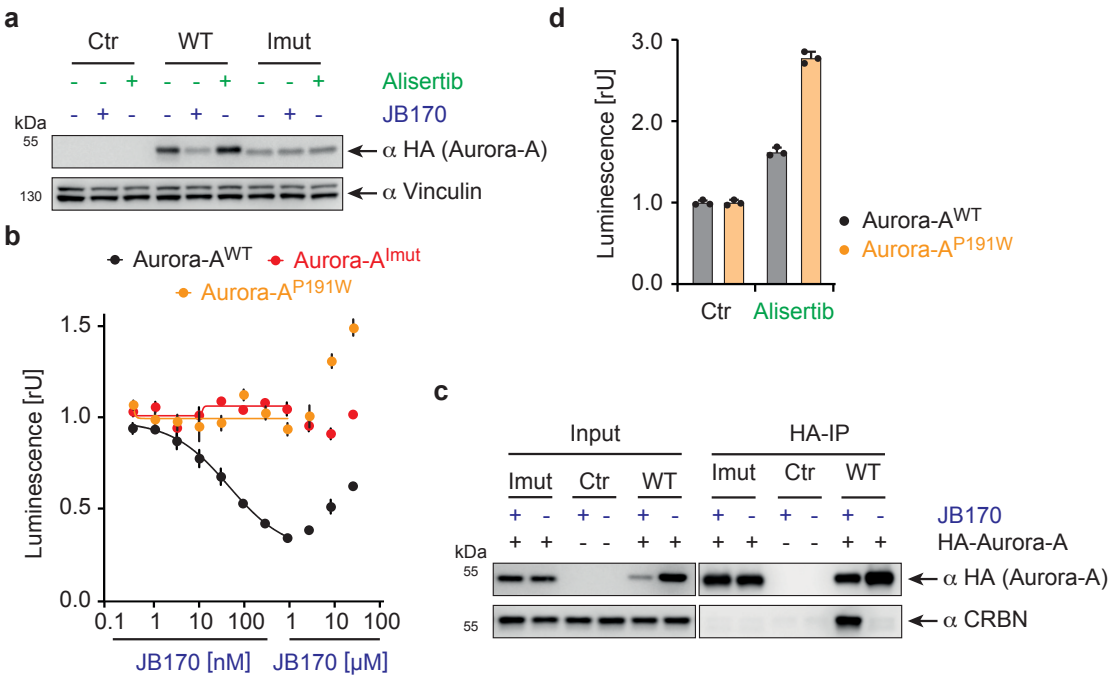

Figure 4.16: PPI is necessary for JB170-mediated Aurora-A degradation.

(a) *Immunoblot of HA-tagged Aurora-A. MV4-11 cells stably expressing HA-tagged wild-type (WT) and the interface mutant (Imut) were treated for 6 hours with 1 µM JB170 or alisertib and expression levels were compared to vehicle-treated cells. Empty vector transduced cells (Ctr) were used as control. The Imut contained 12 amino acids mutation (R137E, K153E, K156E, F157E, I158E, R189E, P191W, K224E, E239R, S266W, A267W, and R375E).* ***(b)*** *Aurora-A levels based on HiBiT assay. MV4-11 cells stably expressing HiBiT-tagged Aurora-A^{WT}, Aurora-A with one mutation (Aurora-A^{P191W}), and Aurora-A interface mutant (Aurora-A^{Imut}) were treated with various concentrations of JB170 for 6 hours, lysed, and complemented with LgBiT, and luminescence was measured to quantify Aurora-A levels. The data represent mean ±*

SD from three replicates. ***(c)*** *Immunoblots of HA-tagged Aurora-A and CRBN. MV4-11 cells expressing HA-tagged Aurora-A^{WT} and Aurora-A^{Imut} were treated with 0.5 μM JB170 for 6 hours. Aurora-A was pulled down using HA-tag, and co-immunoprecipitated CRBN was analyzed by immunoblotting.* ***(d)*** *Aurora-A levels based on HiBiT measurements. MV4-11 cells expressing HiBiT-tagged Aurora-A^{WT} and Aurora-A^{P191W} were treated with 1 μM alisertib for 6 hours, lysed, and complemented with LgBiT, and luminescence was measured to quantify Aurora-A levels. The data represent mean ± SD from three replicates.*
The figures were taken and modified from Adhikari et al., 2020.

Additionally, to check the effect of each amino acid in the interface, twelve different HiBiT-tagged Aurora-A with only a single mutation were cloned. In the HiBiT assay, one of the twelve single mutations, P191W, annihilated the degradation efficiency of JB170 towards Aurora-A (Fig. 4.16b), suggesting that the amino acid P191 of Aurora-A is critical for the PPI with CRBN. To test if the Aurora-A warhead was still able to bind the P191W mutant, the protein levels were analyzed after 6 hours of incubation with alisertib by HiBiT assay. As observed for WT Aurora-A, the P191W Aurora-A levels were increased with alisertib (Fig. 4.16d), implying that the mutant could still bind to alisertib and, thus, potentially, JB170.

Thus, the modeling as well as cellular studies with mutant Aurora-A highlighted the importance of the PPI between Aurora-A and CRBN for JB170 efficacy.

4.1.4.2.2 Degrader efficacy correlates with ternary complex formation ability

To investigate a possible correlation between PROTAC efficiency and the ability of ternary complex formation, the capability of CRBN to co-IP with Aurora-A was analyzed in the presence of all five thalidomide-based degraders. First, MV4-11 cells expressing HA-tagged Aurora-A were lysed with a mild lysis buffer, IP-buffer. Second, 0.5 μM of each PROTAC was pre-incubated with cell lysate for 2 hours before, third, incubation with HA-coupled beads. Finally, the immunoprecipitated Aurora-A and co-immunoprecipitated CRBN levels were detected by western blotting. JB170 induced the maximal co-IP of CRBN, closely followed by JB158, while that for JB159, JB169, and JB171 were less (Fig. 4.17a). The co-IP of CRBN correlated with the degradation efficiency of these PROTACs (Fig. 4.2a and 4.17a). Moreover, a small quantity of CRBN co-IP was seen in vehicle-treated conditions, pointing out that Aurora-A and CRBN might also interact in normal cellular conditions (Fig. 4.16c, 17a). So far, Aurora-A was not known to be a natural substrate of CRBN. However, this interaction gives rise to speculation that either

Aurora-A is a natural substrate of CRBN or that Aurora-A might have some scaffolding functions involving CRBN.

Likewise, the ability of VHL-based degraders to form a ternary complex with VHL was tested using the same pulldown approach as before. MV4-11 cells expressing HA-tagged Aurora-A were treated with two thalidomide- and two VHL-based degraders (0.5 µM) for 6 hours and the protein levels were analyzed. As previously observed, CRBN-recruiting degraders JB170 and JB171 showed co-IP of CRBN, while VHL co-IP was not observed by VHL-recruiting degraders, JB160 and JB161 (Fig. 4.17b). Interestingly, with JB211, which cannot bind to CRBN, small amount of CRBN was co-precipitated, further indicating that Aurora-A and CRBN do interact under normal conditions (Fig. 4.17b). Weak co-IP of CRBN was similarly seen for DMSO, JB160, JB160, and JB161 treated conditions (Fig. 4.17b).

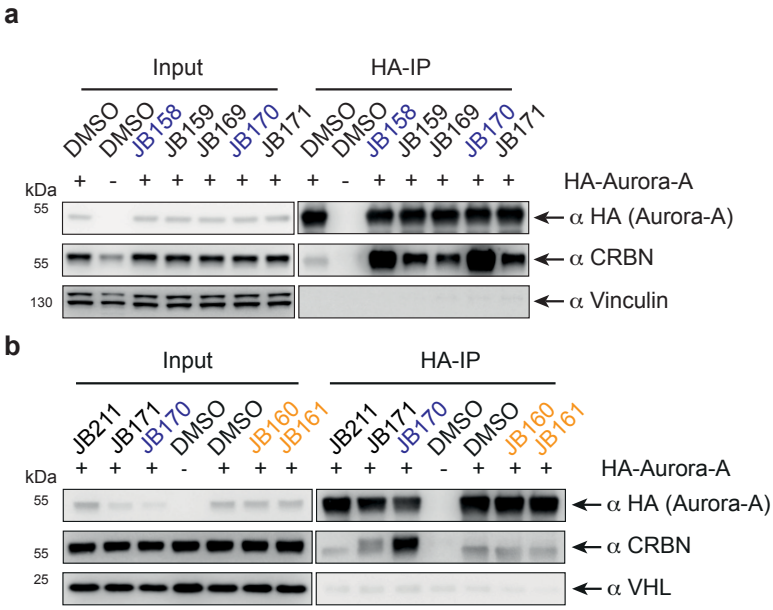

Figure 4.17: Degradation efficiency of PROTACs correlates with ternary complex formation.

(a) *Immunoblots of HA-tagged Aurora-A and CRBN. Lysate of MV4-11 cells expressing HA-tagged Aurora-A was incubated with 0.5 µM JB158, JB159, JB160, JB170, and JB171. Aurora-A was precipitated using HA-tag and the co-precipitated CRBN was evaluated by western blotting.* ***(b)*** *Immunoblots of HA-tagged Aurora-A, CRBN, and VHL. MV4-11 cells expressing HA-tagged Aurora-A were incubated with 0.5 µM CRBN-recruiting (JB170, JB171) and VHL-recruiting (JB160, JB161) degraders. Aurora-A was precipitated using HA-tag, and the co-precipitated CRBN and VHL were evaluated and compared to the vehicle (DMSO) and JB211 treatment by immunoblotting.*

The figures were taken and modified from Adhikari et al., 2020.

4.1.4.2.3 JB170-mediated degradation is impaired in Aurora-B swap mutants

The presumption was that, along with ligand affinity, the PPI plays a vital role in JB170-mediated degradation. The kinase domains of Aurora-A and -B share 71% sequence homology (Fig. 1.4). However, as shown by mass spectrometry, Aurora-B levels were unaffected by JB170. To investigate if Aurora-B would be able to form a PPI with CRBN, like observed for Aurora-A, Aurora-A and -B structures were superimposed. Many residues of Aurora-A within the CRBN interface were not conserved in Aurora-B (Adhikari et al., 2020). Moreover, the protein-protein docking studies showed that the Aurora-B/CRBN complex was less stable than the Aurora-A/CRBN complex (Adhikari et al., 2020).

The ATP-binding pocket of Aurora-A and -B differs only by three amino acid residues. Aurora-A residues L215, T217, and R220, are altered in Aurora-B by R159, E161, and K164 (Dodson et al., 2010). The critical residue, however, is T217 in Aurora-A, which corresponds to negatively charged E161 in Aurora-B (Sloane et al., 2010). By swapping these amino acids of Aurora-B to those of Aurora-A in Aurora-B (swap mutant), the active site of Aurora-A can be mimicked in Aurora-B. The Aurora-B swap mutant likely have a similar affinity to alisertib as Aurora-A and could be used to further analyze the importance of the PPI to the E3-ligase. So, two different HA-tagged swap mutants were cloned: Aurora-B^{E162T} and Aurora-$B^{R160L, E162T, K165R}$ (Aurora-B^{x3}). The cloned Aurora-B here was Isoform 5 (69-69: T → TR). The cloning was done by Markus Vogt from the group of Prof. Dr. Elmar Wolf, University of Wuerzburg. MV4-11 cells were generated stably expressing Aurora-B^{WT}, Aurora-B^{E162T} and Aurora-B^{x3}. These cells were treated with 100 nM and 1 µM JB170 for 6 hours and compared to Aurora-A^{WT} cells. As previously observed, JB170 robustly degraded Aurora-A^{WT}, while Aurora-B^{WT} was not degraded (Fig. 4.18). Both swap mutants displayed only a slight decrease in protein level at higher PROTAC concentrations (Fig. 4.18), suggesting that the binding affinity of the PROTAC-warhead alone does not dictate the efficacy of the PROTAC.

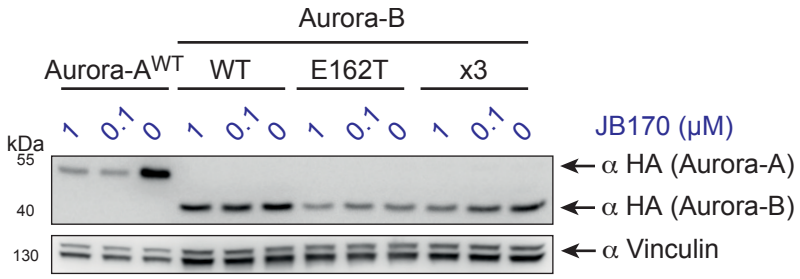

Figure 4.18: PROTAC binding alone does not dictate degradation efficiency.
Immunoblots of HA-tagged Aurora-A and different versions of Aurora-B. MV4-11 cells stably expressing HA-tagged Aurora-A wild-type, Aurora-B wild-type (WT), Aurora-B with single mutation (E162T) and Aurora-B with triple mutations, R160L, E162T, and K165R (x3) were treated for 6 hours with indicated concentrations of JB170 and expression levels were compared to vehicle-treated cells.
The figure was taken and modified from Adhikari et al., 2020.

All the above data showed that CRBN and Aurora-A PPI increased the cooperativity of JB170-mediated ternary complex and contributed to the selectivity of JB170.

4.1.5 Cellular effects of Aurora-A degradation

4.1.5.1 JB170 treatment delays S-phase progression of cells

To evaluate the possible cellular effect of JB170-mediated Aurora-A degradation, cell cycle flow cytometry analysis was conducted. Aurora-A being a mitotic serine-threonine kinase, its degradation was expected to cause cell cycle arrest in the G2/M phase. MV4-11 cells were treated with JB170, alisertib, and vehicle for 12 hours. The cells were additionally pulsed with thymidine analog, Bromodeoxyuridine (BrdU), for the last hour of treatment. BrdU is incorporated into the newly synthesized DNA of replicating cells during the S-phase of the cell cycle. Antibodies against BrdU can then be used to detect the incorporation level of BrdU, thus indicating the cells that are in S-phase. Upon BrdU/propidium iodide (PI) flow cytometry analysis, alisertib-treated cells showed massive G2/M arrest, whereas only small fractions of PROTAC-treated cells showed G2/M arrest (Fig. 4.19a, b). Interestingly, a considerable portion of these cells displayed little to no BrdU incorporation (cells labeled in green, Fig. 4.19a), suggesting that either those cells were arrested in S-phase, or their S-phase progression was delayed. The functions of Aurora-A, potentially non-catalytic, in the S-phase have been reported by multiple publications (Buchel et al., 2017; Isabelle Roeschert et al., 2021).

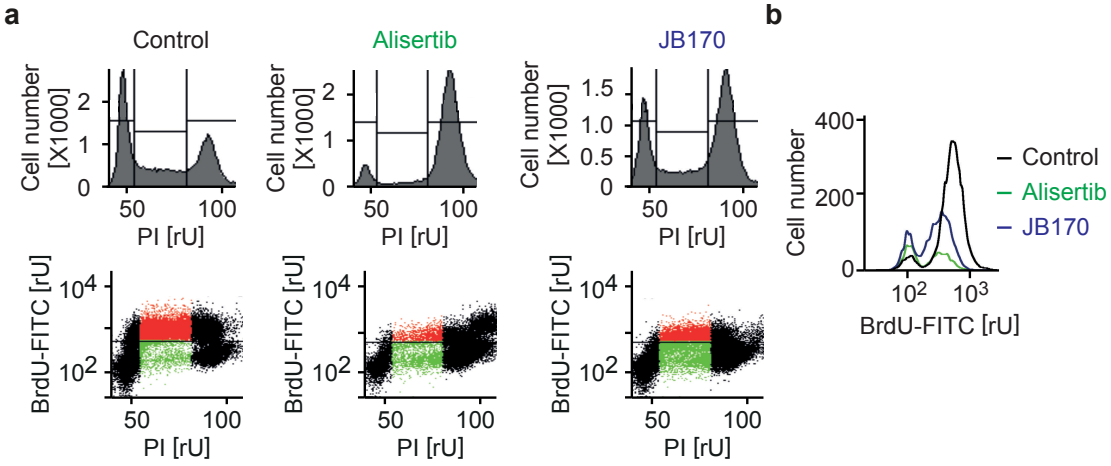

Figure 4.19: JB170 mediated degradation of Aurora-A delays S-phase progression of cells.

(a) *BrdU/PI flow cytometry analysis. MV4-11 cells were treated for 12 hours with 0.5 µM JB170 or 1 µM alisertib and pulsed with BrdU in the last hour. The cells were fixed, stained with propidium iodide (PI) and FITC-labelled anti-BrdU antibody, and analyzed by flow cytometry.* ***(b)*** *Histogram for BrdU incorporation. The quantity of BrdU incorporated by the cells in the S-phase from (a) is shown.*
The figures were taken and modified from Adhikari et al., 2020.

4.1.5.2 GSEA shows no enrichment of the G2/M cell cycle gene set from the JB170 treatment

Next, an RNA-sequencing experiment was performed to investigate if the cell cycle effect of Aurora-A inhibition versus degradation correlated in the transcriptome level. MV4-11 cells were treated with degrader and inhibitor for 18 hours, and complementary DNA (cDNA) was prepared from the harvested RNA and subjected to Illumina sequencing. Then, gene set enrichment analyses (GSEA) were performed by comparing the gene expression of alisertib and JB170 treated samples to vehicle-treated samples. The gene set for the G2/M cell cycle was significantly affected by inhibition but not degradation (Fig. 4.20). The analysis was performed by Apoorva Baluapuri from the group of Prof. Dr. Elmar Wolf, University of Wuerzburg.

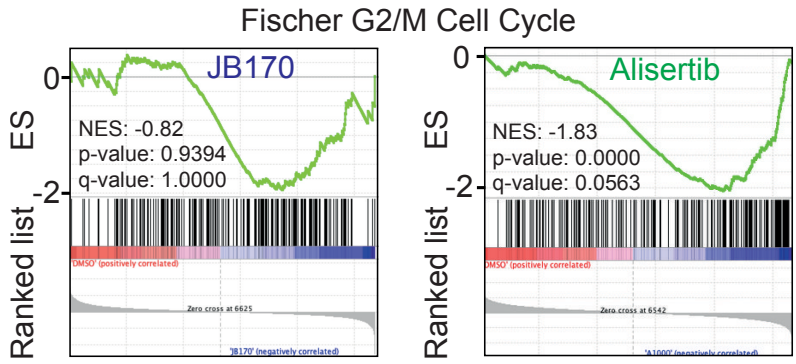

Figure 4.20: G2/M cell cycle gene set are not enriched with JB170 treatment.
Gene set enrichment analysis. MV4-11 cells were treated with 0.1 µM JB170 or 1 µM alisertib for 18 hours. The harvested RNA was processed and subjected to Illumina sequencing. Enrichment plots for the "'Fischer G2/M Cell Cycle" gene set for alisertib and JB170 in comparison to vehicle-treated samples are shown.
The figure was taken and modified from Adhikari et al., 2020.

4.1.5.3 Overexpression of Aurora-A rescues S-phase arrest

To show that the observed S-phase phenotype by JB170 was induced by Aurora-A degradation, an inducible IMR5 cell line was generated, which could express mutant Aurora-A (Aurora-A^{T217D}) upon the addition of doxycycline. Aurora-A^{T217D} is resistant to alisertib inhibition due to its reduced affinity (Sloane et al., 2010). As observed previously in MV4-11 cells (Fig. 4.19a), almost all IMR5 cells were arrested in G2/M cell phase after alisertib treatment (Fig. 4.21a). Similarly, no G2/M arrest but an accumulation of BrdU negative cells was observed upon Aurora-A degradation by JB170. However, expression of Aurora-A^{T217D} effectively rescued the JB170-mediated S-phase defect (Fig. 4.21a, b). Furthermore, the total Aurora-A protein level after Aurora-A^{T217D} induction in the presence of JB170 was not less than the unperturbed condition (Fig. 4.21c). This proved that the S-phase effect seen by JB170 treatment was mediated by Aurora-A degradation. This observation was also recapitulated by the ectopic expression of the Aurora-A^{WT} (Adhikari et al., 2020). Moreover, siRNA-mediated depletion of Aurora-A in IMR5 cells showed a similar S-phase phenotype to Aurora-A degradation (Adhikari et al., 2020). Thus, it can be concluded that Aurora-A has a non-catalytic function in S-phase.

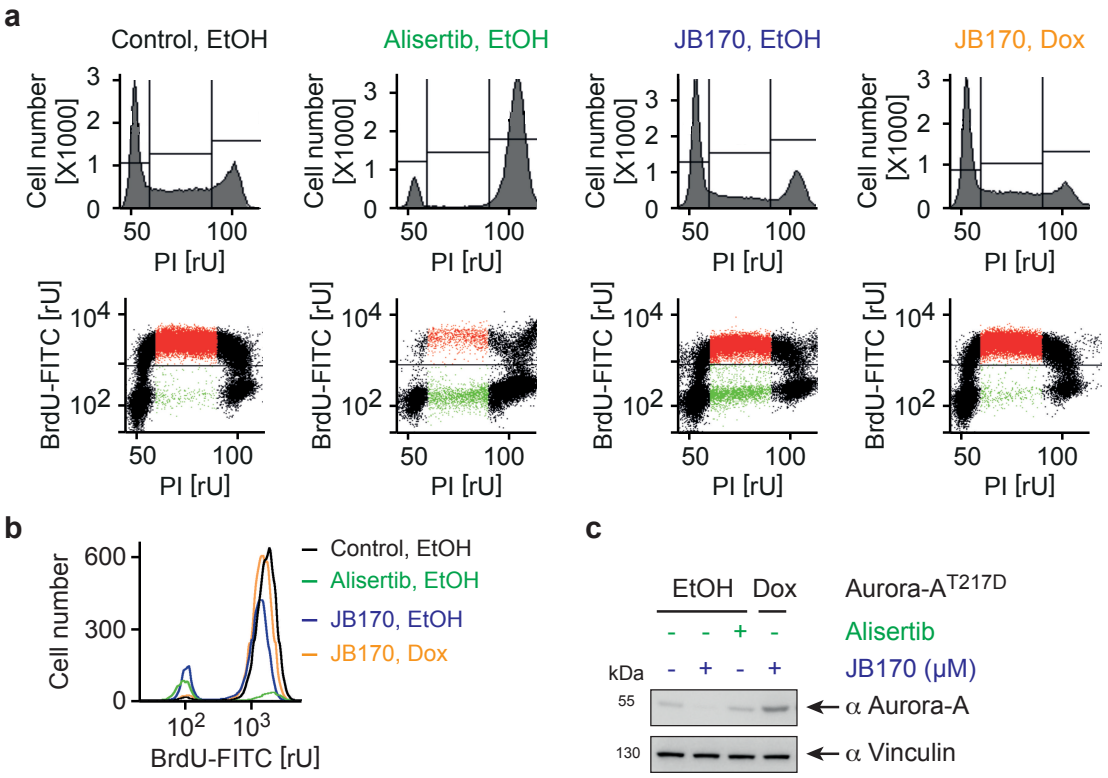

Figure 4.21: Overexpression of Aurora-A rescues S-phase arrest.
(a) *BrdU/PI flow cytometry analysis. IMR5 cells with inducible Aurora-A^{T217D} expression were treated for 18 hours with 1 μM JB170 or 1 μM alisertib in the presence (Dox) or absence (EtOH) of doxycycline. The cells were fixed, stained with propidium iodide (PI) and FITC-labelled anti-BrdU antibody, and analyzed by flow cytometry.* ***(b)*** *Histogram of BrdU incorporation. The quantity of BrdU incorporated by the cells in the S-phase from (a) is shown.* ***(c)*** *Immunoblot of Aurora-A. The Aurora-A expression levels from the cells shown in (a) were analyzed by immunoblotting.*
The figures were taken and modified from Adhikari et al., 2020.

4.1.5.4 Degradation of Aurora-A induces apoptosis in cancer cells

4.1.5.4.1 JB170 decreases cell viability of cancer cells

Subsequently, the effect of long-term degradation of Aurora-A in cancer cell lines was assessed. For this, cell viability of cancer cell lines was measured using the alamarBlue assay. alamarBlue is a resazurin-based dye that can be reduced to a fluorescent compound, resorufin (O'Brien et al., 2000). Living cells actively reduce the resazurin to resorufin; thus, cell viability can be quantified calculating the amount of resorufin by fluorescence measurement.

MV4-11 cells were treated with JB170 for 24, 48, and 72 hours and cell viability were measured. In comparison to the vehicle-treated cells, JB170 significantly decreased cell viability by 6, 33, and 68% after 24, 48, and 72 hours, respectively (Fig. 4.22a). In the cell viability experiments, JB170 was refreshed daily. Similarly,

a significant reduction in cell proliferation was observed by crystal violet staining of IMR5 after four days of degrader treatment (Fig. 4.22b).

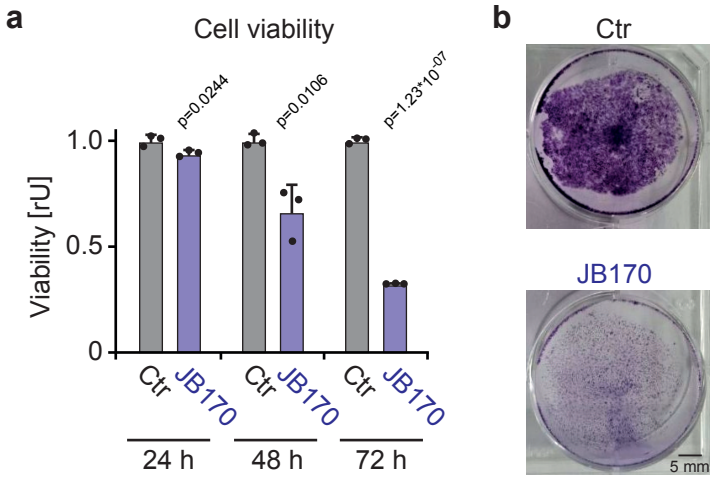

Figure 4.22: JB170 treatment inhibits cell proliferation.
(a) *Cell viability analysis. MV4-11 cells were treated with 1 µM JB170 for 24, 48, and 72 hours, and the cell viability was measured using alamarBlue, and compared to control cells. The data represent mean ± SD from three replicates, and p-values were calculated from a two-tailed unpaired t-test assuming equal variance.* ***(b)*** *Crystal violet staining. IMR5 cells were treated with 1 µM JB170 for four days and stained with crystal violet. Scale bar is 5 mm.*
The figures were taken and modified from Adhikari et al., 2020.

4.1.5.4.2 JB170 induces apoptosis in cancer cells

To study whether the changes in cell viability and proliferation by JB170 were due to apoptosis-mediated cell death, annexin/PI flow cytometry was performed. Annexin-V binds to Phosphatidylserine (PS), a marker of apoptosis, and therefore can be probed to measure apoptosis (Koopman et al., 1994). MV4-11 cells were treated with JB170 for 24, 48, and 72 hours and the annexin/PI profile was compared to control cells. In comparison to control cells (0 h), Aurora-A degradation increased the cellular apoptosis by 15% (24 h), 31% (48 h), and 46% (72 h) (Fig. 4.23a).

To confirm that the apoptosis occurred via Aurora-A degradation, the inducible IMR5 cell line was used. After 72 hours of treatment, 0.5 µM JB170 accumulated 19% annexin-positive IMR5 cells, whereas it was 41% with 1 µM JB170 (Fig. 4.23b). More importantly, the ectopic expression of Aurora-A^{T217D} prevented apoptosis in the presence of JB170 (Fig. 4.23b). Along this line, CRBN non-binding analog JB211 did not show any significant changes in apoptosis. Both findings confirmed that apoptosis by JB170 was solely mediated by Aurora-A degradation.

This experiment was performed by Jessica Schwarz from the group of Prof. Dr. Elmar Wolf, University of Wuerzburg.

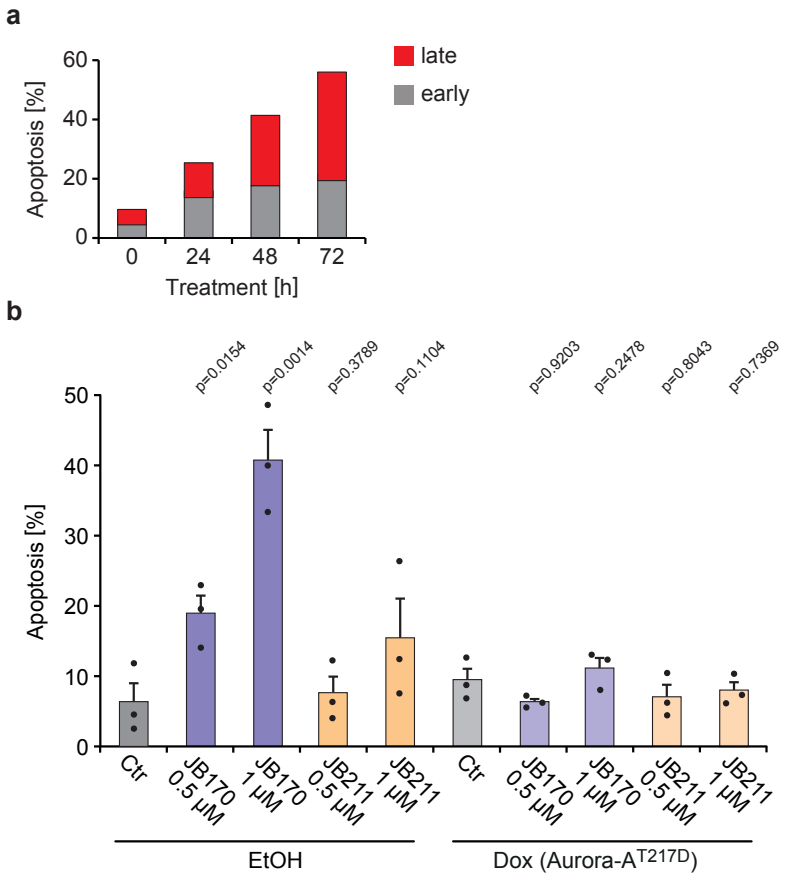

Figure 4.23: JB170-mediated degradation of Aurora-A causes apoptosis in cells. ***(a)*** *Annexin/PI flow cytometry analysis. MV4-11 cells were treated with 0.5 µM JB170 for indicated time points. The cells were stained with annexin and PI, and the apoptotic cells were counted. Early apoptosis (annexin^{+}/PI^{-}) and late apoptosis (annexin^{+}/PI^{+}).* ***(b)*** *Annexin/PI flow cytometry analysis. IMR5 cells with inducible Aurora-A^{T217D} expression were treated for 72 hours with different concentrations of JB170 or JB211 in the presence (Dox) or absence (EtOH) of doxycycline. The cells were stained with annexin and PI, and the total apoptotic cells were counted. The data represent mean ± SEM from three replicates, and p-values were calculated from a two-tailed unpaired t-test assuming equal variance. This experiment was performed by Jessica Schwarz. The figures were taken and modified from Adhikari et al., 2020.*

These experiments indicate that targeting the S-phase function of Aurora-A via degraders could be an alternative option to targeting mitotic function of Aurora-A for cancer therapy.

4.1.6 Aurora-A interacts with a plethora of non-substrates

As described in the above section, JB170-mediated degradation of Aurora-A disclosed a striking function of Aurora-A in the S-phase. This S-phase phenotype was not observed by Aurora-A kinase activity inhibition. So, a scaffolding or kinase-independent function of the protein seemed to be responsible for it. To clarify this, it was investigated if Aurora-A interacts with proteins other than its substrates. Therefore, a quantitative mass spectrometry approach was utilized to analyze Aurora-A interactors. MV4-11 cells transduced with empty vector or expressing HA-tagged Aurora-A were harvested in lysis buffer. Aurora-A and its native complexes were isolated using HA-couple magnetic beads. The analysis was performed by comparing the protein abundance against the empty vector cells. The strongest enrichment was observed for the bait protein, Aurora-A (Fig. 4.24a). 287 more proteins were co-precipitated along with Aurora-A with enrichment of more than 8-fold ($log_2FC>3$). Many Aurora-A substrates like TPX2, INCENP, and TACC3 were enriched (Fig. 4.24a) (Kettenbach et al., 2011). Additionally, numerous proteins were abundantly identified, which were not reported to be substrates of Aurora-A (Fig. 4.24b). Two such interactors, SH3GL1 and DICER1 were validated to interact with Aurora-A in a separate immunoprecipitation experiment using HEK293 cells (Fig. 4.24c). Moreover, DICER1 also interacted with the catalytically inactive versions of Aurora-A, Aurora-A^{K62R} and Aurora-A^{D274N}, suggesting that the kinase-independent function of Aurora-A might be conveyed by such interaction with non-substrate (Fig. 4.24d). Caudron-Herger et al. reported that Aurora-A is present in complexes mediated by RNA (Caudron-Herger et al., 2019). In the same direction, along with DICER1, other members of the microRNA processing, microprocessor complex, like YLPM1 and TARBP2 were identified by mass spectrometry. The interactomic study and western blot validation were performed by Julia Hofstetter from the group of Prof. Dr. Elmar Wolf, University of Wuerzburg, and the mass spectrometry analysis was performed by Andreas Schlosser from Rudolf Virchow Center, University of Wuerzburg.

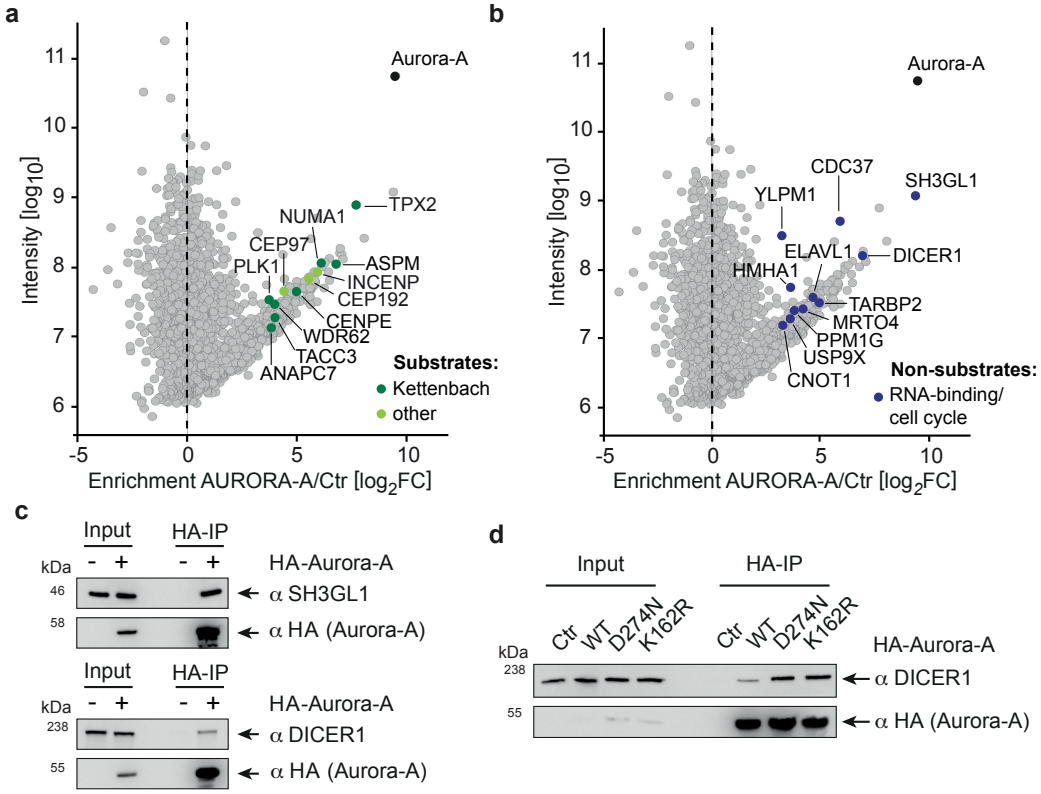

Figure 4.24: Aurora-A interacts with non-substrates.

(a, b) *Enrichment plot for Aurora-A complexes. The X-axis shows enrichment (log_2 fold change) of proteins from HA-tagged Aurora-A expressing over empty vector (Ctr) cells. Y-axis shows the log_{10} intensities of the protein. (a) Aurora-A substrates (Kettenbach et al., 2011) are labeled in green (b) Novel Aurora-A interacting proteins are labeled in blue.* ***(c)*** *Immunoblots of HA-tagged Aurora-A, SH3GL1, and DICER1. HEK293 cells were transfected with HA-tagged Aurora-A, immunoprecipitated, and the co-precipitated SH3GL1 (top) and DICER1 (bottom) were analyzed by immunoblotting.* ***(d)*** *Immunoblots of HA-tagged Aurora-A and DICER1. HEK293 cells were transfected with HA-tagged Aurora-A wild-type (WT), and kinase-dead versions (D274N and K162R), immunoprecipitated using HA-tag and the co-precipitated DICER1 was analyzed by immunoblotting. These experiments were performed by Julia Hofstetter. The figures were taken and modified from Adhikari et al., 2020.*

All in all, Aurora-A PROTAC JB170 showed robust and selective degradation of Aurora-A. Furthermore, the degradation uncovered a non-catalytic role of Aurora-A in the S-phase and eventually induced apoptosis in cancer cells.

4.2 WDR5 degradation

Most of the results in this section are from the publication Dölle, Adhikari et al. (Dolle et al., 2021). The data obtained by others that are shown in this section are acknowledged and cited accordingly. Many figures shown in this section are modified or taken from Dölle et al., 2021.

4.2.1 Design of WDR5 PROTACs

Two series of WDR5 PROTACs were synthesized adopting two published Win-site ligands for WDR5.

4.2.1.1 PROTACs based on OICR-9429 modified WDR5 ligands (AD-series)

A first series of PROTACs targeting WDR5 was synthesized based on OICR-9429 warhead, AD100 (Grebien et al., 2015). The crystal structure of WDR5 bound to the OICR-9429 ligand displayed a solvent-exposed carbonyl moiety, which was utilized to attach the different linkers (Fig. 4.25a, attachment point shown by arrow) (Grebien et al., 2015). Altogether 15 different degraders were synthesized (Fig. 4.25b). Five PROTACs were synthesized with pomalidomide to recruit CRBN, whereas ten were synthesized with VHL-ligand to recruit VHL (Fig. 4.25b). Aliphatic, PEG, and aromatic linkers provided the linker variation (Fig. 4.25b). All the AD-series degraders were synthesized by Anja Dölle from the group of Prof. Dr. Stefan Knapp, Goethe-Universität Frankfurt. The biophysical evaluations (differential scanning fluorimetry, DSF; isothermal titration calorimetry, ITC) and target engagement assays of these compounds showed various binding affinities towards WDR5 (Dolle et al., 2021).

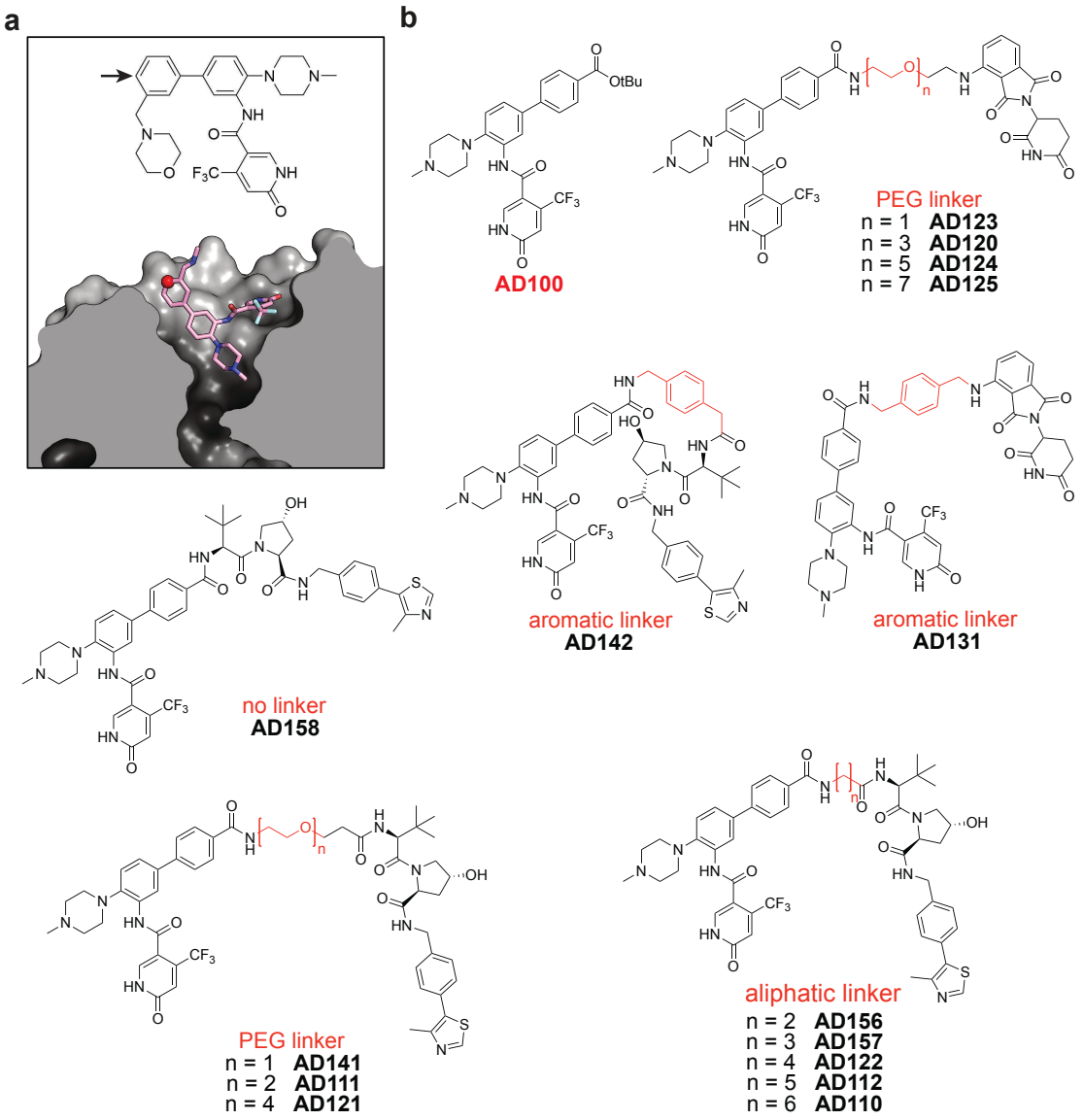

Figure 4.25: Design and structure of AD-series PROTACs.

(a) *Crystal structure of WDR5 and OICR-9429. The structure of WDR5 with OICR-9429 (PDB: 4QL1) shows a carbonyl group (red-colored sphere) exposed to the solvent used for the linker attachment (highlighted by an arrow).* ***(b)*** *The structure of the PROTACs from AD-series. The chemical structure of the ligand (AD100) derived from OICR-9429 and the PROTACs synthesized using AD100 as warhead. These PROTACs were synthesized by Anja Dölle.*

The figures were taken and modified from Dölle et al., 2021.

4.2.1.2 PROTACs based on pyrroloimidazole derived ligands (JW-series)

The second series of PROTACs used a pyrroloimidazole-based inhibitor reported by Wang et al. for the synthesis (Wang et al., 2018). The crystal structure of WDR5 with the inhibitor also presented a solvent-exposed carbonyl group, which was used as an attachment point for the linkers (Fig. 4.26a, attachment point shown by arrow) (Wang et al., 2018). A total of seven PROTACs were synthesized based on

the JW39 ligand to harness VHL with various PEG-linkers (Fig. 4.26b). All the JW-series PROTACs were synthesized by Janik Weckesser from the group of Prof. Dr. Stefan Knapp, Goethe-Universität Frankfurt. The degraders displayed different affinities toward WDR5 from the DSF assays (Dolle et al., 2021).

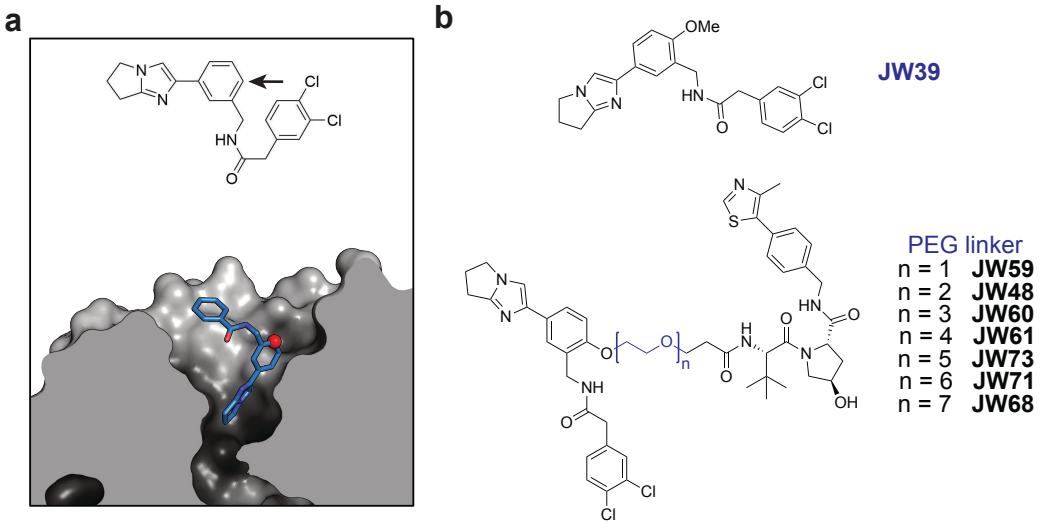

Figure 4.26: Design and structure of JW-series PROTACs.
(a) *Crystal structure of WDR5 and pyrroloimidazole- based inhibitor. The structure of WDR5 with a small molecule published by Wang and colleagues (PDB: 6DAK) shows a carbonyl group (red-colored sphere) exposed to the solvent used to attach the linker (highlighted by an arrow).* ***(b)*** *The structure of the PROTACs from JW-series. The chemical structure of the ligand (JW39) derived from the pyrroloimidazole- based small molecule and the PROTACs synthesized using JW39 as warhead. These PROTACs were synthesized by Janik Weckesser.*
The figures were taken and modified from Dölle et al., 2021.

The AD100 and JW39-based degraders exhibited different linker attachment point in WDR5 pocket, thereby increasing the likelihood of successful ternary complex formation.

4.2.2 PROTAC-induced degradation of WDR5

Next, all the AD- and JW-series PROTACs were tested for their ability to degrade WDR5 using HiBiT assay and immunoblotting.

4.2.2.1 AD122 shows best degradation from AD-series

To test the degradation efficiency of the degraders, a HiBiT-tagged WDR5 (WDR5-HiBiT) expressing cell line was established. Western blot analysis from transduced MV4-11 cells showed similar expression levels for WDR5-HiBiT compared to endogenous WDR5 (Fig. 4.27a). MV4-11$^{WDR5\text{-}HiBiT}$ cells were treated with various

concentrations of degraders from the AD-series. None of the pomalidomide-based degraders, nor the PEG-linker containing VHL-based degraders showed degradation of WDR5 (Table 4.1). In contrast, several VHL-based degraders with aliphatic and aromatic linkers resulted in WDR5 degradation (Table 4.1, Fig. 4.27b, c). The Hook-effect was observed at higher concentrations of all effective degraders (Fig. 4.27b, c). AD122, a butyl linker bearing degrader, was most effective with D_{max} of 58% and DC_{50} value of 53 nM (Table 4.1, Fig. 4.27b). The HiBiT data was validated by immunoblot of MV4-11$^{WDR5\text{-}HiBiT}$ cells incubated with increasing concentrations of AD122 for 24 hours (Fig. 4.27d). Furthermore, to investigate the potency of AD122, MV4-11 cells were treated with a single dose of various concentrations for 72 hours. Immunoblot revealed that even after 72 hours, AD122 was able to form a ternary complex and degrade WDR5 in a concertation-dependent manner (Fig. 4.27e).

Table 4.1: HiBiT data of WDR5 ligand AD100 and its PROTACs after 24 hours treatment.

PROTAC	Linker	E3 ligase	DC_{50} (µM)[a]	DC_{max} (µM)[b]	D_{max} (%)[c]
AD100	-	-	no	no	no
AD123	PEG_1	CRBN	no	no	no
AD120	PEG_3	CRBN	no	no	no
AD124	PEG_5	CRBN	no	no	no
AD125	PEG_7	CRBN	no	no	no
AD131	Aromatic	CRBN	no	no	no
AD141	PEG_1	VHL	no	no	no
AD111	PEG_2	VHL	no	no	no
AD121	PEG_4	VHL	no	no	no
AD158	-	VHL	no	no	no
AD156	Ethyl	VHL	0.625 ± 0.07	3.3	34 ± 3
AD157	Propyl	VHL	0.116 ± 0.01	1.1	40 ± 4
AD122	Butyl	VHL	0.053 ± 0.01	1.1	58 ± 3
AD112	Pentyl	VHL	0.92 ± 0.06	≥10	40 ± 5
AD110	Hexyl	VHL	0.915 ± 0.31	≥10	41 ± 5
AD142	Aromatic	VHL	N/A	0.12	31 ± 2

[a]DC_{50}: half-maximal degradation concentration , calculated with the dose–response (four parameters) equation; [b]DC_{max}: maximal degradation concentration; [c]Dmax: maximal degradation; no: no degradation; N/A: not applicable. Table was adapted from Dölle et al., 2021

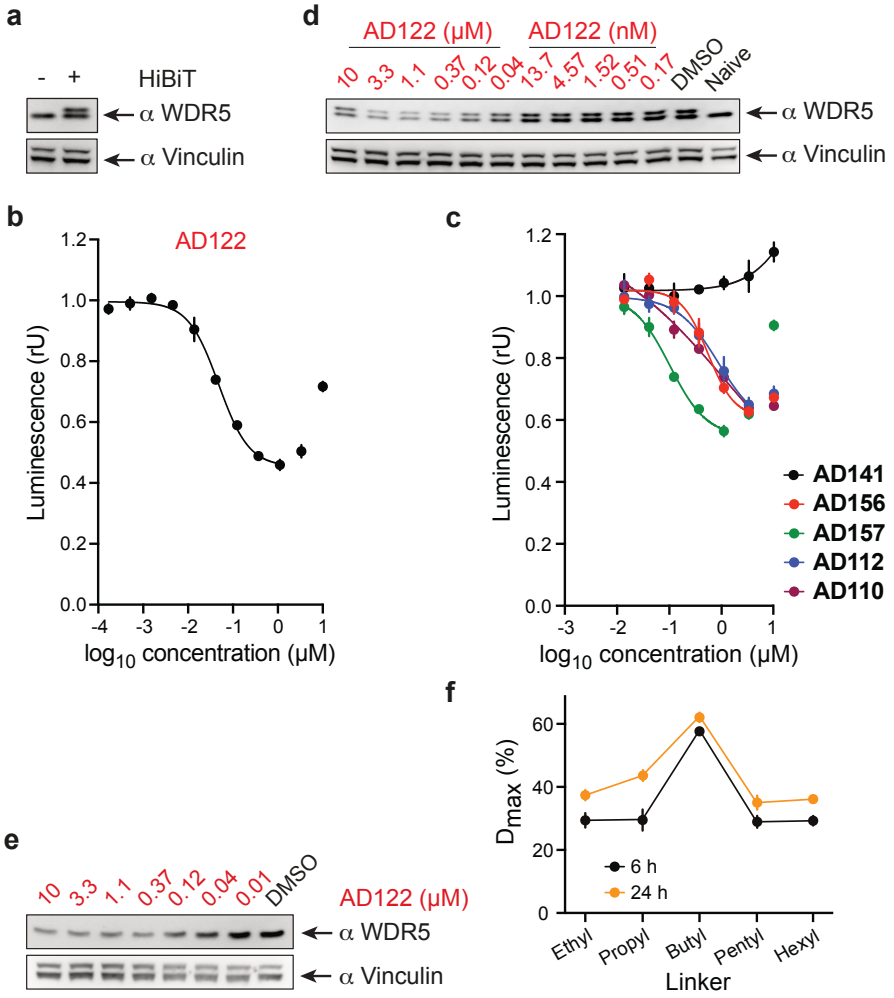

Figure 4.27: PROTAC-induced degradation of WDR5 by AD-series degraders.
(a) *Immunoblot of WDR5. MV4-11 cells stably expressing WDR5 tagged with HiBiT fragment (+) and naive MV4-11 cells (-) were analyzed for WDR5 expression with immunoblot.* ***(b, c)*** *WDR5 levels based on HiBiT assay. MV4-11$^{WDR5\text{-}HiBiT}$ cells were treated with different concentration of (b) AD122, (c) AD110, AD112, AD141, AD156, and AD157 for 24 hours, lysed, and complemented with LgBiT, and luminescence was measured to quantify WDR5 levels. The data represent mean ± SD from three replicates.* ***(d, e)*** *Immunoblot of WDR5. Different concentrations of AD122 were incubated with (d) MV4-11$^{WDR5\text{-}HiBiT}$ cells for 24 hours, (e) MV4-11 cells for 72 hours, and the protein levels were compared to naive, or vehicle-treated cells.* ***(f)*** *Quantification of D_{max} for WDR5-degraders. MV4-11$^{WDR5\text{-}HiBiT}$ cells were treated with different concentration of degraders with aliphatic linkers for 6 or 24 hours, lysed, and complemented with LgBiT, and luminescence was measured to quantify WDR5 levels. The HiBiT assay data for 24 hours is shown in (b) and (c). Ethyl (AD156), Propyl (AD157), Butyl (AD122), Pentyl (AD112), and Hexyl (AD110). The data represent mean ± SD from three replicates.*
The figures were taken and modified from Dölle et al., 2021.

4.2.2.2 Linker length is significant for degradation efficiency

Intriguingly, the HiBiT data unveiled a distinct correlation of linker lengths and degrader efficacy (Table 4.1, Fig. 4.27b, c). Shortening or elongating the linker length from butyl significantly decreased the PROTAC's efficacy (Fig. 4.27b, c). Moreover, AD141, which resembled AD112, but contained PEG_1 instead of pentyl linker, was unable to degrade WDR5 (Fig. 4.27c). To confirm the discrepancy of linker length, MV4-11$^{WDR5\text{-}HiBiT}$ cells were treated with degraders consisting of ethyl (AD156), propyl (AD157), butyl (AD122), pentyl (AD112) and hexyl (AD110) for 6 hours and HiBiT assay was performed. The comparison of the D_{max} of these degraders at 6 hours with the previously analyzed 24 hours showed a similar tendency of degradation (Fig. 4.27f). These result suggested that the linker length is crucial for favorable ternary complex formation.

4.2.2.3 Only JW48 shows degradation from JW-series

Similarly, HiBiT assays were performed to analyze the degradability of the JW-series PROTACs. Only JW48, containing PEG_2 linker, showed degradation of WDR5 (Table 4.2, Fig. 4.28a). JW48 degraded 53% WDR5-HiBiT after 24 hours with the DC_{50} of 1.24 µM. As for AD122, the HiBiT data was validated by immunoblots from JW48-treated MV4-11$^{WDR5\text{-}HiBiT}$ cells (Fig. 4.28b) and for endogenous WDR5 after 72 hours of treatment (Fig. 4.28c).

Table 4.2: HiBiT data of WDR5 ligand JW39 and its PROTACs after 24 hours treatment.

PROTAC	Linker	E3 ligase	DC_{50} (µM)[a]	DC_{max} (µM)[b]	D_{max} (%)[c]
JW39	-	-	no	no	no
JW59	PEG_1	VHL	no	no	no
JW48	PEG_2	VHL	1.24 ± 0.08	3.3	53 ± 1
JW60	PEG_3	VHL	no	no	no
JW61	PEG_4	VHL	no	no	no
JW73	PEG_5	VHL	no	no	no
JW71	PEG_6	VHL	no	no	no
JW68	PEG_7	VHL	no	no	no

[a]DC_{50}: half-maximal degradation concentration, calculated with the dose–response (four parameters) equation; [b]DC_{max}: maximal degradation concentration; [c]D_{max}: maximal degradation; no: no degradation. Table was adapted from Dölle et al., 2021

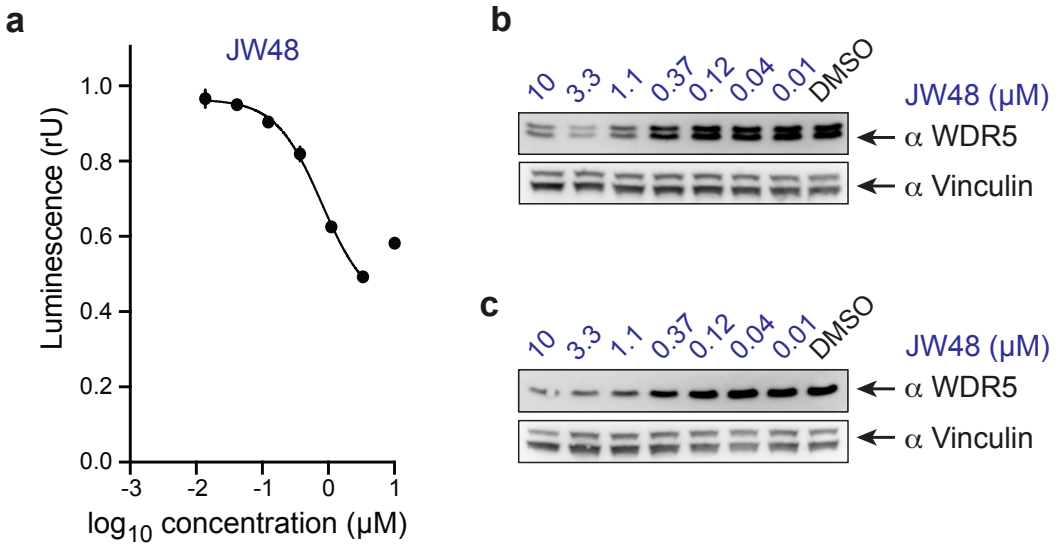

Figure 4.28: JW48-mediated degradation of WDR5.
(a) *WDR5 levels based on HiBiT assay. MV4-11$^{WDR5\text{-}HiBiT}$ cells were treated with different concentration of JW48 for 24 hours, lysed, and complemented with LgBiT, and luminescence was measured to quantify WDR5 levels. The data represent mean ± SD from three replicates.* ***(b, c)*** *Immunoblot of WDR5. Indicated concentrations of JW48 were incubated with (b) MV4-11$^{WDR5\text{-}HiBiT}$ cells for 24 hours, (c) MV4-11 cells for 72 hours, and the protein levels were compared to DMSO-treated cells.*
Figure panel (b) and (c) were taken and modified from Dölle et al., 2021.

4.2.2.4 AD122 and JW48 show degradation in various cancer cell lines

The best degraders from both series, AD122 and JW48, were tested across various cancer cell lines for their ability to degrade WDR5. Both degraders successfully induced WDR5 degradation in colorectal carcinoma (SW620), neuroblastoma (IMR5), hepatocellular carcinoma (HLE), leukemia (HL-60), breast cancer (MCF7), and lung carcinoma (Sk-Mes-1, NCI-H23, and NCI-H1299) cell lines (Fig. 4.29a-h).

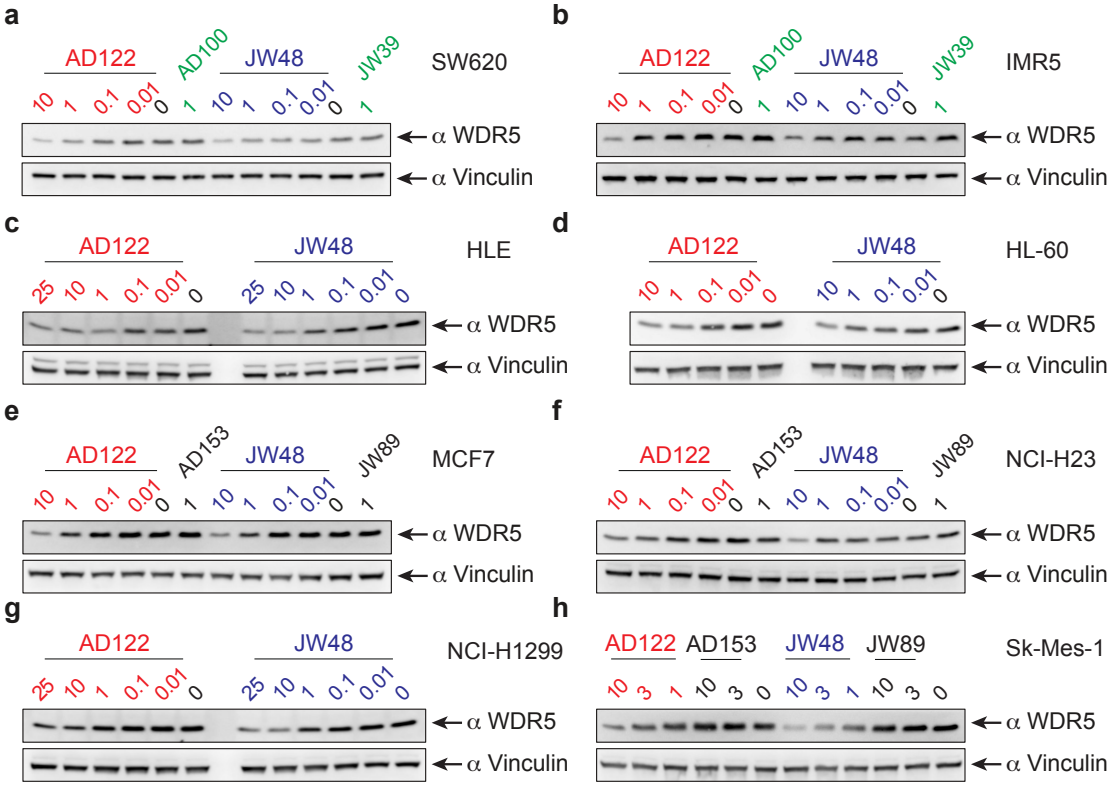

Figure 4.29: AD122- and JW48-mediated WDR5 degradation in various cancer cell lines.

(a-h) *Immunoblots of WDR5. (a) SW620, (b) IMR5, (c) HLE, (d) HL-60, (e) MCF7, (f) NCI-H23, (g) NCI-H1299, and (h) Sk-Mes-1 cells were incubated with the specified concentration of AD122 and JW48 and compared to control cells (0 µM). All cells were treated for 24 hours except Sk-Mes-1 which were treated for 48 hours.*
Part of figure panel (d) was taken and modified from Dölle et al., 2021.

4.2.3 WDR5 degradation is via the PROTAC mechanism

As for Aurora-A degraders, further experiments were conducted to verify the degradation mechanism via induced proximity between WDR5 and VHL and subsequent degradation by UPS.

4.2.3.1 WDR5 mRNA levels do not change upon PROTAC treatment

First, MV4-11 cells were treated with AD122 and JW48, along with their WDR5-ligands, for 24 hours. Even though WDR5 protein levels diminished in immunoblots (Fig. 4.30a), WDR5 transcripts levels did not differ in quantitative PCR analysis (Fig. 4.30b). Thus, a decrease in WDR5 protein level resulting from a transcriptional effect could be ruled out.

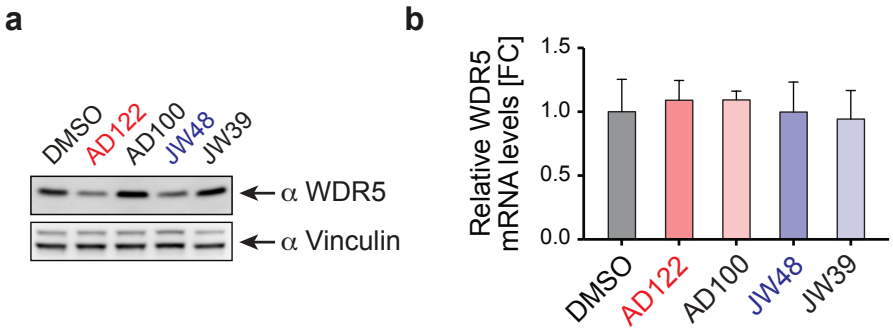

Figure 4.30: WDR5 transcript levels after degrader treatment.
(a) *WDR5 protein levels in response to WDR5 degraders. MV4-11 cells were treated with 1 µM AD100, 1 µM AD122, 3 µM JW39 and 3 µM JW48 for 24 hours. WDR5 protein levels were analyzed by immunoblot.* ***(a)*** *WDR5 mRNA levels in response to WDR5 degraders. MV4-11 cells were treated as in (a) and WDR5 transcript levels were analyzed by quantitative rtPCR. WDR5 expression levels were normalized to vehicle-treated cells (DMSO). Bars represent the mean of technical replicates.*
The figures were taken and modified from Dölle et al., 2021.

4.2.3.2 WDR5 protein stability is decreased by both degraders

Next, the impact of AD122 and JW48 on the stability of WDR5 protein was analyzed using cycloheximide chase assay. MV4-11 cells were treated with cycloheximide in the presence or absence of PROTACs for 1, 2, 6, and 12 hours and WDR5 levels were analyzed by immunoblots. Both AD122 and JW48 demonstrated a decrease in protein stability compared to vehicle-treated control cells (Fig. 4.31a, b). The effect was stronger for AD122 than for JW48.

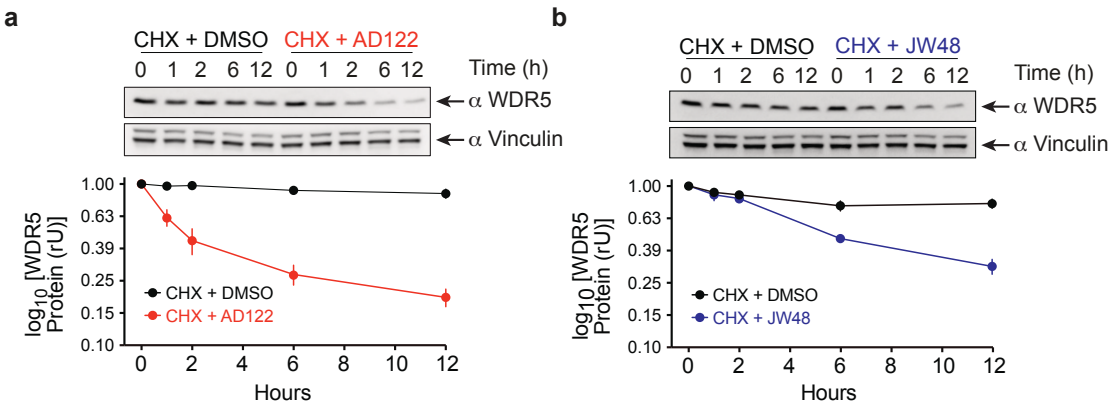

Figure 4.31: WDR5 protein stability after WDR5 degrader treatment.
(a, b) *Cycloheximide (CHX) chase assay with WDR5 degraders. MV4-11 cells were incubated with 50 µg/ml CHX for indicated time points in the presence or absence of (a) 1 µM AD122, (b) 3 µM JW48. WDR5 protein level was evaluated by immunoblotting. The data represent mean ± SD from two biological replicates.*
The figures were taken and modified from Dölle et al., 2021.

4.2.3.3 PROTAC-mediated degradation is prevented by proteasomal and neddylation inhibition

Inhibition experiments were performed to assess the connection of WDR5 level decrease with UPS. Two inhibitors of the UPS system, MG132 (proteasomal inhibitor) and MLN4924 (NAE inhibitor), were used. MV4-11 cells were treated with AD122 and JW48 in combination with the inhibitors or alone. Upon comparison of the WDR5 levels to the DMSO-treated cells, AD122- and JW48-mediated depletion of WDR5 was completely abrogated by both inhibitors (Fig. 4.32a, b).

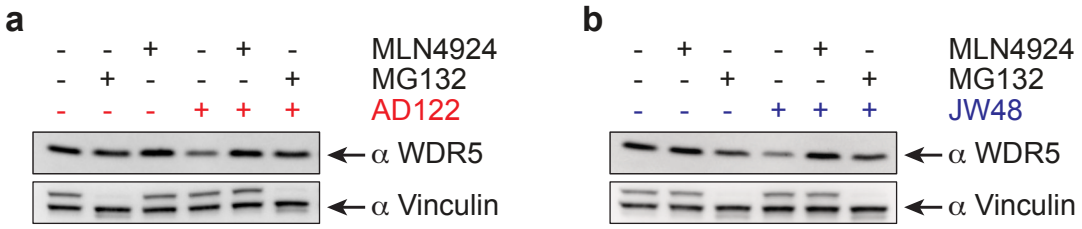

Figure 4.32: Effect of proteasomal and neddylation inhibition on degrader-mediated WDR5 degradation.
(a, b) *Immunoblots of WDR5. MV4-11 cells were incubated with 5 µM MLN4924, 10 µM MG132 or in combination with (d) 1 µM AD122, (e) 3 µM JW48 for 6 hours. The figure panel (b) was taken and modified from Dölle et al., 2021.*

4.2.3.4 WDR5 ligand co-incubation abrogates the degradation by PROTAC

A competition assay was performed to prove that WDR5 binding was necessary for degrader-induced proximity between WDR5 and VHL. MV4-11 cells were treated with the WDR5 ligands (AD100 and JW39), VHL-ligand, degraders alone and degraders in the presence of their corresponding ligands. As expected, degraders decreased WDR5 levels, whereas neither of the WDR5- and VHL-ligands did (Fig. 4.33a, b). More importantly, co-incubation of degraders with their WDR5-ligands successfully rescued WDR5 degradation by competing for WDR5 binding (Fig. 4.33a, b).

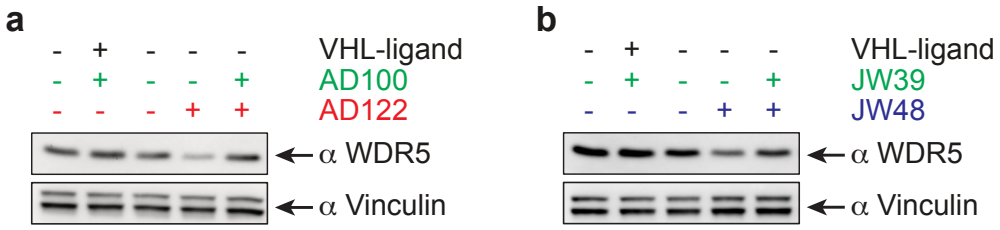

Figure 4.33: Competition assay of WDR5 degraders with their WDR5 ligands.
(a, b) *Immunoblots of WDR5. MV4-11 cells were treated for 6 hours with 10 µM VHL-ligand or (a) 1 µM AD122 and 5 µM AD100, (b) 3 µM JW48 and 10 µM JW39 and compared to single compound or vehicle-treated cells.*
The figure panel (a) was taken and modified from Dölle et al., 2021.

4.2.3.5 Enantiomer analog of WDR5-PROTACs do not degrade WDR5

To demonstrate that VHL-binding is crucial for the degradation, AD122 and JW48 analogs were synthesized with an enantiomer of the VHL ligand, which abolishes binding to VHL, AD153 (AD122 analog) and JW89 (JW48 analog) (Fig. 4.34a, b). The analogs were synthesized by Anja Dölle and Janik Weckesser. To test the efficiency of these compounds, MV4-11$^{WDR5\text{-}HiBiT}$ cells were treated with the degraders, their analogs, and their WDR5 ligands for 24 hours. The degraders induced degradation of WDR5, whereas the inactive analogs and ligands could not degrade WDR5 (Fig. 4.34c, d). Incubation of cells with AD100, however, massively increased WDR5-HiBiT levels, which might be due to increased stability of the protein bound by the ligand (Fig. 4.34c).

From these experiments, it can be concluded that the WDR5 PROTACs AD122 and JW48 mediate WDR5 ubiquitination and eventual degradation by inducing ternary complex formation with VHL.

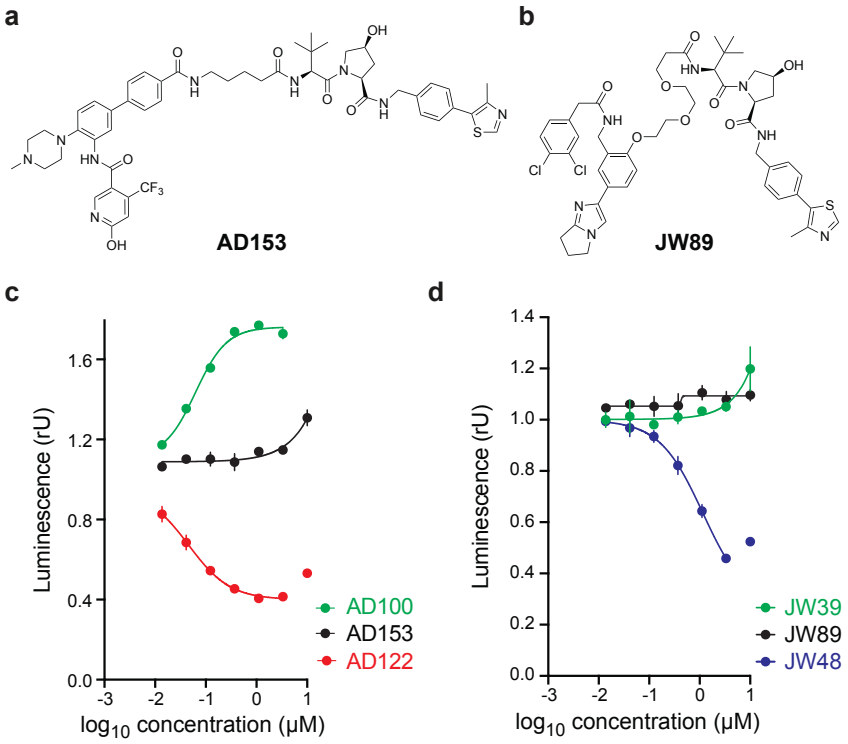

Figure 4.34: Enantiomer analogs of WDR5 PROTACs do not degrade WDR5.
(a, b) *Structure of enantiomer analogs of WDR5 degraders. The inactive epimer analog of (a) AD122, AD153 and (b) JW48, JW89 resembles corresponding degrader but cannot bind VHL.* ***(c, d)*** *WDR5 levels based on HiBiT assay. MV4-11$^{WDR5\text{-}HiBiT}$ cells were treated with different concentration of (c) AD122, AD153 and AD100, (d) JW48, JW89, and JW39, for 24 hours, lysed, and complemented with LgBiT, and luminescence was measured to quantify WDR5 levels. The data represent mean ± SD from three replicates.*
The figures were taken and modified from Dölle et al., 2021.

4.2.4 Both AD122 and JW48 are specific to WDR5

To investigate the selectivity of the PROTACs, quantitative proteomics were performed in MV4-11 cells. MV4-11 cells were treated at least in triplicates with DMSO, AD122, JW48, AD100, and JW39 for 9 hours. After treatment, the cells were lysed and the degradation of WDR5 by the degraders were initially validated by immunoblotting (Fig. 4.35a). Then the cell lysate was subjected to label-free quantitative mass spectrometry analysis. The analysis was performed by Nicola Berner from the group of Prof. Dr. Bernhard Kuster, Technical University of Munich. Of the 5805 proteins reliably detected, only WDR5 was significantly downregulated (p-value <0.001 and $\log_2$FC < -0.5) by both AD122 and JW48 in comparison to DMSO (Fig. 4.35b, c), illustrating that both PROTACs are specific for WDR5. The WDR5 degradation was significant but modest after 9 hours as compared to JB170 for Aurora-A degradation after 6 hours. AD122 degraded 38.2% WDR5 with a p-

value of 9.39x 10^{-5} when compared to DMSO treatment, while JW48 degraded mere 32.1% WDR5 with a p-value of 6.04x 10^{-4}. The degradation efficiency obtained from proteomics was lesser than from the western blot validation where 50% degradation of WDR5 by both degraders were observed (Fig. 35a-c). Furthermore, the abundance of other subunits of SET1/MLL complex (KMT2A, KTM2B, KTM2C, KTM2D, SETD1A, RBBP5, ASH2L, and DPY30) were not decreased by both degraders (Fig. 35b, c, labeled in orange). In contrast, WDR5 levels were not significantly altered by the ligands AD100 and JW39 (Fig. 4.35d, e).

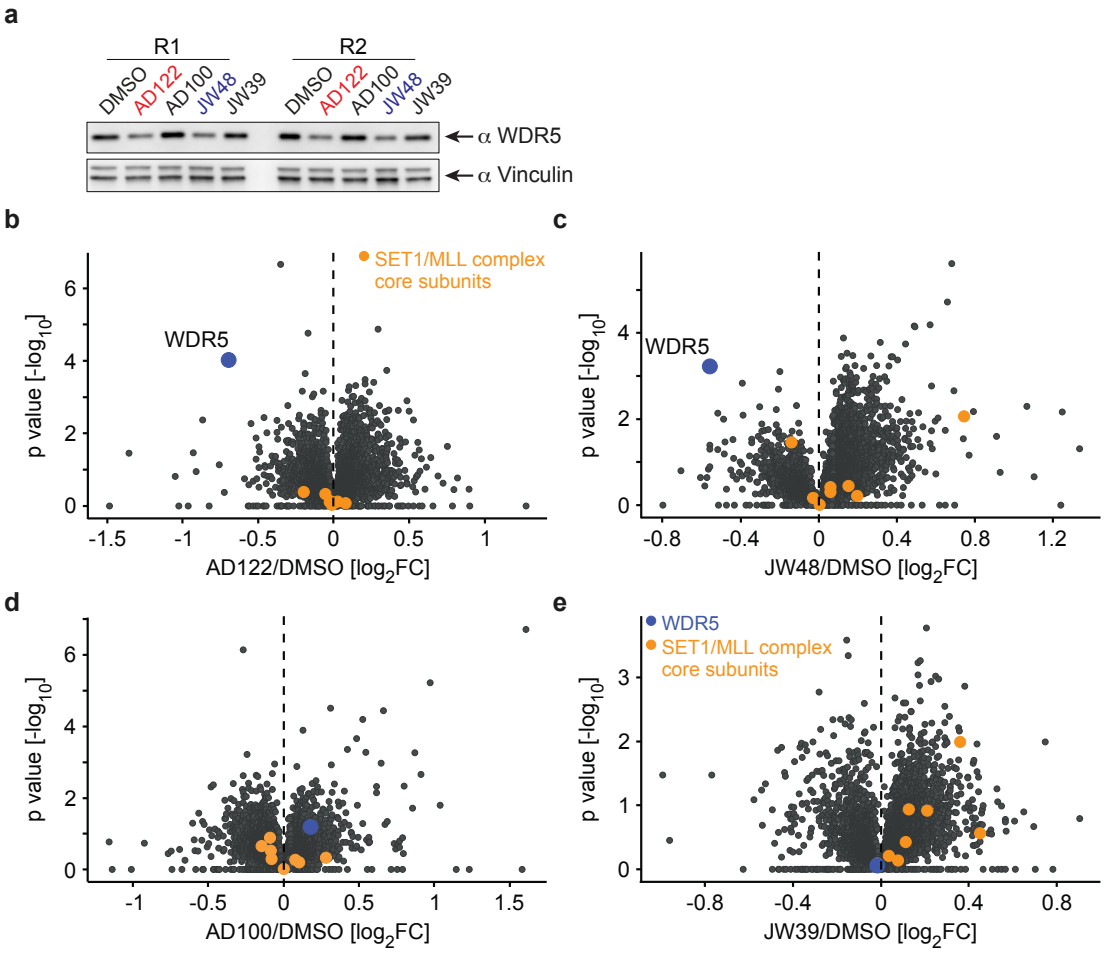

Figure 4.35: AD122 and JW48 are selective to WDR5.

(a) *Immunoblot of WDR5. MV4-11 cells were treated with 1 μM AD122, 5 μM JW48, 1 μM AD100, and 5 μM JW39 for 9 hours, and WDR5 protein levels were analyzed by immunoblotting. R1 and R2 are two replicates.* ***(b-e)*** *Volcano plots showing alteration in cellular proteome. MV4-11 cells were treated with (a) 1 μM AD122, (b) 5 μM JW48, (c) 1 μM AD100, and (d) 5 μM JW39 for 9 hours, and proteins were analyzed by quantitative mass spectrometry. The x-axis shows the log_2 fold change of protein abundance by corresponding treatment compared to DMSO. Y-axis shows a negative log_{10} of the p-value from replicate experiments (triplicates for AD122 and JW39, and*

quadruplicates for DMSO, AD100 and JW48). WDR5 and other SET1/MLL complex core subunits (KMT2A, KTM2B, KTM2C, KTM2D, SETD1A, RBBP5, ASH2L, and DPY30) are labeled in blue and orange, respectively. Immunoblot of WDR5 from two replicates are shown in (a).
The figures were taken and modified from Dölle et al., 2021.

4.2.5 Degradation of WDR5 with JW48 shows modest proliferation defect

The antiproliferative activity of AD122 and JW48 was tested in different cancer cell lines. MV4-11 cells were treated with different concentrations of AD122, AD153, AD100, JW48, JW89, and JW39 for 15 days. The cells were counted every third day and re-seeded to the original density in fresh media with compounds to prevent overgrowth. The cumulative growth curve showed no proliferation defect by AD122, whereas JW48 induced a defect at higher concentration (Fig. 36a, b). The control AD153 did not show any antiproliferative effect in MV4-11 cells. However, the ligand AD100 was very toxic to cells at higher concentrations (Fig. 36a), but the size of AD100 is considerably smaller and more cell-permeable than AD122. Moreover, off-target effects of AD100 had not been ruled out by any experiments so far. Due to the observed toxicity of AD100, it was omitted for further long-term experiments.
Similarly, HL-60 cells were treated for nine days with different concentrations of AD122, AD153, JW48, JW89, and JW39. Like in MV4-11 cells, exclusively higher concentration of JW48 decreased the proliferation of HL-60 cells (Fig. 36c, d).
Likewise, in Sk-Mes-1 lung carcinoma cells crystal violet staining after eight days of treatment revealed that 10 µM JW48 had a strong antiproliferative activity, whereas AD122 did not show any effect (Fig. 36e, f).
It can be speculated from the results that only the high concentration of JW48 maintains durable and adequate WDR5 degradation required to inhibit cellular growth. So, a more substantial depletion of WDR5 might be required to see assertive antiproliferative defects by the PROTACs.

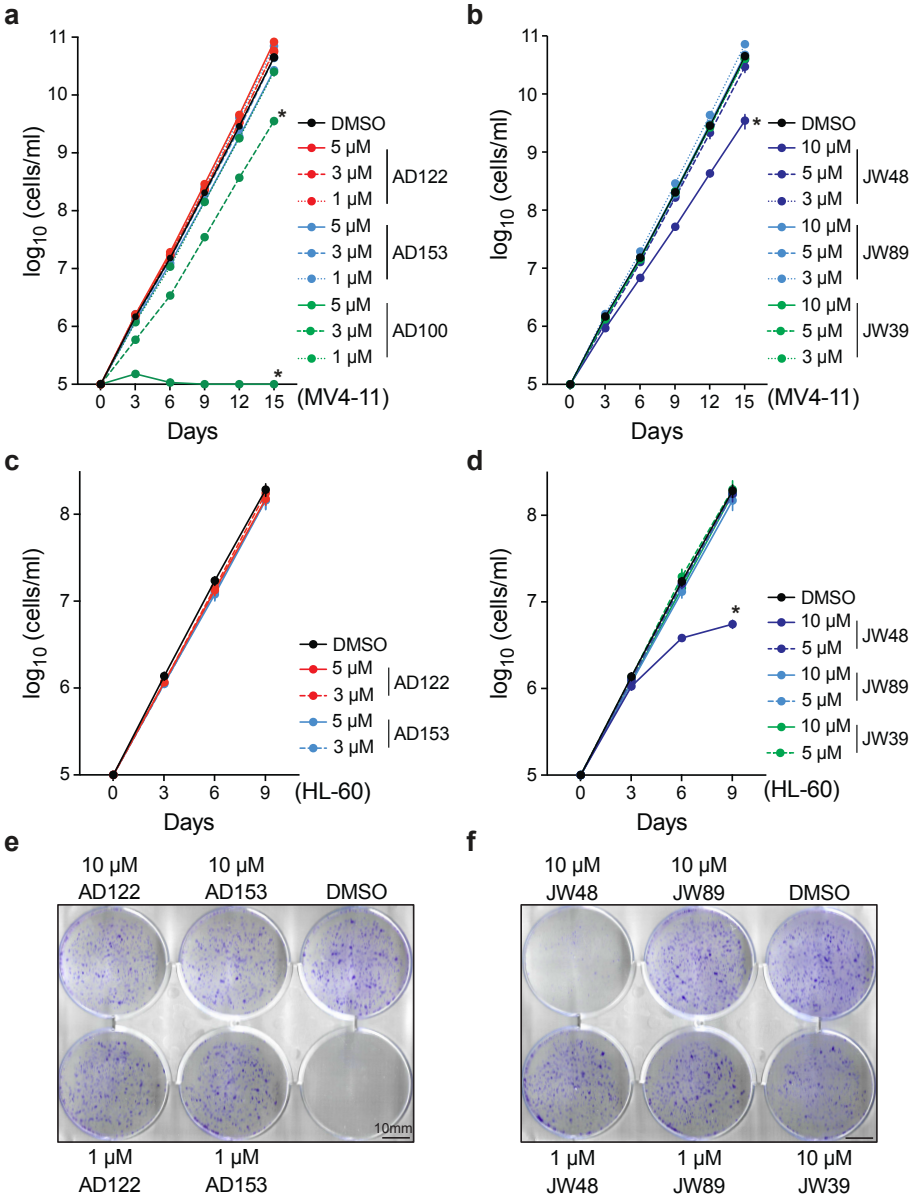

Figure 4.36: JW48-mediated degradation of WDR5 shows proliferation defect. ***(a, b)*** *Growth analysis in MV4-11 cells. MV4-11 cells were treated with indicated concentrations of (a) AD122, AD153 and AD100, (b) JW48, JW89 and JW39 for 15 days and counted at different time points. The cells were reseeded to original density every third day in fresh media with compounds to prevent overgrowth. Data represent mean ± SD of two biological replicates. Asterisks indicate p-value calculated from the 15th day cumulative cell number using two-tailed unpaired t-test assuming equal variance against DMSO treatment. * p ≤ 0.05.* ***(c, d)*** *Growth analysis in HL-60 cells. HL-60 cells were treated with various concentrations of (c) AD122 and AD153, (d) JW48, JW89 and JW39 for 9 days and counted at indicated time points. Cumulative growth curve was generated as in (a, b). Data represent mean ± SD of two biological replicates.* ***(e, f)*** *Crystal violet staining of Sk-Mes-1 cells. Sk-Mes-1 cells were treated with specified concentrations of (e) AD122 and AD153, (f) JW48, JW89 and JW39 for eight days and stained with crystal violet. Scale bar is 10 mm.*
Asterisks indicate p-value calculated from the final day cumulative cell number using two-tailed unpaired t-test assuming equal variance against DMSO treatment. p ≤ 0.05.*

The figure panel (b) was taken and modified from Dölle et al., 2021.

4.2.6 Overexpression of E3-ligase increases efficacy of PROTACs

The amount of all three components of the ternary complex, WDR5, degrader, and VHL are essential for the functionality of the degrader. The effect of various amounts of degrader was already assessed. In quest of improving the degradation of WDR5, it was postulated that VHL expression might be the limiting factor for the PROTACs efficiency.

4.2.6.1 VHL overexpression shows superior degradation of WDR5

To test this hypothesis, VHL was stably expressed in MV4-11$^{WDR5\text{-}HiBiT}$ cells (MV4-11$^{WDR5\text{-}HiBiT/VHL}$) and the degradation efficiency of AD122 and JW48 were evaluated (Fig. 4.37a). Indeed, HiBiT assay after 24 hours of treatment showed that VHL overexpression strongly increased the degradation of WDR5-HiBiT by both degraders (Fig. 4.37b). For AD122, D_{max} increased from 59.5% to 74.7% and DC_{50} decreased from 45 nM to 5.9 nM. Similarly, for JW48, D_{max} increased from 51.3% to 77.8% and DC_{50} decreased from 1.01 µM to 0.155 µM. The result was validated by immunoblot of MV4-11$^{WDR5\text{-}HiBiT/VHL}$ and MV4-11$^{WDR5\text{-}HiBiT}$ cells (Fig. 4.37c).

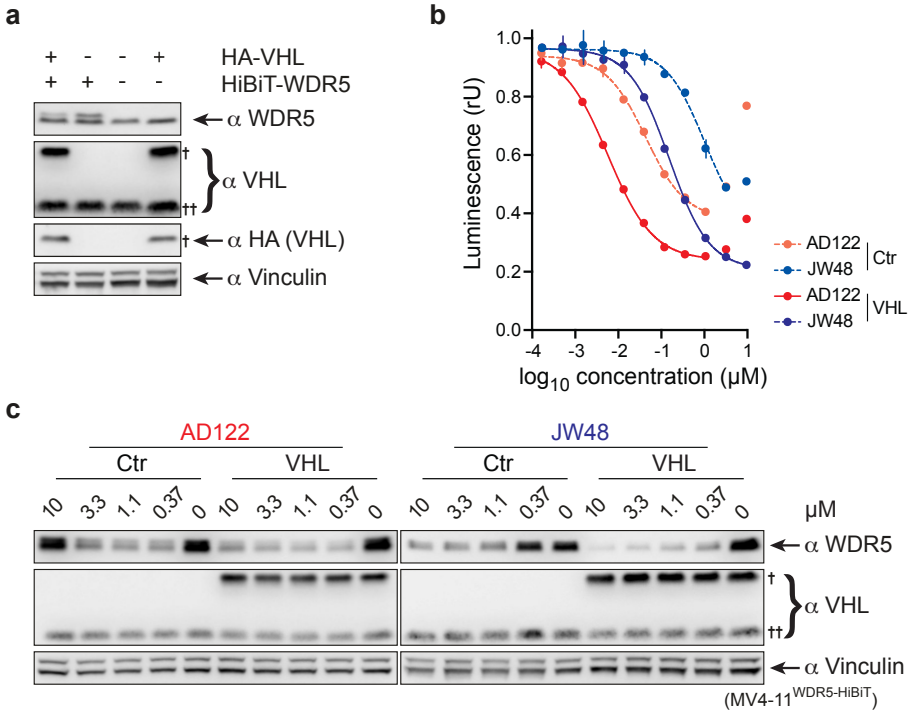

Figure 4.37: VHL overexpression increases degradation efficiency.
(a) *Immunoblot of WDR5 and VHL. HA-tagged VHL was stably expressed in MV4-11 and MV4-11$^{HiBiT\text{-}WDR5}$ cells. † Overexpressed HA-VHL; †† endogenous VHL.* ***(b)*** *WDR5*

levels based on HiBiT assay. MV4-11$^{WDR5\text{-}HiBiT}$ cells (Ctr) and MV4-11$^{HiBiT\text{-}WDR5/VHL}$ cells (VHL) were treated with different concentrations of AD122 and JW48, for 24 hours, lysed, and complemented with LgBiT, and luminescence was measured to quantify WDR5 levels. The data represent mean ± SD from three replicates. ***(c)*** *Immunoblot of WDR5 and VHL. Indicated concentrations of AD122 and JW48 were incubated with MV4-11$^{HiBiT\text{-}WDR5}$ cells (Ctr) and MV4-11$^{HiBiT\text{-}WDR5/VHL}$ cells (VHL) and protein levels were analyzed. † Overexpressed HA-VHL; †† endogenous VHL.*
The figure panels (a), (b) and part of figure panel (c) were taken and modified from Dölle et al., 2021.

4.2.6.2 JW48 shows stronger growth inhibition after VHL overexpression

To further test the effect of VHL overexpression on PROTACs efficiency, MV4-11 cells were transduced with VHL (MV4-11^{VHL}) (Fig. 4.37a). VHL overexpression and its effect on degradation of WDR5 were verified by immunoblotting (Fig. 4.38a). Furthermore, in cumulative growth curve the proliferation defect induced by JW48 was more pronounced upon VHL overexpression (Fig. 4.38b) and occurred with lower concentration of JW48 (5 µM) not observed without VHL overexpression before (Fig. 4.36a). Importantly, none of the controls for JW48 showed any effect (Fig. 4.38b). Surprisingly, AD122 did not show any antiproliferative activity in MV4-11^{VHL} cells (Fig. 4.38c).
Similarly, VHL was ectopically expressed in HL-60 cells (HL-60^{VHL}) and analyzed for growth inhibition by AD122 and JW48. Like in MV4-11^{VHL} cells, the higher concentration of JW48 showed a stronger effect than without VHL overexpression and even lower concertation showed an antiproliferative effect (Fig. 4.38d). Remarkably, both concentrations of AD122 showed growth inhibition in HL-60^{VHL} cells but did not reach statistical significance (Fig. 4.38e). Lower n number (n=2) might be the reason for statistical insignificance. All controls did not show any effect.

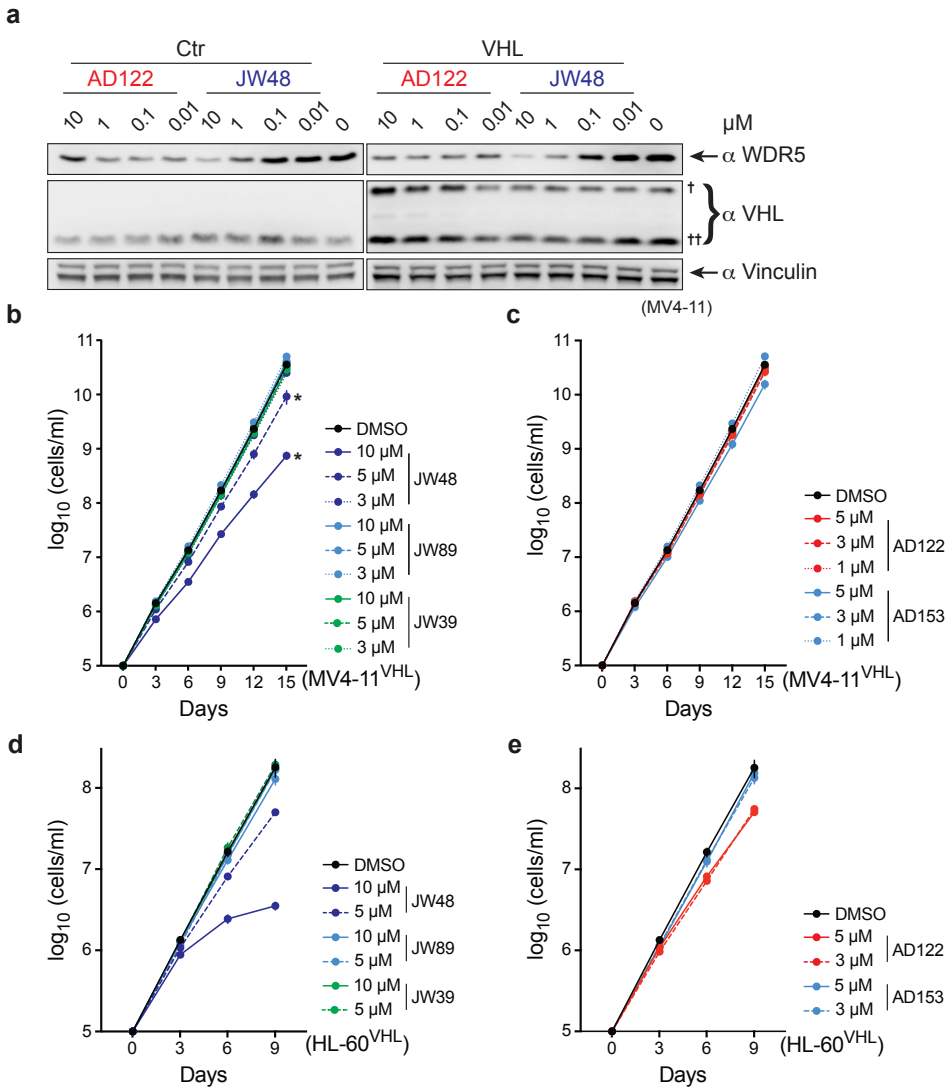

Figure 4.38: VHL overexpression increases the potency of degraders

(a) *Immunoblot of WDR5 and VHL. Indicated concentrations of AD122 and JW48 were incubated with MV4-11 cells (Ctr) and MV4-11^{VHL} cells (VHL). † Overexpressed HA-VHL; †† endogenous VHL.* ***(b, c)*** *Growth analysis in MV4-11^{VHL} cells. MV4-11^{VHL} cells were treated with indicated concentrations of (b) JW48, JW89 and JW39, (c) AD122, AD153 and AD100, for 15 days and counted at different time points. Data represent mean ± SD of two biological replicates.* ***(d, e)*** *Growth analysis in HL-60^{VHL} cells. HL-60^{VHL} cells were treated with various concentrations of (g) JW48, JW89 and JW39, (h) AD122 and AD153, for 9 days and counted at indicated time points. Data represent mean ± SD of two biological replicates.*

Asterisks indicate p-value calculated from the final day cumulative cell number using two-tailed unpaired t-test assuming equal variance against DMSO treatment. p ≤ 0.05. The figure panels (b) and part of figure panel (a) were taken and modified from Dölle et al., 2021.*

In summary, degraders from both series showed incomplete but significant and selective degradation of WDR5 without affecting any other component of the MLL1/SET1 complex. Due to incomplete degradation, the cellular effects of these

degraders were also modest. However, the effects could be excelled by enhancing degrader-induced degradation of WDR5 through the overexpression of the involved E3-ligase, in this case VHL. Moreover, no degradation was observed by CRBN-based degraders and the linker length was crucial for degradation efficiency of VHL-based degraders.

4.3 Assay for prediction of degradative E3-ligase for a target protein

4.3.1 Assay setup

For predicting which E3-ligases that can successfully degrade a target protein a proximity-based assay was established. The assay constitutes of a rapamycin-based heterodimerization system. The heterodimerizer, rapamycin, binds to the 12-kDa FK506 binding protein (FKBP12) and the FKBP-rapamycin binding domain (FRB) of mTOR complex 1 which results in chemically induced proximity (Inobe & Nukina, 2016). Compared to proteins of other heterodimerization systems, FKBP12 and FRB are relatively smaller in size with 12 kDa and 11 kDa, respectively. For the rapamycin-induced proximity assay (RIP assay), the target proteins are tagged with FKBP12, whereas E3-ligase candidates are tagged with the FRB domain (Fig. 4.39). Then, the pair of a target protein and E3-ligase fusion constructs are co-expressed in the cells. After the addition of rapamycin, the proximity between E3 and the target protein is induced, leading to the potential degradation of the target (Fig. 4.39). Finally, the target protein levels are measured by immunoblot (Fig. 4.39). For using a luciferase-based assay, nanoluciferase (NLuc) is added to the target protein to perform quantitative and kinetic measurements of its protein levels.

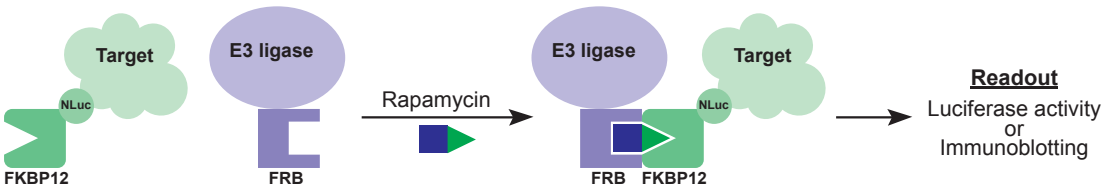

Figure 4.39: RIP assay.

Schematic representation of the rapamycin-induced proximity (RIP) assay. The E3-

ligase and target proteins are tagged with FKBP12 and FRB, respectively, and after rapamycin addition, the target protein levels are analyzed by immunoblotting or by measuring luciferase activity.

4.3.2 Assay development

For RIP assay development, WDR5 and VHL were used as an example, since successful degradation of WDR5 by VHL-based degraders was shown in this study (see section 4.2.2). VHL was N- and C-terminally tagged with FRB and WDR5 with FKBP12 and NLuc (WDR5-NLuc-FKBP12 and NLuc-WDR5-FKBP12). A flexible linker (2x GSSG) was added in between the tags and proteins in all constructs to prevent rigidity. As controls, an FRB construct without VHL and a NLuc tagged FKBP12 construct without WDR5 were also generated. These constructs were cloned within the bachelor thesis of Isabella Kurrer (2021, group of Prof. Dr. Elmar Wolf, University of Wuerzburg), under my supervision.

First, several MV4-11 cell lines expressing the combination of the FRB- and FKBP12-based constructs were generated. The expression of the fusion constructs was verified by immunoblotting (Fig. 4.40a, b). Second, the generated cell lines were incubated for six hours with rapamycin. Luminescence measurement showed that rapamycin treatment decreased a mere 10% of WDR5 protein level in the presence of FRB-tagged VHL when compared to FRB (Fig. 4.40c). The result was validated by immunoblots for cells expressing WDR5 fusion proteins (Fig. 4.40d). Noteworthy, the NLuc-FKBP12 expression was in some conditions increased by rapamycin treatment as analyzed by luciferase activity measurement (Fig. 4.40c). This could not be verified by western blot due to lack of a proper antibody. Stable cell line generation and the follow-up experiments were performed within the bachelor thesis of Isabella Kurrer.

It could be speculated that the inefficiency of the assay might be a result of differences in the expression levels of the chimeric proteins. As revealed in this study higher expression of the involved E3-ligase increased the degradation efficacy of PROTACs (see section 4.2.6). Moreover, from immunoblots it became obvious that the expression level of WDR5 fusion proteins was extremely high compared to endogenous WDR5 levels (Fig. 4.40a). To test this hypothesis, a transfection-based system was utilized where expression level of protein could be tuned easily. Moreover, transfection-based system is faster and more scalable for screening approaches than a stable cell line-based assay. Therefore, HEK293

cells were transfected with WDR5-NLuc-FKBP12 along with VHL-FRB or FRB plasmids in the ratio of 1:1 and 1:10 (FKBP12: FRB) and were treated with rapamycin or DMSO for 6 hours. Both luciferase measurement and immunoblots displayed that WDR5 levels were decreased by rapamycin for a transfection ratio of 1:10 but not for 1:1 (Fig. 4.40.e, f). The result demonstrated that the stoichiometry of the target and E3-ligase was essential for the assay.

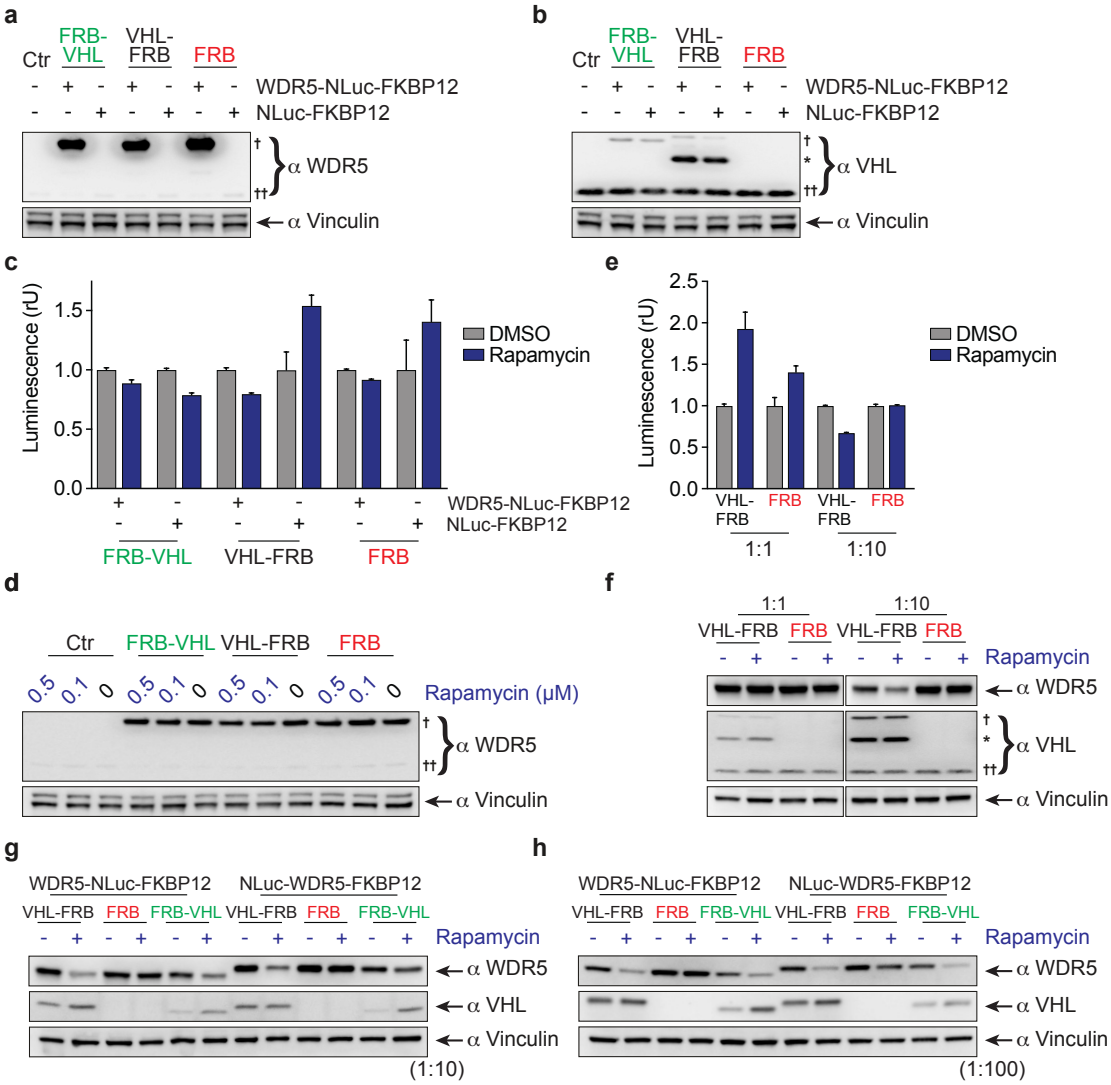

Figure 4.40: Establishment of the RIP assay.

(a, b) *Immunoblots of WDR5 or VHL. MV4-11 cells were transduced to express FKBP12 tagged NLuc or WDR5-NLuc along with N- or C-terminally VHL-tagged FRB or untagged FRB. The expression level of (a) WDR5, (b) VHL was compared to the control cells. † Overexpressed chimeric protein; †† endogenous protein; * free exogenous VHL from its chimeric form. This experiment was performed by Isabella Kurrer.* ***(c)*** *NLuc containing fusion protein levels based on luciferase measurements. MV4-11 cells expressing combination of different FKBP12, and FRB fusion proteins were treated with 0.5 μM rapamycin for 6 hours and compared to DMSO treated cells. This experiment was performed by Isabella Kurrer.* ***(d)*** *Immunoblot of WDR5. MV4-11 cells expressing combination of different WDR5-FKBP12, and FRB fusion proteins*

were treated with indicated concentrations of rapamycin for 6 hours and the expression of WDR5 fusion proteins were compared. † Overexpressed chimeric WDR5; †† endogenous WDR5. This experiment was performed by Isabella Kurrer. ***(e, f)*** *WDR5 levels based on luciferase measurement or immunoblot. HEK293 cells were transfected with vectors encoding WDR5-NLuc-FKBP12 and VHL-FRB/ FRB in the indicated weight to weight ratio. The transfected cells were treated with 100 nM rapamycin for 6 hours and WDR5 protein level was measured and compared using (e) luciferase assay, (f) immunoblotting. † VHL-FRB; †† endogenous VHL; * free exogenous VHL from VHL-FRB.* ***(g, h)*** *Immunoblots of WDR5 and VHL. HEK293 cells were transfected with combinations of WDR5-NLuc-FKBP12/ NLuc-WDR5-FKBP12 and VHL-FRB/ FRB-VHL/ FRB vectors in the ratio of (g) 1:10, (h) 1:100. The transfected cells were treated with 100 nM rapamycin overnight. WDR5 and VHL fusion protein level was compared to the untreated controls and against each other.*

Next, WDR5-NLuc-FKBP12 and NLuc-WDR5-FKBP12 constructs were co-transfected with FRB-VHL, VHL-FRB, and FRB constructs in the ratio of 1:10 and treated with rapamycin or DMSO. Immunoblots illustrated that both chimeric WDR5 proteins were degraded by VHL fusion proteins in the presence of rapamycin, whereas no degradation was observed by FRB without VHL (Fig. 4.40g). Moreover, VHL that was C-terminally tagged to FRB (VHL-FRB) showed better degradation than the one with N-terminal FRB tag (FRB-VHL) (Fig. 4.40g). The experiment was repeated with a transfection ratio of FKBP12: FRB of 1:100 and a similar results to that with 1:10 were observed (Fig. 4.40h).

In summary, these results demonstrated that a transfection-based method was superior to the stable cell line-based method and that the expression of E3-ligase needs to be higher than the target.

4.3.3 Assay validation

After the optimization, RIP assay was used to predict the degradation of WDR5 by another E3 ligase, CRBN. None of the CRBN recruiting PROTACs tested in this study were able to degrade WDR5 (see section 4.2.2). CRBN-FRB and FRB-CRBN vectors were generated and co-transfected in HEK293 cells with WDR5-NLuc-FKBP12. The transfected cells were treated with two different concentrations of rapamycin and the level of WDR5 chimera was evaluated by western blot. The immunoblot corroborated the expression of both tagged versions of CRBN (Fig. 4.41a). However, no significant degradation of the WDR5 fusion protein was observed upon the addition of rapamycin (Fig. 4.41a).

For the validation, a time-course study was performed using WDR5-NLuc-FKBP12, VHL-FRB, CRBN-FRB, and FRB constructs. HEK293 cells were transfected with a combination of vectors and treated with rapamycin for different time points. Luminescence measurement showed that VHL was capable of WDR5 degradation in a time-dependent fashion, whereas CRBN was not (Fig. 4.41b). Immunoblot of WDR5 on samples from 6-hour treatment confirmed the result from the luminescence measurement (Fig. 4.41c).

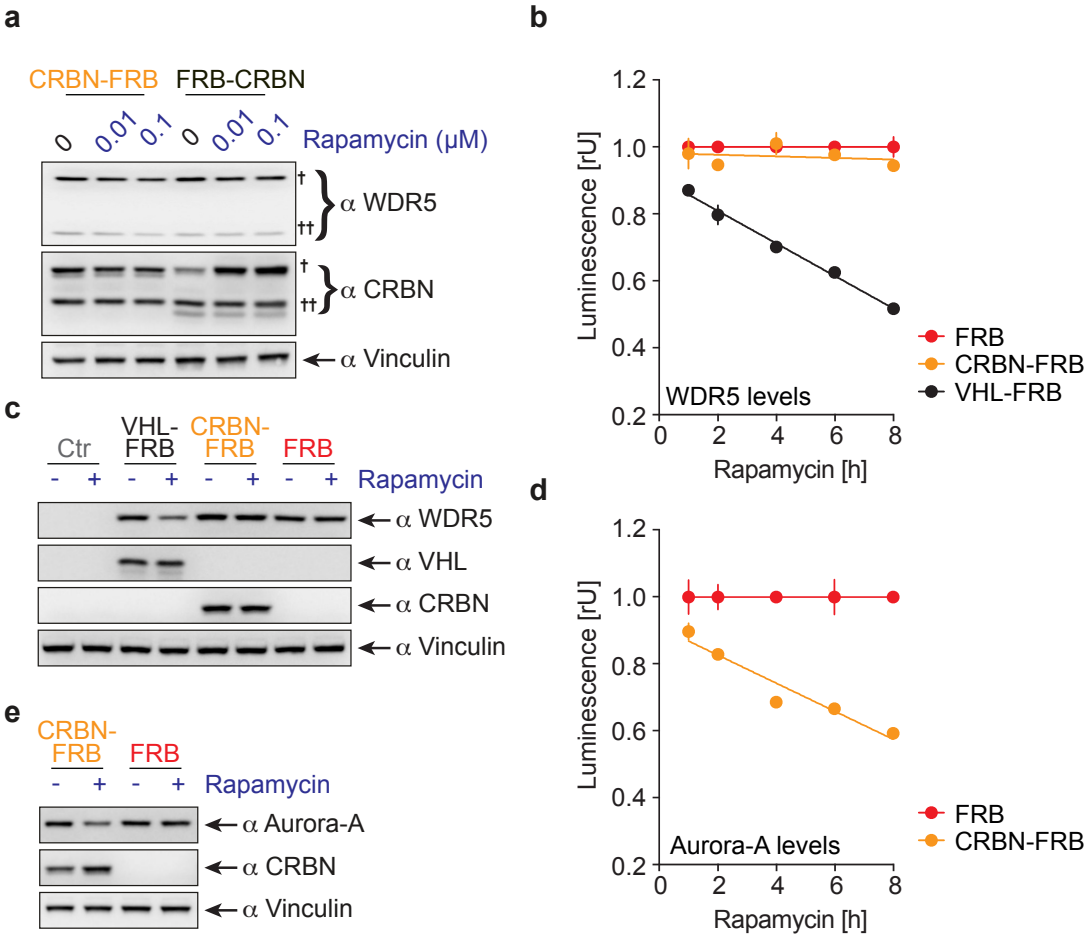

Figure 4.41: Validation of the RIP assay to predict functional E3-ligase.
(a) *Immunoblots of WDR5 and CRBN. HEK293 cells were transfected with WDR5-NLuc-FKBP12 and CRBN-FRB / FRB-CRBN. The transfected cells were treated with different concentrations of rapamycin for 6 hours and WDR5 and CRBN protein levels were analyzed. † transfected chimeric proteins; †† endogenous proteins.* ***(b)*** *WDR5 fusion protein levels based on luciferase measurement. HEK293 cells were transfected with WDR5-NLuc-FKBP12 and CRBN-FRB/ VHL-FRB/ FRB, treated with 10 nM rapamycin for indicated time points and the expression level of WDR5 chimera was measured by luciferase assay.* ***(c)*** *Immunoblots of WDR5, VHL and CRBN fusion proteins. The western blot corresponds to the 6 h time point shown in (b).* ***(d)*** *Aurora-A fusion protein levels based on luciferase measurement. HEK293 cells were transfected with Aurora-A-NLuc-FKBP12 and CRBN-FRB/ FRB, treated with 10 nM rapamycin for indicated time points and the expression level of Aurora-A chimera was*

measured by luciferase assay. ***(e)*** *Immunoblots of Aurora-A and CRBN fusion proteins. The western blot corresponds to the 6 h time point shown in (d).*

In a second validation experiment, the RIP assay was used to test the ability of CRBN for Aurora-A degradation. JB170, a CRBN-based PROTAC, displayed degradation of Aurora-A in this study (see section 4.1.2). The Aurora-A-NLuc-FKBP12 construct was cloned and co-expressed with CRBN-FRB or FRB in HEK293 cells. The transfected cells were treated with rapamycin for various time points. Both luciferase measurement and immunoblot displayed Aurora-A degradation by CRBN in agreement with previous results (Fig. 4.41d, e).

Thus, the RIP assay correctly predicted and validated the productive degradation of WDR5 by VHL but not CRBN and Aurora-A by CRBN.

5 Discussion

The expression of transcription factor Myc is deregulated in many different cancer types. A large body of evidence has indicated that Myc is vital for the development and maintenance of cancer. However, approaches to directly target Myc have not been successful so far due to its structural limitations. In recent years, efforts have been made to study and identify the interactors of Myc that promote its oncogenicity. An alternate approach to indirectly target Myc is by inhibiting Myc-interacting oncoproteins.

In this study, two of such Myc-interacting oncoproteins, Aurora-A and WDR5, were successfully targeted using bifunctional molecules, PROTACs. PROTACs are potent tools and overcome the limitations of traditional modalities. Being a relatively new technique, it has quickly become a powerful tool in biology research and therapeutics (Gao et al., 2022; E. Hamilton et al., 2022; E. P. Hamilton et al., 2022). Aurora-A and WDR5 were chosen as their interaction with Myc was validated by co-crystallization with N-Myc and Myc, respectively (Richards et al., 2016; Thomas et al., 2015). Furthermore, the ligands for both proteins are published and their crystal structures in complex with those ligands were also reported (Grebien et al., 2015; Sloane et al., 2010; Wang et al., 2018). This facilitated the PROTAC design as the linker attachment point could be designated to the solvent-exposed residue of the ligand without affecting its binding to Aurora-A or WDR5.

5.1 Aurora-A degraders

5.1.1 Aurora-A degraders hijacking CRBN degrade Aurora-A

Seven different PROTACs based on the Aurora-A inhibitor alisertib were tested with five of them recruiting CRBN and two VHL. In leukemia MV4-11 cells only the CRBN-based PROTACs successfully degraded the steady state level of Aurora-A. It was not investigated systematically why VHL-based PROTACs were not able to degrade Aurora-A. But the inability of the VHL-based degraders to degrade Aurora-A was not due to their failure to bind Aurora-A, since biophysical measurements showed similar efficient binding to Aurora-A as CRBN-based degraders (Adhikari et al., 2020). Furthermore, a lack of VHL expression in the MV4-11 cells was ruled

out as well, as several proteins have been successfully degraded in MV4-11 cells using VHL-based PROTACs within this study (see section 4.2.2) and other studies (Burslem, Song, et al., 2018; Chan et al., 2018). Presumably it is due to either the lack of a ternary complex formation or unfavorable conditions for ubiquitination within the ternary complex.

Having a closer look at the CRBN-based degraders, the longer PEG linkers (PEG_2, JB170 and PEG_3, JB158) were more efficient than the short PEG linker (PEG_1, JB171) or the short aliphatic linkers (propyl, JB159 and pentyl, JB169). On one hand, a suitable linker is vital for ternary complex formation and target ubiquitination (Burslem & Crews, 2017). On the other hand, the interaction of the linker with residues in the ternary complex increases the cooperativity and thus degradation efficiency and selectivity of PROTACs (Gadd et al., 2017; Roy et al., 2019).

These observations were supported by a recent publication from the Lindon lab on Aurora-A PROTACs using alisertib as the warhead (Wang et al., 2021). In their study, the authors tested eight PROTACs, four VHL-based and four CRBN-based, and only the CRBN-based degraders could degrade Aurora-A. In addition, they observed a similar correlation between linker length and degradation efficacy, as the degrader with a smaller linker length showed lesser degradation (Wang et al., 2021). As a conclusion from study by Wang et al. and my own observations, the linker length and the choice of the E3-ligase are crucial for PROTAC efficiency and need to be optimized for each target.

JB170 was the most potent PROTAC in the here presented study and was further characterized in detail. The degradation of Aurora-A by JB170 was concentration- and time-dependent. The maximum degradation concentration by JB170 at 6 hours was observed between 100 to 1000 nM with a DC_{50} value of 28 nM. These values are in the range of reported concentrations in the PROTAC field (An & Fu, 2018; Y. Wang et al., 2020). The cellular Aurora-A levels were decreased by 25% within one hour to 65% after three hours of treatment and degradation was sustained for 24 hours. However, Aurora-A degradation by JB170 decreased after 24 hours (data not shown). This might be due to the metabolism of the degrader by the cells over time. Therefore, for long-term experiments like cell viability, the compound was either added again or media and compound were refreshed daily.

In addition, it was demonstrated that the JB170-mediated decrease in the Aurora-A level was via successful ternary complex formation followed by degradation. The

addition of the individual CRBN and Aurora-A warheads were not able to decrease the protein level. Furthermore, the coincubation of the ligands with JB170 abrogated the degradation of Aurora-A in a dose-dependent manner. JB211, a N-methylated analog of JB170 disabled in CRBN-binding, did not diminish Aurora-A levels demonstrating that its degradation was due to the induced proximity between CRBN and Aurora-A, mediated by JB170. Notably, Aurora-A transcriptional levels were not affected by JB170 as ruled out by qPCR analysis. In the CHX chase assay it was observed that JB170 decreased the half-life of Aurora-A from 3.8 hours to 1.3 hours. Altogether, these results demonstrated that the JB170-mediated reduction of Aurora-A steady levels was not due to inhibition of transcription or translation but via UPS-mediated degradation.

5.1.2 JB170 is highly selective to Aurora-A

Kinobead selectivity profiling for JB170 along with alisertib in MV4-11 cell lysate was performed to find out which proteins they bind to in a complex cellular system. Apart from Aurora-A, alisertib bound to ACAD10, Aurora-B, ABL2, and AK2, while JB170 lost the binding to ABL2 and AK2 compared to alisertib. ABL2 and AK2 are tyrosine and adenylate kinases, respectively, and ACAD10 is a dehydrogenase but harbors of a serine/threonine kinase domain. The alisertib binders observed in this study were in line with previous kinobead studies (Heinzlmeir et al., 2016; Klaeger et al., 2017). Aurora-B is a mitotic serine/threonine kinase and a member of the Aurora family proteins. Aurora-B shares a remarkable 71% sequence homology of kinase domain to that of Aurora-A (Willems et al., 2018). More importantly, the ATP-binding pocket of Aurora-A to -B differs by just three amino acids (Dodson et al., 2010). With such striking structural similarity, the binding affinity of Aurora-A over Aurora-B for alisertib was 13-fold, but it was increased to 52-fold for JB170. The selectivity of the degrader by the addition of the linker and the E3-recruiting moiety is due to steric hindrances offered by the conjugation of those residues. These findings agree with a work by Bondeson and colleagues, in which they showed that the addition of linker and VHL-ligand to the foretinib warhead, which itself bound to 133 kinases, resulted in the loss of binding to 81 kinases. Likewise, the conjugation to the linker and CRBN-ligand retained 62 kinases (Bondeson et al., 2018).

Comprehensive proteomics studies using two different approaches in two different cell lines revealed that out of >4200 reliably detected proteins, only Aurora-A was

significantly degraded by JB170. No additional proteins were degraded with a p-value less than 0.001 and a decrease of more than 50% abundance in comparison to alisertib, JB211, or the vehicle treatment. Even though JB170 binds to Aurora-B, degradation of Aurora-B was not observed. This could be due to differential ternary complex formation with Aurora-B or constraints in other steps of the degradation cascade. ACAD10 was not detected in both proteomics studies and can therefore not be assessed properly. Increased PROTAC selectivity was also described for CDK6 and BRD4 degraders (Brand et al., 2019; Gadd et al., 2017). When degrader BSJ-03-123 was synthesized using inhibitor palbociclib that binds both CDK4 and CDK6, the degrader selectively degraded CDK6 (Brand et al., 2019). Similarly, Gadd et al. reported selective degradation of BRD4 by VHL recruiting PROTAC AT1 with warhead JQ1, which binds BRD2, BRD3, and BRD4 (Gadd et al., 2017).

Furthermore, PROTACs can achieve ubiquitination of bystander proteins that are associated with target protein (Bond & Crews, 2021; Guenette et al., 2022). PROTACs against a protein complex subunit have been reported to degrade the whole complex or to decrease the level of other subunits. For example, degrader against PRMT5 reduced the abundance of its binding partner WDR77 (Shen et al., 2020). Similarly, PROTACs against EED led to the degradation of Polycomb repressive complex 2 (PRC2) subunits EZH2 and SUZ12 (Hsu et al., 2020; Potjewyd et al., 2020). The degradation of the interactors or complex members could be due to their cross-ubiquitination or destabilization of the complex upon degradation of one subunit. Knockdown of subunits of PRC2 complex have been shown in literature to decrease the protein levels of other members, which points towards the destabilization of complex (Liu et al., 2019; Xu et al., 2015). However, using the EZH2 degrader Liu et al. demonstrated that cross ubiquitination of other subunits is possible (Liu et al., 2021). Degraders affecting a whole complex hold more potency to completely inhibit downstream processes. Nonetheless, JB170 did not significantly degrade any known Aurora-A interactors like TPX2 and TACC3.

Unfortunately, neither Myc (in MV4-11) nor N-Myc (in IMR5) were identified in the total proteomics but using immunoblotting, it was seen that Myc protein levels were not affected by JB170 (data not shown). Aurora-A binding to Myc and N-Myc prevents their FBWX7 mediated degradation and thus stabilizes them (Brockmann et al., 2013; Dauch et al., 2016; Otto et al., 2009). It was expected that degradation

of Aurora-A with JB170 would decrease the Myc protein level either by increased FBXW7-mediated reduction in stability or bystander ubiquitination. However, due to partial degradation of Aurora-A by JB170, remaining Aurora-A might have been enough to stabilize the Myc protein. Moreover, altering the FBXW7 expression levels in the cells in the presence and absence of degrader and analyzing Myc level could give more insight why Myc reduction was not observed by JB170.

5.1.3 The protein-protein interaction supports the ternary complex formation

To investigate the selectivity and efficiency of JB170 to Aurora-A, an in-silico modeling approach was used. Many solutions were generated by protein-protein docking of Aurora-A/alisertib and CRBN/lenalidomide, where the best-ranked solution was ACc1. JB170 fitted to ACc1 without significant rearrangement of the ligands alisertib and lenalidomide. Interestingly, besides JB170, only the second-best degrader, JB158, could fit in ACc1 without significant distortion. Both JB170 and JB158 were compatible with the 15th-ranked solution, Aurora-A-CRBN complex 2 (ACc2). ACc1 and ACc2 showed extensive interface between Aurora-A and CRBN. Such PPI of the target and E3-ligase have been established to display positive cooperativity on the ternary complex formation (Farnaby et al., 2019; Gadd et al., 2017; Law et al., 2021). Positive cooperativity is vital in achieving efficient and selective degradation by the degrader even when low-affinity ligands are used for degrader synthesis (Han et al., 2019; Smith et al., 2019). The docking study was not performed for the analysis of Aurora-A and VHL complex. Nonetheless, the result from Aurora-A and CRBN suggests that modeling is effective tool that could be used in linker design for PROTAC synthesis.

By calculating side-chain energy contributions, twelve critical residues in Aurora-A were identified for the interaction with CRBN. To study the importance of PPI, those twelve residues were mutated in Aurora-A^{Imut}, which resulted in complete abrogation of JB170-mediated Aurora-A degradation. Likewise, Aurora-A^{Imut} did not induce co-precipitation of CRBN in the presence of JB170, while wildtype did. Using single amino acid modifications, proline 191 residue was identified as critical residue for JB170-mediated degradation. As an important control, HiBiT assay showed that binding of alisertib to Aurora-A^{P191W} was not affected. Furthermore, the experiments using Aurora-B swop mutants reinforced the importance of the

PPI for JB170 selectivity and efficacy. In Aurora-B swop mutants the ATP-binding pocket of Aurora-A was mimicked by mutating the three amino acids R159, E161, and K164 in Aurora-B corresponding to L215, T217, and R220 in Aurora-A (Dodson et al., 2010; Sloane et al., 2010; Tsuchiya et al., 2020). The swop mutants Aurora-B^{E162T} and Aurora-B$^{R160L, E162T, K165R}$ were barely degraded by JB170. As alisertib binding affinity should be similar to that of Aurora-A, the distinction was in the amino acid residues for Aurora-B at the interface with CRBN. This result indicates that just by increasing binding affinity of the PROTAC to the target does not increase the degradation potential. This finding was supported by the report that the binding affinity of the ligand to the POI does not correlate to the degradation efficiency of the PROTACs (Bondeson et al., 2018; Chan et al., 2018).

Afterwards, ternary complex formation by both CRBN- and VHL-based degraders was tested by immunoprecipitation assays. Strikingly, the amount of co-precipitated CRBN highly correlated with degradation efficiency with JB170 inducing the strongest co-IP, closely followed by JB158. No co-IP of VHL was observed by the VHL-based PROTACs in line with the fact that none of those PROTACs lead to Aurora-A degradation. As a positive control, BRD4 in the presence of MZ1 had led to efficient co-IP of VHL (Adhikari et al., 2020). Such co-IP experiments could be a useful tool in analyzing the PROTAC efficiency. These results led to the conclusion that JB170 was most suitable for inducing proximity between Aurora-A and CRBN and that ternary complex formation was rate-limiting for degrader efficacy.

Interestingly, a co-IP between Aurora-A and CRBN was even observed without the presence of the degrader. This suggested that CRBN might be a natural E3-ligase for Aurora-A. However, in the literature, CRBN was not reported to interact or to be an E3-ligase for Aurora-A so far. For detailed investigation, a cycloheximide chase experiment was performed in IMR5 cells after siRNA-mediated depletion of CRBN to analyze the half-life of Aurora-A. Biological replicates indicated that in the absence of CRBN, the stability of Aurora-A slightly increased but did not reach statistical significance (data not shown, performed by Jessica Schwarz). Thus, confirming CRBN as a physiological E3-ligase for Aurora-A would require more analysis. *In* vitro ubiquitination assay with CRBN and Aurora-A or DiGly remnant affinity proteomics with altered CRBN expression (overexpression or depletion) could be performed. The observed interaction between CRBN and Aurora-A might be essential in certain cell cycle stages or biological conditions.

5.1.4 Aurora-A degradation shows distinct cellular phenotype

JB170 was further characterized to examine the phenotypic effect of Aurora-A degradation in MV4-11 and IMR5 cells. The inhibition of Aurora-A with alisertib caused G2/M arrest of both cell types as previously reported (Gorgun et al., 2010; Gustafson et al., 2014; Li et al., 2015; Manfredi et al., 2011). In contrast, the degradation of Aurora-A by JB170 led to lesser G2/M arrest and more accumulation of BrdU-negative cells in S-phase. The cells were either arrested in S-phase or the progression of S-phase was delayed. The overexpression of Aurora-A^{T217D}, which is functional but has a lower affinity to alisertib than wildtype Aurora-A, completely rescued the S-phase phenotype in IMR5 cells confirming that the observed cellular effect was due to the degradation of Aurora-A. Depletion of Aurora-A by siRNA also led to an accumulation of BrdU-negative cells in S-phase over time (Adhikari et al., 2020). G2/M arrest was expected with the siRNA-mediated depletion of Aurora-A as a near complete decrease of Aurora-A was observed compared to controls. However, the remaining protein was apparently enough to perform the mitotic functions. As expected, the RNAseq experiment confirmed no enrichment of the gene set for the G2/M cell cycle in the JB170 treated cells.

The disparity between Aurora-A inhibition and degradation could be because of two reasons. On the one hand, JB170 is more specific than alisertib (see section 4.1.3) and the phenotype observed was exclusively by targeting Aurora-A. However, Aurora-A is a mitotic kinase, and alisertib is a fairly Aurora-A selective inhibitor (Klaeger et al., 2017). On the other hand, the phenotype culminated from the non-catalytic or scaffolding role of Aurora-A in S-phase. The second scenario seems more reasonable as alisertib could not target the scaffolding function of Aurora-A, while siRNA mediated decrease of Aurora-A led to the same phenotype as PROTAC-mediated degradation. The interactomic study of Aurora-A also revealed several non-substrate interaction partners. Some interactors like DICER1, TARBP2, AGO2, and DROSHA form large microRNA processor complexes and are linked to RNA metabolism (Chendrimada et al., 2005; Koscianska et al., 2011). In line with this observation, a study showed that Aurora-A is present in RNA-mediated complexes (Caudron-Herger et al., 2019). It could thus be hypothesized that the interaction of RNA-binding proteins mediates this scaffolding function of Aurora-A in S-phase. More studies in this regard are

required to explore this hypothesis. For example, one could check the localization of Aurora-A and its RNA-binding interactors during various cell cycle phases and observe their localization change upon Aurora-A degradation. Alternatively, one could directly deplete the interactors by shRNA or siRNA and investigate the cellular phenotypes. In a study by Zeng et al., silencing DICER1 with siRNA in tongue squamous cell carcinoma increased the number of cells in S- and G2/M phases (Zeng et al., 2014).

The role of Aurora-A in the S-phase has also been explored in other studies. Büchel et al. reported that Aurora-A associates with N-Myc during S-phase and regulates the pause release of RNA polymerase II (Buchel et al., 2017). Similarly, a study by Roeschert and colleagues revealed that Aurora-A phosphorylates histone H3 at S10 in an N-Myc-dependent manner during S-phase and prevents transcription-replication conflicts (I. Roeschert et al., 2021). These findings indicate that Aurora-A has more functions during S-phase than the stabilization of Myc.

Unfortunately, in this study due to limited time no experiments could not be performed to elucidate the role of Myc in the context of Aurora-A degradation. First, the consequences of Aurora-A degradation on Myc levels should be systematically studied. Second, the effect on Myc activity after Aurora-A degradation should be investigated by analyzing the changes in Myc binding to its target genes and the changes in target gene expression. Third, the sensitivity for Aurora-A PROTACs should be examined in various Myc amplified or dependent versus non-amplified or independent cell systems.

Several studies using Aurora-A degraders have also been published recently. The warheads employed for Aurora-A in those works were alisertib, MK-5108 and modified ribociclib, and all the effective degraders recruited CRBN (Bozilovic et al., 2022; Donovan et al., 2020; Rishfi et al., 2022; Tang et al., 2022; Wang et al., 2021). Donovan et al. synthesized a degrader that resembled JB158 and showed its excellent antiproliferative activity over parent compound alisertib in multiple myeloma cell lines (Donovan et al., 2020). In another study, a MK-5108-based degrader showed a significant increase in degradation efficiency and potency than alisertib-based JB170 in MV4-11 cells (Bozilovic et al., 2022). N-Myc amplified neuroblastoma cells has been reported to be sensitive to Aurora-A knockdown and inhibition (Otto et al., 2009; I. Roeschert et al., 2021). However, a recent preprint used PROTACs based on MK-5108, for which they observed no correlation

between the sensitivity to Aurora-A degradation and N-Myc amplification status of neuroblastoma cell lines. Instead, they proposed that sensitivity correlates with Aurora-A and CRBN levels (Rishfi et al., 2022). Another preprint study used a modified CDK4/6 inhibitor, ribociclib, to develop the degraders and showed that their degrader, PROTAC **4**, also degraded N-Myc along with Aurora-A (Tang et al., 2022). N-Myc degradation was only observed after substantial degradation of Aurora-A (greater than 75%). JB170 did not achieve such high degradation of Aurora-A. No decrease in Myc nor N-Myc levels was observed in our study as the remaining amount of Aurora-A might have been sufficient to stabilize the Myc protein. However, in the study by Tang et al., fifteen other proteins apart from Aurora-A and N-Myc were significantly decreased (>30%) after PROTAC **4** treatment and the effect of these proteins on the stability of N-Myc was not further studied (Tang et al., 2022). Finally, Wang and colleagues reported an alisertib-based Aurora-A degrader and demonstrated that the PROTAC degraded only the non-centrosomal Aurora-A pool (Wang et al., 2021). The differential degradation of Aurora-A from different localization was not investigated for JB170 in this thesis. Whether the incomplete degradation of Aurora-A by JB170 is due to the inaccessibility of JB170 for all Aurora-A pools or some other mechanisms needs to be explored.

All in all, along with JB170, all the reported Aurora-A degraders illustrated that targeting the non-catalytic or scaffolding functions rather than the catalytic or mitotic function of Aurora-A would provide an innovative way of tackling this oncoprotein in cancer.

5.2 WDR5 degraders

5.2.1 WDR5 degraders recruiting VHL degrade WDR5

Two different WDR5 ligands were used to synthesize two series of PROTACs: AD-series with OICR-9429-based scaffold (Grebien et al., 2015) and JW-series with pyrroloimidazole-based inhibitor scaffold (Wang et al., 2018). In total, 25 degraders were synthesized to recruit CRBN (5), VHL (17), or MDM2 (3) from both series. The three nutlin-based PROTACs to harness MDM2 exhibited very weak binding affinity and were not used in further cellular degradation analysis (Dolle et al., 2021). On the one hand, the HiBiT assay showed that only JW48 of the JW-series

which recruit VHL was successful in degrading WDR5. However, the degradation was 53% and DC_{50} at 24 hours was 1.24 µM being relatively higher than the range reported in the literature (Y. Wang et al., 2020). The increased DC_{50} of JW48 might be due to its decreased solubility or limited cellular permeability. On the other hand, several VHL-based AD-series PROTACs demonstrated degradation of WDR5. The best was AD122, with 58% degradation and DC_{50} of 53 nM after 24 hours. Strikingly, the increase or decrease of linker length from the butyl linker of AD122 significantly decreased the degradation potential of PROTAC, while the degrader with PEG_1 linker was unable to degrade WDR5. The linkerology is crucial in degrader design for target selectivity, cooperativity, solubility, membrane permeability, and stability (Li & Crews, 2022; Troup et al., 2020). CRBN-based degraders were not able to decrease WDR5 protein levels. The failure of target degradation by CRBN might be due to either incompatibility of WDR5 and CRBN to form a ternary complex, or the absence of lysine residues for ubiquitination on the surface of WDR5 in the vicinity of the CRBN, or the ternary complex is not formed long enough for ubiquitination to occur.

Both AD122 or JW48 only partial degraded WDR5. Incomplete degradation could be due to the inaccessibility of WDR5 in some cellular locations. A similar observation of an undegradable target pool was reported for Aurora-A PROTACs (Wang et al., 2021). Moreover, WDR5 interacts with many proteins through its win-site (Guarnaccia et al., 2021). As AD122 and JW48 are both based on win-site ligands, such interactions might prevent the binding of the degrader to WDR5, thereby decreasing degradation efficiency.

Various experiments validated that AD122- and JW48-mediated decrease in WDR5 levels was a result of proteasomal degradation. As an important control, the enantiomer analogs of AD122, AD153, and JW48, JW89, which could not bind to VHL, did not decrease the protein levels. These analogs are particularly valuable as controls, because with the same molecular weight as their corresponding PROTACs, they share similar solubility and cellular permeability. On the contrary, the ligands itself are characterized by lower molecular weight, increased solubility and permeability compared to the resultant degraders.

5.2.2 AD122 and JW48 are selective for WDR5

Label-free quantitative mass spectrometry in MV4-11 cells attested high selectivity for AD122 and JW48. For both degraders, from the detectable proteome of 5805

proteins, WDR5 was the only significantly decreased protein with a p-value of less than 0.001 and log_2FC of less than -0.5 as compared to DMSO-treated cells, while the ligands AD100 and JW39 did not significantly affect WDR5 abundance. However, JW48 treatment significantly upregulated (p-value <0.001 and log_2FC < 0.5) three enzymes involved in sterol metabolism compared to DMSO treatment. SQLE, CYP51A1, and HMGCS1 were upregulated with log_2FC of 0.5, while two more enzymes of sterol metabolism, FDFT1 and LDLR, were increased by log_2FC of 0.49. Contrarily, these enzymes were not altered by AD122 treatment. Further systematic experiments are required to find if the upregulation of these proteins by JW48 is due to a primary or secondary effect of WDR5 degradation or simply an off-target effect.

For the optimization of both AD122 and JW48, ternary complex crystallization was attempted. Due to the lower solubility of JW48, the crystallization was not feasible. However, for AD122, the co-crystal structure was solved with WDR5, VHL, Elongin B, and Elongin C by Andreas Krämer from the group of Prof. Dr. Stefan Knapp (Fig. 5.1). In the crystal structure, interactions between residues of VHL and WDR5 were observed. Positive cooperativity due to the PPI could be the main reason for successful degradation by AD122. The improvement of AD122, however, seems challenging as the linker is exposed outside towards the solvent, and the chances of increasing the stability of the ternary complex with optimized PROTAC are small. Furthermore, crystal structures with degraders containing longer and shorter linkers than for AD122 could explain the differences observed in degradation efficiency. Moreover, co-IP of E3-ligases with WDR5 immunoprecipitation in the presence of the degraders could give the information on ternary complex formation.

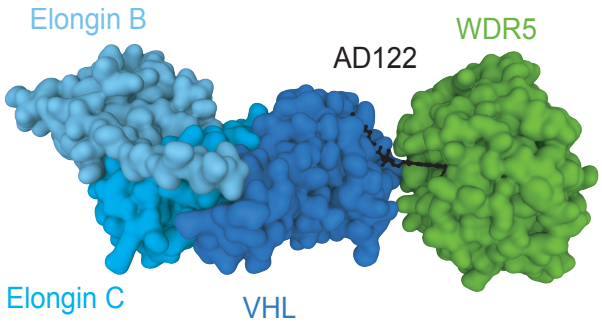

Figure 5.1: Crystal structure of WDR5-AD122-VHL ternary complex.
The molecular surface representation of the ternary complex with PROTAC AD122 (black), WDR5 (green), VHL (blue), Elongin B (sky blue) and Elongin C (aqua). (PDB: 7Q2J)

5.2.3 WDR5 degradation shows modest cellular effects

AD122 did not show any proliferation defect in various cancer cell lines, whereas JW48 showed a significant effect at higher concentrations. It was hypothesized that a higher concentration of JW48 achieved long-term depletion of WDR5 protein below the level required for inhibition of cell growth, while AD122 or lower concentrations of JW48 could not. By further experiments the E3-ligase substrate receptor, VHL, was identified as limiting for efficient degradation in this case. Overexpression of VHL enhanced degradation efficacy of both AD122 and JW48 in MV4-11 and HL-60 cells. Along the same line, some studies have reported a direct correlation between degradation efficiency and expression level of the E3-ligase (Li & Song, 2020; Tang et al., 2022). Indeed, upon VHL overexpression the proliferation assay showed pronounced proliferation inhibition by JW48, even at lower concentrations. For AD122, however, no effect was observed in MV4-11 and moderate effect in HL-60 cells. The discrepancy between the antiproliferative effect of the two degraders, AD122 and JW48, might be due to various reasons. First, AD122 could be less stable for long-term experiments. The stability of both AD122 and JW48 were not studied in cell culture conditions for longer treatment times. Second, as the linker attachment point of AD122 and JW48 are different, their binding to WDR5 alone or recruitment of VHL could sterically prevent interaction to a different subset of WDR5 interactors. The proliferation defect observed by JW48 might be due to the combinatorial effect of WDR5 degradation and loss of WDR5 interaction with its partners. These changes in WDR5 interaction could be studied by incubating the cells with AD122 and JW48 along with controls, immunoprecipitating WDR5, and carefully analyzing its interactome. Third, AD122 and JW48 could target different pools of WDR5, leading to the activation or deactivation of different pathways. Immunofluorescence or fractionation experiments could be implemented to analyze the change in WDR5 levels at different subcellular compartments after degrader treatment. For example, JW48 might induce degradation of chromatin bound WDR5 in comparison to AD122. Fourth, RNAseq or total proteomics could be carried out after long-term PROTAC treatment to identify the pathways they impact.

WDR5 was chosen as a target, since it interacts and recruits Myc to chromatin, regulates genes linked to protein synthesis and promotes oncogenicity of Myc (Thomas et al., 2019; Thomas et al., 2015). Therefore, changes in Myc occupancy

at its target genes should be analyzed after degrader-mediated WDR5 depletion. Furthermore, sensitivity towards these compounds should be tested across various cancer cell lines that are Myc-dependent and independent. Moreover, the VHL overexpression data suggests that sensitive cancer cell lines could be identified by screening for cell lines with higher VHL expression. In blood vessel tumors and renal carcinomas downregulation of VHL and alteration of its localization promotes tumorigenesis (Kaelin, 2018; Shiao et al., 2003). Cell lines from such cancer entities would not be ideal for testing sensitivity of VHL-based degraders.

A recently published work characterized and studied WDR5 PROTACs in many acute myeloid leukemia (AML) cells (Yu et al., 2021). In their study, the WDR5 degrader MS33 was synthesized with OICR-9429 based scaffold and linked to a VHL-ligand with a relatively long aliphatic linker (contains piperazine moiety in upper phenyl ring of OICR-9429 scaffold as compared to AD122, Fig. 5.2a, b). Then the design of MS33 was optimized based on a ternary complex crystal structure. The optimized PROTAC, MS67, contained modifications in the WDR5 warhead, a very short linker and methylated VHL-ligand (Fig. 5.2c). MS67 was more effective than MS33 and suppressed the growth of AML cell lines both *in vitro* and *in vivo*. Comparing the ternary complex crystal structure with AD122 to MS67, MS67 induced more PPIs between VHL and WDR5, which could explain the better degradation efficiency and potency of MS67 than AD122. Based on MS67 and AD122 ternary complex crystal structures, connecting the linker to position 2 of the upper phenyl ring (like in MS67) in AD122 might result in more PPI between VHL and WDR5. Similarly, this could increase the efficiency of the degraders with shorter linkers.

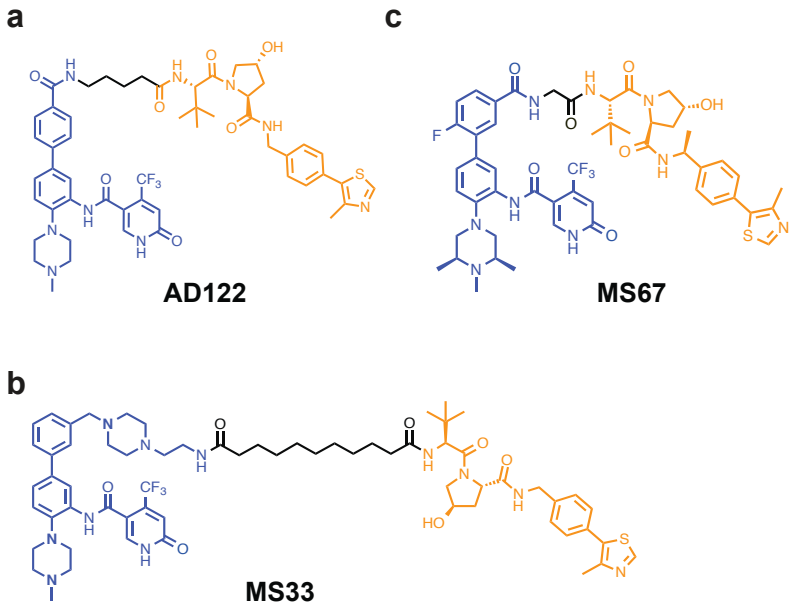

Figure 5.2: Structure of WDR5 degraders.
(a-c) *The structure of OICR-9429 based degrader (a) AD122 (from this study), (b) MS33 and (c) MS67 (optimized based on MS33) from the study by Yu et al, 2021.*

To sum up, identification of WDR5 as oncoprotein has led to discovery of many PPI inhibitors to inhibit WDR5 binding with its interactors, but such inhibitors were not effective to inhibit all oncogenic functions of WDR5. Therefore, degradation of scaffolding proteins like WDR5 offers better therapeutic strategy than inhibition as shown by degraders from this study and other studies.

5.3 RIP assay predicts degradative E3 ligase for a target

As illustrated by the PROTACs developed and tested within this thesis, the PROTAC design approach severely lacks a technique to choose the right E3-ligase leading to successful degradation of the target. For the two targets, Aurora-A and WDR5, PROTACs were tested recruiting several E3-ligases, however, for both targets only one of the tested E3-ligases was able to induce UPS-mediated degradation. That not every E3-ligase is compatible with degrading a particular target of interest could have three reasons: first, an incompatibility to form a stable complex between target and E3-ligase; second, the absence of K48 activity of the E3-ligase required for proteasomal degradation; third, expression of the target and E3-ligase in different cellular compartments.
In a recent study, VHL and CRBN-recruiting PROTACs showed varying degree of dTAG and HaloTAG degradation in different subcellular context (Simpson et al.,

2022). The authors utilized various localization signals to express dTAG and HaloTAG in different subcellular compartments. They showed that outer mitochondrial membrane (OMM) localized dTAG was degraded by CRBN but not by VHL, while HaloTAG expressed in OMM was degraded by VHL. Contrarily, CRBN was less efficient in degradation of dTAG in Golgi-lumen, whereas VHL efficiently degraded both dTAG and HaloTAG in the same compartment. This study highlighted the importance compatibility of the target and E3-ligase and their subcellular context for PROTAC design.

In this thesis, a rapamycin-based proximity (RIP) assay was designed to predict E3-ligases that could induce degradation of the POI. The results demonstrated that the expression level of the E3-ligase is crucial for the assay and a transfection-based method holds superiority over a stable cell line-based method. The transfection-based assay is less time-consuming and scalable to a screening fashion. The RIP assay correctly validated the E3-ligases for degradation of WDR5 and Aurora-A. However, the assay needs to be further validated for other targets and E3-ligases after utilizing successful and unsuccessful targets/ E3-ligases pairs from the literature. Furthermore, this assay could expand the repertoire of the E3-ligases that can be utilized for PROTAC development. Even though more than 600 E3-ligases are found in humans, the type of ubiquitin chains added by many E3 ligases that dictate the substrate's fate is still unknown. Finally, this assay can be applied to screen the best-suited tissue-specific E3-ligase for the degradation of the POI. Most E3-ligases used for developing PROTACs are either ubiquitously expressed or not essential to the cell. Utilizing ubiquitous E3-ligase could cause toxicity to healthy tissues by degrading the target everywhere. Similarly, using non-essential E3-ligases could lead to resistance mechanisms either by simply downregulating E3-ligase expression or by introducing mutation of the E3-ligase that does not support PPI with the target. Tissue-specific and tissue-essential E3-ligase recruiting PROTACs would therefore be ideal for therapeutics.

5.4 Concluding remarks

The field of targeted protein degradation has shown incredible potential in targeting previously thought undruggable targets. With PROTACs and molecular glues in clinical trials, the field holds a bright future. Although the degraders investigated in this thesis need further improvements and characterization, they are a resourceful

tool that will facilitate further understanding of Aurora-A and WDR5 biology and help in the development of Aurora-A and WDR5 degraders for cancer therapeutics.

6 Bibliography

Adams, J. M., Harris, A. W., Pinkert, C. A., Corcoran, L. M., Alexander, W. S., Cory, S., Palmiter, R. D., & Brinster, R. L. (1985). The c-myc oncogene driven by immunoglobulin enhancers induces lymphoid malignancy in transgenic mice. *Nature*, *318*(6046), 533-538. https://doi.org/10.1038/318533a0

Adhikari, B., Bozilovic, J., Diebold, M., Schwarz, J. D., Hofstetter, J., Schroder, M., Wanior, M., Narain, A., Vogt, M., Dudvarski Stankovic, N., Baluapuri, A., Schonemann, L., Eing, L., Bhandare, P., Kuster, B., Schlosser, A., Heinzlmeir, S., Sotriffer, C., Knapp, S., & Wolf, E. (2020). PROTAC-mediated degradation reveals a non-catalytic function of AURORA-A kinase. *Nat Chem Biol*, *16*(11), 1179-1188. https://doi.org/10.1038/s41589-020-00652-y

Agrawal, P., Yu, K., Salomon, A. R., & Sedivy, J. M. (2010). Proteomic profiling of Myc-associated proteins. *Cell cycle*, *9*(24), 4908-4921. https://doi.org/10.4161/cc.9.24.14199

Ahmadi, S. E., Rahimi, S., Zarandi, B., Chegeni, R., & Safa, M. (2021). MYC: a multipurpose oncogene with prognostic and therapeutic implications in blood malignancies. *J Hematol Oncol*, *14*(1), 121. https://doi.org/10.1186/s13045-021-01111-4

Ahn, G., Banik, S. M., Miller, C. L., Riley, N. M., Cochran, J. R., & Bertozzi, C. R. (2021). LYTACs that engage the asialoglycoprotein receptor for targeted protein degradation. *Nat Chem Biol*, *17*(9), 937-946. https://doi.org/10.1038/s41589-021-00770-1

Aho, E. R., Wang, J., Gogliotti, R. D., Howard, G. C., Phan, J., Acharya, P., Macdonald, J. D., Cheng, K., Lorey, S. L., Lu, B., Wenzel, S., Foshage, A. M., Alvarado, J., Wang, F., Shaw, J. G., Zhao, B., Weissmiller, A. M., Thomas, L. R., Vakoc, C. R., . . . Tansey, W. P. (2019). Displacement of WDR5 from Chromatin by a WIN Site Inhibitor with Picomolar Affinity. *Cell Rep*, *26*(11), 2916-2928 e2913. https://doi.org/10.1016/j.celrep.2019.02.047

Ali, H. R., Dawson, S. J., Blows, F. M., Provenzano, E., Pharoah, P. D., & Caldas, C. (2012). Aurora kinase A outperforms Ki67 as a prognostic marker in ER-positive breast cancer. *Br J Cancer*, *106*(11), 1798-1806. https://doi.org/10.1038/bjc.2012.167

Alicea-Velazquez, N. L., Shinsky, S. A., Loh, D. M., Lee, J. H., Skalnik, D. G., & Cosgrove, M. S. (2016). Targeted Disruption of the Interaction between WD-40 Repeat Protein 5 (WDR5) and Mixed Lineage Leukemia (MLL)/SET1 Family Proteins Specifically Inhibits MLL1 and SETd1A Methyltransferase Complexes. *J Biol Chem*, *291*(43), 22357-22372. https://doi.org/10.1074/jbc.M116.752626

Allevato, M., Bolotin, E., Grossman, M., Mane-Padros, D., Sladek, F. M., & Martinez, E. (2017). Sequence-specific DNA binding by MYC/MAX to low-affinity non-E-box motifs. *PLoS One*, *12*(7), e0180147. https://doi.org/10.1371/journal.pone.0180147

An, S., & Fu, L. (2018). Small-molecule PROTACs: An emerging and promising approach for the development of targeted therapy drugs. *EBioMedicine*, *36*, 553-562. https://doi.org/10.1016/j.ebiom.2018.09.005

Arnold, I., & Watt, F. M. (2001). c-Myc activation in transgenic mouse epidermis results in mobilization of stem cells and differentiation of their progeny. *Current Biology*, *11*(8), 558-568. https://doi.org/10.1016/s0960-9822(01)00154-3

Avet-Loiseau, H., Gerson, F., Magrangeas, F., Minvielle, S., Harousseau, J. L., Bataille, R., & Intergroupe Francophone du, M. (2001). Rearrangements of the c-myc oncogene are present in 15% of primary human multiple myeloma tumors. *Blood*, *98*(10), 3082-3086. https://doi.org/10.1182/blood.v98.10.3082

Bai, L., Zhou, H., Xu, R., Zhao, Y., Chinnaswamy, K., McEachern, D., Chen, J., Yang, C. Y., Liu, Z., Wang, M., Liu, L., Jiang, H., Wen, B., Kumar, P., Meagher, J. L., Sun, D., Stuckey, J. A., & Wang, S. (2019). A Potent and Selective Small-Molecule Degrader of STAT3 Achieves Complete Tumor Regression In Vivo. *Cancer Cell*, *36*(5), 498-511 e417. https://doi.org/10.1016/j.ccell.2019.10.002

Baluapuri, A., Hofstetter, J., Dudvarski Stankovic, N., Endres, T., Bhandare, P., Vos, S. M., Adhikari, B., Schwarz, J. D., Narain, A., Vogt, M., Wang, S. Y., Duster, R., Jung, L. A., Vanselow, J. T., Wiegering, A., Geyer, M., Maric, H. M., Gallant, P., Walz, S., . . . Wolf, E. (2019). MYC Recruits SPT5 to RNA Polymerase II to Promote Processive

Transcription Elongation. *Mol Cell*, *74*(4), 674-687 e611. https://doi.org/10.1016/j.molcel.2019.02.031

Baluapuri, A., Wolf, E., & Eilers, M. (2020). Target gene-independent functions of MYC oncoproteins. *Nat Rev Mol Cell Biol*, *21*(5), 255-267. https://doi.org/10.1038/s41580-020-0215-2

Banerjee, S. A., Hoppe, P., Brilliant, M., & Chikaraishi, D. M. (1992). 5' flanking sequences of the rat tyrosine hydroxylase gene target accurate tissue-specific, developmental, and transsynaptic expression in transgenic mice. *The Journal of Neuroscience*, *12*(11), 4460-4467. https://doi.org/10.1523/jneurosci.12-11-04460.1992

Banik, S. M., Pedram, K., Wisnovsky, S., Ahn, G., Riley, N. M., & Bertozzi, C. R. (2020). Lysosome-targeting chimaeras for degradation of extracellular proteins. *Nature*, *584*(7820), 291-297. https://doi.org/10.1038/s41586-020-2545-9

Barr, A. R., & Gergely, F. (2007). Aurora-A: the maker and breaker of spindle poles. *J Cell Sci*, *120*(Pt 17), 2987-2996. https://doi.org/10.1242/jcs.013136

Bayliss, R., Burgess, S. G., & McIntyre, P. J. (2017). Switching Aurora-A kinase on and off at an allosteric site. *Febs Journal*, *284*(18), 2947-2954. https://doi.org/10.1111/febs.14069

Beaulieu, M. E., Jauset, T., Masso-Valles, D., Martinez-Martin, S., Rahl, P., Maltais, L., Zacarias-Fluck, M. F., Casacuberta-Serra, S., Serrano Del Pozo, E., Fiore, C., Foradada, L., Cano, V. C., Sanchez-Hervas, M., Guenther, M., Romero Sanz, E., Oteo, M., Tremblay, C., Martin, G., Letourneau, D., . . . Soucek, L. (2019). Intrinsic cell-penetrating activity propels Omomyc from proof of concept to viable anti-MYC therapy. *Sci Transl Med*, *11*(484). https://doi.org/10.1126/scitranslmed.aar5012

Bekes, M., Langley, D. R., & Crews, C. M. (2022). PROTAC targeted protein degraders: the past is prologue. *Nat Rev Drug Discov*, *21*(3), 181-200. https://doi.org/10.1038/s41573-021-00371-6

Beltran, H., Oromendia, C., Danila, D. C., Montgomery, B., Hoimes, C., Szmulewitz, R. Z., Vaishampayan, U., Armstrong, A. J., Stein, M., Pinski, J., Mosquera, J. M., Sailer, V., Bareja, R., Romanel, A., Gumpeni, N., Sboner, A., Dardenne, E., Puca, L., Prandi, D., . . . Tagawa, S. T. (2019). A Phase II Trial of the Aurora Kinase A Inhibitor Alisertib for Patients with Castration-resistant and Neuroendocrine Prostate Cancer: Efficacy and Biomarkers. *Clin Cancer Res*, *25*(1), 43-51. https://doi.org/10.1158/1078-0432.CCR-18-1912

Bischoff, J. R., Anderson, L., Zhu, Y., Mossie, K., Ng, L., Souza, B., Schryver, B., Flanagan, P., Clairvoyant, F., Ginther, C., Chan, C. S., Novotny, M., Slamon, D. J., & Plowman, G. D. (1998). A homologue of Drosophila aurora kinase is oncogenic and amplified in human colorectal cancers. *EMBO J*, *17*(11), 3052-3065. https://doi.org/10.1093/emboj/17.11.3052

Bischoff, J. R., & Plowman, G. D. (1999). The Aurora/Ipl1p kinase family: regulators of chromosome segregation and cytokinesis. *Trends in Cell Biology*, *9*(11), 454-459. https://doi.org/10.1016/s0962-8924(99)01658-x

Blackwell, T. K., Kretzner, L., Blackwood, E. M., Eisenman, R. N., & Weintraub, H. (1990). Sequence-specific DNA binding by the c-Myc protein. *Science*, *250*(4984), 1149-1151. https://doi.org/10.1126/science.2251503

Blackwood, E. M., & Eisenman, R. N. (1991). Max: a helix-loop-helix zipper protein that forms a sequence-specific DNA-binding complex with Myc. *Science*, *251*(4998), 1211-1217. https://doi.org/10.1126/science.2006410

Blyth, K., Stewart, M., Bell, M., James, C., Evan, G., Neil, J. C., & Cameron, E. R. (2000). Sensitivity to myc-induced apoptosis is retained in spontaneous and transplanted lymphomas of CD2-mycER mice. *Oncogene*, *19*(6), 773-782. https://doi.org/10.1038/sj.onc.1203321

Bode, D., Yu, L., Tate, P., Pardo, M., & Choudhary, J. (2016). Characterization of Two Distinct Nucleosome Remodeling and Deacetylase (NuRD) Complex Assemblies in Embryonic Stem Cells. *Mol Cell Proteomics*, *15*(3), 878-891. https://doi.org/10.1074/mcp.M115.053207

Bond, M. J., & Crews, C. M. (2021). Proteolysis targeting chimeras (PROTACs) come of age: entering the third decade of targeted protein degradation. *RSC Chem Biol*, *2*(3), 725-742. https://doi.org/10.1039/d1cb00011j

Bondeson, D. P., Mares, A., Smith, I. E., Ko, E., Campos, S., Miah, A. H., Mulholland, K. E., Routly, N., Buckley, D. L., Gustafson, J. L., Zinn, N., Grandi, P., Shimamura, S.,

Bergamini, G., Faelth-Savitski, M., Bantscheff, M., Cox, C., Gordon, D. A., Willard, R. R., . . . Crews, C. M. (2015). Catalytic in vivo protein knockdown by small-molecule PROTACs. *Nat Chem Biol*, *11*(8), 611-617. https://doi.org/10.1038/nchembio.1858

Bondeson, D. P., Smith, B. E., Burslem, G. M., Buhimschi, A. D., Hines, J., Jaime-Figueroa, S., Wang, J., Hamman, B. D., Ishchenko, A., & Crews, C. M. (2018). Lessons in PROTAC Design from Selective Degradation with a Promiscuous Warhead. *Cell Chem Biol*, *25*(1), 78-87 e75. https://doi.org/10.1016/j.chembiol.2017.09.010

Borisa, A. C., & Bhatt, H. G. (2017). A comprehensive review on Aurora kinase: Small molecule inhibitors and clinical trial studies. *Eur J Med Chem*, *140*, 1-19. https://doi.org/10.1016/j.ejmech.2017.08.045

Bozilovic, J., Eing, L., Berger, B.-T., Adhikari, B., Weckesser, J., Berner, N. B., Wilhelm, S., Kuster, B., Wolf, E., & Knapp, S. (2022). Novel, highly potent PROTACs targeting AURORA-A kinase. *Current Research in Chemical Biology*, *2*. https://doi.org/10.1016/j.crchbi.2022.100032

Bragelmann, J., Bohm, S., Guthrie, M. R., Mollaoglu, G., Oliver, T. G., & Sos, M. L. (2017). Family matters: How MYC family oncogenes impact small cell lung cancer. *Cell cycle*, *16*(16), 1489-1498. https://doi.org/10.1080/15384101.2017.1339849

Brand, M., Jiang, B., Bauer, S., Donovan, K. A., Liang, Y., Wang, E. S., Nowak, R. P., Yuan, J. C., Zhang, T., Kwiatkowski, N., Muller, A. C., Fischer, E. S., Gray, N. S., & Winter, G. E. (2019). Homolog-Selective Degradation as a Strategy to Probe the Function of CDK6 in AML. *Cell Chem Biol*, *26*(2), 300-306 e309. https://doi.org/10.1016/j.chembiol.2018.11.006

Briassouli, P., Chan, F., Savage, K., Reis-Filho, J. S., & Linardopoulos, S. (2007). Aurora-A regulation of nuclear factor-kappaB signaling by phosphorylation of IkappaBalpha. *Cancer Res*, *67*(4), 1689-1695. https://doi.org/10.1158/0008-5472.CAN-06-2272

Brockmann, M., Poon, E., Berry, T., Carstensen, A., Deubzer, H. E., Rycak, L., Jamin, Y., Thway, K., Robinson, S. P., Roels, F., Witt, O., Fischer, M., Chesler, L., & Eilers, M. (2013). Small molecule inhibitors of aurora-a induce proteasomal degradation of N-myc in childhood neuroblastoma. *Cancer Cell*, *24*(1), 75-89. https://doi.org/10.1016/j.ccr.2013.05.005

Brown, J. R., Hanna, M., Tesar, B., Werner, L., Pochet, N., Asara, J. M., Wang, Y. E., Dal Cin, P., Fernandes, S. M., Thompson, C., Macconaill, L., Wu, C. J., Van de Peer, Y., Correll, M., Regev, A., Neuberg, D., & Freedman, A. S. (2012). Integrative genomic analysis implicates gain of PIK3CA at 3q26 and MYC at 8q24 in chronic lymphocytic leukemia. *Clin Cancer Res*, *18*(14), 3791-3802. https://doi.org/10.1158/1078-0432.CCR-11-2342

Brown, J. R., Koretke, K. K., Birkeland, M. L., Sanseau, P., & Patrick, D. R. (2004). Evolutionary relationships of Aurora kinases: implications for model organism studies and the development of anti-cancer drugs. *BMC Evol Biol*, *4*, 39. https://doi.org/10.1186/1471-2148-4-39

Bryan, A. F., Wang, J., Howard, G. C., Guarnaccia, A. D., Woodley, C. M., Aho, E. R., Rellinger, E. J., Matlock, B. K., Flaherty, D. K., Lorey, S. L., Chung, D. H., Fesik, S. W., Liu, Q., Weissmiller, A. M., & Tansey, W. P. (2020). WDR5 is a conserved regulator of protein synthesis gene expression. *Nucleic Acids Res*, *48*(6), 2924-2941. https://doi.org/10.1093/nar/gkaa051

Buchel, G., Carstensen, A., Mak, K. Y., Roeschert, I., Leen, E., Sumara, O., Hofstetter, J., Herold, S., Kalb, J., Baluapuri, A., Poon, E., Kwok, C., Chesler, L., Maric, H. M., Rickman, D. S., Wolf, E., Bayliss, R., Walz, S., & Eilers, M. (2017). Association with Aurora-A Controls N-MYC-Dependent Promoter Escape and Pause Release of RNA Polymerase II during the Cell Cycle. *Cell Rep*, *21*(12), 3483-3497. https://doi.org/10.1016/j.celrep.2017.11.090

Buckley, D. L., Gustafson, J. L., Van Molle, I., Roth, A. G., Tae, H. S., Gareiss, P. C., Jorgensen, W. L., Ciulli, A., & Crews, C. M. (2012). Small-molecule inhibitors of the interaction between the E3 ligase VHL and HIF1alpha. *Angew Chem Int Ed Engl*, *51*(46), 11463-11467. https://doi.org/10.1002/anie.201206231

Buckley, D. L., Van Molle, I., Gareiss, P. C., Tae, H. S., Michel, J., Noblin, D. J., Jorgensen, W. L., Ciulli, A., & Crews, C. M. (2012). Targeting the von Hippel-Lindau E3 ubiquitin ligase using small molecules to disrupt the VHL/HIF-1alpha interaction. *J Am Chem Soc*, *134*(10), 4465-4468. https://doi.org/10.1021/ja209924v

Buhimschi, A. D., Armstrong, H. A., Toure, M., Jaime-Figueroa, S., Chen, T. L., Lehman, A. M., Woyach, J. A., Johnson, A. J., Byrd, J. C., & Crews, C. M. (2018). Targeting the C481S

Ibrutinib-Resistance Mutation in Bruton's Tyrosine Kinase Using PROTAC-Mediated Degradation. *Biochemistry*, *57*(26), 3564-3575. https://doi.org/10.1021/acs.biochem.8b00391

Burke, M. R., Smith, A. R., & Zheng, G. (2022). Overcoming Cancer Drug Resistance Utilizing PROTAC Technology. *Front Cell Dev Biol*, *10*, 872729. https://doi.org/10.3389/fcell.2022.872729

Burslem, G. M., & Crews, C. M. (2017). Small-Molecule Modulation of Protein Homeostasis. *Chem Rev*, *117*(17), 11269-11301. https://doi.org/10.1021/acs.chemrev.7b00077

Burslem, G. M., Schultz, A. R., Bondeson, D. P., Eide, C. A., Savage Stevens, S. L., Druker, B. J., & Crews, C. M. (2019). Targeting BCR-ABL1 in Chronic Myeloid Leukemia by PROTAC-Mediated Targeted Protein Degradation. *Cancer Res*, *79*(18), 4744-4753. https://doi.org/10.1158/0008-5472.CAN-19-1236

Burslem, G. M., Smith, B. E., Lai, A. C., Jaime-Figueroa, S., McQuaid, D. C., Bondeson, D. P., Toure, M., Dong, H., Qian, Y., Wang, J., Crew, A. P., Hines, J., & Crews, C. M. (2018). The Advantages of Targeted Protein Degradation Over Inhibition: An RTK Case Study. *Cell Chem Biol*, *25*(1), 67-77 e63. https://doi.org/10.1016/j.chembiol.2017.09.009

Burslem, G. M., Song, J., Chen, X., Hines, J., & Crews, C. M. (2018). Enhancing Antiproliferative Activity and Selectivity of a FLT-3 Inhibitor by Proteolysis Targeting Chimera Conversion. *J Am Chem Soc*, *140*(48), 16428-16432. https://doi.org/10.1021/jacs.8b10320

Cai, Y., Jin, J., Swanson, S. K., Cole, M. D., Choi, S. H., Florens, L., Washburn, M. P., Conaway, J. W., & Conaway, R. C. (2010). Subunit composition and substrate specificity of a MOF-containing histone acetyltransferase distinct from the male-specific lethal (MSL) complex. *J Biol Chem*, *285*(7), 4268-4272. https://doi.org/10.1074/jbc.C109.087981

Cancer Genome Atlas, N. (2012). Comprehensive molecular characterization of human colon and rectal cancer. *Nature*, *487*(7407), 330-337. https://doi.org/10.1038/nature11252

Cao, F., Townsend, E. C., Karatas, H., Xu, J., Li, L., Lee, S., Liu, L., Chen, Y., Ouillette, P., Zhu, J., Hess, J. L., Atadja, P., Lei, M., Qin, Z. S., Malek, S., Wang, S., & Dou, Y. (2014). Targeting MLL1 H3K4 methyltransferase activity in mixed-lineage leukemia. *Mol Cell*, *53*(2), 247-261. https://doi.org/10.1016/j.molcel.2013.12.001

Carmena, M., Ruchaud, S., & Earnshaw, W. C. (2009). Making the Auroras glow: regulation of Aurora A and B kinase function by interacting proteins. *Curr Opin Cell Biol*, *21*(6), 796-805. https://doi.org/10.1016/j.ceb.2009.09.008

Carugo, A., Genovese, G., Seth, S., Nezi, L., Rose, J. L., Bossi, D., Cicalese, A., Shah, P. K., Viale, A., Pettazzoni, P. F., Akdemir, K. C., Bristow, C. A., Robinson, F. S., Tepper, J., Sanchez, N., Gupta, S., Estecio, M. R., Giuliani, V., Dellino, G. I., . . . Draetta, G. F. (2016). In Vivo Functional Platform Targeting Patient-Derived Xenografts Identifies WDR5-Myc Association as a Critical Determinant of Pancreatic Cancer. *Cell Rep*, *16*(1), 133-147. https://doi.org/10.1016/j.celrep.2016.05.063

Casorzo, L., Dell'Aglio, C., Sarotto, I., & Risio, M. (2015). Aurora kinase A gene copy number is associated with the malignant transformation of colorectal adenomas but not with the serrated neoplasia progression. *Hum Pathol*, *46*(3), 411-418. https://doi.org/10.1016/j.humpath.2014.11.016

Castro, A., Vigneron, S., Bernis, C., Labbe, J. C., Prigent, C., & Lorca, T. (2002). The D-Box-activating domain (DAD) is a new proteolysis signal that stimulates the silent D-Box sequence of Aurora-A. *EMBO Rep*, *3*(12), 1209-1214. https://doi.org/10.1093/embo-reports/kvf241

Caudron-Herger, M., Rusin, S. F., Adamo, M. E., Seiler, J., Schmid, V. K., Barreau, E., Kettenbach, A. N., & Diederichs, S. (2019). R-DeeP: Proteome-wide and Quantitative Identification of RNA-Dependent Proteins by Density Gradient Ultracentrifugation. *Molecular Cell*, *75*(1), 184-+. https://doi.org/10.1016/j.molcel.2019.04.018

Chacon Simon, S., Wang, F., Thomas, L. R., Phan, J., Zhao, B., Olejniczak, E. T., Macdonald, J. D., Shaw, J. G., Schlund, C., Payne, W., Creighton, J., Stauffer, S. R., Waterson, A. G., Tansey, W. P., & Fesik, S. W. (2020). Discovery of WD Repeat-Containing Protein 5 (WDR5)-MYC Inhibitors Using Fragment-Based Methods and Structure-Based Design. *J Med Chem*, *63*(8), 4315-4333. https://doi.org/10.1021/acs.jmedchem.0c00224

Chamberlain, P. P., Lopez-Girona, A., Miller, K., Carmel, G., Pagarigan, B., Chie-Leon, B., Rychak, E., Corral, L. G., Ren, Y. J., Wang, M., Riley, M., Delker, S. L., Ito, T., Ando,

H., Mori, T., Hirano, Y., Handa, H., Hakoshima, T., Daniel, T. O., & Cathers, B. E. (2014). Structure of the human Cereblon-DDB1-lenalidomide complex reveals basis for responsiveness to thalidomide analogs. *Nat Struct Mol Biol*, *21*(9), 803-809. https://doi.org/10.1038/nsmb.2874

Chan, K. H., Zengerle, M., Testa, A., & Ciulli, A. (2018). Impact of Target Warhead and Linkage Vector on Inducing Protein Degradation: Comparison of Bromodomain and Extra-Terminal (BET) Degraders Derived from Triazolodiazepine (JQ1) and Tetrahydroquinoline (I-BET726) BET Inhibitor Scaffolds. *J Med Chem*, *61*(2), 504-513. https://doi.org/10.1021/acs.jmedchem.6b01912

Chang, D. W., Claassen, G. F., Hann, S. R., & Cole, M. D. (2000). The c-Myc transactivation domain is a direct modulator of apoptotic versus proliferative signals. *Mol Cell Biol*, *20*(12), 4309-4319. https://doi.org/10.1128/MCB.20.12.4309-4319.2000

Chefetz, I., Holmberg, J. C., Alvero, A. B., Visintin, I., & Mor, G. (2011). Inhibition of Aurora-A kinase induces cell cycle arrest in epithelial ovarian cancer stem cells by affecting NFkB pathway. *Cell cycle*, *10*(13), 2206-2214. https://doi.org/10.4161/cc.10.13.16348

Chen, X., Xie, W., Gu, P., Cai, Q., Wang, B., Xie, Y., Dong, W., He, W., Zhong, G., Lin, T., & Huang, J. (2015). Upregulated WDR5 promotes proliferation, self-renewal and chemoresistance in bladder cancer via mediating H3K4 trimethylation. *Sci Rep*, *5*, 8293. https://doi.org/10.1038/srep08293

Chen, Z. J., & Sun, L. J. (2009). Nonproteolytic functions of ubiquitin in cell signaling. *Mol Cell*, *33*(3), 275-286. https://doi.org/10.1016/j.molcel.2009.01.014

Chendrimada, T. P., Gregory, R. I., Kumaraswamy, E., Norman, J., Cooch, N., Nishikura, K., & Shiekhattar, R. (2005). TRBP recruits the Dicer complex to Ago2 for microRNA processing and gene silencing. *Nature*, *436*(7051), 740-744. https://doi.org/10.1038/nature03868

Cheng, J., Blum, R., Bowman, C., Hu, D., Shilatifard, A., Shen, S., & Dynlacht, B. D. (2014). A role for H3K4 monomethylation in gene repression and partitioning of chromatin readers. *Mol Cell*, *53*(6), 979-992. https://doi.org/10.1016/j.molcel.2014.02.032

Chiecchio, L., Dagrada, G. P., White, H. E., Towsend, M. R., Protheroe, R. K., Cheung, K. L., Stockley, D. M., Orchard, K. H., Cross, N. C., Harrison, C. J., Ross, F. M., & Forum, U. K. M. (2009). Frequent upregulation of MYC in plasma cell leukemia. *Genes Chromosomes Cancer*, *48*(7), 624-636. https://doi.org/10.1002/gcc.20670

Chiu, S. C., Chen, K. C., Hsia, J. Y., Chuang, C. Y., Wan, C. X., Wei, T. W., Huang, Y. J., Chen, J. M., Liao, Y. A., & Yu, C. R. (2019). Overexpression of Aurora-A bypasses cytokinesis through phosphorylation of suppressed in lung cancer. *Am J Physiol Cell Physiol*, *317*(3), C600-C612. https://doi.org/10.1152/ajpcell.00032.2019

Choi, S. H., Wright, J. B., Gerber, S. A., & Cole, M. D. (2010). Myc protein is stabilized by suppression of a novel E3 ligase complex in cancer cells. *Genes Dev*, *24*(12), 1236-1241. https://doi.org/10.1101/gad.1920310

Choi, S. R., Wang, H. M., Shin, M. H., & Lim, H. S. (2021). Hydrophobic Tagging-Mediated Degradation of Transcription Coactivator SRC-1. *Int J Mol Sci*, *22*(12). https://doi.org/10.3390/ijms22126407

Cossa, G., Roeschert, I., Prinz, F., Baluapuri, A., Vidal, R. S., Schulein-Volk, C., Chang, Y. C., Ade, C. P., Mastrobuoni, G., Girard, C., Kumar, A., Wortmann, L., Walz, S., Luhrmann, R., Kempa, S., Kuster, B., Wolf, E., Mumberg, D., & Eilers, M. (2021). Localized inhibition of protein phosphatase 1 by NUAK1 promotes spliceosome activity and reveals a MYC-sensitive feedback control of transcription. *Mol Cell*, *81*(11), 2495. https://doi.org/10.1016/j.molcel.2021.05.013

Cotton, A. D., Nguyen, D. P., Gramespacher, J. A., Seiple, I. B., & Wells, J. A. (2021). Development of Antibody-Based PROTACs for the Degradation of the Cell-Surface Immune Checkpoint Protein PD-L1. *J Am Chem Soc*, *143*(2), 593-598. https://doi.org/10.1021/jacs.0c10008

Cox, J., & Mann, M. (2008). MaxQuant enables high peptide identification rates, individualized p.p.b.-range mass accuracies and proteome-wide protein quantification. *Nat Biotechnol*, *26*(12), 1367-1372. https://doi.org/10.1038/nbt.1511

Cromm, P. M., Samarasinghe, K. T. G., Hines, J., & Crews, C. M. (2018). Addressing Kinase-Independent Functions of Fak via PROTAC-Mediated Degradation. *J Am Chem Soc*, *140*(49), 17019-17026. https://doi.org/10.1021/jacs.8b08008

Cui, Z., Li, H., Liang, F., Mu, C., Mu, Y., Zhang, X., & Liu, J. (2018). Effect of high WDR5 expression on the hepatocellular carcinoma prognosis. *Oncol Lett*, *15*(5), 7864-7870. https://doi.org/10.3892/ol.2018.8298

D'Assoro, A. B., Liu, T., Quatraro, C., Amato, A., Opyrchal, M., Leontovich, A., Ikeda, Y., Ohmine, S., Lingle, W., Suman, V., Ecsedy, J., Iankov, I., Di Leonardo, A., Ayers-Inglers, J., Degnim, A., Billadeau, D., McCubrey, J., Ingle, J., Salisbury, J. L., & Galanis, E. (2014). The mitotic kinase Aurora--a promotes distant metastases by inducing epithelial-to-mesenchymal transition in ERalpha(+) breast cancer cells. *Oncogene*, *33*(5), 599-610. https://doi.org/10.1038/onc.2012.628

D'Cruz, C. M., Gunther, E. J., Boxer, R. B., Hartman, J. L., Sintasath, L., Moody, S. E., Cox, J. D., Ha, S. I., Belka, G. K., Golant, A., Cardiff, R. D., & Chodosh, L. A. (2001). c-MYC induces mammary tumorigenesis by means of a preferred pathway involving spontaneous Kras2 mutations. *Nat Med*, *7*(2), 235-239. https://doi.org/10.1038/84691

Dai, X., Guo, W., Zhan, C., Liu, X., Bai, Z., & Yang, Y. (2015). WDR5 Expression Is Prognostic of Breast Cancer Outcome. *PLoS One*, *10*(9), e0124964. https://doi.org/10.1371/journal.pone.0124964

Dalla-Favera, R., Bregni, M., Erikson, J., Patterson, D., Gallo, R. C., & Croce, C. M. (1982). Human c-myc onc gene is located on the region of chromosome 8 that is translocated in Burkitt lymphoma cells. *Proc Natl Acad Sci U S A*, *79*(24), 7824-7827. https://doi.org/10.1073/pnas.79.24.7824

Dang, C. V. (2012). MYC on the path to cancer. *Cell*, *149*(1), 22-35. https://doi.org/10.1016/j.cell.2012.03.003

Dani, C., Blanchard, J. M., Piechaczyk, M., El Sabouty, S., Marty, L., & Jeanteur, P. (1984). Extreme instability of myc mRNA in normal and transformed human cells. *Proc Natl Acad Sci U S A*, *81*(22), 7046-7050. https://doi.org/10.1073/pnas.81.22.7046

Dauch, D., Rudalska, R., Cossa, G., Nault, J. C., Kang, T. W., Wuestefeld, T., Hohmeyer, A., Imbeaud, S., Yevsa, T., Hoenicke, L., Pantsar, T., Bozko, P., Malek, N. P., Longerich, T., Laufer, S., Poso, A., Zucman-Rossi, J., Eilers, M., & Zender, L. (2016). A MYC-aurora kinase A protein complex represents an actionable drug target in p53-altered liver cancer. *Nat Med*, *22*(7), 744-753. https://doi.org/10.1038/nm.4107

Davis, A. C., Wims, M., Spotts, G. D., Hann, S. R., & Bradley, A. (1993). A null c-myc mutation causes lethality before 10.5 days of gestation in homozygotes and reduced fertility in heterozygous female mice. *Genes Dev*, *7*(4), 671-682. https://doi.org/10.1101/gad.7.4.671

De Duve, C., & Wattiaux, R. (1966). Functions of lysosomes. *Annu Rev Physiol*, *28*, 435-492. https://doi.org/10.1146/annurev.ph.28.030166.002251

Delmore, J. E., Issa, G. C., Lemieux, M. E., Rahl, P. B., Shi, J., Jacobs, H. M., Kastritis, E., Gilpatrick, T., Paranal, R. M., Qi, J., Chesi, M., Schinzel, A. C., McKeown, M. R., Heffernan, T. P., Vakoc, C. R., Bergsagel, P. L., Ghobrial, I. M., Richardson, P. G., Young, R. A., . . . Mitsiades, C. S. (2011). BET bromodomain inhibition as a therapeutic strategy to target c-Myc. *Cell*, *146*(6), 904-917. https://doi.org/10.1016/j.cell.2011.08.017

Devi, G. R., Beer, T. M., Corless, C. L., Arora, V., Weller, D. L., & Iversen, P. L. (2005). In vivo bioavailability and pharmacokinetics of a c-MYC antisense phosphorodiamidate morpholino oligomer, AVI-4126, in solid tumors. *Clin Cancer Res*, *11*(10), 3930-3938. https://doi.org/10.1158/1078-0432.CCR-04-2091

Dias, J., Van Nguyen, N., Georgiev, P., Gaub, A., Brettschneider, J., Cusack, S., Kadlec, J., & Akhtar, A. (2014). Structural analysis of the KANSL1/WDR5/KANSL2 complex reveals that WDR5 is required for efficient assembly and chromatin targeting of the NSL complex. *Genes Dev*, *28*(9), 929-942. https://doi.org/10.1101/gad.240200.114

Dikic, I. (2017). Proteasomal and Autophagic Degradation Systems. *Annu Rev Biochem*, *86*, 193-224. https://doi.org/10.1146/annurev-biochem-061516-044908

Dodson, C. A., & Bayliss, R. (2012). Activation of Aurora-A kinase by protein partner binding and phosphorylation are independent and synergistic. *J Biol Chem*, *287*(2), 1150-1157. https://doi.org/10.1074/jbc.M111.312090

Dodson, C. A., Kosmopoulou, M., Richards, M. W., Atrash, B., Bavetsias, V., Blagg, J., & Bayliss, R. (2010). Crystal structure of an Aurora-A mutant that mimics Aurora-B bound to MLN8054: insights into selectivity and drug design. *Biochem J*, *427*(1), 19-28. https://doi.org/10.1042/BJ20091530

Bibliography

Dolle, A., Adhikari, B., Kramer, A., Weckesser, J., Berner, N., Berger, L. M., Diebold, M., Szewczyk, M. M., Barsyte-Lovejoy, D., Arrowsmith, C. H., Gebel, J., Lohr, F., Dotsch, V., Eilers, M., Heinzlmeir, S., Kuster, B., Sotriffer, C., Wolf, E., & Knapp, S. (2021). Design, Synthesis, and Evaluation of WD-Repeat-Containing Protein 5 (WDR5) Degraders. *J Med Chem*, *64*(15), 10682-10710. https://doi.org/10.1021/acs.jmedchem.1c00146

Donovan, K. A., Ferguson, F. M., Bushman, J. W., Eleuteri, N. A., Bhunia, D., Ryu, S., Tan, L., Shi, K., Yue, H., Liu, X., Dobrovolsky, D., Jiang, B., Wang, J., Hao, M., You, I., Teng, M., Liang, Y., Hatcher, J., Li, Z., . . . Fischer, E. S. (2020). Mapping the Degradable Kinome Provides a Resource for Expedited Degrader Development. *Cell*, *183*(6), 1714-1731 e1710. https://doi.org/10.1016/j.cell.2020.10.038

Dou, Y., Milne, T. A., Ruthenburg, A. J., Lee, S., Lee, J. W., Verdine, G. L., Allis, C. D., & Roeder, R. G. (2006). Regulation of MLL1 H3K4 methyltransferase activity by its core components. *Nat Struct Mol Biol*, *13*(8), 713-719. https://doi.org/10.1038/nsmb1128

Douglass, E. F., Jr., Miller, C. J., Sparer, G., Shapiro, H., & Spiegel, D. A. (2013). A comprehensive mathematical model for three-body binding equilibria. *J Am Chem Soc*, *135*(16), 6092-6099. https://doi.org/10.1021/ja311795d

Drygin, D., Siddiqui-Jain, A., O'Brien, S., Schwaebe, M., Lin, A., Bliesath, J., Ho, C. B., Proffitt, C., Trent, K., Whitten, J. P., Lim, J. K., Von Hoff, D., Anderes, K., & Rice, W. G. (2009). Anticancer activity of CX-3543: a direct inhibitor of rRNA biogenesis. *Cancer Res*, *69*(19), 7653-7661. https://doi.org/10.1158/0008-5472.CAN-09-1304

Dubois, N. C., Adolphe, C., Ehninger, A., Wang, R. A., Robertson, E. J., & Trumpp, A. (2008). Placental rescue reveals a sole requirement for c-Myc in embryonic erythroblast survival and hematopoietic stem cell function. *Development*, *135*(14), 2455-2465. https://doi.org/10.1242/dev.022707

Duesberg, P. H., Bister, K., & Vogt, P. K. (1977). The RNA of avian acute leukemia virus MC29. *Proc Natl Acad Sci U S A*, *74*(10), 4320-4324. https://doi.org/10.1073/pnas.74.10.4320

Duffy, M. J., O'Grady, S., Tang, M., & Crown, J. (2021). MYC as a target for cancer treatment. *Cancer Treat Rev*, *94*, 102154. https://doi.org/10.1016/j.ctrv.2021.102154

Ee, L. S., McCannell, K. N., Tang, Y., Fernandes, N., Hardy, W. R., Green, M. R., Chu, F., & Fazzio, T. G. (2017). An Embryonic Stem Cell-Specific NuRD Complex Functions through Interaction with WDR5. *Stem Cell Reports*, *8*(6), 1488-1496. https://doi.org/10.1016/j.stemcr.2017.04.020

Ehrhardt, A., Bartels, T., Geick, A., Klocke, R., Paul, D., & Halter, R. (2001). Development of pulmonary bronchiolo-alveolar adenocarcinomas in transgenic mice overexpressing murine c-myc and epidermal growth factor in alveolar type II pneumocytes. *Br J Cancer*, *84*(6), 813-818. https://doi.org/10.1054/bjoc.2000.1676

Eilers, M., & Eisenman, R. N. (2008). Myc's broad reach. *Genes Dev*, *22*(20), 2755-2766. https://doi.org/10.1101/gad.1712408

Eilers, M., Picard, D., Yamamoto, K. R., & Bishop, J. M. (1989). Chimaeras of myc oncoprotein and steroid receptors cause hormone-dependent transformation of cells. *Nature*, *340*(6228), 66-68. https://doi.org/10.1038/340066a0

Endres, T., Solvie, D., Heidelberger, J. B., Andrioletti, V., Baluapuri, A., Ade, C. P., Muhar, M., Eilers, U., Vos, S. M., Cramer, P., Zuber, J., Beli, P., Popov, N., Wolf, E., Gallant, P., & Eilers, M. (2021). Ubiquitylation of MYC couples transcription elongation with double-strand break repair at active promoters. *Mol Cell*, *81*(4), 830-844 e813. https://doi.org/10.1016/j.molcel.2020.12.035

Erisman, M. D., Rothberg, P. G., Diehl, R. E., Morse, C. C., Spandorfer, J. M., & Astrin, S. M. (1985). Deregulation of c-myc gene expression in human colon carcinoma is not accompanied by amplification or rearrangement of the gene. *Mol Cell Biol*, *5*(8), 1969-1976. https://doi.org/10.1128/mcb.5.8.1969-1976.1985

Facchini, L. M., & Penn, L. Z. (1998). The molecular role of Myc in growth and transformation: recent discoveries lead to new insights. *The FASEB Journal*, *12*(9), 633-651. https://doi.org/10.1096/fasebj.12.9.633

Falchook, G. S., Bastida, C. C., & Kurzrock, R. (2015). Aurora Kinase Inhibitors in Oncology Clinical Trials: Current State of the Progress. *Semin Oncol*, *42*(6), 832-848. https://doi.org/10.1053/j.seminoncol.2015.09.022

Fan, X., Jin, W. Y., Lu, J., Wang, J., & Wang, Y. T. (2014). Rapid and reversible knockdown of endogenous proteins by peptide-directed lysosomal degradation. *Nat Neurosci*, *17*(3), 471-480. https://doi.org/10.1038/nn.3637

Bibliography

Farnaby, W., Koegl, M., Roy, M. J., Whitworth, C., Diers, E., Trainor, N., Zollman, D., Steurer, S., Karolyi-Oezguer, J., Riedmueller, C., Gmaschitz, T., Wachter, J., Dank, C., Galant, M., Sharps, B., Rumpel, K., Traxler, E., Gerstberger, T., Schnitzer, R., . . . Ciulli, A. (2019). BAF complex vulnerabilities in cancer demonstrated via structure-based PROTAC design. *Nat Chem Biol*, *15*(7), 672-680. https://doi.org/10.1038/s41589-019-0294-6

Farrell, A. S., & Sears, R. C. (2014). MYC degradation. *Cold Spring Harb Perspect Med*, *4*(3). https://doi.org/10.1101/cshperspect.a014365

Felsher, D. W., & Bishop, J. M. (1999). Reversible tumorigenesis by MYC in hematopoietic lineages. *Mol Cell*, *4*(2), 199-207. https://doi.org/10.1016/s1097-2765(00)80367-6

Flores, I., Murphy, D. J., Swigart, L. B., Knies, U., & Evan, G. I. (2004). Defining the temporal requirements for Myc in the progression and maintenance of skin neoplasia. *Oncogene*, *23*(35), 5923-5930. https://doi.org/10.1038/sj.onc.1207796

Franco-Serrano, L., Huerta, M., Hernandez, S., Cedano, J., Perez-Pons, J., Pinol, J., Mozo-Villarias, A., Amela, I., & Querol, E. (2018). Multifunctional Proteins: Involvement in Human Diseases and Targets of Current Drugs. *Protein J*, *37*(5), 444-453. https://doi.org/10.1007/s10930-018-9790-x

Fu, J., Bian, M., Jiang, Q., & Zhang, C. (2007). Roles of Aurora kinases in mitosis and tumorigenesis. *Mol Cancer Res*, *5*(1), 1-10. https://doi.org/10.1158/1541-7786.MCR-06-0208

Fu, Y., Chen, N., Wang, Z., Luo, S., Ding, Y., & Lu, B. (2021). Degradation of lipid droplets by chimeric autophagy-tethering compounds. *Cell Res*, *31*(9), 965-979. https://doi.org/10.1038/s41422-021-00532-7

Gabay, M., Li, Y., & Felsher, D. W. (2014). MYC activation is a hallmark of cancer initiation and maintenance. *Cold Spring Harb Perspect Med*, *4*(6). https://doi.org/10.1101/cshperspect.a014241

Gadd, M. S., Testa, A., Lucas, X., Chan, K. H., Chen, W., Lamont, D. J., Zengerle, M., & Ciulli, A. (2017). Structural basis of PROTAC cooperative recognition for selective protein degradation. *Nat Chem Biol*, *13*(5), 514-521. https://doi.org/10.1038/nchembio.2329

Galardi, S., Savino, M., Scagnoli, F., Pellegatta, S., Pisati, F., Zambelli, F., Illi, B., Annibali, D., Beji, S., Orecchini, E., Alberelli, M. A., Apicella, C., Fontanella, R. A., Michienzi, A., Finocchiaro, G., Farace, M. G., Pavesi, G., Ciafre, S. A., & Nasi, S. (2016). Resetting cancer stem cell regulatory nodes upon MYC inhibition. *EMBO Rep*, *17*(12), 1872-1889. https://doi.org/10.15252/embr.201541489

Gao, N., Chu, T.-T., Li, Q.-Q., Lim, Y.-J., Qiu, T., Ma, M.-R., Hu, Z.-W., Yang, X.-F., Chen, Y.-X., Zhao, Y.-F., & Li, Y.-M. (2017). Hydrophobic tagging-mediated degradation of Alzheimer's disease related Tau. *RSC Advances*, *7*(64), 40362-40366. https://doi.org/10.1039/c7ra05347a

Gao, X., Burris Iii, H. A., Vuky, J., Dreicer, R., Sartor, A. O., Sternberg, C. N., Percent, I. J., Hussain, M. H. A., Rezazadeh Kalebasty, A., Shen, J., Heath, E. I., Abesada-Terk, G., Gandhi, S. G., McKean, M., Lu, H., Berghorn, E., Gedrich, R., Chirnomas, S. D., Vogelzang, N. J., & Petrylak, D. P. (2022). Phase 1/2 study of ARV-110, an androgen receptor (AR) PROTAC degrader, in metastatic castration-resistant prostate cancer (mCRPC). *Journal of Clinical Oncology*, *40*(6_suppl), 17-17. https://doi.org/10.1200/JCO.2022.40.6_suppl.017

Ge, Z., Song, E. J., Kawasawa, Y. I., Li, J., Dovat, S., & Song, C. (2016). WDR5 high expression and its effect on tumorigenesis in leukemia. *Oncotarget*, *7*(25), 37740-37754. https://doi.org/10.18632/oncotarget.9312

George, A. J., Hoffiz, Y. C., Charles, A. J., Zhu, Y., & Mabb, A. M. (2018). A Comprehensive Atlas of E3 Ubiquitin Ligase Mutations in Neurological Disorders. *Front Genet*, *9*, 29. https://doi.org/10.3389/fgene.2018.00029

Glickman, M. H., & Ciechanover, A. (2002). The ubiquitin-proteasome proteolytic pathway: destruction for the sake of construction. *Physiol Rev*, *82*(2), 373-428. https://doi.org/10.1152/physrev.00027.2001

Goldenson, B., & Crispino, J. D. (2015). The aurora kinases in cell cycle and leukemia. *Oncogene*, *34*(5), 537-545. https://doi.org/10.1038/onc.2014.14

Gole, B., & Wiesmuller, L. (2015). Leukemogenic rearrangements at the mixed lineage leukemia gene (MLL)-multiple rather than a single mechanism. *Front Cell Dev Biol*, *3*, 41. https://doi.org/10.3389/fcell.2015.00041

Gomez, J. A., Wapinski, O. L., Yang, Y. W., Bureau, J. F., Gopinath, S., Monack, D. M., Chang, H. Y., Brahic, M., & Kirkegaard, K. (2013). The NeST long ncRNA controls microbial susceptibility and epigenetic activation of the interferon-gamma locus. *Cell*, *152*(4), 743-754. https://doi.org/10.1016/j.cell.2013.01.015

Gomez-Roman, N., Felton-Edkins, Z. A., Kenneth, N. S., Goodfellow, S. J., Athineos, D., Zhang, J., Ramsbottom, B. A., Innes, F., Kantidakis, T., Kerr, E. R., Brodie, J., Grandori, C., & White, R. J. (2006). Activation by c-Myc of transcription by RNA polymerases I, II and III. *Biochem Soc Symp*(73), 141-154. https://doi.org/10.1042/bss0730141

Gomez-Roman, N., Grandori, C., Eisenman, R. N., & White, R. J. (2003). Direct activation of RNA polymerase III transcription by c-Myc. *Nature*, *421*(6920), 290-294. https://doi.org/10.1038/nature01327

Gorgun, G., Calabrese, E., Hideshima, T., Ecsedy, J., Perrone, G., Mani, M., Ikeda, H., Bianchi, G., Hu, Y., Cirstea, D., Santo, L., Tai, Y. T., Nahar, S., Zheng, M., Bandi, M., Carrasco, R. D., Raje, N., Munshi, N., Richardson, P., & Anderson, K. C. (2010). A novel Aurora-A kinase inhibitor MLN8237 induces cytotoxicity and cell-cycle arrest in multiple myeloma. *Blood*, *115*(25), 5202-5213. https://doi.org/10.1182/blood-2009-12-259523

Grandori, C., Gomez-Roman, N., Felton-Edkins, Z. A., Ngouenet, C., Galloway, D. A., Eisenman, R. N., & White, R. J. (2005). c-Myc binds to human ribosomal DNA and stimulates transcription of rRNA genes by RNA polymerase I. *Nat Cell Biol*, *7*(3), 311-318. https://doi.org/10.1038/ncb1224

Grebien, F., Vedadi, M., Getlik, M., Giambruno, R., Grover, A., Avellino, R., Skucha, A., Vittori, S., Kuznetsova, E., Smil, D., Barsyte-Lovejoy, D., Li, F., Poda, G., Schapira, M., Wu, H., Dong, A., Senisterra, G., Stukalov, A., Huber, K. V. M., . . . Superti-Furga, G. (2015). Pharmacological targeting of the Wdr5-MLL interaction in C/EBPalpha N-terminal leukemia. *Nat Chem Biol*, *11*(8), 571-578. https://doi.org/10.1038/nchembio.1859

Guarino Almeida, E., Renaudin, X., & Venkitaraman, A. R. (2020). A kinase-independent function for AURORA-A in replisome assembly during DNA replication initiation. *Nucleic Acids Res*, *48*(14), 7844-7855. https://doi.org/10.1093/nar/gkaa570

Guarnaccia, A. D., Rose, K. L., Wang, J., Zhao, B., Popay, T. M., Wang, C. E., Guerrazzi, K., Hill, S., Woodley, C. M., Hansen, T. J., Lorey, S. L., Shaw, J. G., Payne, W. G., Weissmiller, A. M., Olejniczak, E. T., Fesik, S. W., Liu, Q., & Tansey, W. P. (2021). Impact of WIN site inhibitor on the WDR5 interactome. *Cell Rep*, *34*(3), 108636. https://doi.org/10.1016/j.celrep.2020.108636

Guarnaccia, A. D., & Tansey, W. P. (2018). Moonlighting with WDR5: A Cellular Multitasker. *J Clin Med*, *7*(2). https://doi.org/10.3390/jcm7020021

Guelman, S., Kozuka, K., Mao, Y., Pham, V., Solloway, M. J., Wang, J., Wu, J., Lill, J. R., & Zha, J. (2009). The double-histone-acetyltransferase complex ATAC is essential for mammalian development. *Mol Cell Biol*, *29*(5), 1176-1188. https://doi.org/10.1128/MCB.01599-08

Guenette, R. G., Yang, S. W., Min, J., Pei, B., & Potts, P. R. (2022). Target and tissue selectivity of PROTAC degraders. *Chem Soc Rev*, *51*(14), 5740-5756. https://doi.org/10.1039/d2cs00200k

Gugger, M., Burckhardt, E., Kappeler, A., Hirsiger, H., Laissue, J. A., & Mazzucchelli, L. (2002). Quantitative expansion of structural genomic alterations in the spectrum of neuroendocrine lung carcinomas. *J Pathol*, *196*(4), 408-415. https://doi.org/10.1002/path.1065

Guinney, J., Dienstmann, R., Wang, X., de Reynies, A., Schlicker, A., Soneson, C., Marisa, L., Roepman, P., Nyamundanda, G., Angelino, P., Bot, B. M., Morris, J. S., Simon, I. M., Gerster, S., Fessler, E., De Sousa, E. M. F., Missiaglia, E., Ramay, H., Barras, D., . . . Tejpar, S. (2015). The consensus molecular subtypes of colorectal cancer. *Nat Med*, *21*(11), 1350-1356. https://doi.org/10.1038/nm.3967

Guo, J., Parise, R. A., Joseph, E., Egorin, M. J., Lazo, J. S., Prochownik, E. V., & Eiseman, J. L. (2009). Efficacy, pharmacokinetics, tisssue distribution, and metabolism of the Myc-Max disruptor, 10058-F4 [Z,E]-5-[4-ethylbenzylidine]-2-thioxothiazolidin-4-one, in mice. *Cancer Chemother Pharmacol*, *63*(4), 615-625. https://doi.org/10.1007/s00280-008-0774-y

Guo, M., Lu, S., Huang, H., Wang, Y., Yang, M. Q., Yang, Y., Fan, Z., Jiang, B., & Deng, Y. (2018). Increased AURKA promotes cell proliferation and predicts poor prognosis in

bladder cancer. *BMC Syst Biol*, *12*(Suppl 7), 118. https://doi.org/10.1186/s12918-018-0634-2

Gustafson, J. L., Neklesa, T. K., Cox, C. S., Roth, A. G., Buckley, D. L., Tae, H. S., Sundberg, T. B., Stagg, D. B., Hines, J., McDonnell, D. P., Norris, J. D., & Crews, C. M. (2015). Small-Molecule-Mediated Degradation of the Androgen Receptor through Hydrophobic Tagging. *Angew Chem Int Ed Engl*, *54*(33), 9659-9662. https://doi.org/10.1002/anie.201503720

Gustafson, W. C., Meyerowitz, J. G., Nekritz, E. A., Chen, J., Benes, C., Charron, E., Simonds, E. F., Seeger, R., Matthay, K. K., Hertz, N. T., Eilers, M., Shokat, K. M., & Weiss, W. A. (2014). Drugging MYCN through an allosteric transition in Aurora kinase A. *Cancer Cell*, *26*(3), 414-427. https://doi.org/10.1016/j.ccr.2014.07.015

Hamilton, E., Vahdat, L., Han, H. S., Ranciato, J., Gedrich, R., Keung, C. F., Chirnomas, D., & Hurvitz, S. (2022). Abstract PD13-08: First-in-human safety and activity of ARV-471, a novel PROTAC® estrogen receptor degrader, in ER+/HER2- locally advanced or metastatic breast cancer. *Cancer Research*, *82*(4_Supplement), PD13-08-PD13-08. https://doi.org/10.1158/1538-7445.Sabcs21-pd13-08

Hamilton, E. P., Schott, A. F., Nanda, R., Lu, H., Keung, C. F., Gedrich, R., Parameswaran, J., Han, H. S., & Hurvitz, S. A. (2022). ARV-471, an estrogen receptor (ER) PROTACdegrader, combined with palbociclib in advanced ER+/human epidermal growth factor receptor 2–negative (HER2-) breast cancer: Phase 1b cohort (part C) of a phase 1/2 study. *Journal of Clinical Oncology*, *40*(16_suppl), TPS1120-TPS1120. https://doi.org/10.1200/JCO.2022.40.16_suppl.TPS1120

Han, T., Goralski, M., Gaskill, N., Capota, E., Kim, J., Ting, T. C., Xie, Y., Williams, N. S., & Nijhawan, D. (2017). Anticancer sulfonamides target splicing by inducing RBM39 degradation via recruitment to DCAF15. *Science*, *356*(6336). https://doi.org/10.1126/science.aal3755

Han, X., Zhao, L., Xiang, W., Qin, C., Miao, B., Xu, T., Wang, M., Yang, C. Y., Chinnaswamy, K., Stuckey, J., & Wang, S. (2019). Discovery of Highly Potent and Efficient PROTAC Degraders of Androgen Receptor (AR) by Employing Weak Binding Affinity VHL E3 Ligase Ligands. *J Med Chem*, *62*(24), 11218-11231. https://doi.org/10.1021/acs.jmedchem.9b01393

Hanahan, D. (2022). Hallmarks of Cancer: New Dimensions. *Cancer Discov*, *12*(1), 31-46. https://doi.org/10.1158/2159-8290.CD-21-1059

Hanahan, D., & Weinberg, R. A. (2011). Hallmarks of cancer: the next generation. *Cell*, *144*(5), 646-674. https://doi.org/10.1016/j.cell.2011.02.013

Hann, S. R., & Eisenman, R. N. (1984). Proteins encoded by the human c-myc oncogene: differential expression in neoplastic cells. *Molecular and Cellular Biology*, *4*(11), 2486-2497. https://doi.org/10.1128/mcb.4.11.2486

Harper, D. P., & Aplan, P. D. (2008). Chromosomal rearrangements leading to MLL gene fusions: clinical and biological aspects. *Cancer Res*, *68*(24), 10024-10027. https://doi.org/10.1158/0008-5472.CAN-08-2208

He, M., Lv, W., & Rao, Y. (2021). Opportunities and Challenges of Small Molecule Induced Targeted Protein Degradation. *Front Cell Dev Biol*, *9*, 685106. https://doi.org/10.3389/fcell.2021.685106

Heidelberger, J. B., Voigt, A., Borisova, M. E., Petrosino, G., Ruf, S., Wagner, S. A., & Beli, P. (2018). Proteomic profiling of VCP substrates links VCP to K6-linked ubiquitylation and c-Myc function. *EMBO Rep*, *19*(4). https://doi.org/10.15252/embr.201744754

Heinzlmeir, S., Kudlinzki, D., Sreeramulu, S., Klaeger, S., Gande, S. L., Linhard, V., Wilhelm, M., Qiao, H., Helm, D., Ruprecht, B., Saxena, K., Medard, G., Schwalbe, H., & Kuster, B. (2016). Chemical Proteomics and Structural Biology Define EPHA2 Inhibition by Clinical Kinase Drugs. *ACS Chem Biol*, *11*(12), 3400-3411. https://doi.org/10.1021/acschembio.6b00709

Hemann, M. T., Bric, A., Teruya-Feldstein, J., Herbst, A., Nilsson, J. A., Cordon-Cardo, C., Cleveland, J. L., Tansey, W. P., & Lowe, S. W. (2005). Evasion of the p53 tumour surveillance network by tumour-derived MYC mutants. *Nature*, *436*(7052), 807-811. https://doi.org/10.1038/nature03845

Herold, S., Kalb, J., Buchel, G., Ade, C. P., Baluapuri, A., Xu, J., Koster, J., Solvie, D., Carstensen, A., Klotz, C., Rodewald, S., Schulein-Volk, C., Dobbelstein, M., Wolf, E., Molenaar, J., Versteeg, R., Walz, S., & Eilers, M. (2019). Recruitment of BRCA1 limits

MYCN-driven accumulation of stalled RNA polymerase. *Nature*, *567*(7749), 545-549. https://doi.org/10.1038/s41586-019-1030-9

Hershko, A., & Ciechanover, A. (1998). The ubiquitin system. *Annu Rev Biochem*, *67*, 425-479. https://doi.org/10.1146/annurev.biochem.67.1.425

Hochegger, H., Hegarat, N., & Pereira-Leal, J. B. (2013). Aurora at the pole and equator: overlapping functions of Aurora kinases in the mitotic spindle. *Open Biology*, *3*. https://doi.org/ARTN 120185

10.1098/rsob.120185

Hochstrasser, M. (1995). Ubiquitin, proteasomes, and the regulation of intracellular protein degradation. *Current Opinion in Cell Biology*, *7*(2), 215-223. https://doi.org/10.1016/0955-0674(95)80031-x

Hsu, J. H., Rasmusson, T., Robinson, J., Pachl, F., Read, J., Kawatkar, S., DH, O. D., Bagal, S., Code, E., Rawlins, P., Argyrou, A., Tomlinson, R., Gao, N., Zhu, X., Chiarparin, E., Jacques, K., Shen, M., Woods, H., Bednarski, E., . . . Bloecher, A. (2020). EED-Targeted PROTACs Degrade EED, EZH2, and SUZ12 in the PRC2 Complex. *Cell Chem Biol*, *27*(1), 41-46 e17. https://doi.org/10.1016/j.chembiol.2019.11.004

Huang, D., Chen, X., Chen, X., Qu, Y., Wang, Y., Yang, Y., & Cheng, Y. (2020). WDR5 Promotes Proliferation and Correlates with Poor Prognosis in Oesophageal Squamous Cell Carcinoma. *Onco Targets Ther*, *13*, 10525-10534. https://doi.org/10.2147/OTT.S234773

Huang, M., & Weiss, W. A. (2013). Neuroblastoma and MYCN. *Cold Spring Harb Perspect Med*, *3*(10), a014415. https://doi.org/10.1101/cshperspect.a014415

Huang, M. J., Cheng, Y. C., Liu, C. R., Lin, S., & Liu, H. E. (2006). A small-molecule c-Myc inhibitor, 10058-F4, induces cell-cycle arrest, apoptosis, and myeloid differentiation of human acute myeloid leukemia. *Exp Hematol*, *34*(11), 1480-1489. https://doi.org/10.1016/j.exphem.2006.06.019

Hughes, S. J., Testa, A., Thompson, N., & Churcher, I. (2021). The rise and rise of protein degradation: Opportunities and challenges ahead. *Drug Discov Today*, *26*(12), 2889-2897. https://doi.org/10.1016/j.drudis.2021.08.006

Imielinski, M., Berger, A. H., Hammerman, P. S., Hernandez, B., Pugh, T. J., Hodis, E., Cho, J., Suh, J., Capelletti, M., Sivachenko, A., Sougnez, C., Auclair, D., Lawrence, M. S., Stojanov, P., Cibulskis, K., Choi, K., de Waal, L., Sharifnia, T., Brooks, A., . . . Meyerson, M. (2012). Mapping the hallmarks of lung adenocarcinoma with massively parallel sequencing. *Cell*, *150*(6), 1107-1120. https://doi.org/10.1016/j.cell.2012.08.029

Inobe, T., & Nukina, N. (2016). Rapamycin-induced oligomer formation system of FRB-FKBP fusion proteins. *J Biosci Bioeng*, *122*(1), 40-46. https://doi.org/10.1016/j.jbiosc.2015.12.004

Ireland, A. S., Micinski, A. M., Kastner, D. W., Guo, B., Wait, S. J., Spainhower, K. B., Conley, C. C., Chen, O. S., Guthrie, M. R., Soltero, D., Qiao, Y., Huang, X., Tarapcsak, S., Devarakonda, S., Chalishazar, M. D., Gertz, J., Moser, J. C., Marth, G., Puri, S., . . . Oliver, T. G. (2020). MYC Drives Temporal Evolution of Small Cell Lung Cancer Subtypes by Reprogramming Neuroendocrine Fate. *Cancer Cell*, *38*(1), 60-78 e12. https://doi.org/10.1016/j.ccell.2020.05.001

Ishida, T., & Ciulli, A. (2021). E3 Ligase Ligands for PROTACs: How They Were Found and How to Discover New Ones. *SLAS Discov*, *26*(4), 484-502. https://doi.org/10.1177/2472555220965528

Ito, T., Ando, H., Suzuki, T., Ogura, T., Hotta, K., Imamura, Y., Yamaguchi, Y., & Handa, H. (2010). Identification of a primary target of thalidomide teratogenicity. *Science*, *327*(5971), 1345-1350. https://doi.org/10.1126/science.1177319

Ito, T., & Handa, H. (2016). Cereblon and its downstream substrates as molecular targets of immunomodulatory drugs. *Int J Hematol*, *104*(3), 293-299. https://doi.org/10.1007/s12185-016-2073-4

Jain, M., Arvanitis, C., Chu, K., Dewey, W., Leonhardt, E., Trinh, M., Sundberg, C. D., Bishop, J. M., & Felsher, D. W. (2002). Sustained loss of a neoplastic phenotype by brief inactivation of MYC. *Science*, *297*(5578), 102-104. https://doi.org/10.1126/science.1071489

Janghorban, M., Farrell, A. S., Allen-Petersen, B. L., Pelz, C., Daniel, C. J., Oddo, J., Langer, E. M., Christensen, D. J., & Sears, R. C. (2014). Targeting c-MYC by antagonizing

PP2A inhibitors in breast cancer. *Proc Natl Acad Sci U S A*, *111*(25), 9157-9162. https://doi.org/10.1073/pnas.1317630111

Ji, A., Qian, L., Tian, Z., & Cui, J. (2021). WDR5 promotes the proliferation of lung adenocarcinoma by inducing SOX9 expression. *Biomark Med*, *15*(17), 1599-1609. https://doi.org/10.2217/bmm-2021-0184

Ji, C. H., Kim, H. Y., Lee, M. J., Heo, A. J., Park, D. Y., Lim, S., Shin, S., Ganipisetti, S., Yang, W. S., Jung, C. A., Kim, K. Y., Jeong, E. H., Park, S. H., Bin Kim, S., Lee, S. J., Na, J. E., Kang, J. I., Chi, H. M., Kim, H. T., . . . Kwon, Y. T. (2022). The AUTOTAC chemical biology platform for targeted protein degradation via the autophagy-lysosome system. *Nat Commun*, *13*(1), 904. https://doi.org/10.1038/s41467-022-28520-4

Johnson, B. E., Ihde, D. C., Makuch, R. W., Gazdar, A. F., Carney, D. N., Oie, H., Russell, E., Nau, M. M., & Minna, J. D. (1987). myc family oncogene amplification in tumor cell lines established from small cell lung cancer patients and its relationship to clinical status and course. *J Clin Invest*, *79*(6), 1629-1634. https://doi.org/10.1172/JCI112999

Jung, L. A., Gebhardt, A., Koelmel, W., Ade, C. P., Walz, S., Kuper, J., von Eyss, B., Letschert, S., Redel, C., d'Artista, L., Biankin, A., Zender, L., Sauer, M., Wolf, E., Evan, G., Kisker, C., & Eilers, M. (2017). OmoMYC blunts promoter invasion by oncogenic MYC to inhibit gene expression characteristic of MYC-dependent tumors. *Oncogene*, *36*(14), 1911-1924. https://doi.org/10.1038/onc.2016.354

Kaelin, W. G. (2018). The von Hippel–Lindau Tumor Suppressor Protein. *Annual Review of Cancer Biology*, *2*(1), 91-109. https://doi.org/10.1146/annurev-cancerbio-030617-050527

Kalkat, M., De Melo, J., Hickman, K. A., Lourenco, C., Redel, C., Resetca, D., Tamachi, A., Tu, W. B., & Penn, L. Z. (2017). MYC Deregulation in Primary Human Cancers. *Genes (Basel)*, *8*(6). https://doi.org/10.3390/genes8060151

Kalkat, M., Resetca, D., Lourenco, C., Chan, P. K., Wei, Y., Shiah, Y. J., Vitkin, N., Tong, Y., Sunnerhagen, M., Done, S. J., Boutros, P. C., Raught, B., & Penn, L. Z. (2018). MYC Protein Interactome Profiling Reveals Functionally Distinct Regions that Cooperate to Drive Tumorigenesis. *Mol Cell*, *72*(5), 836-848 e837. https://doi.org/10.1016/j.molcel.2018.09.031

Kaposi-Novak, P., Libbrecht, L., Woo, H. G., Lee, Y. H., Sears, N. C., Coulouarn, C., Conner, E. A., Factor, V. M., Roskams, T., & Thorgeirsson, S. S. (2009). Central role of c-Myc during malignant conversion in human hepatocarcinogenesis. *Cancer Res*, *69*(7), 2775-2782. https://doi.org/10.1158/0008-5472.CAN-08-3357

Katayama, H., Sasai, K., Kawai, H., Yuan, Z. M., Bondaruk, J., Suzuki, F., Fujii, S., Arlinghaus, R. B., Czerniak, B. A., & Sen, S. (2004). Phosphorylation by aurora kinase A induces Mdm2-mediated destabilization and inhibition of p53. *Nat Genet*, *36*(1), 55-62. https://doi.org/10.1038/ng1279

Kawate, S., Fukusato, T., Ohwada, S., Watanuki, A., & Morishita, Y. (1999). Amplification of c-myc in hepatocellular carcinoma: correlation with clinicopathologic features, proliferative activity and p53 overexpression. *Oncology*, *57*(2), 157-163. https://doi.org/10.1159/000012024

Kawauchi, D., Robinson, G., Uziel, T., Gibson, P., Rehg, J., Gao, C., Finkelstein, D., Qu, C., Pounds, S., Ellison, D. W., Gilbertson, R. J., & Roussel, M. F. (2012). A mouse model of the most aggressive subgroup of human medulloblastoma. *Cancer Cell*, *21*(2), 168-180. https://doi.org/10.1016/j.ccr.2011.12.023

Kerres, N., Steurer, S., Schlager, S., Bader, G., Berger, H., Caligiuri, M., Dank, C., Engen, J. R., Ettmayer, P., Fischerauer, B., Flotzinger, G., Gerlach, D., Gerstberger, T., Gmaschitz, T., Greb, P., Han, B., Heyes, E., Iacob, R. E., Kessler, D., . . . Koegl, M. (2017). Chemically Induced Degradation of the Oncogenic Transcription Factor BCL6. *Cell Rep*, *20*(12), 2860-2875. https://doi.org/10.1016/j.celrep.2017.08.081

Kettenbach, A. N., Schweppe, D. K., Faherty, B. K., Pechenick, D., Pletnev, A. A., & Gerber, S. A. (2011). Quantitative phosphoproteomics identifies substrates and functional modules of Aurora and Polo-like kinase activities in mitotic cells. *Sci Signal*, *4*(179), rs5. https://doi.org/10.1126/scisignal.2001497

Kimura, M., Kotani, S., Hattori, T., Sumi, N., Yoshioka, T., Todokoro, K., & Okano, Y. (1997). Cell cycle-dependent expression and spindle pole localization of a novel human protein kinase, Aik, related to Aurora of Drosophila and yeast Ipl1. *J Biol Chem*, *272*(21), 13766-13771. https://doi.org/10.1074/jbc.272.21.13766

Kipshidze, N., Iversen, P., Overlie, P., Dunlap, T., Titus, B., Lee, D., Moses, J., O'Hanley, P., Lauer, M., & Leon, M. B. (2007). First human experience with local delivery of novel antisense AVI-4126 with Infiltrator catheter in de novo native and restenotic coronary arteries: 6-month clinical and angiographic follow-up from AVAIL study. *Cardiovasc Revasc Med*, *8*(4), 230-235. https://doi.org/10.1016/j.carrev.2007.04.002

Kistner, A., Gossen, M., Zimmermann, F., Jerecic, J., Ullmer, C., Lubbert, H., & Bujard, H. (1996). Doxycycline-mediated quantitative and tissue-specific control of gene expression in transgenic mice. *Proc Natl Acad Sci U S A*, *93*(20), 10933-10938. https://doi.org/10.1073/pnas.93.20.10933

Klaeger, S., Heinzlmeir, S., Wilhelm, M., Polzer, H., Vick, B., Koenig, P. A., Reinecke, M., Ruprecht, B., Petzoldt, S., Meng, C., Zecha, J., Reiter, K., Qiao, H., Helm, D., Koch, H., Schoof, M., Canevari, G., Casale, E., Depaolini, S. R., . . . Kuster, B. (2017). The target landscape of clinical kinase drugs. *Science*, *358*(6367). https://doi.org/10.1126/science.aan4368

Kocaturk, N. M., & Gozuacik, D. (2018). Crosstalk Between Mammalian Autophagy and the Ubiquitin-Proteasome System. *Front Cell Dev Biol*, *6*, 128. https://doi.org/10.3389/fcell.2018.00128

Koch, H. B., Zhang, R., Verdoodt, B., Bailey, A., Zhang, C. D., Yates, J. R., 3rd, Menssen, A., & Hermeking, H. (2007). Large-scale identification of c-MYC-associated proteins using a combined TAP/MudPIT approach. *Cell cycle*, *6*(2), 205-217. https://doi.org/10.4161/cc.6.2.3742

Kogita, A., Yoshioka, Y., Sakai, K., Togashi, Y., Sogabe, S., Nakai, T., Okuno, K., & Nishio, K. (2015). Inter- and intra-tumor profiling of multi-regional colon cancer and metastasis. *Biochem Biophys Res Commun*, *458*(1), 52-56. https://doi.org/10.1016/j.bbrc.2015.01.064

Kohl, N. E., Kanda, N., Schreck, R. R., Bruns, G., Latt, S. A., Gilbert, F., & Alt, F. W. (1983). Transposition and amplification of oncogene-related sequences in human neuroblastomas. *Cell*, *35*(2), 359-367. https://doi.org/10.1016/0092-8674(83)90169-1

Koopman, G., Reutelingsperger, C. P., Kuijten, G. A., Keehnen, R. M., Pals, S. T., & van Oers, M. H. (1994). Annexin V for flow cytometric detection of phosphatidylserine expression on B cells undergoing apoptosis. *Blood*, *84*(5), 1415-1420. https://doi.org/10.1182/blood.V84.5.1415.1415

Korphaisarn, K., Morris, V. K., Overman, M. J., Fogelman, D. R., Kee, B. K., Raghav, K. P. S., Manuel, S., Shureiqi, I., Wolff, R. A., Eng, C., Menter, D., Hamilton, S. R., Kopetz, S., & Dasari, A. (2017). FBXW7 missense mutation: a novel negative prognostic factor in metastatic colorectal adenocarcinoma. *Oncotarget*, *8*(24), 39268-39279. https://doi.org/10.18632/oncotarget.16848

Koscianska, E., Starega-Roslan, J., & Krzyzosiak, W. J. (2011). The role of Dicer protein partners in the processing of microRNA precursors. *PLoS One*, *6*(12), e28548. https://doi.org/10.1371/journal.pone.0028548

Kronke, J., Udeshi, N. D., Narla, A., Grauman, P., Hurst, S. N., McConkey, M., Svinkina, T., Heckl, D., Comer, E., Li, X., Ciarlo, C., Hartman, E., Munshi, N., Schenone, M., Schreiber, S. L., Carr, S. A., & Ebert, B. L. (2014). Lenalidomide causes selective degradation of IKZF1 and IKZF3 in multiple myeloma cells. *Science*, *343*(6168), 301-305. https://doi.org/10.1126/science.1244851

Landen, C. N., Jr., Lin, Y. G., Immaneni, A., Deavers, M. T., Merritt, W. M., Spannuth, W. A., Bodurka, D. C., Gershenson, D. M., Brinkley, W. R., & Sood, A. K. (2007). Overexpression of the centrosomal protein Aurora-A kinase is associated with poor prognosis in epithelial ovarian cancer patients. *Clin Cancer Res*, *13*(14), 4098-4104. https://doi.org/10.1158/1078-0432.CCR-07-0431

Langmead, B., Trapnell, C., Pop, M., & Salzberg, S. L. (2009). Ultrafast and memory-efficient alignment of short DNA sequences to the human genome. *Genome Biol*, *10*(3), R25. https://doi.org/10.1186/gb-2009-10-3-r25

Law, R. P., Nunes, J., Chung, C. W., Bantscheff, M., Buda, K., Dai, H., Evans, J. P., Flinders, A., Klimaszewska, D., Lewis, A. J., Muelbaier, M., Scott-Stevens, P., Stacey, P., Tame, C. J., Watt, G. F., Zinn, N., Queisser, M. A., Harling, J. D., & Benowitz, A. B. (2021). Discovery and Characterisation of Highly Cooperative FAK-Degrading PROTACs. *Angew Chem Int Ed Engl*, *60*(43), 23327-23334. https://doi.org/10.1002/anie.202109237

Lawlor, E. R., Soucek, L., Brown-Swigart, L., Shchors, K., Bialucha, C. U., & Evan, G. I. (2006). Reversible kinetic analysis of Myc targets in vivo provides novel insights into Myc-mediated tumorigenesis. *Cancer Res*, *66*(9), 4591-4601. https://doi.org/10.1158/0008-5472.CAN-05-3826

Lee, D. H., & Goldberg, A. L. (1998). Proteasome inhibitors: valuable new tools for cell biologists. *Trends in Cell Biology*, *8*(10), 397-403. https://doi.org/10.1016/s0962-8924(98)01346-4

Lemm, I., & Ross, J. (2002). Regulation of c-myc mRNA decay by translational pausing in a coding region instability determinant. *Mol Cell Biol*, *22*(12), 3959-3969. https://doi.org/10.1128/MCB.22.12.3959-3969.2002

Lewis, B. C., Klimstra, D. S., & Varmus, H. E. (2003). The c-myc and PyMT oncogenes induce different tumor types in a somatic mouse model for pancreatic cancer. *Genes Dev*, *17*(24), 3127-3138. https://doi.org/10.1101/gad.1140403

Li, D., Zhu, J., Firozi, P. F., Abbruzzese, J. L., Evans, D. B., Cleary, K., Friess, H., & Sen, S. (2003). Overexpression of oncogenic STK15/BTAK/Aurora A kinase in human pancreatic cancer. *Clin Cancer Res*, *9*(3), 991-997. https://www.ncbi.nlm.nih.gov/pubmed/12631597

Li, J. P., Yang, Y. X., Liu, Q. L., Pan, S. T., He, Z. X., Zhang, X., Yang, T., Chen, X. W., Wang, D., Qiu, J. X., & Zhou, S. F. (2015). The investigational Aurora kinase A inhibitor alisertib (MLN8237) induces cell cycle G2/M arrest, apoptosis, and autophagy via p38 MAPK and Akt/mTOR signaling pathways in human breast cancer cells. *Drug Des Devel Ther*, *9*, 1627-1652. https://doi.org/10.2147/DDDT.S75378

Li, K., & Crews, C. M. (2022). PROTACs: past, present and future. *Chem Soc Rev*, *51*(12), 5214-5236. https://doi.org/10.1039/d2cs00193d

Li, X., & Song, Y. (2020). Proteolysis-targeting chimera (PROTAC) for targeted protein degradation and cancer therapy. *J Hematol Oncol*, *13*(1), 50. https://doi.org/10.1186/s13045-020-00885-3

Li, Z., Wang, C., Wang, Z., Zhu, C., Li, J., Sha, T., Ma, L., Gao, C., Yang, Y., Sun, Y., Wang, J., Sun, X., Lu, C., Difiglia, M., Mei, Y., Ding, C., Luo, S., Dang, Y., Ding, Y., . . . Lu, B. (2019). Allele-selective lowering of mutant HTT protein by HTT-LC3 linker compounds. *Nature*, *575*(7781), 203-209. https://doi.org/10.1038/s41586-019-1722-1

Liao, D. J., Natarajan, G., Deming, S. L., Jamerson, M. H., Johnson, M., Chepko, G., & Dickson, R. B. (2000). Cell cycle basis for the onset and progression of c-Myc-induced, TGFalpha-enhanced mouse mammary gland carcinogenesis. *Oncogene*, *19*(10), 1307-1317. https://doi.org/10.1038/sj.onc.1203430

Lin, C. Y., Loven, J., Rahl, P. B., Paranal, R. M., Burge, C. B., Bradner, J. E., Lee, T. I., & Young, R. A. (2012). Transcriptional amplification in tumor cells with elevated c-Myc. *Cell*, *151*(1), 56-67. https://doi.org/10.1016/j.cell.2012.08.026

Lin, Y. S., Su, L. J., Yu, C. T., Wong, F. H., Yeh, H. H., Chen, S. L., Wu, J. C., Lin, W. J., Shiue, Y. L., Liu, H. S., Hsu, S. L., Lai, J. M., & Huang, C. Y. (2006). Gene expression profiles of the aurora family kinases. *Gene Expr*, *13*(1), 15-26. https://doi.org/10.3727/000000006783991962

Lindon, C., Grant, R., & Min, M. (2015). Ubiquitin-Mediated Degradation of Aurora Kinases. *Front Oncol*, *5*, 307. https://doi.org/10.3389/fonc.2015.00307

Littlepage, L. E., & Ruderman, J. V. (2002). Identification of a new APC/C recognition domain, the A box, which is required for the Cdh1-dependent destruction of the kinase Aurora-A during mitotic exit. *Genes Dev*, *16*(17), 2274-2285. https://doi.org/10.1101/gad.1007302

Liu, J., Farmer, J. D., Lane, W. S., Friedman, J., Weissman, I., & Schreiber, S. L. (1991). Calcineurin is a common target of cyclophilin-cyclosporin A and FKBP-FK506 complexes. *Cell*, *66*(4), 807-815. https://doi.org/10.1016/0092-8674(91)90124-h

Liu, Q., Kaneko, S., Yang, L., Feldman, R. I., Nicosia, S. V., Chen, J., & Cheng, J. Q. (2004). Aurora-A abrogation of p53 DNA binding and transactivation activity by phosphorylation of serine 215. *J Biol Chem*, *279*(50), 52175-52182. https://doi.org/10.1074/jbc.M406802200

Liu, Q., Wang, G., Li, Q., Jiang, W., Kim, J. S., Wang, R., Zhu, S., Wang, X., Yan, L., Yi, Y., Zhang, L., Meng, Q., Li, C., Zhao, D., Qiao, Y., Li, Y., Gursel, D. B., Chinnaiyan, A. M., Chen, K., & Cao, Q. (2019). Polycomb group proteins EZH2 and EED directly regulate androgen receptor in advanced prostate cancer. *Int J Cancer*, *145*(2), 415-426. https://doi.org/10.1002/ijc.32118

Liu, R., Li, Z., Song, E., Hu, P., Yang, Q., Hu, Y., Liu, H., & Jin, A. (2020). LncRNA HOTTIP enhances human osteogenic BMSCs differentiation via interaction with WDR5 and activation of Wnt/beta-catenin signalling pathway. *Biochem Biophys Res Commun*, *524*(4), 1037-1043. https://doi.org/10.1016/j.bbrc.2020.02.034

Liu, Z., Hu, X., Wang, Q., Wu, X., Zhang, Q., Wei, W., Su, X., He, H., Zhou, S., Hu, R., Ye, T., Zhu, Y., Wang, N., & Yu, L. (2021). Design and Synthesis of EZH2-Based PROTACs to Degrade the PRC2 Complex for Targeting the Noncatalytic Activity of EZH2. *J Med Chem*, *64*(5), 2829-2848. https://doi.org/10.1021/acs.jmedchem.0c02234

Llombart, V., & Mansour, M. R. (2022). Therapeutic targeting of "undruggable" MYC. *EBioMedicine*, *75*, 103756. https://doi.org/10.1016/j.ebiom.2021.103756

Lo Iacono, M., Monica, V., Saviozzi, S., Ceppi, P., Bracco, E., Papotti, M., & Scagliotti, G. V. (2011). Aurora Kinase A expression is associated with lung cancer histological-subtypes and with tumor de-differentiation. *J Transl Med*, *9*, 100. https://doi.org/10.1186/1479-5876-9-100

Local, A., Zhang, H., Benbatoul, K. D., Folger, P., Sheng, X., Tsai, C. Y., Howell, S. B., & Rice, W. G. (2018). APTO-253 Stabilizes G-quadruplex DNA, Inhibits MYC Expression, and Induces DNA Damage in Acute Myeloid Leukemia Cells. *Mol Cancer Ther*, *17*(6), 1177-1186. https://doi.org/10.1158/1535-7163.MCT-17-1209

Lorenzin, F., Benary, U., Baluapuri, A., Walz, S., Jung, L. A., von Eyss, B., Kisker, C., Wolf, J., Eilers, M., & Wolf, E. (2016). Different promoter affinities account for specificity in MYC-dependent gene regulation [Different promoter affinities account for specificity in MYC-dependent gene regulation]. *Elife*, *5*. https://doi.org/10.7554/eLife.15161

Lourenco, C., Resetca, D., Redel, C., Lin, P., MacDonald, A. S., Ciaccio, R., Kenney, T. M. G., Wei, Y., Andrews, D. W., Sunnerhagen, M., Arrowsmith, C. H., Raught, B., & Penn, L. Z. (2021). MYC protein interactors in gene transcription and cancer. *Nat Rev Cancer*, *21*(9), 579-591. https://doi.org/10.1038/s41568-021-00367-9

Lu, G., Middleton, R. E., Sun, H., Naniong, M., Ott, C. J., Mitsiades, C. S., Wong, K. K., Bradner, J. E., & Kaelin, W. G., Jr. (2014). The myeloma drug lenalidomide promotes the cereblon-dependent destruction of Ikaros proteins. *Science*, *343*(6168), 305-309. https://doi.org/10.1126/science.1244917

Lu, J., Qian, Y., Altieri, M., Dong, H., Wang, J., Raina, K., Hines, J., Winkler, J. D., Crew, A. P., Coleman, K., & Crews, C. M. (2015). Hijacking the E3 Ubiquitin Ligase Cereblon to Efficiently Target BRD4. *Chem Biol*, *22*(6), 755-763. https://doi.org/10.1016/j.chembiol.2015.05.009

Ma, A., Stratikopoulos, E., Park, K. S., Wei, J., Martin, T. C., Yang, X., Schwarz, M., Leshchenko, V., Rialdi, A., Dale, B., Lagana, A., Guccione, E., Parekh, S., Parsons, R., & Jin, J. (2020). Discovery of a first-in-class EZH2 selective degrader. *Nat Chem Biol*, *16*(2), 214-222. https://doi.org/10.1038/s41589-019-0421-4

Ma, M., Zhang, Y., Weng, M., Hu, Y., Xuan, Y., Hu, Y., & Lv, K. (2018). lncRNA GCAWKR Promotes Gastric Cancer Development by Scaffolding the Chromatin Modification Factors WDR5 and KAT2A. *Mol Ther*, *26*(11), 2658-2668. https://doi.org/10.1016/j.ymthe.2018.09.002

Macdonald, J. D., Chacon Simon, S., Han, C., Wang, F., Shaw, J. G., Howes, J. E., Sai, J., Yuh, J. P., Camper, D., Alicie, B. M., Alvarado, J., Nikhar, S., Payne, W., Aho, E. R., Bauer, J. A., Zhao, B., Phan, J., Thomas, L. R., Rossanese, O. W., . . . Fesik, S. W. (2019). Discovery and Optimization of Salicylic Acid-Derived Sulfonamide Inhibitors of the WD Repeat-Containing Protein 5-MYC Protein-Protein Interaction. *J Med Chem*, *62*(24), 11232-11259. https://doi.org/10.1021/acs.jmedchem.9b01411

Malempati, S., Tibbitts, D., Cunningham, M., Akkari, Y., Olson, S., Fan, G., & Sears, R. C. (2006). Aberrant stabilization of c-Myc protein in some lymphoblastic leukemias. *Leukemia*, *20*(9), 1572-1581. https://doi.org/10.1038/sj.leu.2404317

Manfredi, M. G., Ecsedy, J. A., Chakravarty, A., Silverman, L., Zhang, M., Hoar, K. M., Stroud, S. G., Chen, W., Shinde, V., Huck, J. J., Wysong, D. R., Janowick, D. A., Hyer, M. L., Leroy, P. J., Gershman, R. E., Silva, M. D., Germanos, M. S., Bolen, J. B., Claiborne, C. F., & Sells, T. B. (2011). Characterization of Alisertib (MLN8237), an investigational small-molecule inhibitor of aurora A kinase using novel in vivo pharmacodynamic assays. *Clin Cancer Res*, *17*(24), 7614-7624. https://doi.org/10.1158/1078-0432.CCR-11-1536

Maniaci, C., & Ciulli, A. (2019). Bifunctional chemical probes inducing protein-protein interactions. *Curr Opin Chem Biol*, *52*, 145-156. https://doi.org/10.1016/j.cbpa.2019.07.003

Marinkovic, D., Marinkovic, T., Mahr, B., Hess, J., & Wirth, T. (2004). Reversible lymphomagenesis in conditionally c-MYC expressing mice. *Int J Cancer*, *110*(3), 336-342. https://doi.org/10.1002/ijc.20099

Mayor-Ruiz, C., Bauer, S., Brand, M., Kozicka, Z., Siklos, M., Imrichova, H., Kaltheuner, I. H., Hahn, E., Seiler, K., Koren, A., Petzold, G., Fellner, M., Bock, C., Muller, A. C., Zuber, J., Geyer, M., Thoma, N. H., Kubicek, S., & Winter, G. E. (2020). Rational discovery of molecular glue degraders via scalable chemical profiling. *Nat Chem Biol*, *16*(11), 1199-1207. https://doi.org/10.1038/s41589-020-0594-x

Mayor-Ruiz, C., Jaeger, M. G., Bauer, S., Brand, M., Sin, C., Hanzl, A., Mueller, A. C., Menche, J., & Winter, G. E. (2019). Plasticity of the Cullin-RING Ligase Repertoire Shapes Sensitivity to Ligand-Induced Protein Degradation. *Mol Cell*, *75*(4), 849-858 e848. https://doi.org/10.1016/j.molcel.2019.07.013

Meraldi, P., Honda, R., & Nigg, E. A. (2002). Aurora-A overexpression reveals tetraploidization as a major route to centrosome amplification in p53-/- cells. *EMBO J*, *21*(4), 483-492. https://doi.org/10.1093/emboj/21.4.483

Meyer, N., & Penn, L. Z. (2008). Reflecting on 25 years with MYC. *Nat Rev Cancer*, *8*(12), 976-990. https://doi.org/10.1038/nrc2231

Miao, Y., Gao, Q., Mao, M., Zhang, C., Yang, L., Yang, Y., & Han, D. (2021). Bispecific Aptamer Chimeras Enable Targeted Protein Degradation on Cell Membranes. *Angew Chem Int Ed Engl*, *60*(20), 11267-11271. https://doi.org/10.1002/anie.202102170

Michnick, S. W., Rosen, M. K., Wandless, T. J., Karplus, M., & Schreiber, S. L. (1991). Solution structure of FKBP, a rotamase enzyme and receptor for FK506 and rapamycin. *Science*, *252*(5007), 836-839. https://doi.org/10.1126/science.1709301

Min, M., Mayor, U., & Lindon, C. (2013). Ubiquitination site preferences in anaphase promoting complex/cyclosome (APC/C) substrates. *Open Biol*, *3*(9), 130097. https://doi.org/10.1098/rsob.130097

Min, Z., Xunlei, Z., Haizhen, C., Wenjing, Z., Haiyan, Y., Xiaoyun, L., Jianyun, Z., Xudong, C., & Aiguo, S. (2021). The Clinicopathologic and Prognostic Significance of c-Myc Expression in Hepatocellular Carcinoma: A Meta-Analysis. *Frontiers in Bioinformatics*, *1*. https://doi.org/10.3389/fbinf.2021.706835

Molecular Operating Environment (MOE). (2019). In. 1010 Sherbrooke St. West, Suite #910, Montreal, QC, Canada, H3A 2R7: Chemical Computing Group ULC.

Mollaoglu, G., Guthrie, M. R., Bohm, S., Bragelmann, J., Can, I., Ballieu, P. M., Marx, A., George, J., Heinen, C., Chalishazar, M. D., Cheng, H., Ireland, A. S., Denning, K. E., Mukhopadhyay, A., Vahrenkamp, J. M., Berrett, K. C., Mosbruger, T. L., Wang, J., Kohan, J. L., . . . Oliver, T. G. (2017). MYC Drives Progression of Small Cell Lung Cancer to a Variant Neuroendocrine Subtype with Vulnerability to Aurora Kinase Inhibition. *Cancer Cell*, *31*(2), 270-285. https://doi.org/10.1016/j.ccell.2016.12.005

Mosse, Y. P., Fox, E., Teachey, D. T., Reid, J. M., Safgren, S. L., Carol, H., Lock, R. B., Houghton, P. J., Smith, M. A., Hall, D., Barkauskas, D. A., Krailo, M., Voss, S. D., Berg, S. L., Blaney, S. M., & Weigel, B. J. (2019). A Phase II Study of Alisertib in Children with Recurrent/Refractory Solid Tumors or Leukemia: Children's Oncology Group Phase I and Pilot Consortium (ADVL0921). *Clinical Cancer Research*, *25*(11), 3229-3238. https://doi.org/10.1158/1078-0432.Ccr-18-2675

Muncan, V., Sansom, O. J., Tertoolen, L., Phesse, T. J., Begthel, H., Sancho, E., Cole, A. M., Gregorieff, A., de Alboran, I. M., Clevers, H., & Clarke, A. R. (2006). Rapid loss of intestinal crypts upon conditional deletion of the Wnt/Tcf-4 target gene c-Myc. *Mol Cell Biol*, *26*(22), 8418-8426. https://doi.org/10.1128/MCB.00821-06

Nair, S. K., & Burley, S. K. (2003). X-Ray Structures of Myc-Max and Mad-Max Recognizing DNA. *Cell*, *112*(2), 193-205. https://doi.org/10.1016/s0092-8674(02)01284-9

Nau, M. M., Brooks, B. J., Battey, J., Sausville, E., Gazdar, A. F., Kirsch, I. R., McBride, O. W., Bertness, V., Hollis, G. F., & Minna, J. D. (1985). L-myc, a new myc-related gene amplified and expressed in human small cell lung cancer. *Nature*, *318*(6041), 69-73. https://doi.org/10.1038/318069a0

Neilsen, B. K., Chakraborty, B., McCall, J. L., Frodyma, D. E., Sleightholm, R. L., Fisher, K. W., & Lewis, R. E. (2018). WDR5 supports colon cancer cells by promoting methylation of

H3K4 and suppressing DNA damage. *BMC Cancer*, *18*(1), 673. https://doi.org/10.1186/s12885-018-4580-6

Ni, D., Lu, S., & Zhang, J. (2019). Emerging roles of allosteric modulators in the regulation of protein-protein interactions (PPIs): A new paradigm for PPI drug discovery. *Med Res Rev*, *39*(6), 2314-2342. https://doi.org/10.1002/med.21585

Nie, Z., Guo, C., Das, S. K., Chow, C. C., Batchelor, E., Simons, S. S. J., & Levens, D. (2020). Dissecting transcriptional amplification by MYC. *Elife*, *9*. https://doi.org/10.7554/eLife.52483

Nie, Z., Hu, G., Wei, G., Cui, K., Yamane, A., Resch, W., Wang, R., Green, D. R., Tessarollo, L., Casellas, R., Zhao, K., & Levens, D. (2012). c-Myc is a universal amplifier of expressed genes in lymphocytes and embryonic stem cells. *Cell*, *151*(1), 68-79. https://doi.org/10.1016/j.cell.2012.08.033

Nikiforov, M. A., Chandriani, S., Park, J., Kotenko, I., Matheos, D., Johnsson, A., McMahon, S. B., & Cole, M. D. (2002). TRRAP-dependent and TRRAP-independent transcriptional activation by Myc family oncoproteins. *Mol Cell Biol*, *22*(14), 5054-5063. https://doi.org/10.1128/MCB.22.14.5054-5063.2002

Northcott, P. A., Korshunov, A., Witt, H., Hielscher, T., Eberhart, C. G., Mack, S., Bouffet, E., Clifford, S. C., Hawkins, C. E., French, P., Rutka, J. T., Pfister, S., & Taylor, M. D. (2011). Medulloblastoma comprises four distinct molecular variants. *J Clin Oncol*, *29*(11), 1408-1414. https://doi.org/10.1200/JCO.2009.27.4324

O'Brien, J., Wilson, I., Orton, T., & Pognan, F. (2000). Investigation of the Alamar Blue (resazurin) fluorescent dye for the assessment of mammalian cell cytotoxicity. *Eur J Biochem*, *267*(17), 5421-5426. https://doi.org/10.1046/j.1432-1327.2000.01606.x

O'Connor, O. A., Ozcan, M., Jacobsen, E. D., Roncero, J. M., Trotman, J., Demeter, J., Masszi, T., Pereira, J., Ramchandren, R., Beaven, A., Caballero, D., Horwitz, S. M., Lennard, A., Turgut, M., Hamerschlak, N., d'Amore, F. A., Foss, F., Kim, W. S., Leonard, J. P., . . . Lumiere Study, I. (2019). Randomized Phase III Study of Alisertib or Investigator's Choice (Selected Single Agent) in Patients With Relapsed or Refractory Peripheral T-Cell Lymphoma. *J Clin Oncol*, *37*(8), 613-623. https://doi.org/10.1200/JCO.18.00899

O'Neil, J., Grim, J., Strack, P., Rao, S., Tibbitts, D., Winter, C., Hardwick, J., Welcker, M., Meijerink, J. P., Pieters, R., Draetta, G., Sears, R., Clurman, B. E., & Look, A. T. (2007). FBW7 mutations in leukemic cells mediate NOTCH pathway activation and resistance to gamma-secretase inhibitors. *J Exp Med*, *204*(8), 1813-1824. https://doi.org/10.1084/jem.20070876

O'Shaughnessy, J., McIntyre, K., Wilks, S., Ma, L., Block, M., Andorsky, D., Danso, M., Locke, T., Scales, A., & Wang, Y. (2021). Efficacy and Safety of Weekly Paclitaxel With or Without Oral Alisertib in Patients With Metastatic Breast Cancer: A Randomized Clinical Trial. *JAMA Netw Open*, *4*(4), e214103. https://doi.org/10.1001/jamanetworkopen.2021.4103

Ochi, T., Fujiwara, H., Suemori, K., Azuma, T., Yakushijin, Y., Hato, T., Kuzushima, K., & Yasukawa, M. (2009). Aurora-A kinase: a novel target of cellular immunotherapy for leukemia. *Blood*, *113*(1), 66-74. https://doi.org/10.1182/blood-2008-06-164889

Odho, Z., Southall, S. M., & Wilson, J. R. (2010). Characterization of a novel WDR5-binding site that recruits RbBP5 through a conserved motif to enhance methylation of histone H3 lysine 4 by mixed lineage leukemia protein-1. *J Biol Chem*, *285*(43), 32967-32976. https://doi.org/10.1074/jbc.M110.159921

Ohanian, M., Rozovski, U., Kanagal-Shamanna, R., Abruzzo, L. V., Loghavi, S., Kadia, T., Futreal, A., Bhalla, K., Zuo, Z., Huh, Y. O., Post, S. M., Ruvolo, P., Garcia-Manero, G., Andreeff, M., Kornblau, S., Borthakur, G., Hu, P., Medeiros, L. J., Takahashi, K., . . . Cortes, J. E. (2019). MYC protein expression is an important prognostic factor in acute myeloid leukemia. *Leuk Lymphoma*, *60*(1), 37-48. https://doi.org/10.1080/10428194.2018.1464158

Otte, J., Dyberg, C., Pepich, A., & Johnsen, J. I. (2020). MYCN Function in Neuroblastoma Development. *Front Oncol*, *10*, 624079. https://doi.org/10.3389/fonc.2020.624079

Otto, T., Horn, S., Brockmann, M., Eilers, U., Schuttrumpf, L., Popov, N., Kenney, A. M., Schulte, J. H., Beijersbergen, R., Christiansen, H., Berwanger, B., & Eilers, M. (2009). Stabilization of N-Myc is a critical function of Aurora A in human neuroblastoma. *Cancer Cell*, *15*(1), 67-78. https://doi.org/10.1016/j.ccr.2008.12.005

Papadopoulos, D., Solvie, D., Baluapuri, A., Endres, T., Ha, S. A., Herold, S., Kalb, J., Giansanti, C., Schulein-Volk, C., Ade, C. P., Schneider, C., Gaballa, A., Vos, S.,

Fischer, U., Dobbelstein, M., Wolf, E., & Eilers, M. (2022). MYCN recruits the nuclear exosome complex to RNA polymerase II to prevent transcription-replication conflicts. *Mol Cell*, *82*(1), 159-176 e112. https://doi.org/10.1016/j.molcel.2021.11.002

Park, S. S., Kim, J. S., Tessarollo, L., Owens, J. D., Peng, L., Han, S. S., Tae Chung, S., Torrey, T. A., Cheung, W. C., Polakiewicz, R. D., McNeil, N., Ried, T., Mushinski, J. F., Morse, H. C., 3rd, & Janz, S. (2005). Insertion of c-Myc into Igh induces B-cell and plasma-cell neoplasms in mice. *Cancer Res*, *65*(4), 1306-1315. https://doi.org/10.1158/0008-5472.CAN-04-0268

Patel, A., Dharmarajan, V., & Cosgrove, M. S. (2008). Structure of WDR5 bound to mixed lineage leukemia protein-1 peptide. *J Biol Chem*, *283*(47), 32158-32161. https://doi.org/10.1074/jbc.C800164200

Pekowska, A., Benoukraf, T., Zacarias-Cabeza, J., Belhocine, M., Koch, F., Holota, H., Imbert, J., Andrau, J. C., Ferrier, P., & Spicuglia, S. (2011). H3K4 tri-methylation provides an epigenetic signature of active enhancers. *EMBO J*, *30*(20), 4198-4210. https://doi.org/10.1038/emboj.2011.295

Pelengaris, S., Khan, M., & Evan, G. I. (2002). Suppression of Myc-Induced Apoptosis in β Cells Exposes Multiple Oncogenic Properties of Myc and Triggers Carcinogenic Progression. *Cell*, *109*(3), 321-334. https://doi.org/10.1016/s0092-8674(02)00738-9

Pelengaris, S., Littlewood, T., Khan, M., Elia, G., & Evan, G. (1999). Reversible Activation of c-Myc in Skin. *Molecular Cell*, *3*(5), 565-577. https://doi.org/10.1016/s1097-2765(00)80350-0

Pettersson, M., & Crews, C. M. (2019). PROteolysis TArgeting Chimeras (PROTACs) - Past, present and future. *Drug Discov Today Technol*, *31*, 15-27. https://doi.org/10.1016/j.ddtec.2019.01.002

Pineda-Lucena, A., Ho, C. S., Mao, D. Y., Sheng, Y., Laister, R. C., Muhandiram, R., Lu, Y., Seet, B. T., Katz, S., Szyperski, T., Penn, L. Z., & Arrowsmith, C. H. (2005). A structure-based model of the c-Myc/Bin1 protein interaction shows alternative splicing of Bin1 and c-Myc phosphorylation are key binding determinants. *J Mol Biol*, *351*(1), 182-194. https://doi.org/10.1016/j.jmb.2005.05.046

Pinskaya, M., & Morillon, A. (2009). Histone H3 lysine 4 di-methylation: a novel mark for transcriptional fidelity? *Epigenetics*, *4*(5), 302-306. https://doi.org/10.4161/epi.4.5.9369

Postel-Vinay, S., Herbschleb, K., Massard, C., Woodcock, V., Soria, J. C., Walter, A. O., Ewerton, F., Poelman, M., Benson, N., Ocker, M., Wilkinson, G., & Middleton, M. (2019). First-in-human phase I study of the bromodomain and extraterminal motif inhibitor BAY 1238097: emerging pharmacokinetic/pharmacodynamic relationship and early termination due to unexpected toxicity. *Eur J Cancer*, *109*, 103-110. https://doi.org/10.1016/j.ejca.2018.12.020

Potjewyd, F., Turner, A. W., Beri, J., Rectenwald, J. M., Norris-Drouin, J. L., Cholensky, S. H., Margolis, D. M., Pearce, K. H., Herring, L. E., & James, L. I. (2020). Degradation of Polycomb Repressive Complex 2 with an EED-Targeted Bivalent Chemical Degrader. *Cell Chem Biol*, *27*(1), 47-56 e15. https://doi.org/10.1016/j.chembiol.2019.11.006

Puig-Butille, J. A., Vinyals, A., Ferreres, J. R., Aguilera, P., Cabre, E., Tell-Marti, G., Marcoval, J., Mateo, F., Palomero, L., Badenas, C., Piulats, J. M., Malvehy, J., Pujana, M. A., Puig, S., & Fabra, A. (2017). AURKA Overexpression Is Driven by FOXM1 and MAPK/ERK Activation in Melanoma Cells Harboring BRAF or NRAS Mutations: Impact on Melanoma Prognosis and Therapy. *J Invest Dermatol*, *137*(6), 1297-1310. https://doi.org/10.1016/j.jid.2017.01.021

Punzi, S., Balestrieri, C., D'Alesio, C., Bossi, D., Dellino, G. I., Gatti, E., Pruneri, G., Criscitiello, C., Lovati, G., Meliksetyan, M., Carugo, A., Curigliano, G., Natoli, G., Pelicci, P. G., & Lanfrancone, L. (2019). WDR5 inhibition halts metastasis dissemination by repressing the mesenchymal phenotype of breast cancer cells. *Breast Cancer Res*, *21*(1), 123. https://doi.org/10.1186/s13058-019-1216-y

Rannou, Y., Troadec, M. B., Petretti, C., Hans, F., Dutertre, S., Dimitrov, S., & Prigent, C. (2008). Localization of aurora A and aurora B kinases during interphase: role of the N-terminal domain. *Cell cycle*, *7*(19), 3012-3020. https://doi.org/10.4161/cc.7.19.6718

Richards, M. W., Burgess, S. G., Poon, E., Carstensen, A., Eilers, M., Chesler, L., & Bayliss, R. (2016). Structural basis of N-Myc binding by Aurora-A and its destabilization by kinase inhibitors. *Proc Natl Acad Sci U S A*, *113*(48), 13726-13731. https://doi.org/10.1073/pnas.1610626113

Rickman, D. S., Schulte, J. H., & Eilers, M. (2018). The Expanding World of N-MYC-Driven Tumors. *Cancer Discov*, *8*(2), 150-163. https://doi.org/10.1158/2159-8290.CD-17-0273

Rishfi, M., Krols, S., Martens, F., Sanders, E., Eggermont, A., De Vloed, F., Goulding, J. R., Risseeuw, M., Molenaar, J., Speleman, F., De wilde, B., Van Calenbergh, S., & Durinck, K. (2022). Targeted AURKA degradation: towards new therapeutic agents for neuroblastoma. *ChemRxiv*. https://doi.org/10.26434/chemrxiv-2022-c7lzr

Robinson, M. D., McCarthy, D. J., & Smyth, G. K. (2010). edgeR: a Bioconductor package for differential expression analysis of digital gene expression data. *Bioinformatics*, *26*(1), 139-140. https://doi.org/10.1093/bioinformatics/btp616

Rochlitz, C. F., Herrmann, R., & de Kant, E. (1996). Overexpression and amplification of c-myc during progression of human colorectal cancer. *Oncology*, *53*(6), 448-454. https://doi.org/10.1159/000227619

Roeschert, I., Poon, E., Henssen, A. G., Dorado Garcia, H., Gatti, M., Giansanti, C., Jamin, Y., Ade, C. P., Gallant, P., Schülein-Völk, C., Beli, P., Richards, M., Rosenfeldt, M., Altmeyer, M., Anderson, J., Eggert, A., Dobbelstein, M., Bayliss, R., Chesler, L., . . . Eilers, M. (2021). Combined inhibition of Aurora-A and ATR kinases results in regression of MYCN-amplified neuroblastoma. *Nature Cancer*, *2*(3), 312-326. https://doi.org/10.1038/s43018-020-00171-8

Roeschert, I., Poon, E., Henssen, A. G., Garcia, H. D., Gatti, M., Giansanti, C., Jamin, Y., Ade, C. P., Gallant, P., Schulein-Volk, C., Beli, P., Richards, M., Rosenfeldt, M., Altmeyer, M., Anderson, J., Eggert, A., Dobbelstein, M., Bayliss, R., Chesler, L., . . . Eilers, M. (2021). Combined inhibition of Aurora-A and ATR kinase results in regression of MYCN-amplified neuroblastoma. *Nat Cancer*, *2*(3), 312-326. https://doi.org/10.1038/s43018-020-00171-8

Roussel, M. F., & Robinson, G. W. (2013). Role of MYC in Medulloblastoma. *Cold Spring Harb Perspect Med*, *3*(11). https://doi.org/10.1101/cshperspect.a014308

Roy, M. J., Winkler, S., Hughes, S. J., Whitworth, C., Galant, M., Farnaby, W., Rumpel, K., & Ciulli, A. (2019). SPR-Measured Dissociation Kinetics of PROTAC Ternary Complexes Influence Target Degradation Rate. *ACS Chem Biol*, *14*(3), 361-368. https://doi.org/10.1021/acschembio.9b00092

Sabo, A., Kress, T. R., Pelizzola, M., de Pretis, S., Gorski, M. M., Tesi, A., Morelli, M. J., Bora, P., Doni, M., Verrecchia, A., Tonelli, C., Faga, G., Bianchi, V., Ronchi, A., Low, D., Muller, H., Guccione, E., Campaner, S., & Amati, B. (2014). Selective transcriptional regulation by Myc in cellular growth control and lymphomagenesis. *Nature*, *511*(7510), 488-492. https://doi.org/10.1038/nature13537

Sakamoto, K. M., Kim, K. B., Kumagai, A., Mercurio, F., Crews, C. M., & Deshaies, R. J. (2001). Protacs: chimeric molecules that target proteins to the Skp1-Cullin-F box complex for ubiquitination and degradation. *Proc Natl Acad Sci U S A*, *98*(15), 8554-8559. https://doi.org/10.1073/pnas.141230798

Sakamoto, K. M., Kim, K. B., Verma, R., Ransick, A., Stein, B., Crews, C. M., & Deshaies, R. J. (2003). Development of Protacs to target cancer-promoting proteins for ubiquitination and degradation. *Mol Cell Proteomics*, *2*(12), 1350-1358. https://doi.org/10.1074/mcp.T300009-MCP200

Sala, A. J., Bott, L. C., & Morimoto, R. I. (2017). Shaping proteostasis at the cellular, tissue, and organismal level. *J Cell Biol*, *216*(5), 1231-1241. https://doi.org/10.1083/jcb.201612111

Schaub, F. X., Dhankani, V., Berger, A. C., Trivedi, M., Richardson, A. B., Shaw, R., Zhao, W., Zhang, X., Ventura, A., Liu, Y., Ayer, D. E., Hurlin, P. J., Cherniack, A. D., Eisenman, R. N., Bernard, B., Grandori, C., & Cancer Genome Atlas, N. (2018). Pan-cancer Alterations of the MYC Oncogene and Its Proximal Network across the Cancer Genome Atlas. *Cell Syst*, *6*(3), 282-300 e282. https://doi.org/10.1016/j.cels.2018.03.003

Schlaeger, C., Longerich, T., Schiller, C., Bewerunge, P., Mehrabi, A., Toedt, G., Kleeff, J., Ehemann, V., Eils, R., Lichter, P., Schirmacher, P., & Radlwimmer, B. (2008). Etiology-dependent molecular mechanisms in human hepatocarcinogenesis. *Hepatology*, *47*(2), 511-520. https://doi.org/10.1002/hep.22033

Schneekloth, A. R., Pucheault, M., Tae, H. S., & Crews, C. M. (2008). Targeted intracellular protein degradation induced by a small molecule: En route to chemical proteomics. *Bioorg Med Chem Lett*, *18*(22), 5904-5908. https://doi.org/10.1016/j.bmcl.2008.07.114

Schneider-Poetsch, T., Ju, J., Eyler, D. E., Dang, Y., Bhat, S., Merrick, W. C., Green, R., Shen, B., & Liu, J. O. (2010). Inhibition of eukaryotic translation elongation by cycloheximide and lactimidomycin. *Nat Chem Biol*, *6*(3), 209-217. https://doi.org/10.1038/nchembio.304

Schoenenberger, C. A., Andres, A. C., Groner, B., van der Valk, M., LeMeur, M., & Gerlinger, P. (1988). Targeted c-myc gene expression in mammary glands of transgenic mice induces mammary tumours with constitutive milk protein gene transcription. *EMBO J*, *7*(1), 169-175. https://doi.org/10.1002/j.1460-2075.1988.tb02797.x

Scholes, N. S., Mayor-Ruiz, C., & Winter, G. E. (2021). Identification and selectivity profiling of small-molecule degraders via multi-omics approaches. *Cell Chem Biol*, *28*(7), 1048-1060. https://doi.org/10.1016/j.chembiol.2021.03.007

Scholz, N., Kurian, K. M., Siebzehnrubl, F. A., & Licchesi, J. D. F. (2020). Targeting the Ubiquitin System in Glioblastoma. *Front Oncol*, *10*, 574011. https://doi.org/10.3389/fonc.2020.574011

Schonig, K., & Bujard, H. (2003). Generating conditional mouse mutants via tetracycline-controlled gene expression. *Methods Mol Biol*, *209*, 69-104. https://doi.org/10.1385/1-59259-340-2:69

Schreiber, S. L. (1992). Immunophilin-sensitive protein phosphatase action in cell signaling pathways. *Cell*, *70*(3), 365-368. https://doi.org/10.1016/0092-8674(92)90158-9

Schuetz, A., Allali-Hassani, A., Martin, F., Loppnau, P., Vedadi, M., Bochkarev, A., Plotnikov, A. N., Arrowsmith, C. H., & Min, J. (2006). Structural basis for molecular recognition and presentation of histone H3 by WDR5. *EMBO J*, *25*(18), 4245-4252. https://doi.org/10.1038/sj.emboj.7601316

Schwab, M., Alitalo, K., Klempnauer, K. H., Varmus, H. E., Bishop, J. M., Gilbert, F., Brodeur, G., Goldstein, M., & Trent, J. (1983). Amplified DNA with limited homology to myc cellular oncogene is shared by human neuroblastoma cell lines and a neuroblastoma tumour. *Nature*, *305*(5931), 245-248. https://doi.org/10.1038/305245a0

Schwinn, M. K., Machleidt, T., Zimmerman, K., Eggers, C. T., Dixon, A. S., Hurst, R., Hall, M. P., Encell, L. P., Binkowski, B. F., & Wood, K. V. (2018). CRISPR-Mediated Tagging of Endogenous Proteins with a Luminescent Peptide. *ACS Chem Biol*, *13*(2), 467-474. https://doi.org/10.1021/acschembio.7b00549

Sells, T. B., Chau, R., Ecsedy, J. A., Gershman, R. E., Hoar, K., Huck, J., Janowick, D. A., Kadambi, V. J., LeRoy, P. J., Stirling, M., Stroud, S. G., Vos, T. J., Weatherhead, G. S., Wysong, D. R., Zhang, M., Balani, S. K., Bolen, J. B., Manfredi, M. G., & Claiborne, C. F. (2015). MLN8054 and Alisertib (MLN8237): Discovery of Selective Oral Aurora A Inhibitors. *ACS Med Chem Lett*, *6*(6), 630-634. https://doi.org/10.1021/ml500409n

Shachaf, C. M., Kopelman, A. M., Arvanitis, C., Karlsson, A., Beer, S., Mandl, S., Bachmann, M. H., Borowsky, A. D., Ruebner, B., Cardiff, R. D., Yang, Q., Bishop, J. M., Contag, C. H., & Felsher, D. W. (2004). MYC inactivation uncovers pluripotent differentiation and tumour dormancy in hepatocellular cancer. *Nature*, *431*(7012), 1112-1117. https://doi.org/10.1038/nature03043

Shao, Q., Kannan, A., Lin, Z., Stack, B. C., Jr., Suen, J. Y., & Gao, L. (2014). BET protein inhibitor JQ1 attenuates Myc-amplified MCC tumor growth in vivo. *Cancer Res*, *74*(23), 7090-7102. https://doi.org/10.1158/0008-5472.CAN-14-0305

Sheiness, D., Fanshier, L., & Bishop, J. M. (1978). Identification of nucleotide sequences which may encode the oncogenic capacity of avian retrovirus MC29. *J Virol*, *28*(2), 600-610. https://doi.org/10.1128/JVI.28.2.600-610.1978

Shen, Y., Gao, G., Yu, X., Kim, H., Wang, L., Xie, L., Schwarz, M., Chen, X., Guccione, E., Liu, J., Bedford, M. T., & Jin, J. (2020). Discovery of First-in-Class Protein Arginine Methyltransferase 5 (PRMT5) Degraders. *J Med Chem*, *63*(17), 9977-9989. https://doi.org/10.1021/acs.jmedchem.0c01111

Shiao, Y. H., Forsti, A., Egevad, L., Anderson, L. M., Lindblad, P., & Hemminki, K. (2003). VHL down-regulation and differential localization as mechanisms in tumorigenesis. *Kidney Int*, *64*(5), 1671-1674. https://doi.org/10.1046/j.1523-1755.2003.00257.x

Shirasaki, R., Matthews, G. M., Gandolfi, S., de Matos Simoes, R., Buckley, D. L., Raja Vora, J., Sievers, Q. L., Bruggenthies, J. B., Dashevsky, O., Poarch, H., Tang, H., Bariteau, M. A., Sheffer, M., Hu, Y., Downey-Kopyscinski, S. L., Hengeveld, P. J., Glassner, B. J., Dhimolea, E., Ott, C. J., . . . Mitsiades, C. S. (2021). Functional Genomics Identify Distinct and Overlapping Genes Mediating Resistance to Different Classes of

Heterobifunctional Degraders of Oncoproteins. *Cell Rep*, *34*(1), 108532. https://doi.org/10.1016/j.celrep.2020.108532

Shroff, E. H., Eberlin, L. S., Dang, V. M., Gouw, A. M., Gabay, M., Adam, S. J., Bellovin, D. I., Tran, P. T., Philbrick, W. M., Garcia-Ocana, A., Casey, S. C., Li, Y., Dang, C. V., Zare, R. N., & Felsher, D. W. (2015). MYC oncogene overexpression drives renal cell carcinoma in a mouse model through glutamine metabolism. *Proc Natl Acad Sci U S A*, *112*(21), 6539-6544. https://doi.org/10.1073/pnas.1507228112

Sikora, K., Chan, S., Evan, G., Gabra, H., Markham, N., Stewart, J., & Watson, J. (1987). c-myc oncogene expression in colorectal cancer. *Cancer*, *59*(7), 1289-1295. https://doi.org/10.1002/1097-0142(19870401)59:7<1289::Aid-cncr2820590710>3.0.Co;2-o

Siladi, A. J., Wang, J., Florian, A. C., Thomas, L. R., Creighton, J. H., Matlock, B. K., Flaherty, D. K., Lorey, S. L., Howard, G. C., Fesik, S. W., Weissmiller, A. M., Liu, Q., & Tansey, W. P. (2022). WIN site inhibition disrupts a subset of WDR5 function. *Sci Rep*, *12*(1), 1848. https://doi.org/10.1038/s41598-022-05947-9

Simonetta, K. R., Taygerly, J., Boyle, K., Basham, S. E., Padovani, C., Lou, Y., Cummins, T. J., Yung, S. L., von Soly, S. K., Kayser, F., Kuriyan, J., Rape, M., Cardozo, M., Gallop, M. A., Bence, N. F., Barsanti, P. A., & Saha, A. (2019). Prospective discovery of small molecule enhancers of an E3 ligase-substrate interaction. *Nat Commun*, *10*(1), 1402. https://doi.org/10.1038/s41467-019-09358-9

Simpson, L. M., Glennie, L., Brewer, A., Zhao, J. F., Crooks, J., Shpiro, N., & Sapkota, G. P. (2022). Target protein localization and its impact on PROTAC-mediated degradation. *Cell Chem Biol*, *29*(10), 1482-1504 e1487. https://doi.org/10.1016/j.chembiol.2022.08.004

Slabicki, M., Kozicka, Z., Petzold, G., Li, Y. D., Manojkumar, M., Bunker, R. D., Donovan, K. A., Sievers, Q. L., Koeppel, J., Suchyta, D., Sperling, A. S., Fink, E. C., Gasser, J. A., Wang, L. R., Corsello, S. M., Sellar, R. S., Jan, M., Gillingham, D., Scholl, C., . . . Ebert, B. L. (2020). The CDK inhibitor CR8 acts as a molecular glue degrader that depletes cyclin K. *Nature*, *585*(7824), 293-297. https://doi.org/10.1038/s41586-020-2374-x

Slabicki, M., Yoon, H., Koeppel, J., Nitsch, L., Roy Burman, S. S., Di Genua, C., Donovan, K. A., Sperling, A. S., Hunkeler, M., Tsai, J. M., Sharma, R., Guirguis, A., Zou, C., Chudasama, P., Gasser, J. A., Miller, P. G., Scholl, C., Frohling, S., Nowak, R. P., . . . Ebert, B. L. (2020). Small-molecule-induced polymerization triggers degradation of BCL6. *Nature*, *588*(7836), 164-168. https://doi.org/10.1038/s41586-020-2925-1

Sloane, D. A., Trikic, M. Z., Chu, M. L., Lamers, M. B., Mason, C. S., Mueller, I., Savory, W. J., Williams, D. H., & Eyers, P. A. (2010). Drug-resistant aurora A mutants for cellular target validation of the small molecule kinase inhibitors MLN8054 and MLN8237. *ACS Chem Biol*, *5*(6), 563-576. https://doi.org/10.1021/cb100053q

Smith, B. E., Wang, S. L., Jaime-Figueroa, S., Harbin, A., Wang, J., Hamman, B. D., & Crews, C. M. (2019). Differential PROTAC substrate specificity dictated by orientation of recruited E3 ligase. *Nat Commun*, *10*(1), 131. https://doi.org/10.1038/s41467-018-08027-7

Smith, D. R., Myint, T., & Goh, H. S. (1993). Over-expression of the c-myc proto-oncogene in colorectal carcinoma. *Br J Cancer*, *68*(2), 407-413. https://doi.org/10.1038/bjc.1993.350

Soares, L. M., He, P. C., Chun, Y., Suh, H., Kim, T., & Buratowski, S. (2017). Determinants of Histone H3K4 Methylation Patterns. *Mol Cell*, *68*(4), 773-785 e776. https://doi.org/10.1016/j.molcel.2017.10.013

Sodir, N. M., Kortlever, R. M., Barthet, V. J. A., Campos, T., Pellegrinet, L., Kupczak, S., Anastasiou, P., Swigart, L. B., Soucek, L., Arends, M. J., Littlewood, T. D., & Evan, G. I. (2020). MYC Instructs and Maintains Pancreatic Adenocarcinoma Phenotype. *Cancer Discov*, *10*(4), 588-607. https://doi.org/10.1158/2159-8290.CD-19-0435

Sodir, N. M., Swigart, L. B., Karnezis, A. N., Hanahan, D., Evan, G. I., & Soucek, L. (2011). Endogenous Myc maintains the tumor microenvironment. *Genes Dev*, *25*(9), 907-916. https://doi.org/10.1101/gad.2038411

Song, J. J., & Kingston, R. E. (2008). WDR5 interacts with mixed lineage leukemia (MLL) protein via the histone H3-binding pocket. *J Biol Chem*, *283*(50), 35258-35264. https://doi.org/10.1074/jbc.M806900200

Sos, M. L., Dietlein, F., Peifer, M., Schottle, J., Balke-Want, H., Muller, C., Koker, M., Richters, A., Heynck, S., Malchers, F., Heuckmann, J. M., Seidel, D., Eyers, P. A., Ullrich, R. T.,

Antonchick, A. P., Vintonyak, V. V., Schneider, P. M., Ninomiya, T., Waldmann, H., . . . Thomas, R. K. (2012). A framework for identification of actionable cancer genome dependencies in small cell lung cancer. *Proc Natl Acad Sci U S A*, *109*(42), 17034-17039. https://doi.org/10.1073/pnas.1207310109

Soucek, L., Helmer-Citterich, M., Sacco, A., Jucker, R., Cesareni, G., & Nasi, S. (1998). Design and properties of a Myc derivative that efficiently homodimerizes. *Oncogene*, *17*(19), 2463-2472. https://doi.org/10.1038/sj.onc.1202199

Soucek, L., Jucker, R., Panacchia, L., Ricordy, R., Tato, F., & Nasi, S. (2002). Omomyc, a potential Myc dominant negative, enhances Myc-induced apoptosis. *Cancer Res*, *62*(12), 3507-3510. https://www.ncbi.nlm.nih.gov/pubmed/12067996

Soucek, L., Nasi, S., & Evan, G. I. (2004). Omomyc expression in skin prevents Myc-induced papillomatosis. *Cell Death Differ*, *11*(9), 1038-1045. https://doi.org/10.1038/sj.cdd.4401443

Soucek, L., Whitfield, J., Martins, C. P., Finch, A. J., Murphy, D. J., Sodir, N. M., Karnezis, A. N., Swigart, L. B., Nasi, S., & Evan, G. I. (2008). Modelling Myc inhibition as a cancer therapy. *Nature*, *455*(7213), 679-683. https://doi.org/10.1038/nature07260

Soucek, L., Whitfield, J. R., Sodir, N. M., Masso-Valles, D., Serrano, E., Karnezis, A. N., Swigart, L. B., & Evan, G. I. (2013). Inhibition of Myc family proteins eradicates KRas-driven lung cancer in mice. *Genes Dev*, *27*(5), 504-513. https://doi.org/10.1101/gad.205542.112

Soucy, T. A., Smith, P. G., Milhollen, M. A., Berger, A. J., Gavin, J. M., Adhikari, S., Brownell, J. E., Burke, K. E., Cardin, D. P., Critchley, S., Cullis, C. A., Doucette, A., Garnsey, J. J., Gaulin, J. L., Gershman, R. E., Lublinsky, A. R., McDonald, A., Mizutani, H., Narayanan, U., . . . Langston, S. P. (2009). An inhibitor of NEDD8-activating enzyme as a new approach to treat cancer. *Nature*, *458*(7239), 732-736. https://doi.org/10.1038/nature07884

Soucy, T. A., Smith, P. G., & Rolfe, M. (2009). Targeting NEDD8-activated cullin-RING ligases for the treatment of cancer. *Clin Cancer Res*, *15*(12), 3912-3916. https://doi.org/10.1158/1078-0432.CCR-09-0343

Staff, S., Isola, J., Jumppanen, M., & Tanner, M. (2009). Aurora-A gene is frequently amplified in basal-like breast cancer. *Oncology Reports*, *23*(2). https://doi.org/10.3892/or_00000637

Stewart, M., Cameron, E., Campbell, M., McFarlane, R., Toth, S., Lang, K., Onions, D., & Neil, J. C. (1993). Conditional expression and oncogenicity of c-myc linked to a CD2 gene dominant control region. *Int J Cancer*, *53*(6), 1023-1030. https://doi.org/10.1002/ijc.2910530628

Stewart, M. D., Ritterhoff, T., Klevit, R. E., & Brzovic, P. S. (2016). E2 enzymes: more than just middle men. *Cell Res*, *26*(4), 423-440. https://doi.org/10.1038/cr.2016.35

Stewart, S., & Fang, G. (2005). Destruction box-dependent degradation of aurora B is mediated by the anaphase-promoting complex/cyclosome and Cdh1. *Cancer Res*, *65*(19), 8730-8735. https://doi.org/10.1158/0008-5472.CAN-05-1500

Stewart, T. A., Pattengale, P. K., & Leder, P. (1984). Spontaneous mammary adenocarcinomas in transgenic mice that carry and express MTV/myc fusion genes. *Cell*, *38*(3), 627-637. https://doi.org/10.1016/0092-8674(84)90257-5

Subhash, S., Mishra, K., Akhade, V. S., Kanduri, M., Mondal, T., & Kanduri, C. (2018). H3K4me2 and WDR5 enriched chromatin interacting long non-coding RNAs maintain transcriptionally competent chromatin at divergent transcriptional units. *Nucleic Acids Res*, *46*(18), 9384-9400. https://doi.org/10.1093/nar/gky635

Sun, B., Fiskus, W., Qian, Y., Rajapakshe, K., Raina, K., Coleman, K. G., Crew, A. P., Shen, A., Saenz, D. T., Mill, C. P., Nowak, A. J., Jain, N., Zhang, L., Wang, M., Khoury, J. D., Coarfa, C., Crews, C. M., & Bhalla, K. N. (2018). BET protein proteolysis targeting chimera (PROTAC) exerts potent lethal activity against mantle cell lymphoma cells. *Leukemia*, *32*(2), 343-352. https://doi.org/10.1038/leu.2017.207

Sun, W., Guo, F., & Liu, M. (2018). Up-regulated WDR5 promotes gastric cancer formation by induced cyclin D1 expression. *J Cell Biochem*, *119*(4), 3304-3316. https://doi.org/10.1002/jcb.26491

Sun, Y., Bell, J. L., Carter, D., Gherardi, S., Poulos, R. C., Milazzo, G., Wong, J. W., Al-Awar, R., Tee, A. E., Liu, P. Y., Liu, B., Atmadibrata, B., Wong, M., Trahair, T., Zhao, Q., Shohet, J. M., Haupt, Y., Schulte, J. H., Brown, P. J., . . . Liu, T. (2015). WDR5 Supports an N-Myc Transcriptional Complex That Drives a Protumorigenic Gene Expression

Signature in Neuroblastoma. *Cancer Res*, *75*(23), 5143-5154. https://doi.org/10.1158/0008-5472.CAN-15-0423

Taguchi, S.-i., Honda, K., Sugiura, K., Yamaguchi, A., Furukawa, K., & Urano, T. (2002). Degradation of human Aurora-A protein kinase is mediated by hCdh1. *FEBS Letters*, *519*(1-3), 59-65. https://doi.org/10.1016/s0014-5793(02)02711-4

Takahashi, D., Moriyama, J., Nakamura, T., Miki, E., Takahashi, E., Sato, A., Akaike, T., Itto-Nakama, K., & Arimoto, H. (2019). AUTACs: Cargo-Specific Degraders Using Selective Autophagy. *Mol Cell*, *76*(5), 797-810 e710. https://doi.org/10.1016/j.molcel.2019.09.009

Tang, A., Gao, K., Chu, L., Zhang, R., Yang, J., & Zheng, J. (2017). Aurora kinases: novel therapy targets in cancers. *Oncotarget*, *8*(14), 23937-23954. https://doi.org/10.18632/oncotarget.14893

Tang, J., Moorthy, R., Demir, Ö., Baker, Z. D., Naumann, J. A., Jones, K. F. M., Grillo, M. J., Haefner, E. S., Shi, K., Levy, M. J., Aihara, H., Harris, R. S., Amaro, R. E., Levinson, N. M., & Harki, D. A. (2022). Targeting N-Myc in Neuroblastoma with Selective Aurora Kinase A Degraders. *bioRxiv*, 2022.2004.2009.487756. https://doi.org/10.1101/2022.04.09.487756

Tanner, M. M., Grenman, S., Koul, A., Johannsson, O., Meltzer, P., Pejovic, T., Borg, A., & Isola, J. J. (2000). Frequent amplification of chromosomal region 20q12-q13 in ovarian cancer. *Clin Cancer Res*, *6*(5), 1833-1839. https://www.ncbi.nlm.nih.gov/pubmed/10815905

Taub, R., Kirsch, I., Morton, C., Lenoir, G., Swan, D., Tronick, S., Aaronson, S., & Leder, P. (1982). Translocation of the c-myc gene into the immunoglobulin heavy chain locus in human Burkitt lymphoma and murine plasmacytoma cells. *Proc Natl Acad Sci U S A*, *79*(24), 7837-7841. https://doi.org/10.1073/pnas.79.24.7837

Tesi, A., de Pretis, S., Furlan, M., Filipuzzi, M., Morelli, M. J., Andronache, A., Doni, M., Verrecchia, A., Pelizzola, M., Amati, B., & Sabo, A. (2019). An early Myc-dependent transcriptional program orchestrates cell growth during B-cell activation. *EMBO Rep*, *20*(9), e47987. https://doi.org/10.15252/embr.201947987

Thomas, L. R., Adams, C. M., Wang, J., Weissmiller, A. M., Creighton, J., Lorey, S. L., Liu, Q., Fesik, S. W., Eischen, C. M., & Tansey, W. P. (2019). Interaction of the oncoprotein transcription factor MYC with its chromatin cofactor WDR5 is essential for tumor maintenance. *Proc Natl Acad Sci U S A*, *116*(50), 25260-25268. https://doi.org/10.1073/pnas.1910391116

Thomas, L. R., Wang, Q., Grieb, B. C., Phan, J., Foshage, A. M., Sun, Q., Olejniczak, E. T., Clark, T., Dey, S., Lorey, S., Alicie, B., Howard, G. C., Cawthon, B., Ess, K. C., Eischen, C. M., Zhao, Z., Fesik, S. W., & Tansey, W. P. (2015). Interaction with WDR5 promotes target gene recognition and tumorigenesis by MYC. *Mol Cell*, *58*(3), 440-452. https://doi.org/10.1016/j.molcel.2015.02.028

Thompson, B. J., Buonamici, S., Sulis, M. L., Palomero, T., Vilimas, T., Basso, G., Ferrando, A., & Aifantis, I. (2007). The SCFFBW7 ubiquitin ligase complex as a tumor suppressor in T cell leukemia. *J Exp Med*, *204*(8), 1825-1835. https://doi.org/10.1084/jem.20070872

Ting, T. C., Goralski, M., Klein, K., Wang, B., Kim, J., Xie, Y., & Nijhawan, D. (2019). Aryl Sulfonamides Degrade RBM39 and RBM23 by Recruitment to CRL4-DCAF15. *Cell Rep*, *29*(6), 1499-1510 e1496. https://doi.org/10.1016/j.celrep.2019.09.079

Toure, M., & Crews, C. M. (2016). Small-Molecule PROTACS: New Approaches to Protein Degradation. *Angew Chem Int Ed Engl*, *55*(6), 1966-1973. https://doi.org/10.1002/anie.201507978

Toya, M., Terasawa, M., Nagata, K., Iida, Y., & Sugimoto, A. (2011). A kinase-independent role for Aurora A in the assembly of mitotic spindle microtubules in Caenorhabditis elegans embryos. *Nat Cell Biol*, *13*(6), 708-714. https://doi.org/10.1038/ncb2242

Tracz, M., & Bialek, W. (2021). Beyond K48 and K63: non-canonical protein ubiquitination. *Cell Mol Biol Lett*, *26*(1), 1. https://doi.org/10.1186/s11658-020-00245-6

Treekitkarnmongkol, W., Katayama, H., Kai, K., Sasai, K., Jones, J. C., Wang, J., Shen, L., Sahin, A. A., Gagea, M., Ueno, N. T., Creighton, C. J., & Sen, S. (2016). Aurora kinase-A overexpression in mouse mammary epithelium induces mammary adenocarcinomas harboring genetic alterations shared with human breast cancer. *Carcinogenesis*, *37*(12), 1180-1189. https://doi.org/10.1093/carcin/bgw097

Troup, R. I., Fallan, C., & Baud, M. G. J. (2020). Current strategies for the design of PROTAC linkers: a critical review. *Explor Target Antitumor Ther*, *1*(5), 273-312. https://doi.org/10.37349/etat.2020.00018

Trumpp, A., Refaeli, Y., Oskarsson, T., Gasser, S., Murphy, M., Martin, G. R., & Bishop, J. M. (2001). c-Myc regulates mammalian body size by controlling cell number but not cell size. *Nature*, *414*(6865), 768-773. https://doi.org/10.1038/414768a

Tseng, T. C., Chen, S. H., Hsu, Y. P., & Tang, T. K. (1998). Protein kinase profile of sperm and eggs: cloning and characterization of two novel testis-specific protein kinases (AIE1, AIE2) related to yeast and fly chromosome segregation regulators. *DNA Cell Biol*, *17*(10), 823-833. https://doi.org/10.1089/dna.1998.17.823

Tsuchiya, Y., Byrne, D. P., Burgess, S. G., Bormann, J., Bakovic, J., Huang, Y., Zhyvoloup, A., Yu, B. Y. K., Peak-Chew, S., Tran, T., Bellany, F., Tabor, A. B., Chan, A. E., Guruprasad, L., Garifulin, O., Filonenko, V., Vonderach, M., Ferries, S., Eyers, C. E., . . . Gout, I. (2020). Covalent Aurora A regulation by the metabolic integrator coenzyme A. *Redox Biol*, *28*, 101318. https://doi.org/10.1016/j.redox.2019.101318

Tyanova, S., Temu, T., Sinitcyn, P., Carlson, A., Hein, M. Y., Geiger, T., Mann, M., & Cox, J. (2016). The Perseus computational platform for comprehensive analysis of (prote)omics data. *Nat Methods*, *13*(9), 731-740. https://doi.org/10.1038/nmeth.3901

Ursu, O., Holmes, J., Knockel, J., Bologa, C. G., Yang, J. J., Mathias, S. L., Nelson, S. J., & Oprea, T. I. (2017). DrugCentral: online drug compendium. *Nucleic Acids Res*, *45*(D1), D932-D939. https://doi.org/10.1093/nar/gkw993

van de Wetering, M., Sancho, E., Verweij, C., de Lau, W., Oving, I., Hurlstone, A., van der Horn, K., Batlle, E., Coudreuse, D., Haramis, A.-P., Tjon-Pon-Fong, M., Moerer, P., van den Born, M., Soete, G., Pals, S., Eilers, M., Medema, R., & Clevers, H. (2002). The β-Catenin/TCF-4 Complex Imposes a Crypt Progenitor Phenotype on Colorectal Cancer Cells. *Cell*, *111*(2), 241-250. https://doi.org/10.1016/s0092-8674(02)01014-0

von Eyss, B., Jaenicke, L. A., Kortlever, R. M., Royla, N., Wiese, K. E., Letschert, S., McDuffus, L. A., Sauer, M., Rosenwald, A., Evan, G. I., Kempa, S., & Eilers, M. (2015). A MYC-Driven Change in Mitochondrial Dynamics Limits YAP/TAZ Function in Mammary Epithelial Cells and Breast Cancer. *Cancer Cell*, *28*(6), 743-757. https://doi.org/10.1016/j.ccell.2015.10.013

Walz, S., Lorenzin, F., Morton, J., Wiese, K. E., von Eyss, B., Herold, S., Rycak, L., Dumay-Odelot, H., Karim, S., Bartkuhn, M., Roels, F., Wustefeld, T., Fischer, M., Teichmann, M., Zender, L., Wei, C. L., Sansom, O., Wolf, E., & Eilers, M. (2014). Activation and repression by oncogenic MYC shape tumour-specific gene expression profiles. *Nature*, *511*(7510), 483-487. https://doi.org/10.1038/nature13473

Wang, B., Shen, A., Ouyang, X., Zhao, G., Du, Z., Huo, W., Zhang, T., Wang, Y., Yang, C., Dong, P., Watari, H., Pfeffer, L. M., & Yue, J. (2017). KLF4 expression enhances the efficacy of chemotherapy drugs in ovarian cancer cells. *Biochem Biophys Res Commun*, *484*(3), 486-492. https://doi.org/10.1016/j.bbrc.2017.01.062

Wang, F., Jeon, K. O., Salovich, J. M., Macdonald, J. D., Alvarado, J., Gogliotti, R. D., Phan, J., Olejniczak, E. T., Sun, Q., Wang, S., Camper, D., Yuh, J. P., Shaw, J. G., Sai, J., Rossanese, O. W., Tansey, W. P., Stauffer, S. R., & Fesik, S. W. (2018). Discovery of Potent 2-Aryl-6,7-dihydro-5 H-pyrrolo[1,2- a]imidazoles as WDR5-WIN-Site Inhibitors Using Fragment-Based Methods and Structure-Based Design. *J Med Chem*, *61*(13), 5623-5642. https://doi.org/10.1021/acs.jmedchem.8b00375

Wang, H., Hammoudeh, D. I., Follis, A. V., Reese, B. E., Lazo, J. S., Metallo, S. J., & Prochownik, E. V. (2007). Improved low molecular weight Myc-Max inhibitors. *Mol Cancer Ther*, *6*(9), 2399-2408. https://doi.org/10.1158/1535-7163.MCT-07-0005

Wang, K. C., Yang, Y. W., Liu, B., Sanyal, A., Corces-Zimmerman, R., Chen, Y., Lajoie, B. R., Protacio, A., Flynn, R. A., Gupta, R. A., Wysocka, J., Lei, M., Dekker, J., Helms, J. A., & Chang, H. Y. (2011). A long noncoding RNA maintains active chromatin to coordinate homeotic gene expression. *Nature*, *472*(7341), 120-124. https://doi.org/10.1038/nature09819

Wang, R., Ascanelli, C., Abdelbaki, A., Fung, A., Rasmusson, T., Michaelides, I., Roberts, K., & Lindon, C. (2021). Selective targeting of non-centrosomal AURKA functions through use of a targeted protein degradation tool. *Commun Biol*, *4*(1), 640. https://doi.org/10.1038/s42003-021-02158-2

Wang, S., Han, L., Han, J., Li, P., Ding, Q., Zhang, Q. J., Liu, Z. P., Chen, C., & Yu, Y. (2019). Uncoupling of PARP1 trapping and inhibition using selective PARP1 degradation. *Nat Chem Biol*, *15*(12), 1223-1231. https://doi.org/10.1038/s41589-019-0379-2

Wang, W., Hu, S., Gu, Y., Yan, Y., Stovall, D. B., Li, D., & Sui, G. (2020). Human MYC G-quadruplex: From discovery to a cancer therapeutic target. *Biochim Biophys Acta Rev Cancer*, *1874*(2), 188410. https://doi.org/10.1016/j.bbcan.2020.188410

Wang, Y., Jiang, X., Feng, F., Liu, W., & Sun, H. (2020). Degradation of proteins by PROTACs and other strategies. *Acta Pharm Sin B*, *10*(2), 207-238. https://doi.org/10.1016/j.apsb.2019.08.001

Wang, Y., Wang, Z., Qi, Z., Yin, S., Zhang, N., Liu, Y., Liu, M., Meng, J., Zang, R., Zhang, Z., & Yang, G. (2014). The negative interplay between Aurora A/B and BRCA1/2 controls cancer cell growth and tumorigenesis via distinct regulation of cell cycle progression, cytokinesis, and tetraploidy. *Mol cancer*, *13*, 94. https://doi.org/10.1186/1476-4598-13-94

Wang, Y. L., Faiola, F., Xu, M., Pan, S., & Martinez, E. (2008). Human ATAC Is a GCN5/PCAF-containing acetylase complex with a novel NC2-like histone fold module that interacts with the TATA-binding protein. *J Biol Chem*, *283*(49), 33808-33815. https://doi.org/10.1074/jbc.M806936200

Wei, Y., Resetca, D., Li, Z., Johansson-Akhe, I., Ahlner, A., Helander, S., Wallenhammar, A., Morad, V., Raught, B., Wallner, B., Kokubo, T., Tong, Y., Penn, L. Z., & Sunnerhagen, M. (2019). Multiple direct interactions of TBP with the MYC oncoprotein. *Nat Struct Mol Biol*, *26*(11), 1035-1043. https://doi.org/10.1038/s41594-019-0321-z

Weiss, W. A., Aldape, K., Mohapatra, G., Feuerstein, B. G., & Bishop, J. M. (1997). Targeted expression of MYCN causes neuroblastoma in transgenic mice. *EMBO J*, *16*(11), 2985-2995. https://doi.org/10.1093/emboj/16.11.2985

Welcker, M., Orian, A., Jin, J., Grim, J. E., Harper, J. W., Eisenman, R. N., & Clurman, B. E. (2004). The Fbw7 tumor suppressor regulates glycogen synthase kinase 3 phosphorylation-dependent c-Myc protein degradation. *Proc Natl Acad Sci U S A*, *101*(24), 9085-9090. https://doi.org/10.1073/pnas.0402770101

Welcker, M., Wang, B., Rusnac, D. V., Hussaini, Y., Swanger, J., Zheng, N., & Clurman, B. E. (2022). Two diphosphorylated degrons control c-Myc degradation by the Fbw7 tumor suppressor. *Sci Adv*, *8*(4), eabl7872. https://doi.org/10.1126/sciadv.abl7872

Whitfield, J. R., & Soucek, L. (2021). The long journey to bring a Myc inhibitor to the clinic. *J Cell Biol*, *220*(8). https://doi.org/10.1083/jcb.202103090

Willems, E., Dedobbeleer, M., Digregorio, M., Lombard, A., Lumapat, P. N., & Rogister, B. (2018). The functional diversity of Aurora kinases: a comprehensive review. *Cell Div*, *13*(13), 7. https://doi.org/10.1186/s13008-018-0040-6

Wilson, A., Murphy, M. J., Oskarsson, T., Kaloulis, K., Bettess, M. D., Oser, G. M., Pasche, A. C., Knabenhans, C., Macdonald, H. R., & Trumpp, A. (2004). c-Myc controls the balance between hematopoietic stem cell self-renewal and differentiation. *Genes Dev*, *18*(22), 2747-2763. https://doi.org/10.1101/gad.313104

Winter, G. E., Buckley, D. L., Paulk, J., Roberts, J. M., Souza, A., Dhe-Paganon, S., & Bradner, J. E. (2015). DRUG DEVELOPMENT. Phthalimide conjugation as a strategy for in vivo target protein degradation. *Science*, *348*(6241), 1376-1381. https://doi.org/10.1126/science.aab1433

Wolf, E., & Eilers, M. (2020). Targeting MYC Proteins for Tumor Therapy. *Annual Review of Cancer Biology*, *4*(1), 61-75. https://doi.org/10.1146/annurev-cancerbio-030518-055826

Wu, M. Z., Tsai, Y. P., Yang, M. H., Huang, C. H., Chang, S. Y., Chang, C. C., Teng, S. C., & Wu, K. J. (2011). Interplay between HDAC3 and WDR5 is essential for hypoxia-induced epithelial-mesenchymal transition. *Mol Cell*, *43*(5), 811-822. https://doi.org/10.1016/j.molcel.2011.07.012

Wu, N., Jia, D., Bates, B., Basom, R., Eberhart, C. G., & MacPherson, D. (2017). A mouse model of MYCN-driven retinoblastoma reveals MYCN-independent tumor reemergence. *J Clin Invest*, *127*(3), 888-898. https://doi.org/10.1172/JCI88508

Wu, Y., Diao, P., Li, Z., Zhang, W., Wang, D., Wang, Y., & Cheng, J. (2018). Overexpression of WD repeat domain 5 associates with aggressive clinicopathological features and unfavorable prognosis in head neck squamous cell carcinoma. *J Oral Pathol Med*, *47*(5), 502-510. https://doi.org/10.1111/jop.12708

Xie, T., Lim, S. M., Westover, K. D., Dodge, M. E., Ercan, D., Ficarro, S. B., Udayakumar, D., Gurbani, D., Tae, H. S., Riddle, S. M., Sim, T., Marto, J. A., Janne, P. A., Crews, C. M., & Gray, N. S. (2014). Pharmacological targeting of the pseudokinase Her3. *Nat Chem Biol*, *10*(12), 1006-1012. https://doi.org/10.1038/nchembio.1658

Xu, H., Di Antonio, M., McKinney, S., Mathew, V., Ho, B., O'Neil, N. J., Santos, N. D., Silvester, J., Wei, V., Garcia, J., Kabeer, F., Lai, D., Soriano, P., Banath, J., Chiu, D. S., Yap, D., Le, D. D., Ye, F. B., Zhang, A., . . . Aparicio, S. (2017). CX-5461 is a DNA G-quadruplex stabilizer with selective lethality in BRCA1/2 deficient tumours. *Nat Commun*, *8*, 14432. https://doi.org/10.1038/ncomms14432

Xu, J., Shao, Z., Li, D., Xie, H., Kim, W., Huang, J., Taylor, J. E., Pinello, L., Glass, K., Jaffe, J. D., Yuan, G. C., & Orkin, S. H. (2015). Developmental control of polycomb subunit composition by GATA factors mediates a switch to non-canonical functions. *Mol Cell*, *57*(2), 304-316. https://doi.org/10.1016/j.molcel.2014.12.009

Xu, J., Wu, X., Zhou, W. H., Liu, A. W., Wu, J. B., Deng, J. Y., Yue, C. F., Yang, S. B., Wang, J., Yuan, Z. Y., & Liu, Q. (2013). Aurora-A identifies early recurrence and poor prognosis and promises a potential therapeutic target in triple negative breast cancer. *PLoS One*, *8*(2), e56919. https://doi.org/10.1371/journal.pone.0056919

Yada, M., Hatakeyama, S., Kamura, T., Nishiyama, M., Tsunematsu, R., Imaki, H., Ishida, N., Okumura, F., Nakayama, K., & Nakayama, K. I. (2004). Phosphorylation-dependent degradation of c-Myc is mediated by the F-box protein Fbw7. *EMBO J*, *23*(10), 2116-2125. https://doi.org/10.1038/sj.emboj.7600217

Yamamoto, S., Yamamoto-Ibusuki, M., Yamamoto, Y., Fujiwara, S., & Iwase, H. (2013). A comprehensive analysis of Aurora A; transcript levels are the most reliable in association with proliferation and prognosis in breast cancer. *BMC Cancer*, *13*, 217. https://doi.org/10.1186/1471-2407-13-217

Yang, G., Chang, B., Yang, F., Guo, X., Cai, K. Q., Xiao, X. S., Wang, H., Sen, S., Hung, M. C., Mills, G. B., Chang, S., Multani, A. S., Mercado-Uribe, I., & Liu, J. (2010). Aurora kinase A promotes ovarian tumorigenesis through dysregulation of the cell cycle and suppression of BRCA2. *Clin Cancer Res*, *16*(12), 3171-3181. https://doi.org/10.1158/1078-0432.CCR-09-3171

Yang, N., Wang, C., Wang, J., Wang, Z., Huang, D., Yan, M., Kamran, M., Liu, Q., & Xu, B. (2019). Aurora kinase A stabilizes FOXM1 to enhance paclitaxel resistance in triple-negative breast cancer. *J Cell Mol Med*, *23*(9), 6442-6453. https://doi.org/10.1111/jcmm.14538

Yang, Y. W., Flynn, R. A., Chen, Y., Qu, K., Wan, B., Wang, K. C., Lei, M., & Chang, H. Y. (2014). Essential role of lncRNA binding for WDR5 maintenance of active chromatin and embryonic stem cell pluripotency. *Elife*, *3*, e02046. https://doi.org/10.7554/eLife.02046

Yao, J. E., Yan, M., Guan, Z., Pan, C. B., Xia, L. P., Li, C. X., Wang, L. H., Long, Z. J., Zhao, Y., Li, M. W., Zheng, F. M., Xu, J., Lin, D. J., & Liu, Q. (2009). Aurora-A down-regulates IkappaBalpha via Akt activation and interacts with insulin-like growth factor-1 induced phosphatidylinositol 3-kinase pathway for cancer cell survival. *Mol cancer*, *8*, 95. https://doi.org/10.1186/1476-4598-8-95

Ye, Y., & Rape, M. (2009). Building ubiquitin chains: E2 enzymes at work. *Nat Rev Mol Cell Biol*, *10*(11), 755-764. https://doi.org/10.1038/nrm2780

Yeilding, N. M., Rehman, M. T., & Lee, W. M. (1996). Identification of sequences in c-myc mRNA that regulate its steady-state levels. *Mol Cell Biol*, *16*(7), 3511-3522. https://doi.org/10.1128/MCB.16.7.3511

Yim, W. W., & Mizushima, N. (2020). Lysosome biology in autophagy. *Cell Discov*, *6*, 6. https://doi.org/10.1038/s41421-020-0141-7

Yin, X., Giap, C., Lazo, J. S., & Prochownik, E. V. (2003). Low molecular weight inhibitors of Myc-Max interaction and function. *Oncogene*, *22*(40), 6151-6159. https://doi.org/10.1038/sj.onc.1206641

Yu, X., Li, D., Kottur, J., Shen, Y., Kim, H. S., Park, K. S., Tsai, Y. H., Gong, W., Wang, J., Suzuki, K., Parker, J., Herring, L., Kaniskan, H. U., Cai, L., Jain, R., Liu, J., Aggarwal, A. K., Wang, G. G., & Jin, J. (2021). A selective WDR5 degrader inhibits acute myeloid leukemia in patient-derived mouse models. *Sci Transl Med*, *13*(613), eabj1578. https://doi.org/10.1126/scitranslmed.abj1578

Zanet, J., Pibre, S., Jacquet, C., Ramirez, A., de Alboran, I. M., & Gandarillas, A. (2005). Endogenous Myc controls mammalian epidermal cell size, hyperproliferation,

endoreplication and stem cell amplification. *J Cell Sci*, *118*(Pt 8), 1693-1704. https://doi.org/10.1242/jcs.02298

Zeid, R., Lawlor, M. A., Poon, E., Reyes, J. M., Fulciniti, M., Lopez, M. A., Scott, T. G., Nabet, B., Erb, M. A., Winter, G. E., Jacobson, Z., Polaski, D. R., Karlin, K. L., Hirsch, R. A., Munshi, N. P., Westbrook, T. F., Chesler, L., Lin, C. Y., & Bradner, J. E. (2018). Enhancer invasion shapes MYCN-dependent transcriptional amplification in neuroblastoma. *Nat Genet*, *50*(4), 515-523. https://doi.org/10.1038/s41588-018-0044-9

Zeng, S., Yang, J., Zhao, J., Liu, Q., Rong, M., Guo, Z., & Gao, W. (2014). Silencing Dicer expression enhances cellular proliferative and invasive capacities in human tongue squamous cell carcinoma. *Oncol Rep*, *31*(2), 867-873. https://doi.org/10.3892/or.2013.2903

Zengerle, M., Chan, K. H., & Ciulli, A. (2015). Selective Small Molecule Induced Degradation of the BET Bromodomain Protein BRD4. *ACS Chem Biol*, *10*(8), 1770-1777. https://doi.org/10.1021/acschembio.5b00216

Zhang, C., Ge, S., Gong, W., Xu, J., Guo, Z., Liu, Z., Gao, X., Wei, X., & Ge, S. (2020). LncRNA ANRIL acts as a modular scaffold of WDR5 and HDAC3 complexes and promotes alteration of the vascular smooth muscle cell phenotype. *Cell Death Dis*, *11*(6), 435. https://doi.org/10.1038/s41419-020-2645-3

Zhang, H., Han, Y., Yang, Y., Lin, F., Li, K., Kong, L., Liu, H., Dang, Y., Lin, J., & Chen, P. R. (2021). Covalently Engineered Nanobody Chimeras for Targeted Membrane Protein Degradation. *J Am Chem Soc*, *143*(40), 16377-16382. https://doi.org/10.1021/jacs.1c08521

Zhang, L., Riley-Gillis, B., Vijay, P., & Shen, Y. (2019). Acquired Resistance to BET-PROTACs (Proteolysis-Targeting Chimeras) Caused by Genomic Alterations in Core Components of E3 Ligase Complexes. *Mol Cancer Ther*, *18*(7), 1302-1311. https://doi.org/10.1158/1535-7163.MCT-18-1129

Zhang, R., McIntyre, P. J., Collins, P. M., Foley, D. J., Arter, C., von Delft, F., Bayliss, R., Warriner, S., & Nelson, A. (2019). Construction of a Shape-Diverse Fragment Set: Design, Synthesis and Screen against Aurora-A Kinase. *Chemistry*, *25*(27), 6831-6839. https://doi.org/10.1002/chem.201900815

Zhao, L., Zhao, J., Zhong, K., Tong, A., & Jia, D. (2022). Targeted protein degradation: mechanisms, strategies and application. *Signal Transduct Target Ther*, *7*(1), 113. https://doi.org/10.1038/s41392-022-00966-4

Zhao, X., Su, J., Wang, F., Liu, D., Ding, J., Yang, Y., Conaway, J. W., Conaway, R. C., Cao, L., Wu, D., Wu, M., Cai, Y., & Jin, J. (2013). Crosstalk between NSL histone acetyltransferase and MLL/SET complexes: NSL complex functions in promoting histone H3K4 di-methylation activity by MLL/SET complexes. *PLoS Genet*, *9*(11), e1003940. https://doi.org/10.1371/journal.pgen.1003940

Zheng, F., Yue, C., Li, G., He, B., Cheng, W., Wang, X., Yan, M., Long, Z., Qiu, W., Yuan, Z., Xu, J., Liu, B., Shi, Q., Lam, E. W., Hung, M. C., & Liu, Q. (2016). Nuclear AURKA acquires kinase-independent transactivating function to enhance breast cancer stem cell phenotype. *Nat Commun*, *7*, 10180. https://doi.org/10.1038/ncomms10180

Zheng, N., & Shabek, N. (2017). Ubiquitin Ligases: Structure, Function, and Regulation. *Annu Rev Biochem*, *86*, 129-157. https://doi.org/10.1146/annurev-biochem-060815-014922

Zhou, Q., Chen, X., He, H., Peng, S., Zhang, Y., Zhang, J., Cheng, L., Liu, S., Huang, M., Xie, R., Lin, T., & Huang, J. (2021). WD repeat domain 5 promotes chemoresistance and Programmed Death-Ligand 1 expression in prostate cancer. *Theranostics*, *11*(10), 4809-4824. https://doi.org/10.7150/thno.55814

Zorba, A., Buosi, V., Kutter, S., Kern, N., Pontiggia, F., Cho, Y. J., & Kern, D. (2014). Molecular mechanism of Aurora A kinase autophosphorylation and its allosteric activation by TPX2. *Elife*, *3*, e02667. https://doi.org/10.7554/eLife.02667

List of Figures

List of Tables

Abbreviations

Prefixes

n	nano
µ	micro
m	milli
k	kilo

Units

°C	degree celsius
A	ampere
Da	dalton
g	gram
h	hour
l	liter
M	molar, mol/l
rU	relative unit
v/v	volume per volume
w/v	weight per volume

Amino acids

A	Alanine, Ala
D	Aspartatic acid, Asp
E	Glutamatic acid, Glu
F	Phenylalanine, Phe
G	Glycine, Gly
I	Isoleucine, Ile
K	Lysine, Lys
L	Leucine, Leu
N	Asparagine, Asn
P	Proline, Pro
Q	Glutamine, Gln
R	Arginine, Arg
S	Serine, Ser
T	Threonine, Thr
V	Valine, Val
W	Tryptophan, Trp
x	Variable amino acid

Others

AID	Auxin-inducible degron
ALP	Autophagy-lysosome pathway
AML	Acute myeloid leukemia

APS	Ammonium persulfate
AR	Androgen receptor
ATAC	Ada2-containing
ATP	Adenosine triphosphate
ATTEC	Autophagosome-tethering compound
AUTAC	Autophagy targeting chimera
AUTOTAC	AUTOphagy-TArgeting Chimera
BCA	Bicinchoninic acid
BET	Bromodomain and extra-terminal domain
BR	Basic region
BrdU	Bromodeoxyuridine
BSA	Bovine serum albumin
CDK	Cyclin-dependent kinase
cDNA	Complementary DNA
CDS	Coding sequence
ChIP	Chromatin immunoprecipitation
ChRIP	Chromatin RNA immunoprecipitation
CHX	Cycloheximide
CMA	Chaperone-mediated autophagy
CRBN	Cereblon
CRC	Colorectal cancer
CRL	Cullin-RING ligase
Ctr	Control
DC_{50}	Half-maximal degradation concentration
DC_{max}	Maximal degradation concentration
D_{max}	Maximal degradation
DMEM	Dulbecco's Modified Eagle's Medium
DMSO	Dimethyl sulfoxide
DNA	Deoxyribonucleic acid
dNTP	Deoxynucleotide triphosphate
Dox	Doxycycline
dTAG	Degradation tag
DTT	Dithiothreitol
E-box	Enhancer-box
E1	Ubiquitin-activating enzyme
E2	Ubiquitin-conjugating enzyme
E3	Ubiquitin-protein ligase
EC_{50}	Half maximal effective concentration
EDTA	Ethylenediamine tetraacetic acid
ER	Estrogen receptor
ESC	Embryonic stem cell
EtOH	Ethanol
FBS	Fetal bovine serum
FBXW7	F-box/WD repeat containing 7
FC	Fold change
FDR	False discovery rate

FKBP12	12-kDa FK506 binding protein
FRB	FKBP-rapamycin binding
G2/M phase	Gap 2/ Mitosis phase
GFP	Green fluorescent protein
GSEA	Gene set enrichment analyses
HA	Hemagglutinin
HCC	Hepatocellular carcinoma
HEPES	4-(2-hydroxyethyl)-1-piperazineethanesulfonic acid
HLH	Helix-loop-helix
HMT	Histone methyltransferases
HRP	Horseradish peroxidase
IgG	Immunoglobulin G
IMiD	Immunomodulatory drug
IP	Immunoprecipitation
K_d^{app}	Apparent dissociation constant
LB	Lysogeny broth
LC	Liquid chromatography
LDS	Lithium dodecyl sulfate
LFQ	Label-free quantification
lncRNA	Long non-coding RNA
$\log_{10}$	Decadic logarithm
$\log_2$	Binary logarithm
LZ	Leucine zipper
Max	MYC-associated factor X
MB	Myc homology box
MD	Molecular dynamics
MLL	Mixed lineage leukemia
MOPS	3-(N-morpholino)propanesulfonic acid
mRNA	Messenger RNA
MS	Mass spectrometry
MYC	MYC proto-oncogene, BHLH transcription factor
n	Number
N/A	Not applicable
NAE	NEDD8-activating enzyme
NLuc	Nanoluciferase
nM	Nanomolar
NP-40	Nonidet P-40
NSCLC	Non-small-cell lung cancer
NSL	Non-specific lethal
NuRD	Nucleosome remodeling and deacetylase
OHT	4-Hydroxytamoxifen
p	P-value
PAGE	Polyacrylamide gel electrophoresis
PBS	Phosphate buffered saline
PCR	Polymerase chain reaction
PDAC	Pancreatic ductal adenocarcinoma

PDB	Protein Data Bank
PEG	Polyethylene glycol
PEI	Polyethyleneimine
PI	Propidium iodide
pK_d^{app}	Negative decadic logarithm of K_d^{app}
POI	Protein of interest
PPI	Protein-protein interaction
PROTAC	Proteolytic targeting chimera
PVDF	Polyvinylidene difluoride
qPCR	Quantitative polymerase chain reaction
RB	Retinoblastoma
RCC	Renal cell carcinoma
RIP	Rapamycin-induced proximity
RIPA	Radioimmunoprecipitation assay
RNA	Ribonucleic acid
RNAseq	RNA sequencing
RPMI	Roswell Park Memorial Institute
RT	Room temperature
rtPCR	Reverse transcription-polymerase chain reaction
rtTA	Reverse tetracycline-controlled transactivator
S-phase	Synthesis phase
SCF	Skp1-Cullin-F box
SCLC	Small cell lung cancer
SD	Standard deviation
SDS	Sodium dodecyl sulfate
SEM	Standard error of mean
SILAC	Stable isotope labeling with amino acids in cell culture
siRNA	Small interfering RNA
$t_{1/2}$	Half-life
TAD	Transactivation domain
TAE	Tris-Acetate-EDTA
TBS	Tris-buffered saline
TCGA	The Cancer Genome Atlas
TE	Tris-EDTA
TEMED	N,N,N′,N′-tetramethylethan-1,2-diamine
TMT	Tandem mass tag
TPD	Targeted protein degradation
Tris	Tris(hydroxymethyl)aminomethane
tTA	Tetracycline-controlled transactivator
Ub	Ubiquitin
UPS	Ubiquitin proteasome system
VHL	von Hippel-Lindau disease tumor suppressor
WBM	WDR5 Binding Motif
WDR5	WD repeat-containing protein 5
Win	WDR5 interacting
WT	Wildtype

Acknowledgements

Appendix

Publication list

Bozilovic J., Eing L., Berger B., **Adhikari B.**, Weckesser J., Berner N., Wilhelm S., Kuster B., Wolf E. and Knapp S., 2022. Novel, highly potent PROTACs targeting AURORA-A kinase. *Current Research In Chemical Biology*, 2, p100032

Adhikari B.*#, Narain A.* and Wolf E.#, Generation of auxin inducible degron (AID) knock-in cell lines for targeted protein degradation in mammalian cells. *STAR Protocols*, 2021, 2(4), p.100949.

Narain A., Bhandare P., **Adhikari B.**, Backes S., Eilers M., Dölken L., Schlosser A., Erhard F., Baluapuri A. and Wolf E., Targeted protein degradation reveals a direct role of SPT6 in RNAPII elongation and termination. *Molecular Cell,* 2021, 81(15), pp.3110-3127.e14.

Dölle A.*, **Adhikari B.***, Krämer A., Weckesser J., Berner N., Berger L., Diebold M., Szewczyk M., Barsyte-Lovejoy D., Arrowsmith C., Gebel J., Löhr F., Dötsch V., Eilers M., Heinzlmeir S., Kuster B., Sotriffer C., Wolf E. and Knapp S., Design, Synthesis, and Evaluation of WD-Repeat-Containing Protein 5 (WDR5) Degraders. *Journal of Medicinal Chemistry*, 2021, 64(15), pp.10682-10710.

Adhikari B.*, Bojilovic J.*, Diebold M., Schwarz J.D., Hofstetter J., Schröder M., Wanior M., Narain A., Vogt M., Dudvarski Stankovic N., Baluapuri A., Schönemann L, Eing L., Bhandare P., Kuster B., Schlosser A., Heinzlmeir S., Sotriffer C., Knapp S. and Wolf E., PROTAC-mediated degradation reveals a non-catalytic function of AURORA-A kinase. *Nature Chemical Biology*, 2020, 16(11), 1179-1188

Zivanovic J., Kouroussis E., Kohl J., **Adhikari B.**, Bursac B., Schott-Roux S., Petrovic D., Miljkovic J., Thomas-Lopez D., Jung Y., Miler M., Mitchell S., Milosevic V., Gomes J., Benhar M., Gonzalez-Zorn B., Ivanovic-Burmazovic I., Torregrossa R., Mitchell J., Whiteman M., Schwarz G., Snyder S., Paul B., Carroll K. and Filipovic M., Selective Persulfide Detection Reveals Evolutionarily Conserved Antiaging Effects of S-Sulfhydration. *Cell Metabolism*, 2020, 31(1):207.

Baluapuri A., Hofstetter J., Stankovic N.D., Endres T., Bhandare P., Vos S.M., **Adhikari B.**, Schwarz J.D., Narain A., Vogt M., Wang S-W., Düster R., Jung L.A., Vanselow J., Wiegering A., Geyer M., Maric H., Gallant P., Walz S., Schlosser A., Cramer P., Eilers M. and Wolf E., MYC recruits SPT5 to RNA polymerase II to promote processive transcription elongation. *Molecular Cell*, 2019, 16(74), 674-687

Kouroussis E., **Adhikari B.**, Zivanovic J. and Filipovic M., Measurement of Protein Persulfidation: Improved Tag-Switch Method. *Methods in Molecular Biology*, 2019; 37-50.

Appendix

Vitvitsky V., Miljkovic J., Bostelaar T., **Adhikari B.**, Yadav P., Steiger A., Torregrossa R., Pluth M., Whiteman M., Banerjee R. and Filipovic M., Cytochrome c Reduction by H_2S Potentiates Sulfide Signaling. *ACS Chemical Biology*, 2018, 13(8):2300-2307

***** authors contributed equally
# corresponding author

Curriculum Vitae

Affidavit

I hereby confirm that my thesis entitled "*Targeted degradation of Myc-interacting oncoproteins*" is the result of my own work. I did not receive any help or support from commercial consultants. All sources and / or materials applied are listed and specified in the thesis.

Furthermore, I confirm that this thesis has not yet been submitted as part of another examination process neither in identical nor in similar form.

Place, Date Signature

Eidesstattliche Erklärung

Hiermit erkläre ich an Eides statt, die Dissertation "*Gezielte Degradation von mit Myc interagierenden Onkoproteinen*" eigenständig, d.h. insbesondere selbständig und ohne Hilfe eines kommerziellen Promotionsberaters, angefertigt und keine anderen als die von mir angegebenen Quellen und Hilfsmittel verwendet zu haben.

Ich erkläre außerdem, dass die Dissertation weder in gleicher noch in ähnlicher Form bereits in einem anderen Prüfungsverfahren vorgelegen hat.

Ort, Datum Unterschrift